

LEVEL 1

AGARD-CP-277

AGARD-CP-277

AGARD

ADVISORY GROUP FOR AEROSPACE RESEARCH & DEVELOPMENT

7 RUE ANCELLE 92200 NEUILLY SUR SEINE FRANCE

ADA 080451

AGARD CONFERENCE PROCEEDINGS No. 277

Damping Effects in Aerospace Structures

DDC
REFINER
FEB 8 1980
REGISTRATION
E

This document has been approved
for public release and sale, its
distribution is unlimited.

DDC FILE COPY

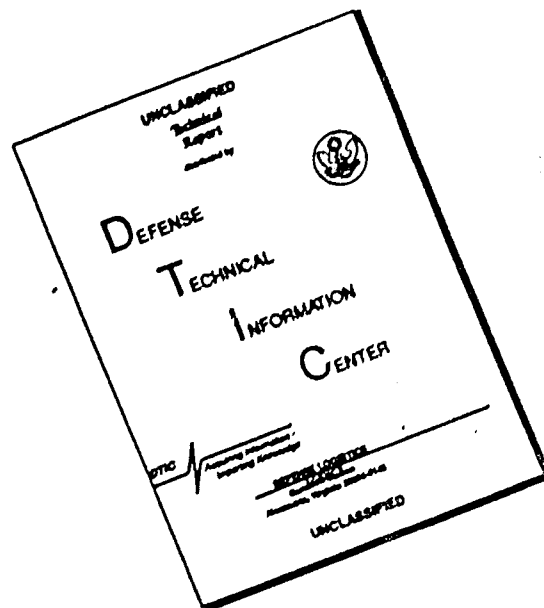
NORTH ATLANTIC TREATY ORGANIZATION



DISTRIBUTION AND AVAILABILITY
ON BACK COVER

80 2 1 068

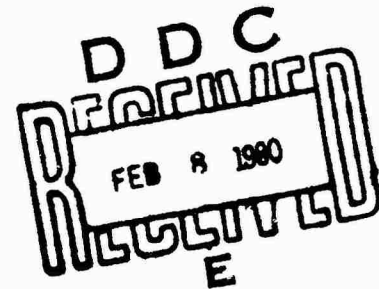
DISCLAIMER NOTICE



THIS DOCUMENT IS BEST QUALITY AVAILABLE. THE COPY FURNISHED TO DTIC CONTAINED A SIGNIFICANT NUMBER OF PAGES WHICH DO NOT REPRODUCE LEGIBLY.

①

NORTH ATLANTIC TREATY ORGANIZATION
ADVISORY GROUP FOR AEROSPACE RESEARCH AND DEVELOPMENT
(ORGANISATION DU TRAITE DE L'ATLANTIQUE NORD)



⑨

AGARD Conference Proceedings No. 277

⑥

DAMPING EFFECTS IN AEROSPACE STRUCTURES

⑪ Oct 72

⑬ 2001

This document has been approved
for public release and sale; its
distribution is unlimited.

Papers presented at the 48th Meeting of the AGARD Structures and Materials Panel
held in Williamsburg, VA, USA on 2-3 April 1979

400043

VB

THE MISSION OF AGARD

The mission of AGARD is to bring together the leading personalities of the NATO nations in the fields of science and technology relating to aerospace for the following purposes:

- Exchanging of scientific and technical information;
- Continuously stimulating advances in the aerospace sciences relevant to strengthening the common defence posture;
- Improving the co-operation among member nations in aerospace research and development;
- Providing scientific and technical advice and assistance to the North Atlantic Military Committee in the field of aerospace research and development;
- Rendering scientific and technical assistance, as requested, to other NATO bodies and to member nations in connection with research and development problems in the aerospace field;
- Providing assistance to member nations for the purpose of increasing their scientific and technical potential;
- Recommending effective ways for the member nations to use their research and development capabilities for the common benefit of the NATO community.

The highest authority within AGARD is the National Delegates Board consisting of officially appointed senior representatives from each member nation. The mission of AGARD is carried out through the Panels which are composed of experts appointed by the National Delegates, the Consultant and Exchange Programme and the Aerospace Applications Studies Programme. The results of AGARD work are reported to the member nations and the NATO Authorities through the AGARD series of publications of which this is one.

Participation in AGARD activities is by invitation only and is normally limited to citizens of the NATO nations.

The content of this publication has been reproduced
directly from material supplied by AGARD or the authors.

Published October 1979

Copyright © AGARD 1979
All Rights Reserved

ISBN 92-835-0244-2



*Printed by Technical Editing and Reproduction Ltd
Harford House, 7-9 Charlotte St, London, W1P 1HD*

A050 271

PREFACE

The Specialists' Meeting on Damping Effects in Aerospace Structures stemmed from a proposal made by the writer, leading to the formation of a Sub-Committee on Structural Damping during the 44th Panel Meeting in Lisbon, April 1977. I do believe, in fact, that the effects of damping on the problems of elastic stability are of the highest interest for several NATO countries, for their national activities and also for some multi-national co-operative programmes, e.g. POGO effect, dynamic response of structures, flutter.

In view of the need to have available pertinent information and reliable rules to account for these effects, which in some cases are of vital importance, the Sub-Committee undertook the organisation of the present Specialists' Meeting. The first step was the preparation of two pilot papers, presented at the 45th SMP Meeting in September 1977 and published as AGARD Report No.663/ "An Introduction to the Problem of Dynamic Structural Damping" by P.Santini, A.Castellani and A.Nappi. The interest shown in this subject enabled all details of the Specialists' Meeting to be established by the following April.

The Specialists' Meeting covered the most general aspects of structural damping; physical roots, mathematical formulation, damping characteristics of aerospace structural components, effects on dynamic response, investigation of damping in composites and effects in joints.

The Meeting was very successful, as was agreed by all the Sub-Committee members; this was essentially due to the spectrum of practical information presented by the participants, covering the whole area of the subject. The importance of the problem and the need for updating technical information is such that AGARD will be requested to consider the possibility of continuing the activity in the future in order to disseminate as much as possible all pertinent data, as is the aim of the present volume.

P.SANTINI
Chairman, Sub-Committee on
Structural Damping

Accession For	
NTIS GRA&I	<input checked="checked" type="checkbox"/>
DDC TAB	<input type="checkbox"/>
Unannounced	<input type="checkbox"/>
Justification	
By _____	
Distribution/	
Availability Codes	
Dist	Availand/or special
A	

CONTENTS

	Page
PREFACE by P.Santini	iii
TECHNICAL EVALUATION REPORT by P.Santini	v
	Reference
 <u>SESSION I</u> 	
MATHEMATICAL FORMULATION OF DAMPING FOR STRUCTURAL RESPONSE ANALYSIS by H.H.Ottens	1
PREDICTION OF THE STRUCTURAL DAMPING OF A VIBRATING STIFFENED PLATE by D.J.Mead	2
NUMERICAL MODELLING OF STRUCTURES TO ACCOUNT FOR INTERNAL DAMPING by R.F.Baldacci, A.Corsanego and A.Del Grosso	3
 <u>SESSION II</u> 	
SOME RECENT MEASUREMENTS OF STRUCTURAL DYNAMIC DAMPING IN AIRCRAFT STRUCTURES by E.J.Phillips	4
EFFECT OF STRUCTURAL DAMPING ON THE DYNAMIC RESPONSE OF SPACECRAFT by M.Degener	5
SPACECRAFT DAMPING CONSIDERATIONS IN STRUCTURAL DESIGN by B.K.Wada and D.T.DesForges	6
VIBRATION DAMPING ON SAN MARCO SATELLITES -- RESULTS AND COMMENTS by C.Arduini and A.Agneni	7
DAMPING PROBLEMS IN ACOUSTIC FATIGUE by V.Giavotto, M.Borri and G.Cavallini	8
 <u>SESSION III</u> 	
DYNAMIC DAMPING INVESTIGATIONS ON COMPOSITES by H.Georgi	9
VISCOELASTIC DAMPING IN USAF APPLICATIONS by D.I.G.Jones, J.P.Henderson and L.C.Rogers	10
BILAN SUR LA MISE EN OEUVRE DE TECHNIQUES D'AMMORTISSEMENT POUR DES PROBLEMES LIES AUX VIBRATIONS ET AU BRUIT par B.Duperray and L.Gaudriot	11
DAMPING EFFECTS IN JOINTS AND EXPERIMENTAL TESTS ON RIVETED SPECIMENS by L.Balis Crema, A.Castellani and A.Nappi	12

TECHNICAL EVALUATION REPORT

by

Paolo Santini
Scuola di Ingegneria Aerospaziale
Rome University
Rome, Italy

I. INTRODUCTION

There are many aerospace problems of engineering interest where structural damping plays a basic role. Suffice here to list just some of them:

- (i) It is well known that, for an undamped structure, the response near resonance peaks increases without limits. If damping is present (e.g., of a viscous kind) a very elementary analysis shows that the response is roughly in inverse ratio to the damping coefficient. Therefore, if one has to evaluate design stresses, uncertainties in damping coefficient are exactly equal to uncertainties in such stresses.
- (ii) The aeroelastic behaviour of a panel in supersonic flow is such that a pre-critical phase is followed by the critical phase at a certain dynamic pressure - q_c ; the value of q_c is little influenced by damping, although in special cases a dangerous reduction may be observed. The postcritical phase (dyn. press. $q > q_c$) corresponds to the appearance of a "limit cycle", the amplitude of which is governed by the balance between energy input (from air) and energy dissipation (from structural damping). It is easily understood that, again, the dynamic damping coefficient is of paramount importance.
- (iii) A typical problem of large liquid fuel booster structures is the so-called "POGO" effect, i.e., a case of dynamic instability where structure, propulsion system, and fuel pipelines are involved. The overall loop is equivalent to a system with negative damping; so that structural damping is the only source from which stability can be obtained. This phenomenon is associated with a particularly dangerous and uncertain situation, since loss of stability inevitably leads to the loss of the rocket.

Several other examples might be given. From analysis of all of them, one can conclude that what is missing is the basic conception of damping, and the numerical values of the relevant coefficients, for which only empirical rules are available.

It seemed therefore quite important to have a Specialists' Meeting on the subject, so as to gather as much information as possible from scientists and technical personnel of NATO countries. Some of the results of the meeting are summarised here.

2. GENERAL ASPECT OF DAMPING IN AEROSPACE STRUCTURES

2.1 General Papers

Ottens¹ presented a survey of damping models, ranging from the very simple viscous model to the more sophisticated hysteretic damping concept, and to multiparameter approaches. Special attention is given to implementation of models in response calculations; although the mathematical formulation can be very simple, reliable numerical values are still missing for a complete structure. In other words, if the damping properties of each individual component are known, this by no means implies that, by finite element analysis, or any other similar technique, the complete damping matrix for the structure may be constructed. According to Ottens, this method does not seem feasible, and damping can be represented only by quantities dealing with the energy dissipation in the entire structure; so one is led to the concept of modal damping factor. For a particular structure, measured modal damping values are the most reliable, in spite of the fact that they are generally available at a late stage of design. A reasonable collection of data is also presented for European spacecraft: the values of damping ratio (actual damping coefficient/critical damping coefficient) are centered around 4×10^{-3} , with a rather large scatter.

Mead² presented a very interesting attempt at entering into the physics of the problem. Of all the sources of damping, for a vibrating stiffened plate, the most important seems to be the one associated with the riveted joints

Reference numbers refer to Paper numbers published in this Conference Proceedings (CP-277).

attaching the skin to the stringers. Each structural joint is characterized as a "semi-rigid dissipator", quantified by the "joint dissipation coefficient (JDC)"; i.e., the ratio of cyclic energy dissipation to the square of the force transmitted across the joint. The Author then shows, in a very ingenious way, how it is possible to obtain, from measured values of JDC, modal damping values in a structure whose vibration modes are known. However, comparison of calculated and measured values (for a given stiffened flat plate) shows that the latter are one third of the former. In the author's opinion, this result is "disappointing", in my opinion it is encouraging, if one considers that nothing is known on the prediction of damping of complex structures. It appears that the single joint, on which the dissipation coefficient measurement was made, did not adequately represent the actual joint in the reinforced plate. Mead also discussed the linear behaviour of the joint. According to his results, such linear behaviour holds reasonably well for joints loaded in tension or by moments, but, for joints loaded in shear, there is a sudden rise in the JDC above a given level.

Baldacci et al.³ discussed different techniques of analysis (from the point of view of the structural behaviour) when finite element models including damping effects are introduced. Also, the most popular de-coupling approaches are reviewed; such techniques are only approximate when the damping matrix pertinent to the structural model exhibits a non-proportional trend. The authors also presented various diagonalization schemes, and special emphasis is given to evaluation of errors arising in computations. Such errors can be identified on an "a posteriori" basis, through parametric numerical studies or, in many cases, an "a priori" evaluation is possible. Thus one is led to define a set of "admissibility" criteria.

2.2 Experimental Results

Phillips⁴ presented values of structural damping obtained from tests upon a complete aircraft and upon aircraft components. For the first case, the wing was excited by vertical impulses, reasonably careful elimination of aerodynamic damping being ensured. Damping of each mode of the structure (a typical integrally machined one) was determined from the logarithmic decrement of the signal. Examination of the results shows that damping was consistently higher in anti-symmetric modes than in symmetric modes the values of the former being centered around 3.5%, those of the latter around 2%. It would be of great interest to ascertain whether these results can be extended to many other kinds of similar wings.

The second typical structure tested by Phillips was an underwing mounted pod, (a component that recently became famous on account of a series of cracks). Here amplification factors, and not damping itself, were measured: however, comparison of the response amplitudes gave important information about the variation of damping vs vibration amplitude; clearly, a non linear effect.

One of the main results was that decrease or increase of damping is strongly related to the type of suspension. For excitation at pod nose and tail, damping was directly measured; a very useful set of data was presented, which seems to be rather low if compared to similar other results.

The third series of tests was concerned with a box-type structure, on the upper and lower surfaces of which various items of avionics equipment were mounted. The results are centered around a rather high value; (about 5-6%), and this is easily understood since the primary objective of the test program was to demonstrate that vibrations attenuation by the shelf and the anti-vibration mounts were satisfactory. In my opinion the results are far from general, but the technique reported in the paper could usefully be applied to space instrumentation supports, so as to help in avoiding undue acceleration peaks, which might jeopardize the integrity of electronic equipment. In any case, this seems to be a very important paper for design purposes.

Experimental data on composite materials (with reinforcement by boron-, carbon-, glass-, and synthetic-fibres), structural components (sandwich and I-beams); composite structures (wing box beam, rotor blades) were presented by Georgi⁵. The main goal of the tests was directed towards a collection and comparison of damping data of such different composite materials and structural components, and a discussion of a semiempirical approach to damping behaviour of composite beams in different configurational and operational conditions. Here too, while the prediction of structural damping of composite systems based on damping measurements of simpler, but similar configurations seems to be possible, prediction of structural damping of more complex structures (rotor blades) is not yet achieved. The author proposes a future damping program on composites that should be directed towards a systematic completion of experimental damping data and a study of damping behaviour under severe environmental conditions.

Further experimental results were presented by Balis Crema et al.¹². In this paper the importance of damping in riveted joints is considered in detail. The state of the art in the field of joint damping was illustrated and a general demand for development of experimental research was pointed out, since available theoretical approaches do not seem to be adequate to make satisfactory predictions on complex structures. Further, a series of tests on riveted specimens of different types is described and discussed. The purpose of the research was to evaluate the contribution of riveted joints to global damping properties and the analysis of the results obtained for elementary structural components shows that significant data concerning energy losses in riveted joints can be obtained by means of standard test facilities. Future programs should be directed towards evaluation of temperature and vacuum conditions.

2.3 Influence of Damping Upon Response

Degener's paper⁵ was chiefly concerned with one of the major items listed in the Introduction, i.e., the response of a structure to sinusoidal excitation at frequencies near resonance. Satellite structures were mainly investigated. Firstly, a general survey of mathematical manipulation for obtaining structural response is reported; it is shown that neglecting intermodal coupling would drastically reduce computing time. The question then arises, whether or not such coupling can actually be neglected. In order to give an answer to this question, two methods were used: firstly, a five-mass dynamic model, with realistic values for dampers was studied; secondly, experimental results of satellite ground vibration tests were employed for dynamic response analysis. In both cases, the Author finds just small differences between diagonal and nondiagonal damping matrix, "in spite of large [artificially introduced] off-diagonal elements in such generalised damping matrix". A very important result (that should however be taken with some caution) is therefore that influence of intermodal coupling is very small and may be neglected in response analysis; for the example reported by the Author, computing time was reduced by a factor of 4. Intermodal coupling could be very important in other problems, e.g., modal synthesis.

A survey of test results was then presented, with the following conclusions:

- In general, damping of spacecraft structures is an increasing function of input level.
- Damping properties are different for each normal mode.
- Typical damping values of reduced damping for spacecraft structures are between 0.5% and 5%.

The third important subject considered by Degener was dynamic response in the case of nonlinear damping, where reduced damping is linearly dependent on mode amplitude. A numerical iterative method is presented: results based on such method indicate that, in frequencies far from eigenfrequencies, the effect of damping is quite small, but, in their vicinity, dynamic amplification decreases rapidly with increasing input.

Giavotto et al.⁸ presented a paper on Damping Problems in Acoustic Fatigue. Firstly the Authors point out the importance of a more accurate knowledge of the damping values on prediction of durability and safety of structures operating in an acoustic fatigue environment. They then considered the different mechanisms developing some damping, such as material damping, joint damping and acoustic radiation damping. The wide gap existing between the needs for structural analysts and data collected by researchers was pointed out. In particular, the Authors remark that, all that is available now are experimental data on damping ratio plotted vs frequency, and such plots have the aspect of clouds of points; so it seems obvious that mode frequency alone is not enough to obtain a reasonable correlation of damping ratios. So the authors launch a program of tests, with the aim of clarifying damping phenomena in riveted joints and, possibly, of evaluating damping from acoustic sources.

2.4 Design Problems

Wada⁶ emphasized the circumstance that damping plays a significant role in the prediction of spacecraft structural response and loads, that in turn influence the structural design. The Author reviews some of the techniques adopted to incorporate such effects in the overall model, but, again, the main problem is that of defining clearly damping characteristics. A design rule is that of subdividing the spacecraft into subcomponents, estimating the kinetic contributions of each of them in the various modes, and performing a weighted sum of the component modal damping ratio, each weighted by its kinetic energy fraction. When a launcher is coupled to a payload, individual damping matrices are combined via the coupled modal matrix to obtain a nondiagonal modal damping matrix. In some other cases (Space Shuttle, HEAL) a constant damping ratio is assigned to payload modes (0.5 to 1.5%). The importance of such damping values on POGO qualities are illustrated. Model Test/Data Reduction can be performed in many ways; results obtained for the Voyager spacecraft indicate considerable variations between methods in many instances. Another factor is the test article, which is not always flight hardware, but engineering models, or dynamic simulators, so that wiring harness, electronic equipment and mounting hardware which do not add to the integrity of the structure may contribute to damping values. Also, response amplitude level should be considered. Air damping (influence of the air of the total damping in a vibrating structure) may be negligible in some cases and significant in other cases; general methods to account for such effects are still missing.

As a conclusion by the Author, for to-day's spacecraft current methods of predicting damping appear to be adequate; new methods do not seem to be forthcoming, although improvements in current methods are expected. Good engineering judgement and design practice are the best basis. More sophisticated analysis will surely be required for future larger spacecraft.

Jones, et al.¹⁰ discussed Viscoelastic Damping in USAF applications. Main application in the future may be damping technology for vibration control in large flexible space structures, e.g., extremely exacting requirements for positional stability requires passive damping to supplement active controls. Other areas are jet engines, printed circuit boards, aircraft avionics and equipment structures. Current technological problems involve: (i) damping materials data; (ii) techniques of treatment for protecting from severe environments; (iii) cost reduction; (iv) more advanced design techniques; (v) technology transfer to industry; (vi) damping at very high (200°-450°C) and very low (< -20°C) temperatures.

Once the above problems are solved, design of damping treatments on a rational basis will be possible. (Most of such treatments used at present time consist of one or more layers of viscoelastic material bonded between metallic or other stiff structural members.) As a matter of fact, equations providing multilayer beams or plate flexural rigidity can be used to derive elastic modulus and loss factor (the pair of parameters used commonly to describe viscoelastic materials) from observed resonant frequencies and modal damping. Applications are widely described; jet engines, inlets and components, avionics, as said above. From an aeronautical standpoint, however, the most important applications are constrained layers of elastomeric damping materials, either to increase service life or to reduce noise; so, fatigue cracks in secondary structures can frequently be prevented or minimized through the application of additive damping.

2.5 Special Problems

Arduini⁷ analyzed some anomalous behaviour observed in the San Marco satellite. The anomalies can be explained if one introduces damping into the equation of motion of the satellite. Detailed analysis (and suggestions for future work in this area) proves the importance of the subject, for which further data may be of significant value.

Gaudriot et al.¹¹ examined the effects of instrumentation to be applied to a structure when applied for damping purposes. Several examples of special techniques developed for general and for special purposes are given by the Authors. The results could be applied also to non-aerospace structures.

In my opinion, some of the ideas and concepts of this paper can be considered to be a real guide in mounting of anti-vibration and shock devices. The reader is referred to the written version of the paper for technical details.

3. RESULT OF THE MEETING

It is now possible to draw a general conclusion on the result of the Meeting. Was it successful? Was it useful?

It was certainly successful, also on account of the interesting discussions with which every session was concluded, and which cannot even be summarized here. However, such discussions proved the great interest of the subject of damping to the aerospace community.

As far as the usefulness of the Meeting is concerned we must define the different areas of the aerospace community to which it was directed:

- (i) Universities – In my opinion, the general papers (e.g., Ottens, Mead, Baldacci) are of prime interest from a didactical point of view. In courses of Applied Mechanics, Aerospace Structures, Aircraft Vibration, very little is said about the problem of incorporating damping into the frame of the general mechanical problem. Also, the complete Report can be considered as the first textbook on Damping in Aerospace Structures.

On the basis of a careful selection of the topics listed in all the papers, a basic implementation of such items is possible. Bibliographic references (some 239 altogether) are such that also preparation of a complete teaching course on the subject seems to be possible.

- (ii) Industry – Nearly all the papers presented at the Meeting are of interest for industrial applications. Designers may find useful data in the work done, e.g., by Georgi, Degener, Phillips, Jones and Wada. Procedures for experimental determination of coefficients, numerical values to be used, practical rules to account for damping effects, are basic information that can be found in such papers. The reader might sometimes be surprised or disappointed by the data scattering, it should be borne in mind, however, that this is a feature of the phenomenon itself, reflecting the state of the art of our present knowledge. It is also important to notice, however that scattering is greatly reduced if damping for wide classes of structures (e.g., "aircraft"; "spacecraft"; "rockets") is considered and a basic improvement may be reached only if such areas shall be considerably reduced (e.g., "wing"; "aileron"; "mounting pod", etc.).
- (iii) Research – Substantially similar considerations will hold also for research. Many papers, even those devoted to special problems, contain observations and description of phenomena which are really starting points for new research areas.

4. WHAT IS MISSING?

A deeper insight into the physical mechanism and the inherent reasons of damping is a goal that has not yet been achieved. This is a feature common to many other fields, such as stress, strain analysis, heat conduction, electricity, etc.; until the "core" of such phenomena is discovered and studied, there is little hope that significant advances in the prediction of them may really be obtained. Such goals may be achieved only from cooperation between engineers and physicists.

Also, another objective was missing (and this is my fault): the "design" of a material with specified damping properties (although a first example of this approach is provided by Jones' paper in this collection). Here again, however, a closer insight into the real understanding of the phenomenon will be necessary.

From a practical standpoint, the review and listing of experimental data is far from being complete. What is known to us to-day is that typical values may be given for special classes of structures: but, as said before, such classes are too broad to be of a real help to the designer. Factors of uncertainty of 10 are far from being uncommon, and the same factor is applicable to related design quantities. A more careful review of existing data and classification into narrower categories should be performed. This is a very big, time consuming, and expensive job, and doubts might be inferred whether this is within AGARD's scope. This is, however, in my opinion, the most ambitious medium term objective that the aerospace technical community can reasonably consider reaching in the future for so important a problem. Because this at least has been a great result of our meeting — damping is a real problem.

5. ACKNOWLEDGEMENT

I am indebted to all the colleagues of the SMP who cooperated in the Technical Sub Committee. A special thanks also to the Chairmen of the three sessions: Mr Coupry and Dr Rogers, who volunteered for chairing two sessions instead of one.

I also found a wonderful response from the Authors, most of them young scientists, who devoted much of their invaluable time to the success of the meeting.

Finally, I am happy to give my thanks to our friend John Willis, for the patience he demonstrated with respect to my delays, and for his help in carefully reviewing the English of the text.

SUMMARY

A survey is presented of damping models that are commonly used in the structural response analysis of aerospace structures. The various damping models are evaluated with respect to the required knowledge of structural damping, the mathematical complexity and the accuracy of the calculated response. The survey is limited to linear damping models and special attention has been given to models which represent lightly damped structures.

LIST OF SYMBOLS

a	= maximum amplitude of mass spring system
c	= viscous damping factor
c_{cr}	= critical viscous damping factor
C	= generalized viscous damping factor
D	= dissipated energy
F_D	= damping force
$f(t)$	= force
$F(t)$	= generalized force
h	= hysteric damping factor
H	= generalized hysteretic damping factor
i, j, n	= indices referring to vibration modes
k	= stiffness
m	= mass
M	= generalized mass
q	= generalized coordinate
V	= potential energy
x	= displacement
α	= proportionality factor
β	= viscous damping ratio (c/c_{cr})
β_{eq}	= equivalent viscous damping ratio
η	= loss factor ($D/2\pi V$)
$\phi(t)$	= memory function
ϕ	= mode shape function
ω	= frequency
$\{ \}$	= vector
$[]$	= matrix

1. INTRODUCTION

The effect of material damping on the vibrations of structures is easily observable. When the driving forces are removed, each vibration decays and comes to rest (leaving additional effects, e.g. due to rotation, out of consideration). This almost vulgar observation does not alter the fact that the physical understanding of the damping mechanism and the theoretical models to describe them are far from complete. But even with the knowledge of damping on microscale available it is hardly possible to predict overall damping of e.g. a complex built-up structure.

For structural response analyses mathematical models to describe the damping are necessary. One way may be to base these models on the mathematical formulation of the physical mechanism. They should at least involve the experimental evidence obtained in laboratory tests with suitable test specimens.

A different way is the phenomenological approach, where models are designed which are able to select observed damping characteristics of a wide range of structures. It is clear that the latter approach is commonly preferred in response analyses of complex structures.

In agreement with the prime interest of this symposium it is particularly the phenomenological approach that is considered. The commonly used damping models will be discussed and illustrated with a single degree of freedom system (chapter 2). Their application in the dynamic analysis of complex structures is discussed and evaluated.

2. MODELS OF THE DAMPING MECHANISM

In a vibrating structure an exchange takes place between kinetic and potential energy. During this interaction damping removes energy from the vibrating structure by radiation and dissipation. The radiated part is associated with acoustic or aerodynamic damping, the dissipated part with structural damping. This distinction, however, is rather formal as in many cases the two parts cannot be separated. Anyway, the damping models treated in this paper will be concentrated on structural damping.

With that, nothing has been said about the way in which the energy dissipates: by internal friction, friction of slipping surfaces or other sources. The effect of these damping mechanisms has to be incorporated in the specific damping models.

According to the phenomenological approach it is necessary to apply damping models in response analyses which are adequately manageable in calculations and which are able to stand the confrontation of analytical and experimental response results. The question remains unresolved as to which extend these models should be inherently consistent in their physical features. It may come out, therefore, that different linear damping models have to be used for low and for high amplitudes.

A damping measure which is commonly employed in setting up damping models is the quantity of the energy, D , that is dissipated during one cycle of a harmonic motion. This quantity is related to the maximum potential energy stored in the structure, V , by the introduction of a loss factor η

$$\eta = D/2\pi V$$

In general this loss factor is a function of frequency and amplitude. For aerospace structures the loss factor is usually small (10^{-5} to 0.2) although larger values may occur when special dampers are implemented in the structure.

In looking for an adequate mathematical formulation for the damping model an important point that has to be decided is whether the loss factor should depend on amplitude or not, in other words whether the model should be linear. In a vast majority of the publications linearity has been adopted, mainly because of two reasons (Ref.1):

- a the models are sufficiently accurate
- b they are computationally more economical

In engineering practice the idea is generally accepted that linearity is allowed in the case of low amplitudes levels. When the loss factor is expected to depend on the amplitude different loss factors are estimated for various amplitude levels.

In specific cases, however, it is admitted that linear damping models are not accurate enough. Studying e.g. phenomena where friction of joints plays an important role a nonlinear damping model, where the damping force depends on the sign of the relative velocity, should be adopted. Effects of nonlinearities for aircraft structures are discussed e.g. by Haidl (Ref.2) and Breithach (Ref.3).

In this paper a restriction will be made to linear damping models as they govern a major part of structural response problems. Various damping models have been proposed and used. Reviews of these models are given e.g. by Fraeyss de Veubeke (Ref.4), by Bert (Ref.1), by Crandall (Ref.5) or by Graham (Ref.6). The most usual models will be discussed here in some detail in application to a simple mass-spring system.

2.1 Viscous damping model

This model has a clear physical meaning. Energy is dissipated by fluid friction and a typical application is the dash pot. The damping force, F_D , is proportional to the velocity of the motion, \dot{x} :

$$F_D = -c\dot{x}$$

where c is the viscous damping factor. The dissipated energy during one cycle of a harmonic motion with frequency ω is

$$D = \pi c a^2 \omega$$

where a is the amplitude of the motion.

Commonly, the damping factor is given as a fraction of the critical damping which is the damping for which the motion is just not harmonic anymore. This critical value is

$$c_{cr} = 2m\omega_n$$

where m and ω_n are the mass and the natural frequency of the mass-spring system. The viscous damping ratio, δ , is

$$\delta = c/c_{cr}$$

The maximum stored potential energy is

$$V = \frac{1}{2} k a^2$$

where k is the spring stiffness. The relationship between δ and the loss factor η is

$$\eta = 2 \beta \omega / \omega_n$$

This shows that the loss factor is proportional with ω .

When the viscous damping model is applied to represent the structural damping its phenomenological value fades away as the frequency dependence of the loss factor is not observed generally. In reference 5 it is discussed that the role of damping is only important when the frequency of the driving force is near the resonance frequency of the structure. This is illustrated in figure 1, where differences in frequency response functions emerge only near the resonance frequency.

A constant equivalent viscous damping ratio, β_{eq} , may be established which matches the loss factor value for $\omega = \omega_n$, no matter how the factor depends on frequency:

$$\beta_{eq} = 2 \eta \omega = \omega_n$$

This is shown in figure 2. Although this equivalent damping value may be incorrect for all other frequencies except the resonance frequency the response results will still be sufficiently accurate.

A great advantage of the use of the viscous damping model is its applicability in both transient and steady state response analyses without being troubled by inherent inconsistency in the damping model.

2.2 Hysteretic damping model

For many structures it has been observed that the loss factor is independent of the frequency, at least in a certain frequency range. The hysteretic damping model has been designed to cover this observation. The damping force is proportional to the displacement of the motion, x , and 90° out of phase

$$F_D = -i h x$$

where h is the hysteretic damping factor. The dissipated energy per cycle of a harmonic motion is

$$D = \pi h a^2$$

where a is the amplitude of the motion.

The maximum stored potential energy is $V = \frac{1}{2} k a^2$ and the resulting loss factor is

$$\eta = \frac{h}{k}$$

which is indeed independent on frequency.

It should be noted that material hysteresis due to the plasticity is not included as this is nonlinear in nature.

A main disadvantage of using the hysteretic damping model is discussed by Fraeys de Veubeke, Crandall and others (Ref.4,5,7). It was shown that using a hysteretic damping model the response on a unit impulse is not causal that means the response depends not only on the previous history of the excitation but also on the future behaviour. It is therefore stated that the hysteretic damping model can only be used for steady state response analyses but not for transient analyses.

2.3 More advanced models

For the description of the damping characteristics the previously described models can be considered as first approximations. For the hysteretic damping model only the stiffness has to be known besides the damping factor, and for the equivalent viscous damping model also the resonance frequency. More advanced damping models have been designed by taking the freedom to choose one or more additional system parameters. This implies of course that more experimental data concerning material and structure should be available.

An extension of the simple viscous damping or Kelvin-Voigt model (shown in figure 3) is the so-called standard linear solid. This three parameter model is shown in figure 4. In this model not only the instantaneous applied force but also the previously applied loading is taken into account. Formally written the damping force is

$$F_D = \int_{-\infty}^t \phi(t, \tau) x(\tau) d\tau$$

where x is the displacement and ϕ is a memory function. Fraeys de Veubeke (Ref.4) has shown that this model can be interpreted as a viscous damping model with frequency dependent damping and stiffness parameter.

An evaluation of more parameter models is given by Milne (Ref.8). A wide class of frequency dependent damping behaviour can be constructed if only enough experimental data are available to establish all necessary parameters.

The application of these more complicated damping models for response calculations on aerospace structures is very limited. They are mainly useful for damping investigations on specific material rather than on complex structures.

3. IMPLEMENTATION OF DAMPING MODELS IN RESPONSE CALCULATIONS

Besides reflecting essential physical features, the damping mechanisms should allow proper implementation in response calculation formulations. These calculations can be as simple as modelling the structure into a single beam element but also as complicated as using a finite element representation. The refinement of the model depends of course on the available information and the desired accuracy of the results.

When the structure is built up from elements with known damping characteristics a proper damping matrix can be determined leading to the equations of motion, for viscous damping

$$[m] \{\ddot{x}\} + [c] \{\dot{x}\} + [k] \{x\} = \{f(t)\}$$

and for hysteretic damping

$$[m] \{\ddot{x}\} + ([k] + i [h]) \{x\} = \{f(t)\}$$

$\{x\}$ is a vector representing the displacements in a number of points of the structure. The elements of the damping matrix $[c]$ or $[h]$ may be derived from results of investigations in which the damping characteristics have been determined of more or less homogeneous test specimens. These characteristics have provided sometimes the basis to design the more advanced damping models pointed out before.

A large number of publications on damping deals with this kind of investigations. In particular damping of joints (e.g. Ref.9,10), of stiffened panels (e.g. Ref.11,12), of sandwich plates and beams (e.g. Ref.13,14) and of multilayered beams with visco-elastic layers (e.g. Ref.15) have been reported.

The results of these investigations are used in the design phase of a structure in order to pursue an optimal solution. For example, while designing an acoustically loaded stiffened panel the results of comparative studies of damping of various panel configurations may be very useful. An optimal panel can be designed and the danger of acoustic fatigue can be diminished. Another important application of the results of these specimen studies is the improvement of damping properties of existing structure e.g. by adding visco-elastic layers.

Theoretically it is possible using the damping data for each component to construct a damping matrix for a complex structure e.g. by applying a finite element method. In practice, however, the damping data of the individual components show a wide scatter. This is illustrated in figure 5 where damping data of stiffened panels are shown, as gathered by Hay (Ref.11). A complex aerospace structure consists of a large number of panels and joints each with its own uncertainties with respect to damping that an accurate determination of the damping in this way seems unfeasible.

For these structures damping can only be represented by quantities dealing with the energy dissipation of the total structure disregarding the damping in the individual components. In that case introduction of modal damping factors is appropriate. Because of the importance of this category a separate discussion is given in the next chapter.

4. MODAL METHODS FOR STRUCTURAL RESPONSE ANALYSIS

A very common way to analyse damped structures is to use a modal approach, which is permitted when only the response of the structure within a certain frequency range is of interest. Then the response can be expressed by means of a limited number of vibration modes. The reduction of the extent of the calculations is the advantage of this approach.

4.1 Methods using vibration modes of the undamped structure

For lightly damped structures the vibration modes of the undamped structure are taken in the modal representation. These modes follow from the equations of motion

$$[m] \{\ddot{x}\} + [k] \{x\} = \{0\}$$

Substitution of a harmonic solution $\{x\} = \{\phi\} e^{i\omega t}$ leads to an eigenvalue problem from which the natural frequencies ω_i and their corresponding mode shapes $\{\phi\}_i$ can be established. Introduction of the amplitudes of the modes q_i as generalized coordinates the following transformation

$$\{x\} = \sum_i \{\phi\}_i q_i$$

leads to the uncoupled, modal equations of motion

$$M_{ii} \ddot{q}_i + \omega_i^2 M_{ii} q_i = F_i(t)$$

where M_{ii} and $F_i(t)$ are the generalized masses and forcing functions defined by

$$M_{ii} = \{\phi\}_i^T [m] \{\phi\}_i$$

$$F_i(t) = \{\phi\}_i^T \{f(t)\}$$

Using the same transformation generalized damping matrices can be derived

$$C_{ij} = \{\phi\}_i^T [c] \{\phi\}_j$$

$$H_{ij} = \{\phi\}_i^T [h] \{\phi\}_j$$

In general the generalized damping matrices are nondiagonal so that the modal equations are coupled.

Hasselman (Ref.16) has shown that for viscous damping the influence of the coupling terms on the response can be neglected if

$$\sqrt{\frac{\beta_i}{\omega_j^2/\omega_i^2 - 1}} \left| \frac{C_{ij}}{C_{ii}} \right| \ll 1$$

where β_i is the viscous damping ratio of the i th mode. This inequality holds depending on three parameters:

- 1 magnitude of β_i
- 2 ratio of off-diagonal and diagonal terms (C_{ij}/C_{ii})
- 3 frequency separation ($\omega_j^2/\omega_i^2 - 1$)

Writing the derivation of the generalized damping matrix in this way is a bit formal as the proper determination of the matrices $[c]$ or $[h]$ is nearly impossible for a complex aerospace structure, as discussed in the previous chapter.

Sometimes the concept of the proportional damping matrix, introduced by Rayleigh, is used

$$[c] = \alpha_1 [m] + \alpha_2 [k]$$

or the extension given by Caughey (Ref.17)

$$c = [m] \sum_i \alpha_i ([m]^{-1} [k])^i$$

This damping matrix is introduced for mathematical convenience, as it does not couple the modal equations of motion. But as this matrix has no physical meaning proper determination of the proportionality factors is difficult. Usually these factors are related to the modal damping factors, but then the modal damping factors can better be used directly instead of firstly derive a proportional damping matrix which will be used in the modal equations.

Commonly damping is introduced on modal level. This means that each mode has its own viscous or hysteretic damping value. These modal damping values have to be estimated from previous experience on similar structures or can be measured afterwards by means of ground vibration tests.

An assessment of the modal damping values can be obtained using the method proposed by Biggs. The modal damping value is derived from the loss factor of the various used materials

$$\beta_i = \frac{\sum_j \eta_j / 2 \cdot v_j^{(i) \max}}{\sum_j v_j^{(i) \max}}$$

where η_j is the loss factor of element j and $v_j^{(i) \max}$ is the maximum potential energy of element j in the i th mode. This method is used to determine the damping values of structural components. Application to aerospace structures has not been reported and may be rather difficult also because Loup (Ref.19) has reported that for spacecraft structures up to 25 % of the damping results from non-load carrying parts such as cable booms and thermal blankets.

For a particular structure measured modal damping values are the most reliable but, as they can only be obtained from ground vibration tests, they are only available in a rather late stage of the design. This disadvantage can partly be overcome when vibration tests are performed on substructures. Kana et al (Ref.20) have proposed a method to derive modal damping data for the complete structure from measured modal damping values for the substructures. The method has been applied analyzing the Space Shuttle (Ref. 21).

4.2 Methods using vibration modes of the damped structure

When the modal equations are uncoupled the response is obtained by summation of the response of the individual modes. The modal response can be calculated by direct stepwise integration or using Duhamel integrals.

When the equations of motion are coupled a direct stepwise integration method can still be applied. For transient analyses this may be an appropriate method but for harmonic response analyses this method may be unwieldy as it takes some time before the steady state solution is obtained.

For harmonic loading and also for random loading decoupling of the equations by introducing damped vibration modes may be useful. For structures with viscous damping the derivation is given by Poes (Ref.24) and for structures with hysteretic damping by Mead (Ref.25). The amplitudes of the damped vibration modes are chosen as new generalized coordinates which now depend on the damping. Mead has applied this method in

analyzing sandwich beams and plates (Ref.13). Changes in the damping, however, alter the generalized coordinates which is unattractive as damping is a rather uncertain parameter. Further, the modal response analysis using damped vibration modes is slightly more complicated as all generalized quantities are complex.

Reviews of the features of various general purpose computer programmes for vibration analyses are given by Nelson (Ref.26) and by Imbert (Ref.27). In table 1 a list is presented taken from reference 27 showing the modelling features available in the various programmes.

5. RESPONSE CALCULATIONS

When response calculations are made damping values have to be quantified. Even for a simple damping representation using modal damping values it is difficult to obtain proper damping values already in the design phase. As the role of damping on the response is important the question arises whether incorrect damping values lead to an improper basic design of the structure. This is true for spacecraft structures but hardly true for aircraft structures.

Consider for example the response of an aircraft on a landing impact or store separation. For these calculations the structural damping is only a small part of the total damping as the aerodynamic loading provides the major contribution. For the design of specific parts, such as panels which are acoustically loaded, the structural damping is an important parameter. If no proper damping information is available low values are taken as a conservative measure. Such a proceeding does hardly not affect the basic design of the structure.

An important design criterium for a spacecraft, on the other hand, is that the spacecraft structure must withstand severe dynamic tests. Having calculated the transient response of a spacecraft-launcher combination on ignition of one of the various stages the maximum loading is used in the dynamic tests as an upper limit. An example of these calculations is given in figure 7. The response is calculated of the AHS satellite and SCOUT launcher on the ignition of the third stage. (Ref.22,23)

If during the tests these limit load levels are still exceeded the input test levels may be notched. As these load levels are derived from response calculations the role of damping is obvious: the limit load levels in the spacecraft structure are more or less dictated by the used damping values.

A review of all available damping data for spacecraft structures will be very helpful. For European spacecraft such a review has been given in figure 7 (Ref.18).

6. EXPERIMENTAL VERIFICATION

The choice of the method to calculate the response is also influenced by the possibility to adjust the damping factor afterwards so as to agree with measured results. When the modal approach using undamped vibration modes is applied not only the final response but also intermediate results can be checked. By performing a ground vibration test, modal quantities (natural frequencies, mode shapes, generalized masses and modal damping factors) can be measured. These quantities can be used to improve the analytical model. As already discussed in chapter 4 this vibration test may be the first opportunity to obtain proper damping data for this particular structure.

Also basic assumptions, such as whether the intermodal coupling can be neglected or not, can be experimentally verified. The difficulties and possibilities of measuring modal coupling terms are discussed by Coupry (Ref.28).

When damped vibration modes are used in the modal representation experimental verification of the modal results is very difficult as measuring damped vibration modes is nearly impossible. Then, and also when the original set of equations of motion is directly integrated, only the final response can be verified. If the agreement between calculated and measured results is poor little is known about the defects in the analytical model.

7. CONCLUSIONS

At this moment various damping models are available to describe structural damping mechanisms. Success in applying them depends on the fortunate choice of the various parameters which, however, is not guaranteed by current experience.

For response analyses of complex aerospace structures a modal approach and the consequent use of modal damping values is appropriate. The modal damping can be considered either viscous or hysteretic.

In the design phase the damping values that have to be chosen are often only conjectured. For aircraft structures this does not lead to uncertainty in the basic design but for spacecraft structures the limit load levels are dependent on the applied damping values. Incorrect damping values may lead to an improper design.

Collection and evaluation of available measured damping data of satellite structures seem a rational first step to clear up the design uncertainties.

8. REFERENCES

1. Bert, C.W., "Material damping: An introductory review of mathematical models, measures and experimental techniques", Journ. of Sound and Vibration (1973) 29(2) pp 129-153.

2. Haidl, G., "Non-linear effects in aircraft ground and flight vibration tests". Agard report no. 652, 1976.
3. Breithbach, E., "Effects on structural non-linearities on aircraft vibration and flutter", Agard report no. 665, 1977.
4. Fraeys de Veubeke, B.M., "Influence of internal damping on aircraft resonance", Agard manual on aeroelasticity, Vol.1, Chapt.3, 1960.
5. Crandall, S.H., "The role of damping in vibration theory". Journ. of Sound and Vibr. (1970) 11(1), pp 3-18.
6. Graham, W.B., "Material damping and its role in linear dynamic equations", Univ. of Toronto, Institute for Aerospace Studies UTIAS review no.36, 1973.
7. Caughey, T.K., "Vibration of dynamic systems with linear hysteretic damping", Proc. Fourth US Nat. Congress Applied Mech. 87, New York, 1962.
8. Milne, R.D., "A constructive theory of linear damping", Proc. Symp. on structural dynamics, Loughborough, 1970.
9. Ungar, E.E., "Energy dissipation at structural joints; mechanism and magnitudes", FDL-TDR 64-98 US Air Force, Aug. 1964.
10. Pian, T.H.H., "Structural damping of simple built-up beam with riveted joints in bending", J. Applied Mech., Vol.24, No.1, 1957, pp 35-38.
11. Hay, J.A., "Experimentally determined damping factors", Agard CP 113 Symposium on Acoustic Fatigue, May 1973.
12. Ungar, E.E., "Damping of vibrating panels and panel systems", Proc. Seminar on vibr. of damped structures", Pennsylvania Univ., 1975.
13. Mead, D.J., "The damping properties of elastically supported sandwich plates", J. Sound Vibr. 24(3) pp 275-295, 1972.
14. Mead, D.J., "Vibration of sandwich beams and plates", Proc. Seminar on vibr. of damped structures, Pennsylvania Univ., 1975.
15. Jones, D.I.G., "Damping of stiffened plates by multiple layer treatment", J. Sound and Vibr. 35(3), pp 417-427, 1974.
16. Hasselman, T.K., "Modal coupling in lightly damped structures", AIAA Journal, Vol.14 No.11, pp 1627-1628, Nov. 1976.
17. Caughey, T.K., "Classical normal modes in damped linear dynamic systems", J. Applied Mech., Vol.27, pp 269-271, June 1960.
18. Carrington, H.G. and Ottens, H.H., "A survey of data on damping in spacecraft structures", ESRO CR - 539.
19. Loup, J., "Recherche sur l'amortissement en vibration des structures de satellites", ESRO CR - 633, Mai 1975.
20. Kana, D.D. and Huzar, S., "Synthesis of shuttle vehicle damping using substructure test results", J. Spacecraft, Vol.10, No.12, pp 790-797, Dec. 1973.
21. Kana, D.D. and Unruh, F.J., "Substructure energy method for prediction of space shuttle modal damping", J. Spacecraft, Vol.12, No.5, pp 294-301, May 1975.
22. Case, W.R., "ANS structural analyses", Goddard Space Flight Center, rep. 721-4, Febr. 1972.
23. Ottens, H.H., "Some investigations on the notching procedure used in shaker tests on satellites", NLR TR 76134 C, 1976.
24. Foss, K.A., "Coordinates which uncouple the equations of motion of damped linear dynamic systems", J. Applied Mech., Vol.25, pp 361-364, Sept. 1958.
25. Mead, D.J., "Existence of normal modes of linear systems with arbitrary damping", Proc. Symp. on struct. dyn., Loughborough Paper C5, 1970.
26. Nelson, F.C. and Creif, R., "Damping", Shock and Vibr. Information Center, Shock and Vibr. Computer Programs, Tufts Univ. Medford, Mass., pp 603-623.
27. Inbert, J.F., "A survey of current capability for dynamic analysis of complex structures", Proc. Conf. Finite Element Methods in the Commercial Environment, Bournemouth, U.K. 1978.
28. Coupry, G., "Mesure des amortissements généralisés non diagonaux d'une structure lors d'un essai au sol de vibration", La recherche aérospatiale no.4, pp 239-244, 1977.

9. ACKNOWLEDGEMENT

This paper has been partly prepared under contract for the Scientific Research Branch, Air Material Directorate, Royal Netherlands Air Force (RNLAF).

TABLE 1 Linear dynamic modelling features in general purpose computer programmes (Ref.27)

CODES	masses		rigid element	linear constraint	matrix input	damping						modal composite damping	freq. dependent	fluid-structure interaction	loading					
	lumped	consistent				viscous				hyst.					surface	inertia	base excit.	initial stress	centrifugal	others
						proportional	diag. modal	general from element damp.	discrete dampers	uniform	general from element damp.									
ADINA	x	x	x	x	x				x					x	x	x	x			
ANSYS	x	x	x	x	x	x		x	x	x	x			x	x	x	x	x		
ASAS	x	x		x			x						x		x		x			
ASKA	x	x		x	x	x	x		x						x	x	x			
BERDYNE		x	x	x	x	x	x			x					x	x	x		x	x
MARC	x	x				x	x							x	x	x	x		x	
NASTRAN	x	x	x	x	x		x	x	x	x	x	x	x	x	x	x	x	x	x	
PAFEC		x				x	x			x					x	x				
PAM	x	x		x		x	x							x	x	x	x	x	x	
SAMCEF	x	x		x	x	x	x	x		x				x	x	x	x	x	x	x
SAP	x			x		x														
SESAM	x	x	x	x	x	x	x							x						
STARDYNE	x	x	x	x	x		x			x		x	x			x	x			
STRUDEL-DYNAL	x				x		x					x					x			
TITUS	x	x			x	x	x								x	x		x	x	x

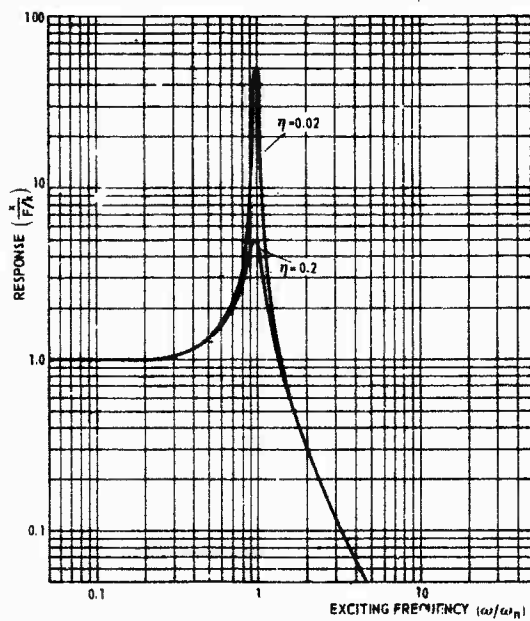


Fig. 1 Frequency response function of a single degree of freedom oscillator with a viscous damper (Ref.5)

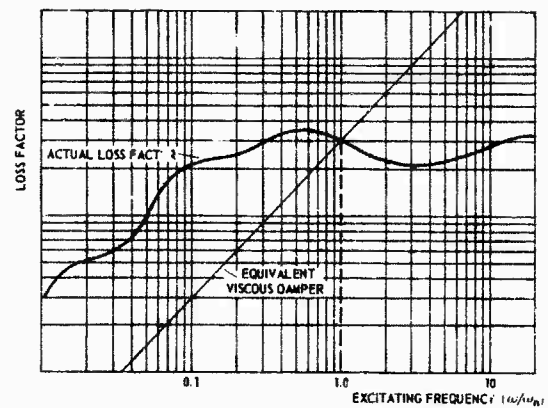


Fig. 2 Frequency dependence of an actual loss factor and the loss factor of an equivalent viscous damper (Ref.5)

KELVIN-VOIGT MODEL

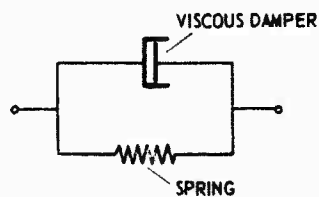


Fig. 3 Viscous damping model

STANDARD LINEAR SOLID MODEL

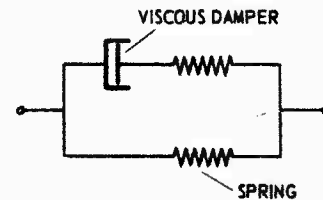
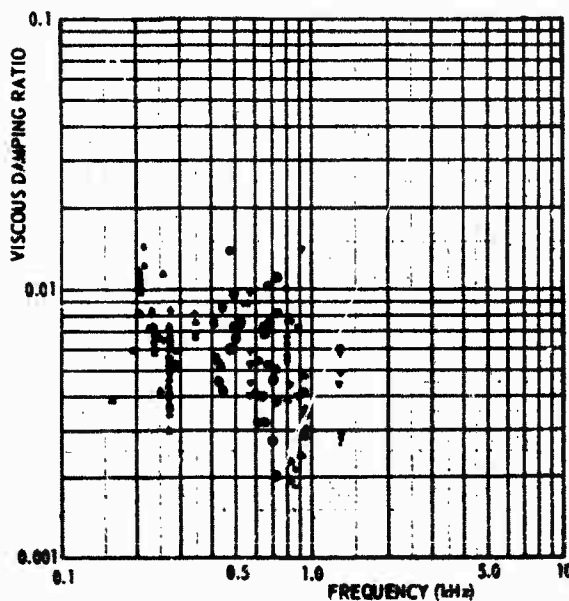
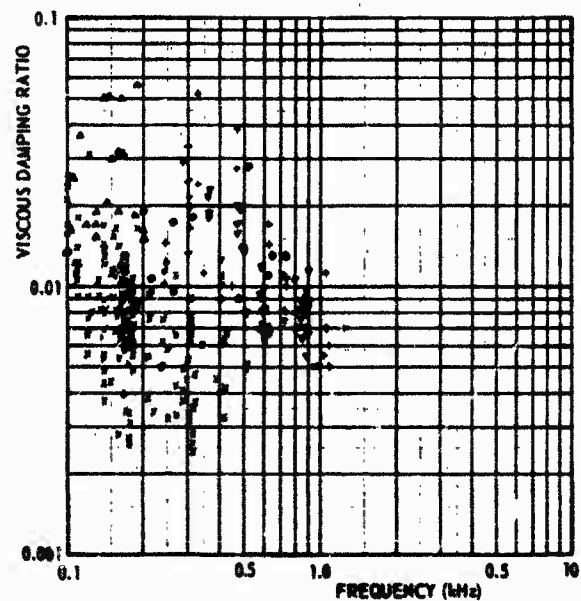


Fig. 4 Three parameter damping model

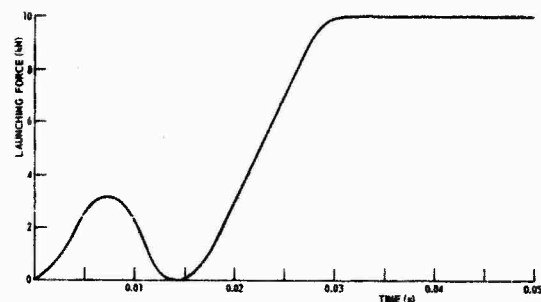


RIVETED STRUCTURES WITH VISCO-ELASTIC SEALANT
(MACHINED SKINS)

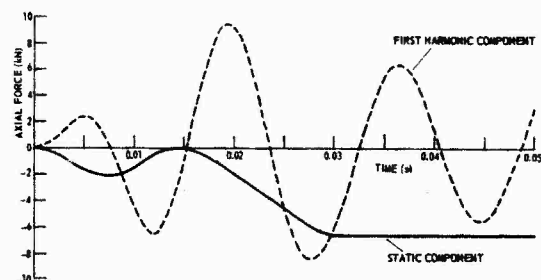


RIVETED STRUCTURES WITH VISCO-ELASTIC SEALANT
(PLAIN SKINS)

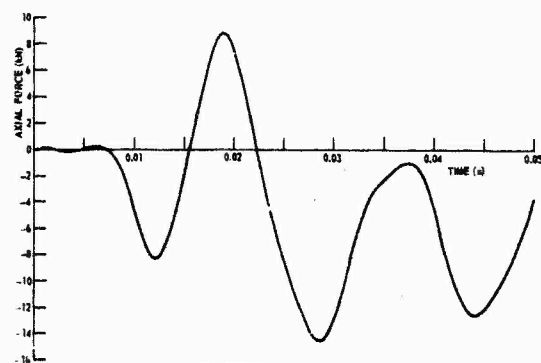
Fig. 5 Measured damping values of stiffened panels (Ref.11)



LAUNCHING HISTORY AT IGNITION OF THIRD STAGE OF THE SCOUT LAUNCHER



MODAL RESPONSES: AXIAL FORCES IN THE ANS-SATELLITE



TOTAL RESPONSE: AXIAL FORCE IN THE ANS-SATELLITE

Fig. 6 Transient response of the SCOUT-ANS at the third stage ignition (Ref. 22, 23)

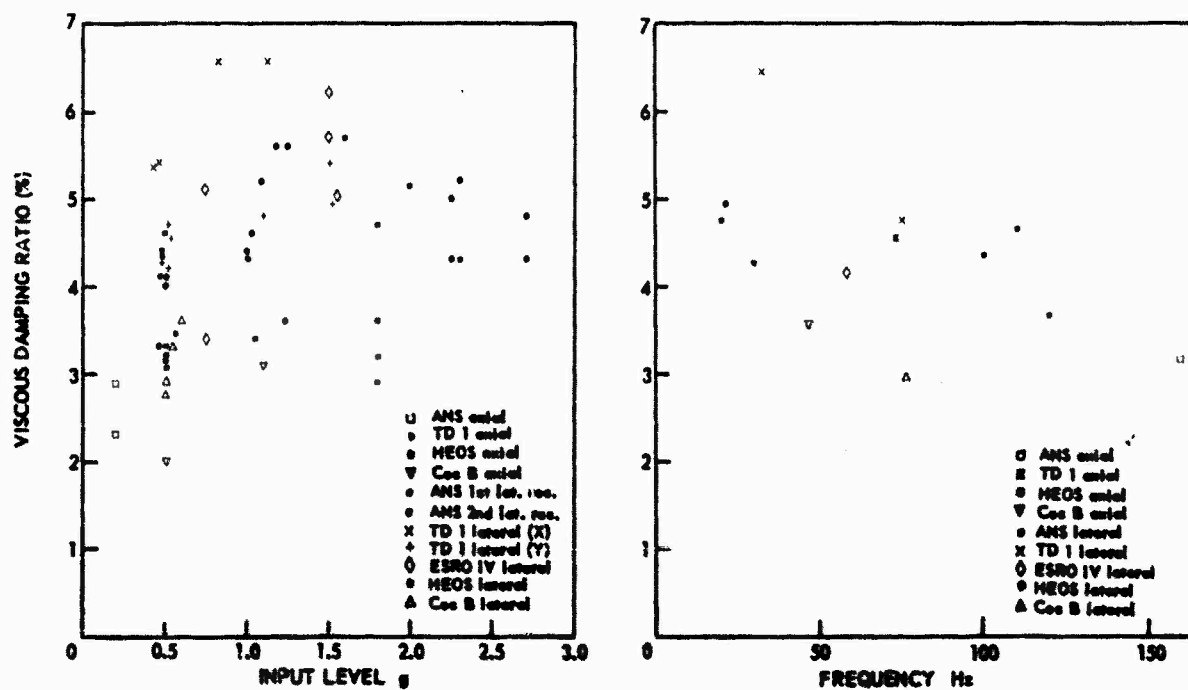


Fig. 7 Modal viscous damping ratios of European spacecraft (Ref.18)

PREDICTION OF THE STRUCTURAL DAMPING OF A VIBRATING STIFFENED PLATE

by

Denys J. Mead

Department of Aeronautics & Astronautics
University of Southampton
Southampton, SO9 5NH, England

SUMMARY

This paper outlines the sources of energy dissipation in a vibrating stiffened plate, typical of a fuselage stringer-skin structure. For a particular specimen, the principal source was identified as the riveted joints attaching the skin to the stringer. These undergo oscillating tension / compression loads (in the direction of the rivet axis) when the plate vibrates.

An experiment is described which attempted to measure the basic damping characteristic of a single riveted joint loaded harmonically in this way. The non-linearity of the damping was clearly demonstrated, as was the effect of an air-pumping mechanism in the joint. The results of the experiment were used to predict the damping of a riveted stringer-skin structure containing many such joints. The predicted damping is compared with the value actually measured. The results are of the same order of magnitude, but the numerical difference highlights the difficulties involved in undertaking such damping studies.

1. INTRODUCTION

Several different energy sinks contribute to the damping of the high frequency vibrations of stiffened plate structures. The material of the structure is never perfectly elastic, and dissipates energy as it undergoes stress cycles. As the surface of the structure vibrates in its plate flexural modes, the surrounding medium (air) is made to vibrate and acoustic energy is radiated away from the surface. If there is an aerodynamic flow over the surface, further vibrational energy can be lost to the air by a different mechanism.

It is well-known that a jointed structure is more highly damped than one which is continuous and machined out of a solid block. As the riveted or bolted joints are subjected to oscillating loads due to the vibration, the inherent flexibility of the joint permits some degree of relative motion between the joint interfaces. This may only be due to high shear strains in the surface layers, but on account of the high strain more energy is dissipated in the layers than would be dissipated if the structure were continuous. The local discontinuities and stress concentrations due to joints therefore cause extra energy to be dissipated. If the relative motion involves actual slipping and dynamic friction, much more energy will be lost at the interface.

Further structural damping can derive from non-structural items attached to the structure, e.g. pipes and cables, passenger chairs and luggage pallets. The attachments of these components will not be perfectly rigid, will allow some relative movements and so will allow energy to be dissipated. However, it is in those regions of the aerospace vehicle which do not have such attached items that the damping is lowest, and of greatest importance. In those regions, the resonant vibration responses are likely to be highest. It is of value, therefore, to study the sources and mechanisms of damping in lightly-damped built-up structures.

The material damping of aluminium alloy structures is known to contribute only a tiny proportion to the total damping (1). Acoustic damping (2) can sometimes be the major damping sink, but this has a frequency-dependent damping mechanism which is amenable to analytical study and is now well-understood. Some modes of vibration of stiffened plates have very low acoustic damping. Aerodynamic damping depends on the speed of the flow over the structure and vanishes at zero flow speed. For some structural modes and under some operating conditions, the structural damping from the joints is the largest contributor to the total damping and for this reason this present work was undertaken.

When a stiffened plate vibrates, the mode of flexural plate vibration along a line across the stiffeners (stringers) may be of the form indicated in Figure 1. In some modes (e.g. 1c) the plate inertia forces tend to pull the plate away from the stiffeners, and put the attachment rivets in a state of fluctuating 'normal tension'. In other modes (e.g. 1a) the plate is tending to twist the stiffener, and is subjecting the attachment rivet and joint to a moment which is transferred into the stiffener. The joint then has a 'moment' loading. When the stiffener itself bends, the same joints are subjected to shear forces which lead to the rate of change of bending loads in the stiffener-beam components. The joint then has a 'shear loading'.

These three types of loading, to be known as Mode A, Mode B and Mode C, are illustrated in further detail in Figure 2. Notice that in both Modes A and B, the oscillating curvature in the plate must cause a periodic opening and closing of a gap between the plate and the stiffener flange, provided there is no jointing compound between the interfaces. This may cause an actual periodic impact of the plate and flange surfaces which may cause energy to be dissipated through macroscopic local plastic deformation.

It will certainly cause air to be pumped in and out of the fluctuating gap and this results in a powerful air-pumping damping mechanism (3). This is partially due to viscous aerodynamic losses in the small gap but also to acoustic energy losses as the air gap acts as an acoustic line source.

The rivet in Mode A is subjected to oscillating normal tension and it is conceivable that high shear strains (and relative slipping?) can occur between the rivet sides and the internal surface of the rivet hole. Oscillating compression stresses will exist between the rivet head and the plate surface, and at all such points of stress concentration, energy will be dissipated. It will be assumed that the amount of energy dissipated per cycle in this mode depends on the amplitude of the normal tension force acting on the rivet.

In Mode B, the whole joint is subjected to an oscillating moment. If the joint interfaces are initially in good contact, this moment will cause oscillating tension/compression forces on the rivet, with associated oscillating compression forces on the adjacent interface surfaces. Some of the moment may also be transmitted along the rivet in a rivet bending mode. Each of these fluctuating forces can cause energy to be dissipated as described for Mode A. The energy dissipated per cycle depends on the amplitude of the moment transmitted from plate to stiffener.

In Mode C, the joint is subjected to simple shear in the mode for which a rivet is designed. The mechanism of the interface damping has been described previously (4) and is clearly associated with shear deformation and ultimately with relative slipping of the interfaces. The energy dissipated per cycle depends on the amplitude of the shear force transmitted across the joint.

Attempts have been made to analyse the energy dissipation of very ideal joints under Mode C loading (5). The frictional shear stresses and degree of slipping all depend upon the normal pressure between the plates, and in a riveted joint this depends upon the technique of forming the rivet. For the average riveted joint the normal pressure is unknown and almost uncontrollable. There seems to be little hope of a mathematical analysis of the damping of such a riveted joint. Analysis of the damping of the joints under the Mode A and B types of loading is even more intractable, and its magnitude is even more sensitive (it would seem) to manufacturing inconsistencies from one joint to another. A series of experiments has therefore been conducted to measure the energy dissipation in specially prepared single-joint specimens, designed to subject the joints to either Mode A, B or C type loading. Several joints of each type were made in order to investigate consistency of damping (or otherwise) between different specimens. Each specimen consisted basically of two Alclad strips 25 mm wide, 1.2 mm thick, joined with a single mushroom-head rivet (Dural) of 3 mm diameter.

When the energy dissipation characteristics of a joint are known, it is possible to estimate the contribution of that joint to the total damping of a structure in which the joint is incorporated. The mode of vibration of the structure must, of course, be known. This paper presents a simple theory for predicting the total damping of a multi-jointed structure, vibrating in a known mode. Also derived is the cross-damping coefficient deriving from the joint dissipation which couples a pair of the otherwise normal modes of vibration of the structure.

This theory, and the measured values of the joint energy dissipation rate, are then used to predict the damping of a plate with multiple stiffening, all of which is attached to the plate by rivets of the same type as used in the single-joint tests. Only one mode of vibration has been considered, in which the riveted joints between plate and stiffening were subjected to Mode A loads. This mode of vibration was chosen as it was relatively simple to calculate the joint loads. In the other modes, the joint loads could only be found approximately and with great difficulty.

The work described in this paper is associated only with steady-state harmonic (or near-harmonic) vibration. Further work is required to investigate its relevance to transient or random vibration.

2. THE CHARACTERIZATION OF STRUCTURAL JOINTS

A joint possesses both flexibility and damping capacity. To incorporate its effect in a vibration analysis one requires a model of its stiffness and damping mechanisms. The stiffness must take account of the loss of stiffness in the adjacent structure due to the stress re-distributions close to the joint, as well as of the stiffness of the joining element itself. The damping must take account of any slipping and Coulomb friction occurring within the joint, as well as the effects of macroscopic plastic deformations at the joint stress concentrations.

To obtain a detailed model of spring-damper-friction elements for only one particular joint would involve a formidable analysis. It would be unthinkable to examine all the different joints in a typical aero-space vehicle. However, it will be argued that a detailed model of the joint is not required. It is only necessary to know the amount of energy dissipated in one cycle of given load on the joint, rather than a detailed load-deflection relationship for the joint. The former is easy to determine experimentally. The latter is not. It is also desirable (but not always necessary) to know the overall stiffness of the joint, and this can sometimes be measured, though with difficulty. These two quantities can be associated with just two series elements in a model of the joint. The dissipation will be associated with a 'SEMI-RIGID DISSIPATOR' represented by D on Figure 3a, and the stiffness by the spring k_j on Figure 3a.

A 'Semi-Rigid Dissipator' is a hypothetical element which dissipates energy at a cyclic rate which is dependent on the amplitude of the force acting on it. It is called 'semi-rigid' because the relative displacement across its extremities A and B is negligibly small. If it were actually zero, of course, no energy could be dissipated in a real element of this type, but in a real joint the actual displacement across the elements which do the dissipating is certainly much less than the displacement across the spring k_j which represents the stiffness (and flexibility) of the surrounding part of the joint. Furthermore, the potential energy associated with displacements within the dissipating part of the joint is likely to be much less than the potential energy associated with displacements of the surrounding parts. Altogether, then, it is justifiable to separate the joint into the two components - one which deflects

and stores energy, and the other which does not deflect but dissipates energy.

The semi-rigid dissipator will be quantified by the 'Joint Dissipation Coefficient', J . If the joint (and the element) is subjected to a cyclic load of amplitude P , then the cyclic energy dissipation D is given by

$$D = J \cdot P^2. \quad (1)$$

If the dissipator is linear, J is constant and then represents the cyclic dissipation at unit load amplitude. When dissipation stems from non-linear mechanisms, such as Coulomb friction or plastic deformation, J depends on the magnitude of P . Experimental evidence (as will be seen later) suggests that J is constant at low load levels but increases at higher load levels.

For further justification of the semi-rigid dissipator hypothesis, consider Figure 3b which represents the joint by three simple (and conventional) elements - two springs and a linear hysteretic damper. This is the next-to-simplest model of a real joint. Separate values cannot reliably be assigned to the three elements. Experiments can determine the overall stiffness and the overall cyclic dissipation, but a third quantity must be measured if the three element values are to be determined. The quantity required is the ratio of relative displacements A to C and A to B . The relative displacement A to C clearly cannot be measured as point C is inaccessible inside the real joint. The two-element model of Figure 3a can just as adequately represent the joint, at least for harmonic vibration conditions.

3. THE DAMPING OF STRUCTURES DUE TO DISSIPATION AT JOINTS

Suppose the r th joint in a structure is characterized by J_r and k_r , and is used to connect two flexible linear elements characterized by K_A and K_B (see Figure 3c). The displacements at A and D are X_1 and X_2 . Elements k_r and K_B can be combined into the simple linear stiffness $(1/k_r + 1/K_B)^{-1} = K_{CD}$. If the stiffness of the joint, k_r , is much greater than that of the element K_B , then $K_{CD} \approx K_B$, and the joint can be regarded as being effectively rigid. The relative displacement across CD is, by the hypothesis regarding the dissipator, the same as that across AD . The force in the combined spring K_{CD} is then $K_{CD}(X_2 - X_1)$. If X_1 and X_2 are varying harmonically, the amplitude of the force in the spring is $K_{CD}(X_2 - X_1)$, and this is also the amplitude of the force on the dissipator. The energy dissipated per cycle by this joint is then

$$D_r = J_r K_{CD}^2 (\overline{X_2 - X_1})^2. \quad (2)$$

Now suppose the whole system of all such elements together with the system masses is forced to vibrate harmonically at frequency ω in two principal modes whose principal co-ordinates are $q_m \cos \omega t$ and $q_n \cos (\omega t + \epsilon)$. The displacements X_1 and X_2 are now given by

$$X_1 = \alpha_{1m} q_m \cos \omega t + \alpha_{1n} q_n \cos (\omega t + \epsilon)$$

$$\text{and } X_2 = \alpha_{2m} q_m \cos \omega t + \alpha_{2n} q_n \cos (\omega t + \epsilon).$$

α_{1m} , α_{2m} , etc., clearly define the mode of vibration. The amplitude of the relative motion, $\overline{X_1 - X_2}$ can now be evaluated, from which one finds the following expression for the cyclic dissipation at the joint:

$$D_r = J_r \left\{ K_{CD}^2 (\alpha_{2m} - \alpha_{1m})^2 q_m^2 + K_{CD}^2 (\alpha_{2n} - \alpha_{1n})^2 q_n^2 + 2 K_{CD}^2 (\alpha_{2m} - \alpha_{1m})(\alpha_{2n} - \alpha_{1n}) q_m q_n \cos \epsilon \right\}. \quad (3)$$

Let the generalized direct hysteretic damping coefficients for the two modes be H_{mm} and H_{nn} , and the cross-damping coefficient be H_{mn} . In terms of these coefficients, the energy dissipated per cycle when the two modes co-exist is given by

$$\pi \left\{ H_{mm} q_m^2 + H_{nn} q_n^2 + 2 H_{mn} q_m q_n \cos \epsilon \right\}. \quad (4)$$

Comparing the above two expressions, it is evident that the contributions from the joint dissipation to the generalized damping coefficients are

$$\Delta H_{mm} = \frac{J_r}{\pi} K_{CD}^2 (\alpha_{2m} - \alpha_{1m})^2 \quad (5a)$$

$$\Delta H_{nn} = \frac{J_r}{\pi} K_{CD}^2 (\alpha_{2n} - \alpha_{1n})^2 \quad (5b)$$

$$\Delta H_{mn} = \frac{J_r}{\pi} K_{CD}^2 (\alpha_{2m} - \alpha_{1m})(\alpha_{2n} - \alpha_{1n}). \quad (5c)$$

Now the term $K_{CD}(\alpha_{2m} - \alpha_{1m})$ is the amplitude of the force in the spring K_{CD} (= the force on the r th joint) when the system vibrates with unit q_m in the mode m . Likewise, $K_{CD}(\alpha_{2n} - \alpha_{1n})$ is the amplitude of the force on the r th joint when the system vibrates with unit q_n in mode n . Denote these force amplitudes by P_{rm} and P_{rn} , so that $\Delta H_{mm} = J_r P_{rm}^2 / \pi$ etc. If there are R such joints in the whole system, the general form for the total hysteretic damping coefficient from all the joints will be given by

$$H_{mm} = \sum_{r=1}^R J_r P_{rm}^2 / \pi. \quad (6)$$

This is true for $m = n$ and $m \neq n$.

The generalized hysteretic damping coefficient is therefore related very simply to the energy dissipation coefficients and to the modal forces acting on the joints.

The LOSS FACTOR of a mode of vibration of the whole system can be defined by the dimensionless quantity

$$\eta_m = \frac{1}{2\pi} \frac{\text{Energy dissipated per cycle of displacement in mode } m}{\text{Maximum energy stored during the cycle}} \quad (7)$$

When the system vibrates harmonically at its natural frequency, ω_m , the maximum potential and kinetic energies are equal, so that

$$V_{\max} = T_{\max} = |q_m|^2 \omega_m^2 M_m / 2 \quad (8)$$

where M_m is the generalized mass of the mode and is given by

$$M_m = \int_V \rho \phi_m^2(x_1, y_1, z) dV \quad (9)$$

ρ is the material density, ϕ_m is the modal displacement function from which α_{1m} , α_{2m} etc. are derived, and the integration extends throughout the volume of the vibrating system.

The energy dissipated by all the joints in the system in the course of one cycle of mode m is

$$\sum_{r=1}^R J_r P_{rm} |q_m|^2$$

The loss factor of the m^{th} mode is then

$$\eta_m = \frac{\sum_{r=1}^R J_r P_{rm}^2 / \omega_m^2 M_m}{2} \quad (10)$$

Now the generalized stiffness of this mode, K_m , is equal to $\omega_m^2 M_m$. Using this in equation (10), together with the expression for H_{mm} from equation (6), one finds

$$\eta_m = H_{mm} / K_m \quad (11)$$

This is the alternative, frequently-quoted form for the loss factor of a hysteretically damped system.

4. THE MEASUREMENT OF JOINT DISSIPATION COEFFICIENTS

4.1 The general method

Joint dissipation coefficients may be measured by incorporating a single joint in a simple vibrating system. Ideally, that system should have no other significant damping sinks. From measurements of the system loss factor, natural frequency and mode ϕ_m , J_r can be found from the re-arranged form of equation (10) with $R = 1$:

$$J_r = \frac{\eta_m \omega_m^2 M_m}{P_{rm}^2} \quad (12)$$

The joint load per unit generalised displacement, P_{rm} can be calculated when ϕ_m , ω_m and the system mass distribution are known.

If the joint has non-linear damping characteristics, η_m will vary with amplitude and may be difficult to measure reliably. In that case, the actual power input required to maintain vibration at different levels should be measured. Denote this by W . If the joint is the only damping sink, then $W = D_r = J_r |q_m|^2 P_{rm}^2$. Hence $J_r = W / |q_m|^2 P_{rm}^2$. (13)

Some joints are subjected to moments (bending or twisting) rather than forces. In that case, P_{rm} must be the moment acting on the joint per unit q_m and J_r has the units of work ÷ moment². Otherwise its units are those of work ÷ force².

The joints to be considered in Section 5 are subjected to three principal types of load. These are

- (a) An oscillating tension-compression load along the rivet axis,
- (b) An oscillating bending moment transmitted through the rivet,
- (c) An oscillating shear load perpendicular to the rivet axis.

To measure the joint dissipation for these different loading actions, three different types of test specimen were required, each with a single joint. When each specimen vibrated in its fundamental mode the joint in that specimen was loaded in one of the above ways only. The joints in the different specimens were, however, nominally identical, being made with the same size and type of rivet (3.175 mm (1/8 in) diameter, duralumin, mushroom head) and with the joint plates of the same thickness and material

(1.2 mm (= 0.048 in) Alclad L73) and made by the same manufacturer.

4.2 The specimens used.

Specimen A subjected the joint to the oscillating tension-compression load of Mode A. Figure (4a) shows the cross-beam layout of the specimen and its dimensions. In the fundamental mode of flexural vibration of the specimen (displacements normal to the plate surfaces) the two cross-beams bent in anti-phase as shown in Figure (5a). The inertia loading due to this motion imposed a pure tension-compression force on the joint along the line of the rivet axis.

Specimen B subjected the joint to the oscillating bending moment of Mode B loading. Figure (4b) shows its layout and dimensions and Figure (5b) shows the specimen deformed in its fundamental mode. The inertia loading on the vibrating plates subjects the joint to pure bending, provided both the mode of vibration and the specimen are symmetrical about the centre of the specimen.

Specimen C subjected the joint to the oscillating shear load of Mode C. The joint was incorporated in a "top-hat" section beam (Figure (4c)) at the centre of which the crown and the side webs were cut away. A joint plate with two rivets in single shear restored the continuity of the crown across the cut. The beam vibrated in its fundamental mode of free-free flexural vibration in a direction normal to the crown and flanges. The oscillating bending moment in the beam at its centre generated a tension-compression load along the crown and imparted the oscillating shear load of Mode C to the joint.

Three nominally identical specimens of types A and B, and two of type C, were manufactured and tested with a view to checking the reproducibility of results from different, but nominally identical specimens. The nature of the specimens was such that aerodynamic damping was expected to contribute appreciably to the total damping. Damping measurements were therefore made in air and in vacuo in order to assess the aerodynamic effects. Furthermore, specimens A and B were expected to be damped additionally by electro-magnetic effects due to the proximity of the vibration exciter magnet. The magnitude of this effect was investigated on plain, unjointed specimens similar to specimens A and B, tested in air and in vacuo.

4.3 The vibration measurement and excitation.

To measure the damping of the specimens, they were suspended from a massive frame by thin threads or wires attached at (or close to) their nodal points. Vibration of the specimens was perpendicular to the plane of the threads, to minimize restraint of the motion by the threads.

The specimens were excited electro-dynamically. A small coil was attached to one end of specimens A and B and was free to move in a permanent magnetic field. A similar coil was attached at the other end of specimens A and B to measure the amplitude of the velocity of motion. The exciter coil was supplied with alternating current from a standard LF oscillator and power amplifier. Frequencies of vibration were measured on a digital frequency meter of high resolution. Specimen C had a crystal strain gauge attached to measure vibration amplitudes.

Modes of vibration were measured with a non-contacting capacitive vibration meter. This was also used to calibrate the coils for the exciter and velocity transducer, and to calibrate the crystal strain gauge output in terms of the beam displacement.

4.4. The experimental methods

Initially, damping measurements were made by exciting the specimens with a force of constant amplitude (i.e. constant exciter current) and by varying the frequency through the fundamental resonance. The bandwidth of the frequency-response curve at the half-power point yielded a loss factor (= bandwidth \div resonant frequency). However, the force-velocity relationship at the resonant frequency was not always linear, so the accuracy of this measured loss-factor was at times in doubt.

Two alternative methods were therefore used:

(e) The energy input method

At the frequency for maximum response (ω_m) the amplitude of displacement at the exciter (\bar{w}) was measured for different measured exciting force amplitudes (F). The input force was genuinely simply harmonic and the displacement was almost simply harmonic. (Higher harmonic contents were very small). The cyclic energy input is given by \sqrt{Fw} , provided the harmonic contents are small and the phase difference between force and displacement is close to 90° . These conditions were satisfied in the experiments. The loss factor is then given by

$$\eta_m = \frac{\bar{F}\bar{w}}{\omega_m^2 \bar{w}^2}$$

and the joint dissipation coefficient by

$$J_T = \frac{\sqrt{F}}{\omega_m^2 \bar{w}_{Tm}}$$

where the actual joint load is given by \bar{w}_{Tm} .

(b) The bandwidth method at constant displacement amplitude.

The frequency of excitation was varied in the region of the resonant frequency while the displacement amplitude was kept at a constant level by adjusting the force amplitude. The two frequencies, ω_a and ω_b , were identified at which the force amplitude was $\sqrt{2}$ times the force amplitude at resonance (the minimum value). The 'equivalent linear half-power bandwidth' of this frequency response curve is $(\omega_a - \omega_b)$. The equivalent linear loss factor of the system, corresponding to the displacement amplitude of test, is $\eta_m = (\omega_a - \omega_b)/\omega_m$.

Loss factors were measured by these alternative methods for a range of displacement amplitudes. The tests were carried out both in still air at normal temperature and pressure, and in vacuo ($< 1 \text{ mm Hg}$).

To determine the modes of vibration of the specimen, the non-contacting vibration transducer was traversed over the surfaces and amplitudes measured at a number of points. For this part of the experiment, the specimens were supported in the horizontal plane on pieces of soft foam rubber at (or near) the nodal points. This prevented swaying motion of the specimens and facilitated measurement.

For the energy input method, accurate calibration constants were required to relate the exciter current to the force exerted, and the velocity transducer voltage to the actual velocity of motion. These constants were obtained at frequent intervals during the whole test programme by calibrating the coils in situ. To do this, the vibration amplitude and voltage output of each coil were measured at a known frequency using the displacement transducer, while the other coil was being used to excite the system. From these measurements the coil constant Γ was obtained, i.e. $\Gamma = \text{Voltage output amplitude} \div \text{coil velocity amplitude}$. By the reciprocity law, this is also equal to the force amplitude \div supply current amplitude, S.I. units being used.

4.5 Calculation of J_r from measured results.

The amplitude of the exciting force is given by $\bar{F} = \Gamma_e i_0$ where i_0 is the amplitude of the supply current to the exciter. The amplitude of the velocity at the velocity transducer location is given by V_0/Γ_v where V_0 is amplitude of the output voltage from the velocity coil. The measured mode of transverse (flexural) vibration is $\phi(x)$. Let this be normalized to have unit value at the exciter coil location. At the velocity coil location, its value is $\phi(x_v)$. It follows that the velocity amplitude at the exciter point is $V_0/(\Gamma_v \phi(x_v))$ and the displacement amplitude at that point is

$$\bar{w} = V_0/(\Gamma_v \phi(x_v) \omega_m)$$

The joint load, P_{jm} , corresponding to unit displacement at the exciter location was found by appropriate integration of the inertia forces of vibration corresponding to $\phi(x)$. For specimen A, it takes the form of $\omega_m^2/\mu \phi(x) dx$, where μ is the mass per unit length of the cross-beam and the integration extends over one of the cross-beams. For specimen B, in which the joint is subjected to an oscillating moment, the moment amplitude is proportional to $\omega_m^2 \int \mu \phi(x) dx$

where the integration extends from the end of the specimen up to the centre of the joint. For specimen C, in which the joint load is the direct load produced in the crown by the beam bending moment, the load is proportional to $\omega_m^2 \int \mu \phi(x) dx \div \text{depth of beam at the joint}$.

It follows that the joint dissipation coefficient for specimen A is found from the equation

$$J_r = \frac{\pi \Gamma_e \Gamma_v \phi(x_v)}{\omega_m^2 \int \mu \phi(x) dx} \left(\frac{i_0}{V_0} \right)$$

For specimens B and C, the double integrals replace the single integral in the denominator.

J_r can therefore be evaluated, using measured values of i_0 and V_0 and the other quantities. The corresponding amplitude of joint load, P_r , for specimen A is $\bar{w} P_{jm}$, which is seen to be given by

$$P_r = V_0 \omega_m \int \mu \phi(x) dx / (\Gamma_v \phi(x_v))$$

From the values of J_r calculated in this way, it is possible to compute the corresponding loss factor of the specimens, using equation (10). This value can be compared with the loss factors measured by the two other methods.

5. MEASURED VALUES OF THE JOINT DISSIPATION COEFFICIENTS

Figures 6, 7 and 8 show the values of J_r for the joints loaded in normal tension (Specimens A), bending (Specimens B) and shear (Specimens C). Specimen A experiments were carried out at (or about) 143 Hz, Specimen B at 184 Hz and Specimen C at 195 Hz.

Consider first the joints loaded in normal tension (Figure 6). J_r does not vary appreciably over the range of joint loads covered. The surrounding air makes the major contribution to the joint damping, (say 1/2 to 2/3 of the total). When tested in vacuo, the values of J_r from each specimen are almost the same, showing that the actual rivet/joint damping is reproducible from one similar specimen to another. The same is not true for the contribution of the air damping which comes predominantly from the air pumping mechanism between the two joint plates. (This is suggested by the very small contribution of air damping to the unjointed specimen, No.4). The damping due to air pumping must depend considerably on the initial closeness of the plate interfaces at the joint. If this closeness varies

from specimen to specimen, considerable variations can be expected in the damping. This may account for the variability of the J_r 's for the different specimens of Type A when measured in air. The same may be said for the specimens of Type B.

Specimen No.4 had no joint but an equivalent J_r has been calculated for it using the measured i_0 and V_0 values. The corresponding curves of J_r on Figure 6 show that the sources of energy dissipation apart from the joint are small, being due to material hysteresis, electro-magnetic effects (eddy-currents), support damping, and aerodynamic viscous losses around the edges of the specimen.

When the joints are loaded by moments (Figure 7) the air pumping mechanism is still predominant, and is still very variable in magnitude from one specimen to another. Whereas its contribution to J_r increases with increasing moment for one joint, it decreases for another. On the other hand, the J_r values measured in vacuo are more consistent and are scattered by about $\pm 20\%$ around the mean value. There is a slight tendency for J_r in vacuo to increase with increasing moment on the joint. The unjointed specimen behaves almost linearly and its J_r remains constant with moment amplitude.

The joints loaded in shear (Figure 8) behave almost linearly at low amplitudes of load with constant J_r , but J_r rises very steeply after the load amplitude exceeds about 70N. This steep increase has been observed in previous work ⁽⁴⁾ and can be associated with increasing relative slipping of contiguous interfaces. The two different specimens of Type C yield very similar values for J_r at low amplitude, so the joint dissipation characteristics are repeatable on different but nominally-identical joints. The values of J_r for these joints with mushroom-head rivets are about one-fiftieth of those previously measured for countersunk rivets ⁽⁴⁾. This is probably associated with the fact that the shear stiffness of a countersunk rivet is less than that of a mushroom head rivet.

The magnitudes of J_r for the joints under normal tension and those under shear may be compared, as the dimensions of J_r are the same for these two types of loading. It will be seen that the joint under normal tension has a J_r value of about $0.6 \times 10^{-5} \text{ N}^{-1} \text{ m}$ (when electro-magnetic effects, etc., have been subtracted), but under shear, the low-load value of J_r is about $0.3 \times 10^{-9} \text{ N}^{-1} \text{ m}$. These values differ by several orders of magnitude but as quite different mechanisms of energy dissipation are involved, this is not unexpected.

Figure 9 compares the loss factors of specimen C measured by the different methods at different amplitude levels. The agreement between values obtained from the different methods is not as close as could be desired but is not unexpected from previous experience of measuring damping in different ways.

6. THE MEASUREMENT AND PREDICTION OF THE DAMPING OF A STIFFENED FLAT PLATE

6.1 The Plate Structure

A rectangular flat plate, 1.18m x 0.41m x 1.22mm, of the same material as the jointed specimens (L73) was reinforced by 'frame' type members down each long edge, and by seven 'stringer' type members at equal intervals (0.17m) perpendicular to the long edges. Figure 10 shows the panel and reinforcing member dimensions. The reinforcing members were all of L73 and were 1.22mm thick. They were riveted to the plate by the same type of rivet as used in the jointed specimens and were formed by the same process and operator as used for the small jointed specimens. The frames were cut away to allow the stringers to pass through and were attached to the stringers at the intersection points by small cleats, riveted with the same type of rivet as before. The rivets between the plate and the reinforcing members were at 38mm pitch throughout.

6.2 Measurement of the Loss Factor and Mode

The reinforced plate was suspended from a rigid frame by two thin wires and was excited electro-dynamically using light-weight coils at the centre of each inter-stringer panel. The exciters were so inter-connected as to produce forces which were in the same phase on all panels. The mode which was thus most readily and intentionally excited was the so-called "stringer-bending" mode and this was driven at and around its resonant frequency of 240.3 Hz. All the panels vibrated in phase with one another and exerted forces on the stringers which tended to bend the stringers, albeit by imperceptible amounts. These forces between the panels and stringers constituted 'normal tension' forces on the riveted joints of the Mode A type.

The loss factor of this mode was determined from accurate measurements of the bandwidth of the frequency response curve, the response being measured with a strain gauge attached to the centre of one panel. It was confirmed firstly that the response varied in direct proportion to the coil exciting current at the resonant frequency, i.e. the system was behaving linearly. The bandwidth was measured at several different levels below the peak response level, and the different bandwidths so obtained were suitably used to improve the accuracy of the loss factor measurement. The value of the modal loss factor so obtained was 0.017. Measurement of the loss factor in vacuo gave almost the same result.

The mode of plate vibration was measured along the longitudinal centre-line, and also across the lateral centre-line of one of the panels. The non-contacting displacement transducer was used for this measurement. Figure 11 shows the modal displacement patterns so obtained.

6.3 Prediction of the Loss Factor

To predict the loss factor, use was made of equation (10). The amplitude of load on each rivet, P_{rm} , is required, corresponding to vibration of a given magnitude of the plate in the measured mode. The rivets joining the plate and stringer, and plate and frame, are subjected to normal tension due to the plate inertia forces, and to shear due to the stringer or frame bending.

In calculating the normal tension force on the stringer-plate rivets, it was assumed that each rivet carried the inertia force on a rectangular element of plate bounded by the lines mid-way between adjacent pairs of rivets and by the lateral centre lines of the panels (see Figure 12). It was assumed that the displacement of a point (x,y) on the plate was given by

$$w = q_m \phi(x,y) = q_m f_m(x) g_m(y) .$$

$f_m(x)$ is given by the lengthwise mode of Figure 11 and $g_m(y)$ by the lateral mode. $g_m(y)$ was assumed to be the same for each panel. The inertia force on the rivet 'R' for unit value of q_m is therefore given by

$$P_{rm} = \omega_m^2 \rho h \int_{x_1}^{x_2} \int_{y_1}^{y_2} f_m(x) g_m(y) dy dx .$$

This is a good approximation for the loads on rivets near to the longitudinal centre-line, but is poor for rivets close to the frame. However, these latter rivets only sustain very small loads, so even large percentage errors in their magnitudes lead to very small errors in the calculated loss factor which requires $\sum J_r P_{rm}^2$.

The shear loads (Mode C) on these rivets are zero at the longitudinal centre line, and close to the frame have magnitudes of the order of $4 \times P_{rm}$ for the central rivet normal tension load. Values of J_r for rivets under shear are orders of magnitude less than J_r for rivets under normal tension. Energy dissipation due to shearing of these rivets is therefore negligible compared with energy dissipated due to normal tension.

The total inertia force on the plate and stringers is transmitted to the frames through riveted cleats at the stringer-frame junctions. From the normal tension loads on the plate-stringer rivets, one can deduce the shear force on the stringer-frame-plate rivets. Once again, the energy dissipation due to this shearing was found to be negligible.

It now follows that the energy dissipation term $\sum J_r P_{rm}^2$ in the loss factor expression (Equation 10) derives predominantly from the rivets loaded in normal tension, for all of which the value of J_r is the same. This term can therefore be evaluated as $J_r \sum P_{rm}^2$. The value of $\sum P_{rm}^2$ calculated for all the rivets of the panel which were loaded in normal tension was $8.39 \times 10^9 \text{ N}^2$.

Equation 10 also requires the generalized mass, given by

$$M_m = \iint \rho h f_m^2(x) g_m^2(y) dy dx$$

all panels

+ contributions from stringers and frames

The frame contribution in this particular case included inertia associated with distortion of its cross-section, together with inertia associated with deflection normal to the plate surface. The value so obtained for M_m was 0.148 kg.

With $\omega_m = 240.3 \times 2\pi$ rads/sec, the loss factor is found to be

$$\eta = 7.92 \cdot 10^3 J_r .$$

It remains now to use the appropriate value of J_r for the rivets under normal tension. From the in vacuo tests on single joints (Figure 6) the average value of J_r from three specimens is $1.1 \times 10^{-5} \text{ N}^{-1} \text{ m}$. This includes a contribution from electro-magnetic and suspension damping, which, on the unjointed specimen gave an equivalent J_r of $0.4 \times 10^{-5} \text{ N}^{-1} \text{ m}$. The difference between these (0.7×10^{-5}) can be attributed to the riveted joint alone, and should be used to find the plate loss factor. This then yields

$$\eta = 0.0554$$

6.4 Comparison of Calculated and Measured Values

The calculated value is seen to be about three times the measured value of 0.017, and does not include any contribution from air-pumping dissipation at the joints. The best that can be said is that the calculated loss factor is of the same order of magnitude as the measured value, but the discrepancy is nevertheless disappointing. Two possible reasons can be advanced for the discrepancy.

- (a) Although the joints on the plate and cross-beam specimens were made by the same basic process, it is possible that there were significant differences between the mass-produced multiple joints of the stiffened plate, and the hand-made single joints of each cross-beam specimen. The value of J_r found from the cross-beams may not have represented that of the joints in the stiffened plate.
- (b) The simple cross-beam, single joint specimens may not have adequately represented the actual joints on the structure. They consisted of two 25mm wide flat strips riveted together. Around the single rivet were four plate edges in contact with two adjacent plate faces. On the reinforced plate structure where the plate was riveted to a stringer, there were only two stringer edges associated with each rivet which were in contact with the plate, and one of these edges was the rounded edge of the bend between the stringer flange and web. If the cyclic energy dissipation were associated primarily with fluctuating contact, pressure or clipping at such edges, the dissipation coefficient

of the joint in the simple cross-beam could be expected to be at least twice that of a joint in the reinforced plate.

This latter possibility casts doubt upon the premise that the energy dissipated at the cross-beam joints depends upon the amplitude of the normal tension load acting on the joint. Fluctuating pressure between the joint plate surfaces and relative (slipping) displacements of the joint surfaces in this mode must depend upon the fluctuating curvature of each plate surface. The magnitude of this, of course, depends upon the magnitude of the bending moment in each plate close to the joint, and not just upon the magnitude of the normal tension load on the joint.

As a preliminary investigation into this point, damping measurements were made on the 'A' specimens after one of the cross-beams had been 'cropped', and reduced in span from 127 mm (5 in) to 65 mm (2½ in). The degree of curvature in the cropped beam when the whole specimen vibrated in its fundamental mode was now greatly reduced, although the other beam was bending by the same amount as before. This should have led to a marked change in J_r if the amplitude of curvature was the important controlling parameter. In fact, there was no detectable change in J_r , as deduced from in vacuo results. (The air-pumping energy dissipation changed quite considerably, but erratically.) It was therefore concluded that the energy dissipation was associated primarily with the normal tension load on the joint, but further confirmation and investigation into this point would be desirable.

7. CONCLUSIONS

The damping and flexibility of a structural joint may be conveniently represented in vibration analyses by a 'rigid dissipator' in series with an elastic spring. The characteristic value of the dissipator has been called the 'joint dissipation coefficient' and may be determined from measured values of the energy dissipated in a given joint when loaded harmonically with a force (or moment) of known magnitude. To predict the total damping of a structural mode, or the cross-damping between two structural modes, knowledge is required of the load on each joint when the structure vibrates in each mode, and of the dissipation coefficients of all the significant joints.

The structural damping of high-frequency modes of reinforced plates originates in joints which may be loaded by normal tension forces, shear forces, or by moments. In different modes, the joints will be loaded in different ways. Experiments on typical joints loaded in these three ways have shown that the damping characteristics of nominally identical joints (in vacuo) are almost the same. Joint structural damping appears therefore to be reproducible. The energy dissipated by air-pumping between joint surfaces is not reproducible. The structural damping of joints loaded in normal tension or by moments appears to be sensibly linear, but for joints loaded in shear, there is a rapid rise in the joint dissipation coefficient when the load amplitude exceeds a certain level.

When the joint dissipation coefficients so measured were used to predict the damping of a reinforced plate structure, the predicted damping was found to be about three times the measured damping. It appears that the single joint, on which the dissipation coefficient measurement was made, did not adequately represent the actual joints in the reinforced plate. Further careful work is required to establish the ideal form for a single joint specimen.

REFERENCES

1. P.B. WALKER, 1936 Royal Aircraft Establishment Report No. A.D.3079. Note on material and structural damping.
2. L. CREMER, M. HECKL, E.E. UNGAR, 1973 Structure-Borne Sound (especially Ch.6) New York; Springer-Verlag.
3. E.E. UNGAR, G. MAIDANIK, 1968 Journal of the Acoustical Society of America 44, 1, p.292. High frequency plate damping due to gas pumping in riveted joints.
4. D.J. MEAD, 1961 USAF WADC Technical Report 59-676 (ed.W.J. Trapp, D.M. Forney, Jr). The damping, stiffness and fatigue properties of joints and configurations representative of aircraft structures. (pp 235-261)
5. E.E. UNGAR, 1964 USAF FDL-TDR-64-98 Energy dissipation at structural joints; mechanisms and magnitudes.

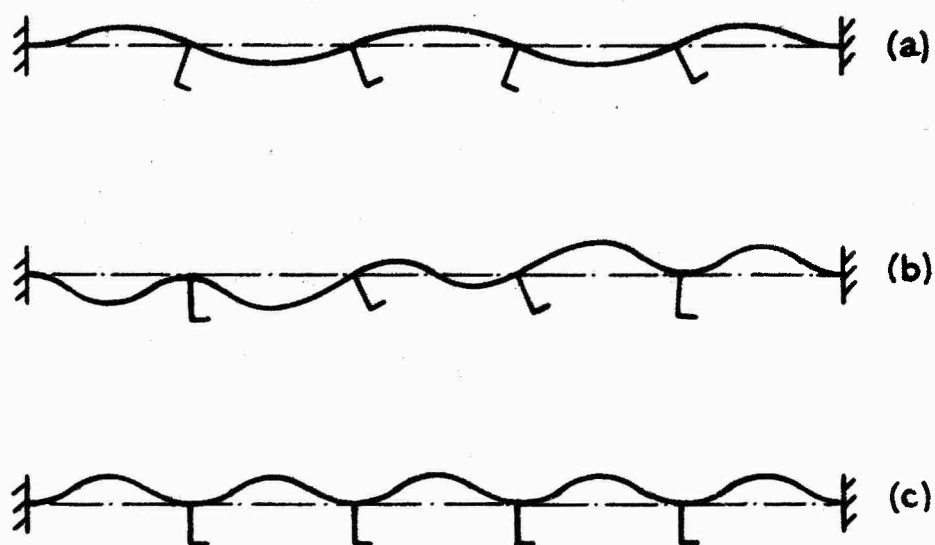


FIG. 1 TYPICAL MODES OF VIBRATION OF A STRINGER-STIFFENED PLATE; TRANSVERSE DISPLACEMENTS ALONG THE PLATE CENTRE-LINE (a) STRINGER-TORSION MODE (b) INTERMEDIATE MODE (c) STRINGER-BENDING MODE.

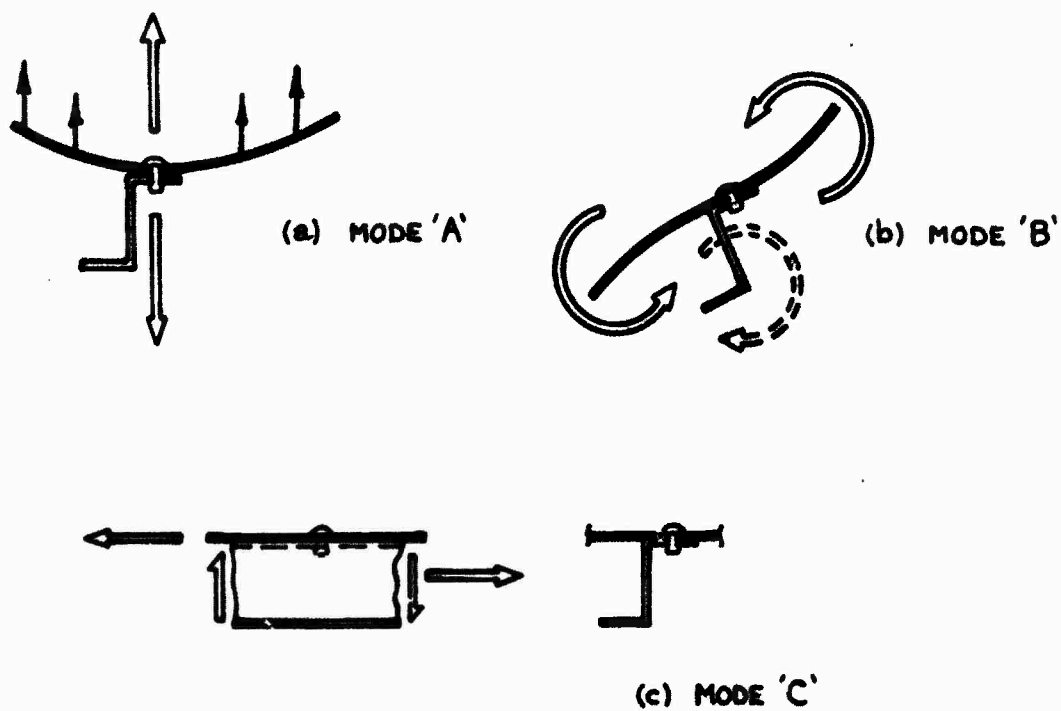


FIG. 2 LOADING ACTIONS ON A RIVETED JOINT BETWEEN THE PLATE AND STRINGER.

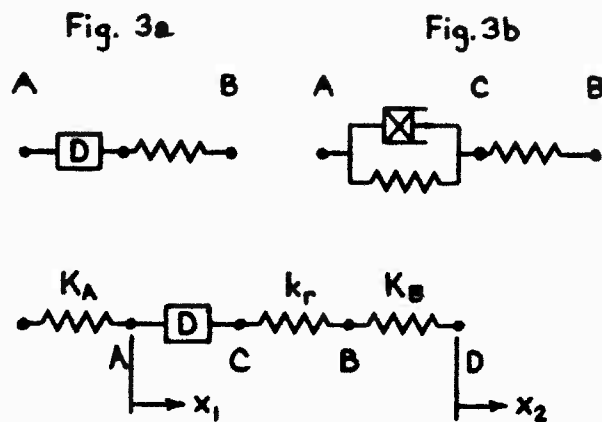


FIG. 3 (a) & (b) DIFFERENT REPRESENTATIONS OF A JOINT.
(c) THE JOINT OF FIG. 3a BETWEEN TWO OTHER STIFFNESSES.

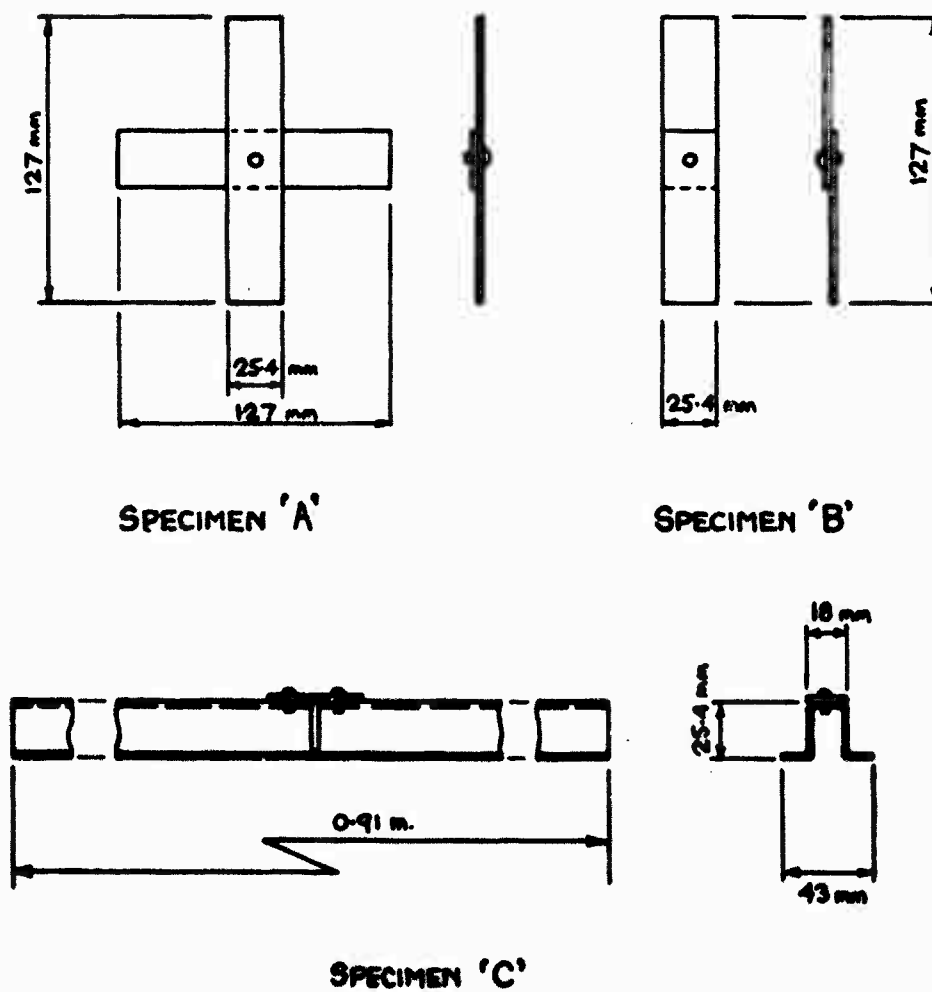


FIG. 4 DIMENSIONS OF THE SPECIMENS USED FOR JOINT-DAMPING MEASUREMENTS.

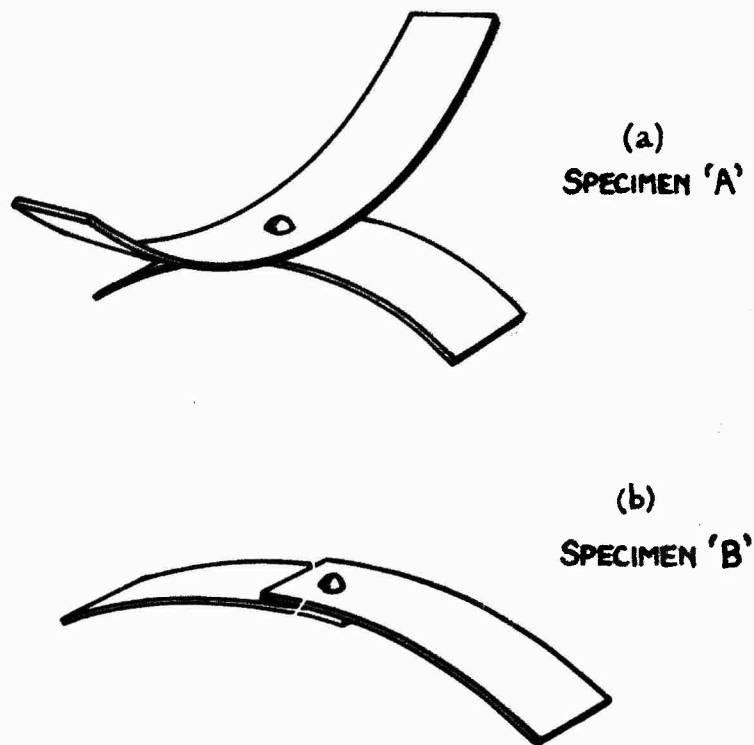


FIG. 5 THE MODES OF BENDING VIBRATION OF SPECIMENS A AND B.

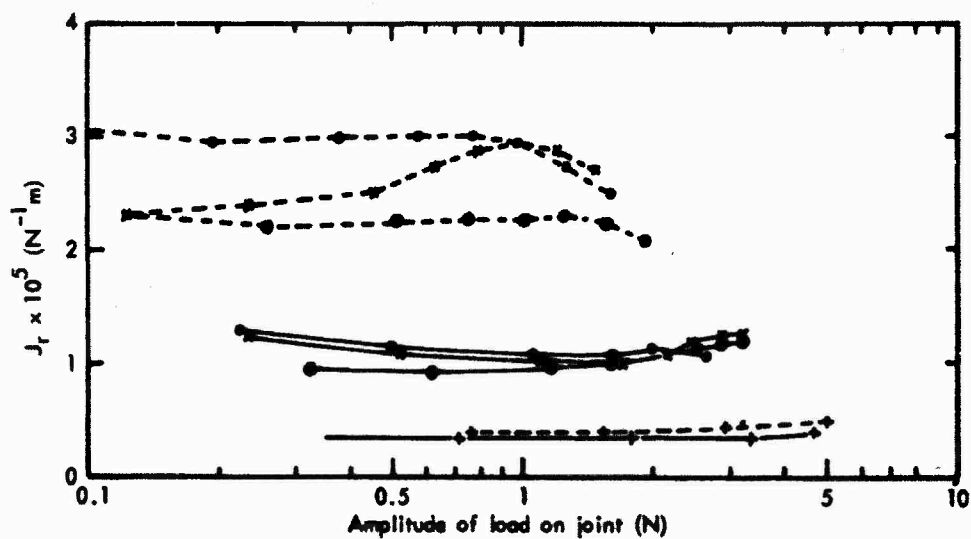


FIG. 6 THE JOINT DISSIPATION COEFFICIENT, J_r , FOR THE MODE 'A' TYPE LOADING.

(—, in vacuo; ----, in air; —●—, specimen A1;
—■—, specimen A2; —○—, specimen A3; —△—, unjointed specimen)

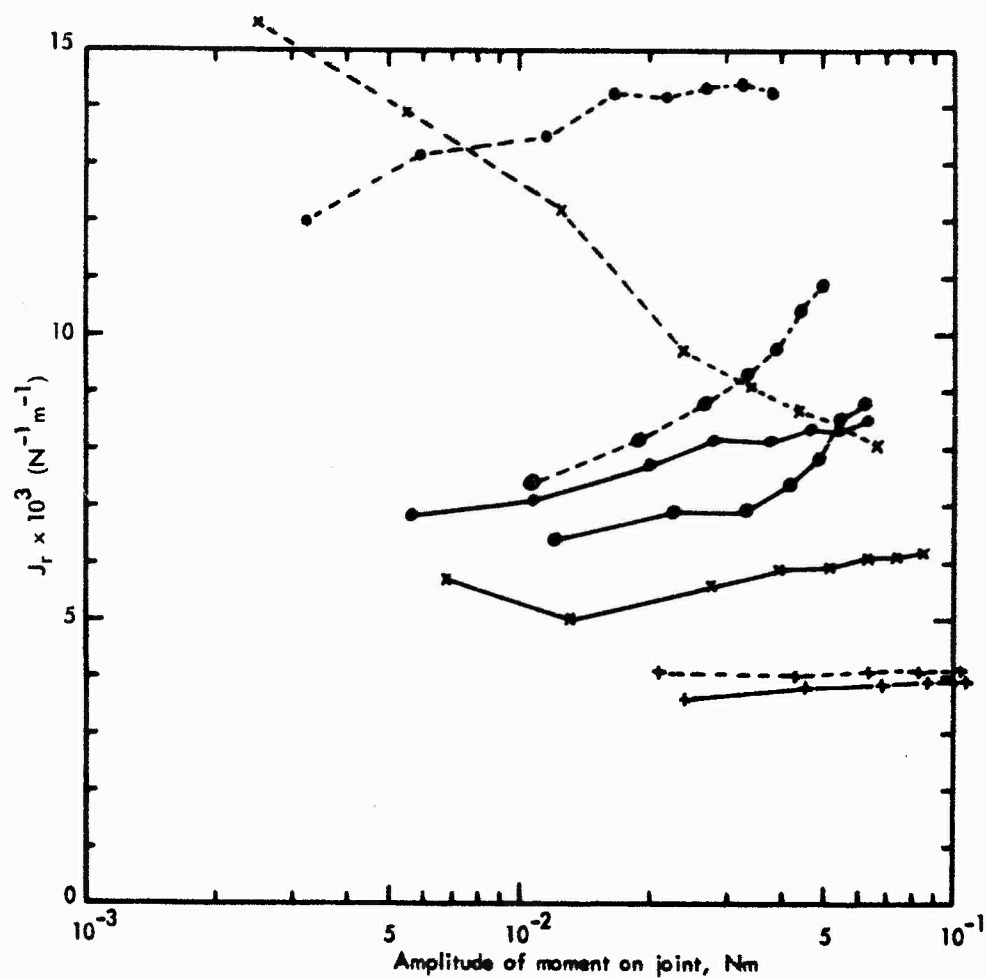


FIG. 7 THE JOINT DISSIPATION COEFFICIENT, J_r , FOR THE MODE 'B' TYPE LOADING. (—, in vacuo; ----, in air; —●—, specimen B1; —x—, specimen B2; —●—, specimen B3; —+—, unjointed specimen)

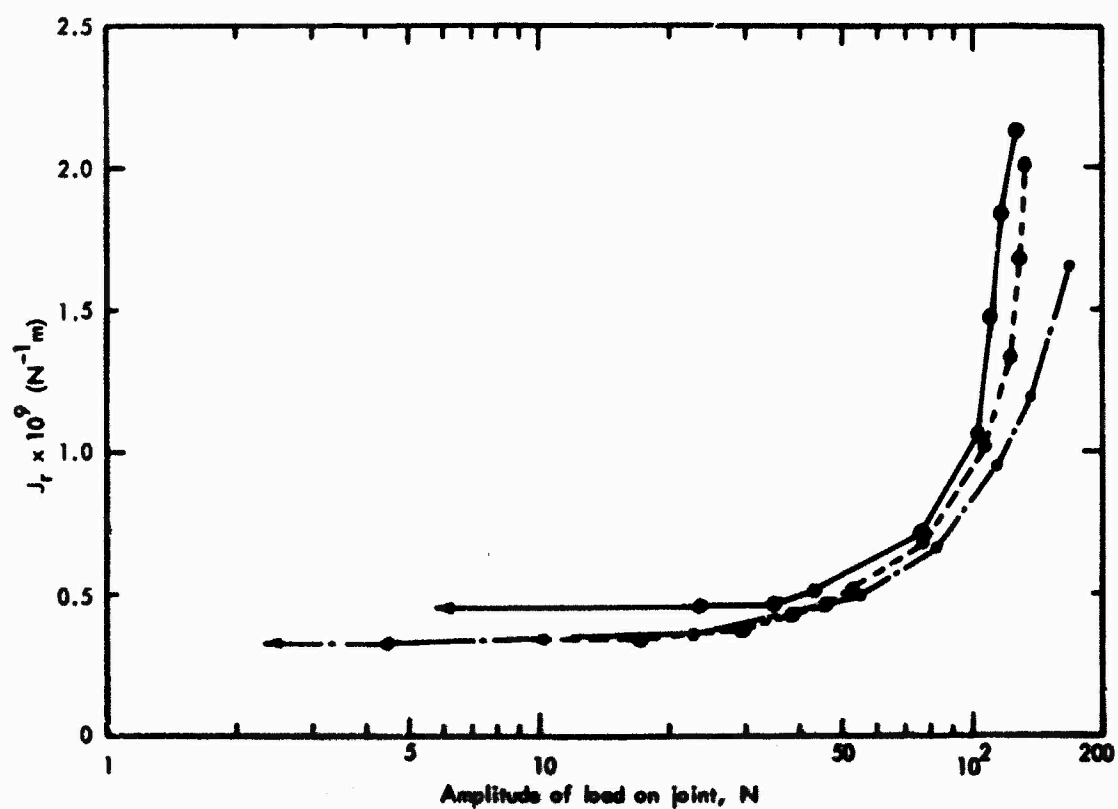


FIG. 8 THE JOINT DISSIPATION COEFFICIENT, J_r , FOR THE MODE 'C' TYPE LOADING. (—●—, specimen C1 in vacuo; ---●---, specimen C2 in vacuo; —●—, specimen C2 in air)

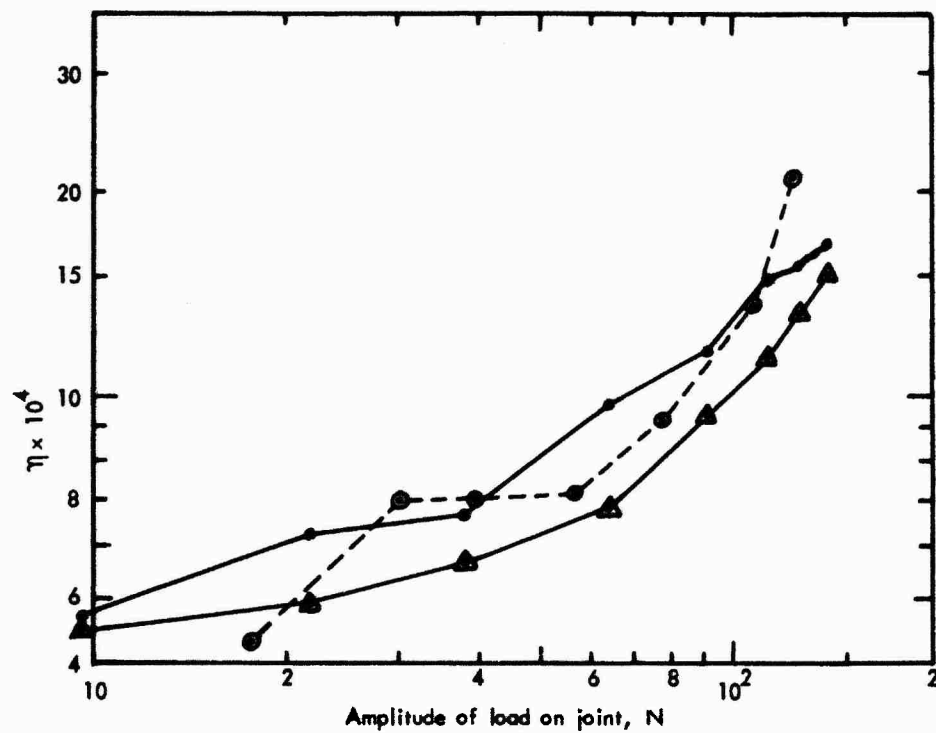


FIG. 9 THE VARIATION OF THE BEAM LOSS FACTOR, η , WITH AMPLITUDE OF LOAD ON THE JOINT, SPECIMEN C.

(—●—, bandwidth method, constant exciting force; ---●---, bandwidth method, constant response amplitude; —▲—, calculated from measured energy input)

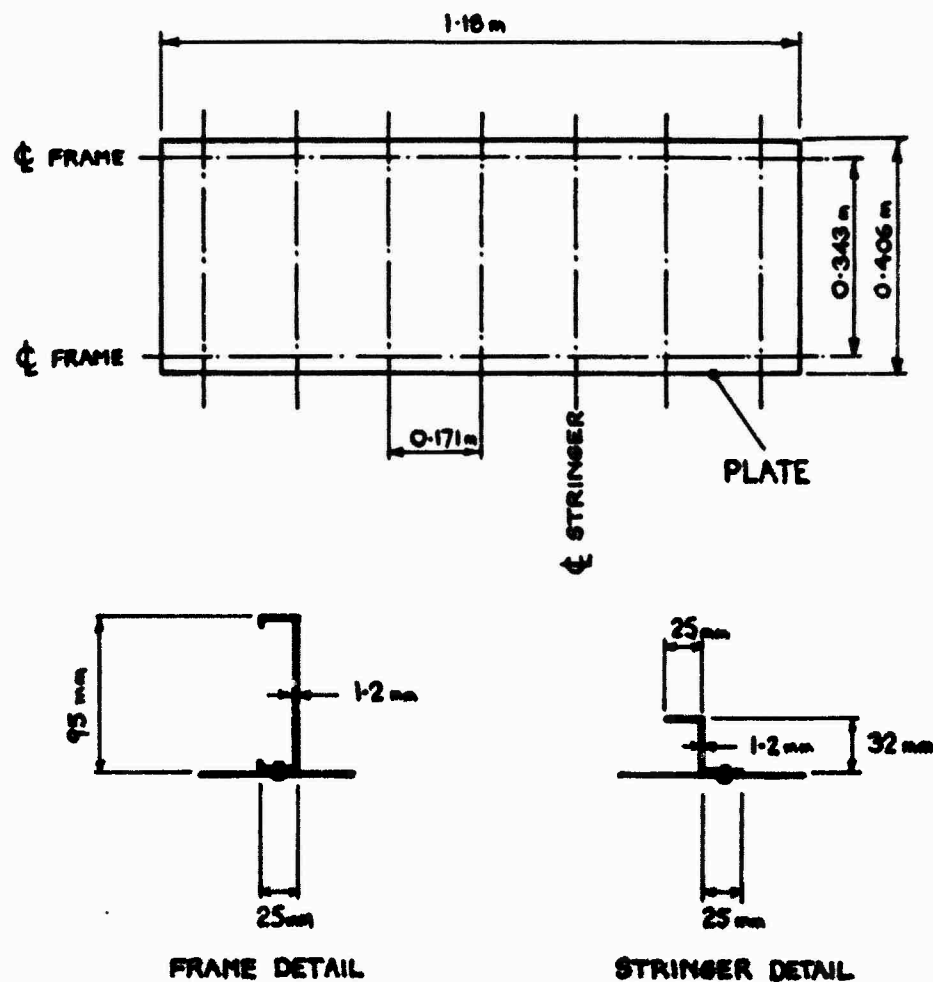


FIG. 10 DETAILS OF THE STIFFENED PLATE.

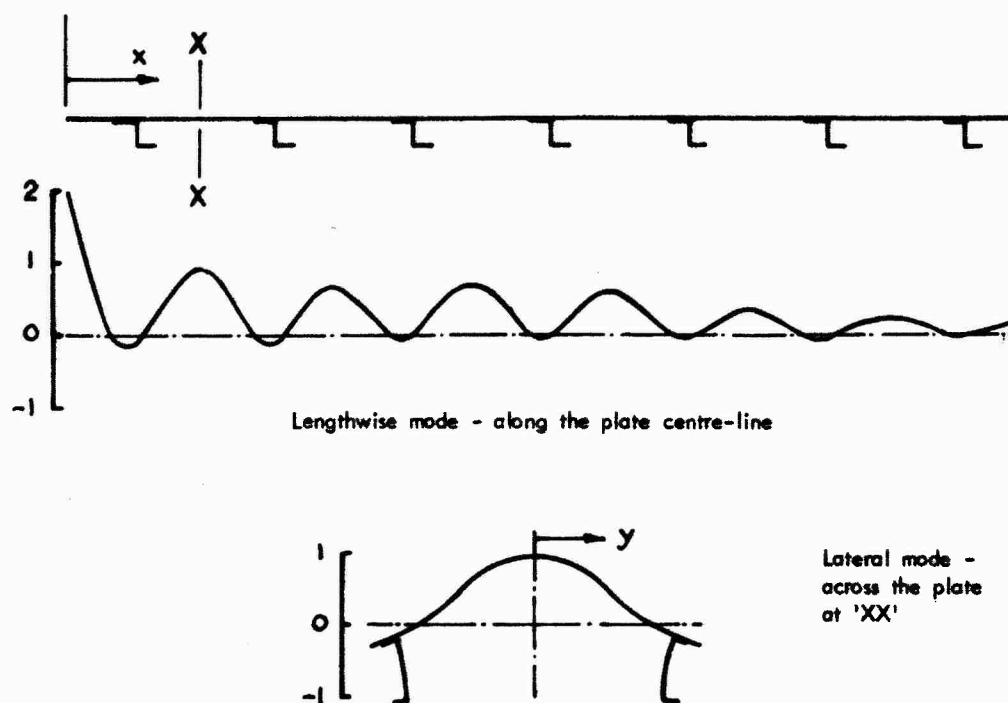


FIG. 11 THE MODE OF VIBRATION OF THE STIFFENED PLATE.

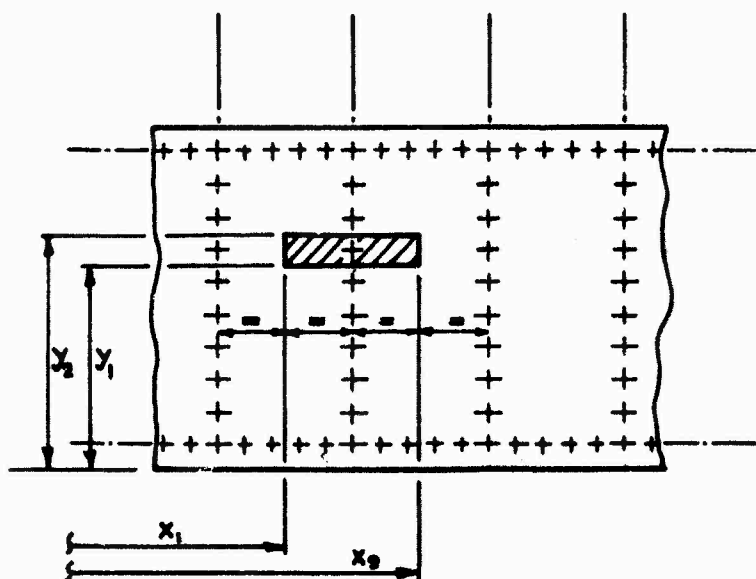


FIG. 12 DIAGRAM SHOWING THE AREA OF PLATE CONTRIBUTING TO THE INERTIA LOAD ON A RIVET. (+, rivet centre locations)

NUMERICAL MODELLING OF STRUCTURES TO ACCOUNT FOR
INTERNAL DAMPING

by

Riccardo F. BALDACCI, Alfredo CORSANEGO and Andrea DEL GROSSO
Istituto di Scienza delle Costruzioni
University of Genova
Via Montallegro, 1
16145, Genova
Italy

SUMMARY

From the point of view of the representation of the structural behaviour by means of finite element models, the various analysis techniques are discussed, as concerning the inclusion of the structural damping effects. The different consequences of assuming some of the most widely used damping models are examined, from the point of view of the solution algorithms. In particular, the most popular uncoupling techniques, that are only approximate when the structural models possess a non proportional damping matrix, are criticized.

Various diagonalization schemes are presented for the damping matrix and particular emphasis is given to the evaluation of the errors involved in the computation. The errors can be identified on an "a posteriori" basis, through parametric numerical studies or, alternatively, can be, in the majority of the cases, estimated "a priori". This consideration leads to a variety of admissibility criteria; some of these are also discussed in the paper.

1. INTRODUCTORY REMARKS

In the context of dynamic structural analysis, the term "numerical model" is referred to a process, typically reproducible into a computer program, able to simulate the dynamic behaviour of a given structural system.

The mathematical structure of the model does not need to be chosen "a priori". Sufficiently well established procedures are known, indeed, [1],[2], to select from a general class of functionals the most appropriate model, provided experimental data taken from vibration measurements are given.

In engineering practice, however, it is more usual to derive "a priori" the mathematical structure of the models from the general principles of the structural dynamics. Such models involve analytically defined quantities and parameters which still need to be determined from field observations.

Some of the methods available to perform this latter task are discussed in [1], [3-8]. By the other hand, the main purpose of the present paper is to deal with the mathematical structure of the models themselves.

In particular, from the point of view of the representation of the structural behaviour by means of finite element models, the various analysis techniques are discussed, as concerning the inclusion of the structural damping effects.

Structural damping is responsible of a removal of energy from the system. The energy removed is dissipated within the system itself by some physical mechanism belonging either to the nature of the material or to the characteristics of the structural details.

It is well known that many structural situations are strictly dependent from the presence of internal damping. Some of these situations are described, for instance, in [9], [10].

The damping mechanism can be very different in nature; many attempts to mathematically describe the phenomenon can be found in the literature together with papers offering comprehensive reviews of the various formulations (e.g.: [11]).

To be consistent with the purpose of the paper, it will be herein assumed that the above mentioned formulations can be classified in two broad categories: a) viscous damping, and b) hysteretic damping. Regardless to the physical nature of the phenomena that the two categories describe, it is intended that the so-called Coulomb damping, plasticity and other similar kinds of dissipation are included, as special cases, into the second category.

From the mathematical point of view, the damping effect is visualized by the equation of motion of a single degree-of-freedom system where a term of resistive force is added:

$$m\ddot{x} + kx + r = f(t) \quad (1)$$

In the case of viscous damping, to the force r can be given a form:

$$r = \sum_{\alpha=1}^s C_{\alpha} \dot{x}^{\alpha} \quad (2)$$

while, in the case of hysteretic damping, the most general expression of the resistive force is:

$$r = g(x, \operatorname{sgn} \dot{x}, \operatorname{sgn} \ddot{x}) \quad (3)$$

In very general terms, the resistive force arising from material damping, can be evaluated on the basis of the linear hereditary theory by the integral:

$$r = \int_{-\infty}^t \phi(t, \tau) \dot{x}(\tau) d\tau \quad (4)$$

in which the kernel has, in some instances, an expression of the Volterra's type. Eq. (4) is derived from the most general constitutive law for linear viscoelasticity. Nevertheless, suitable techniques can be applied in order to give a similar representation to the hysteretic damping.

The idealization of a structural system into a finite element model substantially consist in attributing to that structural system a finite number of degrees of freedom. The dynamic behaviour of the system can be defined mathematically either by a set of differential equations valid in a domain F :

$$D(\{u\}) = \{0\} \quad (5)$$

together with the associated boundary conditions on the boundaries C of F

$$B(\{u\}) = \{0\} \quad (6)$$

or by a variational principle requiring stationarity of some scalar functional M

$$M = \int_F A(\{u\}) dF + \int_C T(\{u\}) dC \quad (7)$$

where $u(x, y, z, t)$ denotes the state of displacement within the system. [14].

In both cases the problem is discretized [15], [16] by introducing a finite number of parameters $\{\Delta\}$ and piecewise defined trial functions $[N]$ such that the unknown functions are approximated by:

$$\{u\} = [N] \{\Delta\} \quad (8)$$

or, breaking the domain F into m subdomains F_i :

$$\{u\}_i = [N]_i \{\Delta\}_i \quad (i = 1, \dots, m) \quad (9)$$

The discretization can be performed according to two alternative criteria.

a) The trial functions $[N]$ are only functions of the space coordinates, that is: $[N] = [N(x, y, z)]$, while $\{\Delta\} = \{\Delta(t)\}$. This approach leads to resulting equations which are algebraic with respect to the space variables and differential with respect to the time.

By introducing, according to the usual finite element techniques, the global stiffness matrix $[K]$ and the consistent or lumped mass matrix $[M]$ one gets the following matrix ordinary differential equation:

$$[M] \ddot{\Delta} + [K] \Delta + \{r\} = \{f(t)\} \quad (10)$$

b) The trial functions $[N]$ are also functions of time, that is: $[N] = [N(x, y, z, t)]$. In other words, the domain F , which is a space-time domain, is broken into subdomains F_i , that still are space-time domains. The resulting equations are, of course, fully algebraic.

It should be observed that, in Eq. (10), the vector $\{r\}$ represents the resistive force arising from damping.

The traditional approach, within the context of the finite element practice, takes advantage of damping formulations of the type shown in Eqs. (2), (3). This approach will be taken as a basis for the future developments.

Although they will not be treated in this paper, alternative approaches exist and must be, for sake of completeness herein referenced. These formulations use damping representations analogous to eq. (4). Important contributions to the subject can be found in [12], [13].

2. SOLUTION ALGORITHMS

In Eq. (10), the resistive force $\{r\}$, for certain kinds of damping can be written as:

$$\{r\} = [C] \dot{\Delta} \quad (11)$$

with:

$$[M]^{-1} [C] = \sum_{i=0}^{n-1} a_i ([M]^{-1} [K])^i \quad (12)$$

where a_i are arbitrary constants and n is the total number of degrees of freedom of the model [17]. In this case the modal superposition method can be applied. It should be observed that Eq. (11) corresponds to the linear viscous damping derived from Eq. (2).

In particular, an important form of the matrix $[C]$, satisfying condition (12), is the following:

$$[C] = \beta [K] + \gamma [M] \quad (13)$$

Under the above assumptions, calling $[Z]$ the modal matrix of the eigenvalue problem:

$$([K] - \omega^2 [M]) \{z\} = \{0\} \quad (14)$$

normalized as follows:

$$[Z]^T [M] [Z] = [I] \quad (15)$$

Eq. (10) can be transformed into the uncoupled system:

$$[I] \{\ddot{q}\} + [B] \{\dot{q}\} + [A] \{q\} = \{a\} \quad (16)$$

where:

$$\begin{aligned} \{q\} &= [Z]^{-1} \{\Delta\} \\ [B] &= [Z]^T [C] [Z] \\ [A] &= [Z]^T [K] [Z] \\ \{a(t)\} &= [Z]^T \{f(t)\} \end{aligned}$$

Eq. (16) can now be solved either in closed form, in a very restricted variety of cases, or numerically, by the evaluation of the Duhamel's integral or by some time-stepping procedure. This latter method presents many analogies with the direct integration of the equations of motion and will be, therefore, discussed later in this section, while the other solution procedures do not involve particular consideration of the damping phenomenon.

It should be observed, however, that the condition (13) physically implies that the damping phenomenon must be the same for all the elements of the model. Eq. (12) states the condition in more general terms but the physical requirements are not substantially modified. Nevertheless, modal analysis represents a very powerful tool, when applicable, especially if the dynamic behaviour is controlled by the first few natural modes.

The solution of the eigenvalue problem (14) constitutes, for models characterized by a large number of degrees of freedom, a very expensive effort. Various techniques are applicable, however, to reduce the total number of degrees of freedom.

Mass lumping or special kinds of consistent mass matrices, obtained by employing reduced interpolation techniques, can be used for this purpose. Detailed discussions of the subject are contained in [18], [19], [22]. Guyan reduction and dynamic substructuring can also be utilized in the condensation process, as described in [20], [21].

In these techniques, the choice of the master degrees of freedom is usually made "a priori", on the basis of an effective subdivision of the structure into substructures or, alternatively, is left to some automatic criterion as the one presented in [23], which is based on the examination of the stiffness and mass matrices of the complete model.

In order to keep the applicability of the modal analysis for the reduced model the damping matrix must be of the kind (13) for each substructure and the constants β and γ must be the same for all the components. If a static condensation is applied, however, condition (13) is not violated when a damping matrix of the same type is superimposed to the one obtained by the condensation process. This latter consideration provides the possibility of constructing simple models in which a localized energy dispersion is present.

When the resistive force is still represented by Eq. (11), condition (12) can be omitted if, instead of the modal superposition, the method of the complex response is applied. By making the Fourier transform of Eq. (10) one obtains:

$$(-\omega^2 [M] + [K] + i\omega [C]) \{\bar{\Delta}\} = \{\bar{f}\} \quad (17)$$

where:

$$\{\bar{\Delta}\} = \int_{-\infty}^{\infty} \{\Delta(t)\} e^{-i\omega t} dt; \quad \{\bar{f}\} = \int_{-\infty}^{\infty} \{f(t)\} e^{-i\omega t} dt$$

Eq. (17) is a set of complex algebraic equations in the unknowns $\{\Delta\}$. The response in the time domain is given by the inverse Fourier transform.

Numerically the procedure is realized by projecting displacement and load time histories into a discrete spectrum of frequencies ω_j ($j = 1, \dots, s$) via the discrete finite Fourier transform thus generating s sets of linear algebraic complex equations of the type (17). The inverse discrete finite Fourier transform gives the time history of the response. The fast Fourier transform algorithm (Cooley-Tuckey or equivalent) can be used as an efficient computational procedure for the direct and inverse Fourier transforms.

Often Eq. (17) is written in terms of a complex stiffness matrix derived from the complex moduli:

$$\begin{aligned} G^* &= G(1 + 2i\beta) \\ E^* &= 2(1 + \nu)G^* \end{aligned}$$

where ν is the Poisson's ratio, G is the (real) shear modulus and β is a measure of the internal dissipation of the material. The coefficient β is a constant in the case of hysteretic damping and is a function of the frequency ω if the damping is of a viscous type.

It should be pointed out that, in a finite element model, each element can have different damping characteristics [24] while substructuring techniques apply to eq. (17) in a way analogous to the static condensation process.

If the damping representation falls in one of the categories described above, either the modal superposition or the complex response method is applicable depending from further conditions or analyst's choice. Often, structures possessing a dissipation mechanism suitable for such representation are said to be "classically damped".

Alternatively or in all the other cases, the matrix equations of the motion (10) can be directly solved by means of a numerical integration procedure. In very general terms a time-step integration consists in calculating starting from initial values, a set of "state vectors" to be associated with a corresponding finite number of instants originated by the stepping of the total interval in which the behaviour of the structure has to be investigated.

It is interesting to point out that time-stepping schemes do not suffer, in principle, any limitation on the representation of the resistive force provided a suitable algorithm is chosen. Unless otherwise specified, however, it will be assumed in the following that a representation (11) holds without restrictions on the nature of the matrix $[C]$.

Under this assumption the "state vector" at the i -th point in time can be expressed as:

$$\{X_i\} = \sum_{k=0}^p [A_k] \{X_{i-k}\} + \sum_{k=0}^q [B_k] \{f_{i-k}\} \quad (19)$$

where:

$$\{X_j\}^T = (\{A_j\}^T \quad \{\dot{A}_j\}^T \quad \{\ddot{A}_j\}^T)$$

is the state vector containing the computed values of the displacements, velocities and accelerations at the j -th point, $[A_k]$ and $[B_k]$ are transformation matrices.

The matrices $[A_k]$ and $[B_k]$ can have different mathematical structures depending on the particular integration algorithm and obviously involve manipulations of the $[M]$, $[K]$ and $[C]$ matrices.

As concerning the algorithms, many of these, old and new ones, are currently in use within the context of a finite element representation of the structural behaviour, each one possessing advantages and disadvantages for certain types of problem. However, although a great amount of work has been done on the subject and authoritative papers can be found in the literature (see for instance Refs. [25-27]), a general procedure is lacking which can be used to compare the merits of these methods in practical applications for complex structural systems.

Essentially, the various integration schemes can be derived within two different general contexts. The first one is based on a finite-difference approximation of the response, leading to expansions of the kind:

$$\{\Delta_{t+\tau}\} = \sum_{i=0}^n \frac{(\tau)^i}{i!} \cdot \frac{d^i \{\Delta_t\}}{dt^i} \quad (20)$$

or:

$$\{\Delta_t\} = \sum_{i=0}^n \frac{(-\tau)^i}{i!} \cdot \frac{d^i \{\Delta_{t+\tau}\}}{dt^i} \quad (21)$$

The second one gives an approximation of the response in a finite element sense, i.e.:

$$\{\hat{\Delta}\} = \sum_{i=1}^n [N_{t+i\tau}] \{\Delta_{t+i\tau}\} \quad (22)$$

where $\{N_{t+i\tau}\}$ are "shape functions" and $\{\Delta_{t+i\tau}\}$ are determined in such a way to give the best average approximation.

Generations of modern algorithms or discussions on old ones can be found in the specific literature. We refer, among the others, to [28-32].

In the choice of a time-stepping method, particular care must be given to the structure of the transformation matrices appearing in Eq. (19). This structure is indeed related to the performance of the method as concerning stability, accuracy, convergence and filtering of high frequency components.

It is generally agreed that for a method to be competitive it should possess the following attributes [27] :

- a) unconditional stability
- b) no more than one set of implicit equations should have to be solved at each step
- c) second-order accuracy
- d) controllable algorithmic dissipation in the higher modes
- e) self-starting

It should be noticed that the above mentioned properties not only depend from the nature of the algorithm (it is recognized, for instance, that explicit linear multi-step schemes are generally only conditionally stable) but some of these properties may be influenced by the step size and by the physical damping of the system.

It is possible to determine an optimal choice of the step size, related to the resonant periods of the system. There is, therefore, a difference between the application of the method to the uncoupled equations (16), where the periods are known and each equation can be independently solved, and its application to the coupled set (10). In this latter case the time step must be unique and can only be guessed, for instance on the basis of the frequency contents of the loads, thus producing a filtering of some modes as an effect of the integration error. By the other hand, if the step size would be determined in order to get accurate integration of high frequency components, its value could result too small with respect to other requirements such as solution economy or round-off error propagation.

In most real situations, however, participation of higher modes is undesirable or unnecessary and an algorithm is needed which is able to filter out any unwanted frequency without losing accuracy in the low range. This implies the availability of parameters other than the step-length. A detailed discussion of the subject together with a continuously controllable scheme is contained in Ref. [33].

Algorithmic dissipation is one of the major aspects to deal with when physical damping is present in the system. The two effects are simply superimposed when the $[C]$ matrix is of the form (12) while for purely hysteretic damping or more general cases the consequences on the participation of the various frequencies cannot be so clearly estimated.

In conclusion, the direct integration of the equations of motion is the most general procedure which can be applied to the solution of dynamic structural problems but a certain amount of uncertainty is also involved. Time-stepping procedures can show a better performance with respect to modal analysis when all the frequencies of the system are clustered together but modal analysis can be superior due to its simplicity, reliability and availability through general purpose finite element codes, especially when eigenvalue economizers can be used.

Fourier analysis is more general and even simpler than modal analysis but a design philosophy based on response and load spectra is usually required.

Moreover, in standard modal analysis the definition of a suitable damping matrix involves a significant amount of engineering judgement. This problem may be avoided, however, if the damping matrix is so cast as to make the computed response as close as possible to a measured one thus using the internally dissipated energy as a flywheel for all the uncertainties of the numerical model.

Condition (12) is also in this context a severe limitation and in any case the question arises to what extent classical modal analysis can represent more complex phenomena or how the procedure can be modified to account for non-classical damping representation.

3. MODAL ANALYSIS FOR NON-CLASSICAL LINEAR DAMPING

The idealization of a structure into a finite element model with a non-classical damping matrix leads to a $[B]$ matrix in Eq. (16) which is no longer diagonal. This fact can be of little importance if Eq. (16) are numerically integrated in time while the knowledge of the natural frequencies can serve as a guide in choosing the appropriate integration parameters. This knowledge does not justify, in general, the combined effort of solving an eigenvalue problem and of directly integrating the complete set of equations of motion in modal coordinates.

The crudest way of overcoming this difficulty and still have all the simplifications of the classical modal analysis is to disregard the off-diagonal terms. This technique is in fact widely used under the hypothesis that the resulting error will be acceptable. Admissibility criteria can be formulated and depend from the amount of damping, the ratio between off-diagonal and on-diagonal terms in the matrix $[B]$, the frequency spacing and the mode shapes. The subject was studied by several Authors. Among them we refer to [34]

-36]. They give, in particular, the following criteria:

$$\text{Ref. [34]} \quad \gamma_r \leq \frac{\epsilon}{2} \left| \frac{\omega_s^2}{\omega_r^2} - 1 \right| \min s \quad (23)$$

$$\text{Ref. [35]} \quad \gamma_r \leq \frac{\epsilon}{2} \left| \frac{b_{rr}}{b_{rs}} \left(\frac{\omega_s^2}{\omega_r^2} - 1 \right) \right| \min s \quad (24)$$

$$\text{Ref. [36]} \quad \left| \frac{1}{\omega_s^2 - \omega_r^2} \left[\frac{b_{rs}^2}{b_{rr}^2} \alpha_r Z_{rk} - \frac{b_{rs}}{b_{rr}} (\alpha_s Z_{rk} + \alpha_r Z_{sk}) \right] \right| \leq \epsilon \left| \frac{Z_{rk}}{\omega_r b_{rr}} \alpha_r \right| \quad (25)$$

where: γ_r is the modal damping factor $b_{rr}/2\omega_r$ and ϵ is a tolerance parameter. It should be noticed that formulas (23) and (24) must hold true for all or the most relevant modes, while formula (25) must be verified also for all or the most meaningful degrees of freedom.

All the above criteria are deduced, for small damping, by comparison of the responses when the models are excited, in resonance, by a harmonic load with a frequency ω_r . Moreover, in Ref. [34] it is assumed $b_{rs} > b_{rr}$ while in Ref. [35] Z_{rk} and Z_{sk} are assumed to be of the same order. The parameter ϵ is not defined in Ref. [34], while it is taken as 0.05 in Ref. [35] and is given by $\epsilon^2 = 8E$ in Ref. [36], where E is the relative error and β is a coefficient which can be taken as unity for a large class of problems.

The applicability of the criteria is, therefore, restricted to the case of small damping but numerical evidence shows that formulas (24) and (25) can predict the order of magnitude of the error also beyond this limit.

The next step is to define a diagonal damping matrix for the modal equations of motion, to be used instead of the matrix [B]. This can be accomplished by means of several procedures.

A first class of methods consists in minimizing, over a given frequency interval, the sum of a measure of the error between the Fourier transforms of the response in one or more points of the models (see for instance [37]). This method is absolutely general but leads to very complicated analytical developments. A similar approach is to equate the moduli of the transfer functions for one particular node of the models over a discrete set of n frequencies, being n the total number of degrees of freedom [38]. Alternatively it could be proposed a method equating such moduli for one particular frequency over n nodal points. This approach is relatively simpler but implies a suitable choice of the nodal points and of the frequencies. As observed in [37] the two approaches give approximately the same results and, consequently, the first one seems not to be fully justifiable.

It should be noticed [39] that the method presented in Ref. [38] can be substantially simplified if the damping is small and if the natural frequencies are not very close to each other. In this case, however, it can be proved that if the comparison is made for the natural frequencies, the modified matrix (diagonal) is practically equal to the original matrix in which only the diagonal coefficients are retained.

A second class of methods can be derived from energy criteria, analogous to the ones used to define equivalent viscous damping models [40]. In particular, a simple procedure [41] is based on the fact that, for steady-state resonant vibrations of a single mode of a linear (uncouplable) system, the modal damping factor may be expressed as:

$$\gamma_r = \frac{D_r}{4\pi U_r} \quad (26)$$

where D_r is the energy dissipated per cycle of motion and U_r is the maximum potential energy per cycle of motion. If the system is not uncouplable, an equivalent modal damping factor is still defined by Eq. (26), provided D_r and U_r are intended as relative to the actual system. As, in the majority of the real cases, non-proportional damping arises from non-homogeneity of the structural components, the energy is always the sum of the contributions of the single components and the equivalent modal damping factors result as a weighted average:

$$\gamma_r = \frac{\sum_{i=1}^p \lambda^i U_r^i}{U_r} \quad (27)$$

where $\lambda^i = D^i / 4\pi U^i$. The contributions of the single elements can be analytically computed, derived from experiments or based on intuition. A method belonging to this class is the Biggs method, which is very po

pular among earthquake engineers [42]. It can be observed that all these methods bypass the computation of the damping matrix [C].

When the on-diagonal coefficients of the matrix [B] are dominant, a third class of methods can be applied. These methods are essentially of an iterative nature and improve, by repeated calculations, an approximate solution obtained with the on-diagonal coefficients alone. An application to steady-state vibrations, limited to the first-order iteration (and therefore of a perturbative nature) is presented in Ref. [43]. Of course the algorithm can also be applied when the on-diagonal coefficients are not dominant, provided the damping is small. It should be noticed that in this case the undamped solution can be taken as the approximate one (zero-order), but the load may not put the structure in resonance. A proof of the convergence of this latter technique is offered in Ref. [44].

When the influence of the modes on the response of the system can be estimated "a priori", in the sense that few dominant modes can be individuated, a fourth approach is applicable. The method, presented in [45], is based on the direct integration of a subset of the coupled modal equations of motion. In particular, only the equations related to the dominant modes are solved. Of course, if the dominant modes are the first ones, the disregarded equations need not to be explicitly generated. In Ref. [45], however, it is suggested that the number of coordinates to be retained could be determined numerically by observing the convergence of the results with increasing number of modes. Theoretically, the procedure can be interpreted as a standard Ritz analysis, in which the assumed shapes are the free vibration mode shapes of the undamped system.

All the above described methods are essentially approximate. It is always possible, however, to generate a diagonal damping matrix by projecting the equations (10) on the eigenvectors of the true, damped system. The basic procedure was introduced in [46] and fully developed in [47]. By considering the velocities $\{\dot{v}\}$ as independent variables, Eq. (10) can be rewritten as:

$$\begin{bmatrix} [O] & [M] \\ [M] & [C] \end{bmatrix} \begin{Bmatrix} \{\dot{v}\} \\ \{v\} \end{Bmatrix} + \begin{bmatrix} -[M] & [O] \\ [O] & [K] \end{bmatrix} \begin{Bmatrix} \{\dot{\Delta}\} \\ \{\Delta\} \end{Bmatrix} = \begin{Bmatrix} \{f(t)\} \\ \{f(t)\} \end{Bmatrix} \quad (28)$$

The homogeneous problem associated with Eq. (28) possesses $2n$ (complex) eigenvalues and corresponding eigenvectors, both in complex conjugate pairs. Calling $[W]$ the modal matrix, the modal decomposition still applies, formally as in the undamped case, leading to a set of $2n$ uncoupled equations in the unknowns $\{p\}$:

$$\{\dot{p}\} = [W]^{-1} \begin{Bmatrix} \{\dot{\Delta}\} \\ \{\Delta\} \end{Bmatrix} \quad (29)$$

analogous to Eq. (16). Although, for systems controlled by the first few modes, substantial economies can be obtained, it may be observed that the determination of the complex eigenvalues and eigenvectors of Eq. (28) represents a serious computational problem.

An algorithm taking advantage of the banded structure of the matrices appearing in Eq. (28) is presented in Ref. [48]. An analysis procedure substantially contained in this approach is applied in [49].

The procedures described in this section can be regarded as the more widely used. It should be noticed, however, that other approaches can be conveniently applied to the analysis of non-classically damped systems. One of these approaches is, for instance, the characteristic phase lag method, reviewed in Ref. [50].

4. CONCLUSIONS

Numerical modelling of structures to account for internal damping must represent an accurate agreement between the simulation of a physical phenomenon and the use of certain solution algorithms.

As shown in the previous sections, the attempt to describe more realistically the material behaviour can lead to a loss in the computational efficiency and in the immediateness of the solution offered by certain algorithms.

For instance, a linear viscous damping model, when proportional, can be included in any of the previously described numerical models and, in particular, allows a straightforward use of the modal superposition technique. Nevertheless, when proportionality is not admitted, classical modal analysis is only an approximate tool, being its applicability dependent from the way in which the method is employed and from the related error criteria.

Moreover, classical and complex modal analysis are no longer applicable when a linear hysteretic kind of damping is of concern. Finally, non linear models, either viscous or hysteretic ones, can only be included in direct integration procedures as the validity of both modal and Fourier analyses ceases, apart from very particular situations.

In conclusion, physical and numerical models are very deeply related and their optimal choice is one of the most important aspects of the structural analyst's activity.

REFERENCES

- [1] GOODWIN G.C. & PAYNE R.L.: Dynamic System Identification: Experiment Design and Data Analysis, Academic Press, New York (1977)
- [2] UDWADIA F.E. & MARMARELIS P.Z.: The Identification of Building Structural Systems, I. The Linear Case, II. The Non-linear Case, Bull. of the Seism. Soc. of America, vol. 66, n° 1 (1976).
- [3] NOVAK M.: Data Reduction from Nonlinear Response Curves, Journal of the Engng. Mech. Div. ASCE, vol. 97, n° EM4 (1971).
- [4] BERMAN A. & FLANNELLY W.G.: Theory of Incomplete Models of Dynamic Structures, AIAA Journal, vol. 9, n° 8 (1971).
- [5] GERSH W.: On the Achievable Accuracy of Structural System Parameter Estimates, Journal of Sound and Vibration, vol. 34, n° 1 (1974).
- [6] GAUKROGER D.R., HERON K.H. & SKINGLE C.W.: The Processing of Response Data to obtain Modal Frequencies and Damping Ratios, Journal of Sound and Vibration, vol. 35, n° 4 (1974).
- [7] DISTEFANO N. & PENA-PARDO B.: System Identification of Frames under seismic loads, Journal of Engng. Mech.Div. ASCE, vol. 102, n° EM2 (1976).
- [8] GERSH W., TAOKA G.T. & LIU R.: Structural System Parameter Estimation by Two-Stage Least Square Method, Journal of the Engng.Mech.Div. ASCE, vol. 102, n° EM5 (1976).
- [9] CRANDALL S.H.: The Role of Damping in Vibration Theory, Journal of Sound and Vibration, vol. 11, n° 1, (1970).
- [10] SANTINI P.: Current Problems in the Area of Dynamic Damping, AGARD 45th Meeting, Voss, Norway, (1977).
- [11] BERT C.W.: Material Damping: An Introductory Review of Mathematical Models, Measures and Experimental Techniques, Journal of Sound and Vibration, vol.29, n°2 (1973).
- [12] ODEN J.T. & RAMIREZ G.A.: Formulation of General Discrete Models of Thermomechanical Behaviour of Materials with Memory, Int. Journal of Solids and Structures, vol. 5 (1969).
- [13] MALONE D.W. & CONNOR J.J.: Finite Elements and Dynamic Viscoelasticity, Journal of the Engng.Mech.Div. ASCE, vol. 97, n° EM4 (1971).
- [14] BALDACCI R.F.: Scienza delle Costruzioni, vol. I, II, U.T.E.T., Torino (1970).
- [15] ZIENKIEWICZ O.C.: An Overview and Categorization of Modern Computational Methods in Engineering, I. C.C.A.D., Lecture Series n° 1/74, Genova (1974).
- [16] ZIENKIEWICZ O.C.: The Finite Element Method, 3d Edition, Mc Graw-Hill, London (1977)
- [17] CAUGHEY T.K. & O'KELLY M.E.J.: Classical Normal Modes in Damped Linear Dynamic Systems, J. of Applied Mechanics, vol. 32, (1965).
- [18] HINTON E., ROCK T. & ZIENKIEWICZ O.C.: A Note on Mass Lumping and related Processes in the Finite Element Method, Earthq.Engng.Struct.Dyn., vol. 4 (1976).
- [19] VYSLOUK V.A., KANDIDOV V.P. & CHESNOKOV S.S.: Reduction in the Degrees of Freedom in Solving Dynamic Problems in the Finite Element Method, Int. J.Num.Meth.Engng., vol. 7, (1973).
- [20] GALLAGHER R.H.: Approximation Procedures; Reduced Stiffness and Mass Matrices; Substructuring; Component Mode Synthesis, I.C.C.A.D. Lecture Series n° 1/74, Genova (1974).
- [21] GUTIERREZ J.A. & CHOPRA A.K.: A Substructure Method for Earthquake Analysis of Structures including Structure-Soil Interaction, Earthq.Engng.Struct.Dyn., vol. 6 (1978).
- [22] HUGHES T.J.R.: Reduction scheme for some Structural Eigenvalue Problems by a Variational Theorem, Int. J.Num.Meth.Engng., vol. 10 (1976).
- [23] HENSHELL R.D. & ONG J.H.: Automatic Masters for Eigenvalue Economization, Earthq.Engng.Struct.Dyn., vol. 3 (1975).
- [24] CARMIGNANI C., CELLA A. & DE PAULIS A.: Structural Dynamics by Finite Elements: Modal and Fourier Analysis, Proc. 2d Int. Conf. on Struct. Mech. in Reactor Techn., Berlin, vol. K (1973).
- [25] BATHE K.J. & WILSON E.L.: Stability and Accuracy Analysis of Direct Integration Methods, Earth.Engng. Struct.Dyn., vol. 1 (1973).
- [26] PARK K.C.: Practical Aspects of Numerical Time Integration, Computers & Structures, vol. 7 (1977).
- [27] HILBER H.M. & HUGHES T.J.R.: Collocation, Dissipation and "Overshoot" for Time Integration Schemes in Structural Dynamics, Earth.Engng.Struct.Dyn., vol. 6 (1978).
- [28] ZIENKIEWICZ O.C. & LEWIS R.W.: An Analysis of Various Time-stepping Schemes for Initial Value Problems, Earth.Engng.Struct.Dyn., vol. 1 (1973).
- [29] ARGYRIS J.H., DUNNE P.C. & ANGELOPULOS T.: Dynamic Response by Large Step Integration Earth.Engng. Struct.Dyn., vol. 2 (1973).

- [30] MELOSH R.J.: Integration of Linear Equations of Motion, ASCE Journal of the Struct.Div., vol.101,n. ST7 (1975).
- [31] ZIENKIEWICZ O.C.: A New Look at the Newmark, Houbolt and other Time-stepping formulas. A Weighted Residual Approach, Earth.Engng.Struct.Dyn., vol. 5 (1977).
- [32] TRUJILLO D.M.: An Unconditionally Stable Explicit Algorithm for Structural Dynamics, Int. Journal for Num.Meth. in Engng., vol. 11 (1977).
- [33] HILBER H.M., HUGHES T.J.R. & TAYLOR R.L.: Improved Numerical Dissipation for Time Integration Algorithms in Structural Dynamics, Earth.Engng.Struct.Dyn., vol. 5 (1977).
- [34] HASSELMAN T.K.: Modal Coupling in lightly Damped Structures, A.I.A.A. Journal, vol. 14 (1976).
- [35] WARBURTON G.B. & SONI S.R.: Errors in Response Calculations for Nonclassically Damped Structures, Earth. Engng.Struct.Dyn., vol. 5 (1977).
- [36] CORSANEGO A. & SOLARI G.: Valutazione dell'accoppiamento modale in strutture con piccolo smorzamento, Ist. Scienza Costr. Genova, publ. 7, series IV (1978).
- [37] THOMSON W.T., CALKINS T. & CARAVANI P.: A Numerical Study of Damping, Earth.Engng.Struct.Dyn., vol. 3 (1974).
- [38] TSAI N.C.: Modal Damping for Soil-Structure Interaction, ASCE Journal of the Engng.Mech.Div., vol.100 (1974).
- [39] CORSANEGO A. & SOLARI G.: Analisi modale classica di strutture con smorzamento non classico, Ist.Scienza Costr. Genova, Publ. 8, series IV (1978).
- [40] JACOBSEN L.S. & AYRE R.S.: Engineering Vibrations, Mc Graw-Hill, New York (1958).
- [41] RAGGET J.D.: Estimating Damping of Real Structures, ASCE Journal of the Struct.Div., vol. 101 (1975).
- [42] WHITMAN R.V.: Soil-Structure Interaction, Seismic Design for Nuclear Power Plants, R.J. Hansen, ed., MIT Press, Cambridge, Mass. (1970).
- [43] CRONIN D.L.: Approximation for Determining Harmonically Excited Response of Nonclassically Damped Systems, J.Engng.Ind., vol. 98 (1976).
- [44] BENVENUTO E. & CORSANEGO A.: Condizioni sufficienti per l'ammissibilità di un procedimento approssimato nella dinamica dei sistemi dissipativi, Atti Ist. Scienza Costr. Genova, vol. 2 (1968).
- [45] CLOUGH R.W. & MOJTAHEDI S.: Earthquake Response Analysis considering Non-proportional Damping, Earth. Engng.Struct.Dyn., vol. 4 (1976).
- [46] FRAZER R.A., DUNCAN W.J. & COLLAR A.R.: Elementary Matrices, Cambridge University Press, (1963).
- [47] FOSS K.A.: Co-ordinates which Uncouple the Equations of Motion in Damped Linear Dynamic Systems, J.of Appl.Mech., vol. 25 (1958).
- [48] GUPTA K.K.: Eigenproblem Solution of Damped Structural Systems, Int. J. for Num.Meth. in Engng., vol. 8 (1974).
- [49] ITOH T.: Damped Vibration Mode Superposition Method for Dynamic Response Analysis, Earth.Engng.Struct. Dyn., vol. 2 (1973).
- [50] NELSON F.C.: Damped Vibration Theory: A State-of-the-Art-Assessment, Conf. on Aerosp. Polymeric Viscoelastic Damping Techn. for the 1980's, L. Rogers Ed., AFFDL-TM-78-78-FBA, Dayton (1978).

E.J. Phillips
 Chief Structural Engineer (Research and Dynamics)
 British Aerospace - Aircraft Group
 Kingston-Brough Division
 Brough North Humberside HU15 1EQ

SUMMARY

The paper presents values of structural damping obtained during a flutter investigation of a strike aircraft in several wing store configurations, in which the wings were excited by impulses at the wing tips; a vibration test on a large underwing pylon mounted pod during which three suspensions were represented; and a vibration test on a box section shelf, mounted on anti-vibration mounts, upon which items of avionic equipment were attached. In the flutter investigation the structural damping was determined from the time decay of filtered accelerometer signals. In the vibration tests, the test items were excited sinusoidally and damping was obtained from accelerometer response curves at resonance. The test techniques are briefly described.

1. INTRODUCTION

This paper presents values of structural damping obtained from tests, upon an aircraft and upon aircraft components, undertaken at the Brough, North Humberside, site of the Kingston/Brough Division of British Aerospace. The test techniques employed are also briefly reviewed.

The measurements were made on structures excited by impulses or constant amplitude sinusoidal excitation. The tests were unconnected and were undertaken over a period of time. The determination of damping was not a primary reason for the tests and it is not suggested that the techniques described are the only, or the best, methods of measuring structural damping. No attempt has been made to collect data from other sources.

The first series of tests were on an aircraft, the second on a pylon mounted pod and the third on an avionic equipment shelf. Each series is described separately.

2. STRUCTURAL DAMPING OF AN AIRCRAFT WING

The structural damping of a Buccaneer S Mk.2 wing was measured during a wing flutter investigation. The purpose of the flight trial was to ascertain the flutter clearance of a version of the aircraft in several alternative wing store configurations. The technique employed was to excite the wing by 'bonkers' - cartridges located at the wing tips providing vertical impulses with specific characteristics. The transient response of the wing was recorded by accelerometers attached at stiff points, e.g. spar rib intersections.

The wing is a typical stiff strike aircraft wing, the construction ensuring high strength and contributing to an excellent 'ride' in high speed low level conditions. The outer wing has integrally machined aluminium alloy skins and ribs. The front and rear spars are steel for part of the span and aluminium alloy for the remainder. The inner wing has aluminium alloy sheet covers, machined steel or aluminium alloy ribs, and steel spars. Skin fasteners on both the outer and inner wings have countersunk heads and a jointing compound was used on assembly. The wing does not contain fuel.

Figure 1 shows the location of the accelerometers in the aircraft. In addition accelerometers were positioned on wing pylons, store bodies, and wing tanks, as required.

All accelerometers were Endevco type 233, and signals were passed through low pass filters before being recorded on an Ampex AR 200 twelve channel recorder. The 'bonkers' were situated in two magazines, one aft, one forward, at each wing tip and firing sequences were chosen to excite particular modes. The bonkers were fired in batches producing a nominal force of 3.6kN for 50 m.secs. for symmetric excitation, and 5.3kN for 25 m.secs for antisymmetric excitation.

For the damping measurements, in order to eliminate aerodynamic damping, the bonkers were fired with the aircraft standing on its undercarriage, the tyre pressures being as low as possible. Measurements were made for a variety of wing store configurations, the transient response of the wing to the bonker impulses being recorded for subsequent analysis. Plots of amplitude of response versus frequency were obtained by passing each accelerometer signal through a series of narrow band filters using a development of the Mazet^{1,2} technique in which signals are played backwards through the filter to prevent the filter 'ringing' when encountering a sharp discontinuity. Having identified the modes and modal frequencies, for selected modes the signal was replayed through a filter tuned to the frequency of the mode to obtain the modal amplitude/time history of the response. The damping in the mode was then obtained from the logarithmic decrement of the signal.

Table 1 contains a summary of the values derived. For configurations A, B and F, the wing carried pylon mounted stores only, for configurations C, D, E and G wing tanks were fitted in addition to stores. Examination of Table 1 shows that the damping was consistently higher in antisymmetric vibration modes than in symmetric modes, with the exception of tank pitch. For symmetric modes, the average structural damping was of the order of 2% critical, for antisymmetric modes of the order of 3.5% critical, a significant increase.

3. VIBRATION TESTS ON AN UNDERWING MOUNTED POD

3.1 Test objectives

The pod is approximately 3600 mm long and 420 mm in diameter. Its mass, including equipment, is approximately 340 Kg. It is basically a cylindrical shell fabricated from aluminium alloy with aluminium alloy and steel internal structure. Fasteners are conventional aluminium alloy rivets and steel bolts. The pod is normally carried suspended below the wing on a pylon.

Minimum values for the pod fundamental bending frequency and for the pitching stiffness were specified in the design requirements. In the initial design stage, the natural modes and frequencies were predicted using a finite element idealization of the structure. Compliance with the design requirements was demonstrated by stiffness and vibration tests on a production standard pod complete with internal equipment or dynamically equivalent space models. The pod was designed to be capable of carriage on several aircraft and each type of suspension was simulated in turn during the tests.

The structural response of such a pod in flight is due to structure borne vibration, exciting the pod through its suspension, and due to fluctuating aerodynamic forces, for example buffet or shock waves, acting on the pod itself, usually near the extremities. Past experience on underwing stores has shown that the two excitations produce quite different structural responses. For this reason vibration tests were performed with excitation applied both through the suspension and then at the pod nose and tail.

3.2 Excitation through suspension

Figure 2 depicts the test arrangement when excitation was applied, vertically and in line with the centre of gravity of the assembly, through the suspension. Forty-two accelerometers were attached to the structure at various locations, including reference points on the pod structure close to the suspension points. The pod was subjected to a slow sinusoidal sweep excitation at constant 0.5g peak input to find the major structural resonances. Having determined the resonant frequencies, the amplification factors at these frequencies were measured for selected positions on the pod structure, where amplification factor at a point is defined as the ratio of the amplitude of acceleration of the structure at that point to the amplitude of the input acceleration measured at a datum point on the stiff beam. To do this the system was tuned to a selected resonance frequency and the accelerometer signals recorded at a range of fixed input acceleration levels, retuning the excitation frequency to resonance, if necessary. The results were analysed to give; (i) the variation in resonance frequency with increase in input acceleration; (ii) the variation of amplification factor with increase in input acceleration; and (iii) the acceleration mode shapes by plotting the acceleration magnitudes and relative phase relationships at selected accelerometer positions.

Structural damping was not measured when the excitation was applied through the suspension. However the variation of amplification factors with excitation level is shown in table 2.

For suspension system A there is a clear indication of an increase in damping as the amplitude of vibration increases. This was expected and agrees with earlier test results on a fuselage mounted pod. The results for suspension system C generally indicate a similar trend although the amount of change is less. Suspension systems A and C are very similar, the pod being suspended via two suspension hooks from an ejector release unit having four sway brace arms. There are however, geometric differences. In each case the pod was crutched against crutch pads on the sway brace arms. With suspension system A the pod is crutched much more tightly but in both cases the amount of crutching was sufficient to ensure that the pod surface remained firmly in contact with the pads during all levels of vibration. A further difference in the test conditions was that with suspension system A the ejector release unit was suspended from a pylon which in turn was attached to a stiff beam, the whole assembly being suspended on the low frequency support and excited by the shaker, whereas with suspension system C the ejector release unit was attached directly to the stiff beam, no pylon being available.

Suspension system B was fundamentally different from A or C, the ejector release unit not having sway brace arms and the pod consequently not being crutched in position. In this case Table 2 shows an increase in amplification factor with vibration level, suggesting that structural damping has decreased with increasing vibration amplitude. A convincing reason for this change in characteristics has not been found.

Table 3 shows the variation of resonance frequency with input acceleration level. Mode 1 is the fundamental symmetric vertical bending mode, mode 2 is a 'free-free' vertical bending mode. For suspension A, there was a

clear reduction in the resonance frequency of mode 1 as the input acceleration level increased. There was no change for suspension B and no significant change for suspension C. The reason for the decrease in resonance frequency has not been ascertained but it is considered unlikely that it was due solely to a change in structural damping in view of the large change in the latter which would be required. Also the reason for a change for one suspension system only has not been found.

3.3 Excitation at pod nose and tail

The pod, ejector release unit and, in the case of suspension A, pylon, were bolted to a stiff test frame. Two exciters were used, either both forcing vertically, as shown on figure 3, or both laterally, at the pod nose and tail. Additionally, for suspension A, the exciters were positioned in turn at the pod nose and tail, one on each side of the pod, to excite torsional modes. The exciters could be operated in phase and at 180° out of phase.

Slow sinusoidal sweep resonance searches were made with a nominally constant force applied at the excitation points, obtaining paper trace records of acceleration against frequency for each accelerometer. The structural damping at resonance was obtained from selected response curves using the half power point method.

Table 4 lists the observed resonance frequencies for the three suspension configurations. Figures 4 to 6 show the response curves for selected accelerometers and the associated mode shapes are shown on figures 7 and 8. The test results indicate the existence of several closely spaced modes where only one was found in the tests applying excitation through the suspension.

The damping levels in the various modes for all three suspension configurations are summarized in tables 5 to 8. It should be noted that the excitation level was low and that the variation of damping with excitation level was not investigated. The quoted levels of damping in the closely spaced modes, e.g. suspension system A, 0.57% critical damping (average) in the 46.6 Hz vertical bending mode, are low. It is doubtful that some of the closely spaced modes were separate modes, although they appeared to be clearly indicated on test. In such circumstances the half power point method becomes questionable for the measurement of damping.

4. DAMPING MEASUREMENTS ON AN AVIONIC EQUIPMENT SHELF

The third series of tests were concerned with a box type structure, on the upper and lower surfaces of which various items of avionic equipment were mounted. The dimensions of the shelf are shown on figure 9. In service the shelf is supported at each corner by an anti-vibration mount attached to a stiff point on the aircraft structure. The cover plates and internal members are fabricated from aluminium alloy sheet and components are rivetted together and assembled with a jointing compound.

The primary objective of the test programme was to demonstrate that vibration attenuation by the shelf and the anti vibration mounts would be satisfactory. To achieve this a shelf, with actual equipment or correct dynamical simulation of equipment, was mounted in a stiff test frame via the anti-vibration mountings, the whole assembly suspended from low frequency supports and vibrated by a 13.5kN thrust exciter. Excitation was applied vertically and horizontally through the centre of gravity of the assembly. Ideally the aircraft fuselage vibration environment would have been reproduced by the exciter but the control equipment available for the test allowed only sinusoidal vibration to be applied. Therefore the assembly was excited sinusoidally, stepping at 5 Hz intervals over a range 5 Hz to 500 Hz. At each step the exciter current was adjusted so that the mean of the levels of vibration (in mm/sec), monitored at reference points on the test frame adjacent to the anti-vibration mounts, remained constant over predetermined frequency bandwidths. The actual levels were chosen to represent the peak power spectral density of the fuselage vibration level over the frequency bandwidth, using an assumed relationship between random and sinusoidal vibration.

Approximately sixty accelerometers were attached at points on the shelf and on equipment mounting brackets to measure response. The frequency steps and data print out were controlled by a computer. Subsequently, a computer program was written to produce from the test data an envelope of the highest level of vibration recorded by any accelerometer versus excitation frequency. This was compared with the specified allowable vibration amplitude and also with the theoretically predicted vibration level on the shelf. The latter was obtained from a finite element representation of the shelf structure and a modal analysis using the resulting flexibility matrix, assuming 2% critical damping in the shelf structural modes.

The foregoing tests were followed by 'modal tests', the purpose of these being to identify modal frequencies and shapes, and to measure modal damping for comparison with the values assumed in the theoretical analyses. For the modal tests the shelf, together with its associated equipment, was removed from the stiff test frame and supported via the anti-vibration mounts on rigid supports. A 200N exciter was placed below each corner of the

shelf to excite it vertically. The drive current for each exciter was supplied by one of four matched amplifiers, the amplifiers being fed by a common controlled oscillator signal. Switching of the amplifier output signals permitted all exciters to be driven in phase or pairs to be 180° out of phase. Twenty accelerometers were placed on the shelf surface on a five by four grid and their outputs logged automatically.

Initially the exciters were driven sinusoidally in phase, stepping through the frequency range 6 Hz to 300 Hz in 2 Hz steps at constant exciter force to excite symmetric modes.

Then two diagonally opposite exciters were driven in phase and the remaining two 180° out of phase to the first pair, stepping as before, to excite antisymmetric modes.

The frequency response curves were examined for resonance peaks and several frequencies chosen for closer examination. Testing was repeated, stepping through the frequencies at three input force levels. The mid-range level was chosen to give a level of vibration at a reference point on the shelf corresponding to the highest expected service level. From the resulting response curves damping was determined using the half power point method. Also plots of the deflected shape of the shelf were obtained using phase data from the accelerometers.

Damping values are given in table 9. Mode 1 is a mode involving torsion of the structure and some rigid body rocking about a diagonal, occurring around 68 Hz. Mode 2 has been identified as a fundamental bending mode occurring at about 90 Hz. The measured damping levels appear high but reasonably consistent. The shelf contains a large number of rivets in proportion to its surface area, due to the internal structure and due to the equipment mounting brackets attached to its exterior. It also supports relatively heavy equipment and contains quite sizeable cable looms, closely clipped to the structure. These facts probably explain the high level of damping. There is evidence of an increase in structural damping with excitation level.

Figure 10 shows the mode 2 response curves obtained from accelerometer 13 for the three excitation levels. The decrease of resonance frequency with increase of excitation level was typical of most accelerometer signals.

5. CONCLUDING REMARKS

This paper has presented values of structural damping measured during bonking tests on an aircraft wing and during vibration tests on an underwing pylon mounted pod and an avionic equipment shelf. It should be noted that in the latter two cases the primary reason for the tests was to check that a required natural frequency of vibration had been achieved or to demonstrate satisfactory vibration attenuation characteristics. In both these cases the measurement of damping was a secondary objective. The disadvantages of sinusoidal testing techniques were apparent in both tests, particularly so in the avionic equipment shelf tests. It was also apparent that the determination of damping from a frequency response curve at resonance is not satisfactory for structures where modes are close and non-linearities may be present, affecting the behaviour of the structure at resonance.

6. REFERENCES

- | | | |
|---|----------------|--|
| 1 | Mazet, R. | Some aspects of ground and flight vibration tests. April 1956, AGARD Report 40-T. |
| 2 | Bellerby, P.J. | A note on in-flight flutter testing using the method of decaying oscillations. September 1961 ARC 31930. |

ACKNOWLEDGEMENTS

The author wishes to thank Mr. D.C. Lang of the Aerodynamics Dept., Brough, for the provision of data on wing bonking tests, and staff of the Structural Dynamics group and the Structures Test Laboratory, Brough, for advice during the preparation of the paper.

EXCITATION	MODE	STORE CONFIGURATION						
		A	B	C	D	E	F	G
SYMMETRIC	WING BENDING	1.8	1.5	2.0	1.7		1.75	1.5
	WING TORSION			1.8		1.5	2.5	2.5
	WING BENDING 1st OVERTONE	2.0						
	WING TORSION 1st OVERTONE					2.0		
	FUSELAGE BENDING					1.5		
	AILERON ROTATION						2.5	
	O/B PYLON BENDING					1.8	1.5	2.0
	TANK PITCH					2.0		
ANTI-SYMMETRIC	WING BENDING	3.0	3.6	3.2	4.0	3.0		
	WING TORSION	2.5		4.0		2.5		
	WING TORSION 1st OVERTONE	5.0						
	AILERON ROTATION							4.5
	TANK PITCH					1.5		

Table 1 Strike aircraft with underwing stores
% critical structural damping

ACCELEROMETER	AMPLIFICATION FACTOR (MODE 1)											
	SUSPENSION A				SUSPENSION B				SUSPENSION C			
	INPUT ACCEL ⁿ . (PEAK 'g')				INPUT ACCEL ⁿ . (PEAK 'g')				INPUT ACCEL ⁿ . (PEAK 'g')			
	0.25	0.50	0.75	1.00	0.25	0.50	0.75	1.00	0.25	0.50	0.75	1.00
S23	33.84	24.26	20.68	16.92	7.80	7.15	7.80	8.97	11.70	14.30	12.57	10.73
S17	54.15	35.35	25.48	21.50	9.60	8.90	13.24	14.72	15.07	19.18	16.44	16.10
S5	15.44	9.80	7.90	6.62	3.57	4.16	4.76	4.76	7.74	7.44	5.95	5.06
S1	7.24	4.84	4.43	3.80	2.72	2.26	2.52	2.64	5.28	3.02	3.80	2.27
S3	6.92	4.76	3.90	3.36	2.16	2.16	3.24	2.97	4.86	3.24	1.80	2.16
S8	16.70	9.90	7.20	5.72	4.31	4.62	5.85	5.00	7.70	7.32	5.13	4.62
S20	42.20	26.70	19.70	16.90	10.53	11.70	14.04	14.92	10.53	15.21	13.65	12.87
S24	29.90	23.10	14.50	12.22	10.45	9.22	8.61	10.15	9.84	11.68	9.84	9.23

Table 2 Variation of amplification factors
with excitation level

INPUT ACCELERATION (PEAK 'g')	RÉSONANCE FREQUENCY (Hz)					
	SUSPENSION A		SUSPENSION B		SUSPENSION C	
	MODE 1	MODE 2	MODE 1	MODE 2	MODE 1	MODE 2
0.25	47.5	102.5	49.0	118.9	47.7	111.7
0.50	46.5	103.0	49.0	117.7	46.7	110.2
0.75	45.5	103.4	49.0	117.3	47.5	109.3
1.00	44.0	103.8	49.0	116.6	46.8	110.0
1.25		104.2		116.5		110.4
1.50		104.5		116.4		

Table 3 Variation of resonance frequency
with excitation level - excitation through suspension

MODE	FREQUENCY (Hz)		
	SUSPENSION A	SUSPENSION B	SUSPENSION C
YAW	12.8	12.2	13.1
PITCH	21.3	19.3	19.8
ROLL	20.0 22.0	18.9 20.1	20.7 22.8
VERTICAL BENDING	46.6 47.6 52.6	47.1 47.9 53.2	45.9 54.1
LATERAL BENDING	62.4 76.8	59.5 70.6	59.7 70.3
POD NOSE TORSION	89 90		
AFT POD TORSION	89.5		

Table 4 Resonance frequencies, excitation at
pod nose and tail

MODE	FREQ. (Hz)	% CRITICAL DAMPING											
		ACCELEROMETER NO.											
		VERT. S5	LAT. S7	VERT. S3	LAT. S10	VERT. S17	LAT. S18	LAT. S19	VERT. S20	LAT. S21	LAT. S22	VERT. S23	VERT. S24
YAW	12.8		2.2		2.1			2.2			2.0		
PITCH	21.3	3.0		2.9		3.0			2.9			3.2	2.8
ROLL	20.0 22.0		2.1 1.5		2.1 1.4			2.0 1.5			2.1 1.5		
VERT. BENDING	46.6 47.6 52.6	0.6 0.5 1.1		0.6 0.5 1.3		0.6 0.5 1.1			0.6 0.6 1.2			0.6 0.6 0.9	0.4 0.4 1.2
LAT. BENDING	62.8 76.8		1.2 1.1		1.3 1.2			1.2 1.2			1.4 1.1		
POD NOSE TORSION	89.0 90.0						2.3	2.0 1.7					
AFT POD TORSION	89.5									2.1	1.6		

Table 5 Damping factors, suspension system A

MODE	FREQ. (Hz)	% CRITICAL DAMPING									
		ACCELEROMETER NO.									
		VERT. S5	LAT. S7	VERT. S8	LAT. S10	VERT. S17	LAT. S19	VERT. S20	LAT. S22	VERT. S23	VERT. S24
YAW	12.2		4.8		4.6		5.5		4.3		
PITCH	19.3	3.3		3.2		2.2		2.9		3.1	2.5
ROLL	18.9 20.1		1.8 2.3		1.9 2.8		1.8 1.9		2.0 2.6		
VERTICAL BENDING	47.9 53.2	0.8 1.5		0.7 1.4		0.8 1.5		0.7 1.5		0.8 1.4	0.8 1.2
LATERAL BENDING	59.5 70.6		1.2 0.6		1.2 0.6		1.2 0.6		1.3 0.6		

Table 6 Damping factors, suspension system B

MODE	FREQ. (Hz)	% CRITICAL DAMPING									
		ACCELEROMETER NO.									
		VERT. S5	LAT. S7	VERT. S8	LAT. S10	VERT. S17	LAT. S19	VERT. S20	LAT. S22	VERT. S23	VERT. S24
YAW	13.1		3.0		3.6		3.3		2.3		
PITCH	19.8	1.8		1.9		1.9		1.8		2.0	1.8
ROLL	20.7		1.5		1.2		2.2		1.2		
	22.8		1.3		1.2		1.3		1.1		
VERTICAL BENDING	45.9	1.1		1.1		1.0		1.1		1.1	1.1
	54.1	1.0		1.1		0.9		1.1		1.1	1.0
LATERAL BENDING	59.7		1.5	1.4			1.4		1.4		
	70.3		0.8		0.8		0.8		0.9		

Table 7 Damping factors, suspension system C

MODE	SUSPENSION SYSTEM A	SUSPENSION SYSTEM B	SUSPENSION SYSTEM C	OVERALL AVERAGE
YAW	2.13	3.30	3.05	2.99
PITCH	2.97	2.87	1.87	2.57
ROLL	2.08	1.88	1.53	1.83
	1.48	2.40	1.23	1.70
VERTICAL BENDING	0.57	0.77	1.08	0.81
	0.52			0.52
	1.13	1.42	1.03	1.19
LATERAL BENDING	1.28	1.23	1.43	1.31
	1.15	0.60	0.83	0.86
TORSION	1.94			1.94

Table 8 Average % critical damping

ACCEL- EROMETER NO.	EXCITER CURRENT (AMPS)	% CRITICAL DAMPING	
		MODE 1	MODE 2
1	7.5	5.3	4.0
	10.0	-	4.9
	12.5	6.4	6.7
6	7.5	4.1	5.3
	10.0	4.8	5.2
	12.5	5.0	5.7
9	7.5	3.7	2.9
	10.0	5.0	3.5
	12.5	5.0	4.2
10	7.5	4.6	-
	10.0	5.0	4.2
	12.5	5.2	4.3
13	7.5	3.9	5.6
	10.0	5.0	5.4
	12.5	6.0	5.4
14	7.5	4.9	5.1
	10.0	5.5	5.4
	12.5	5.2	5.8

Table 9 Avionic equipment shelf, measured damping

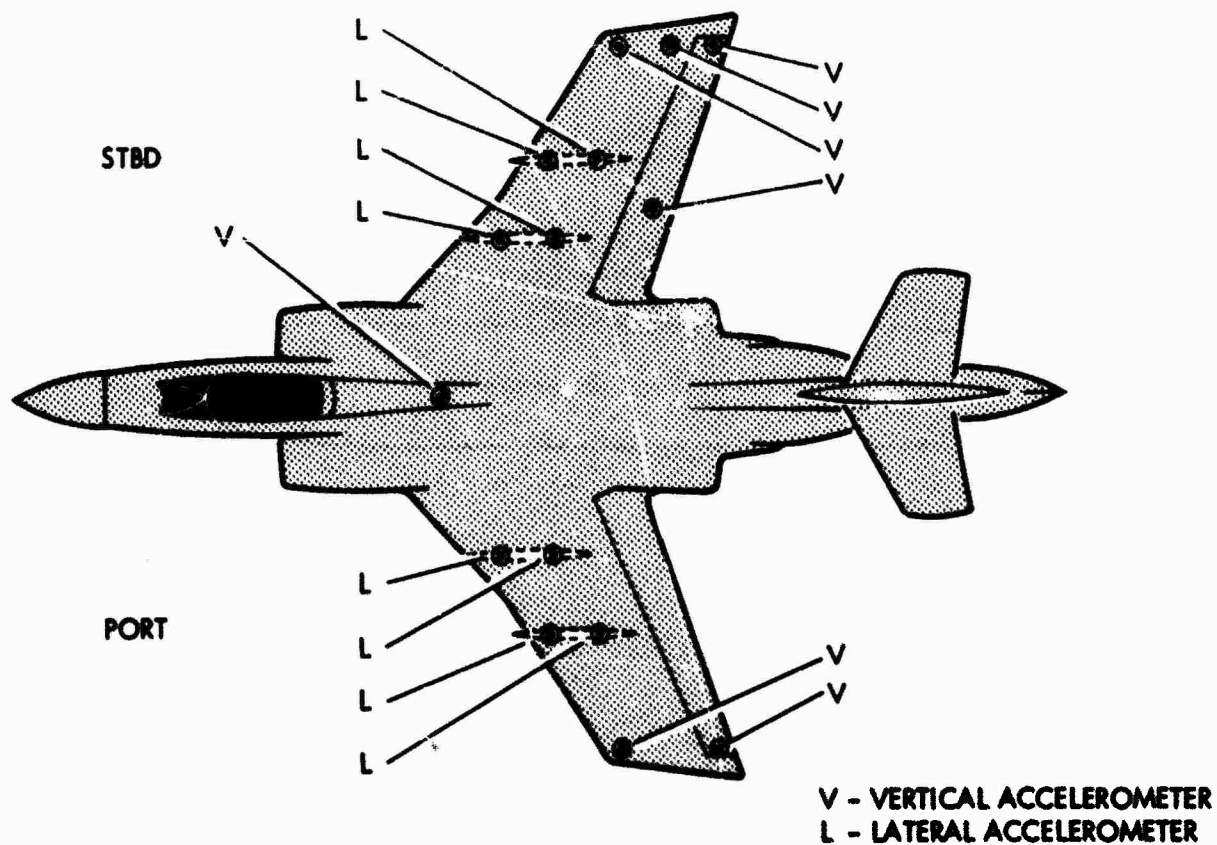


Fig.1 Location of accelerometers

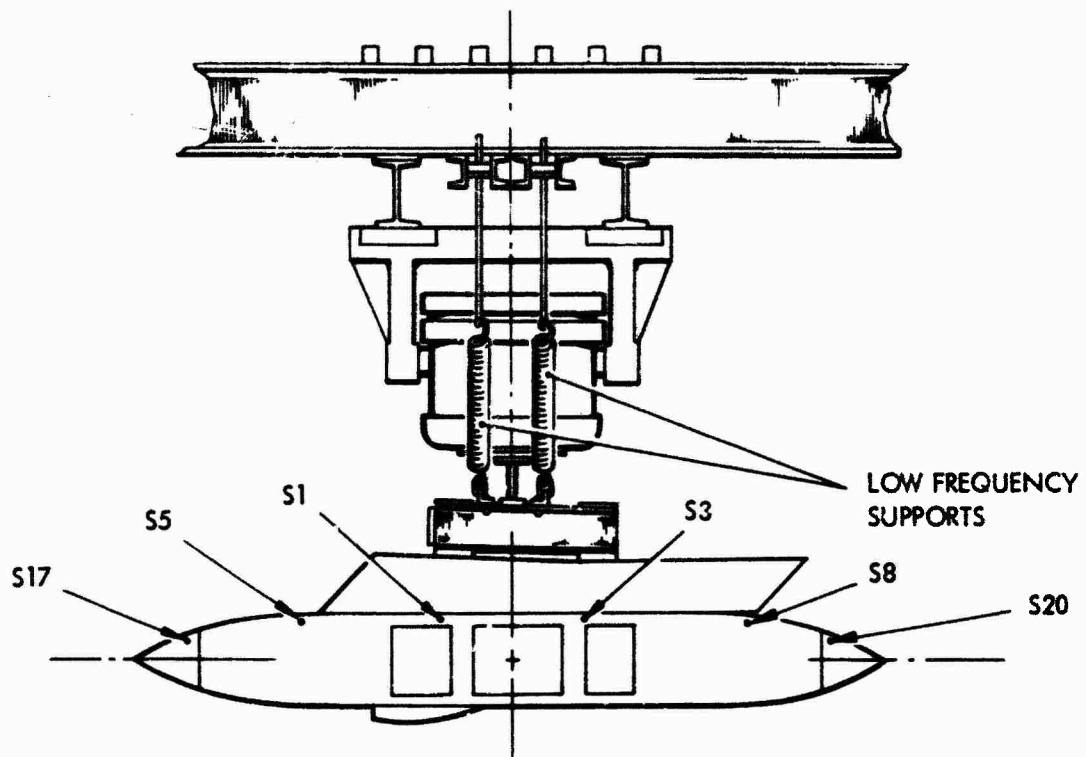


Fig.2 Test rig, excitation through suspension system

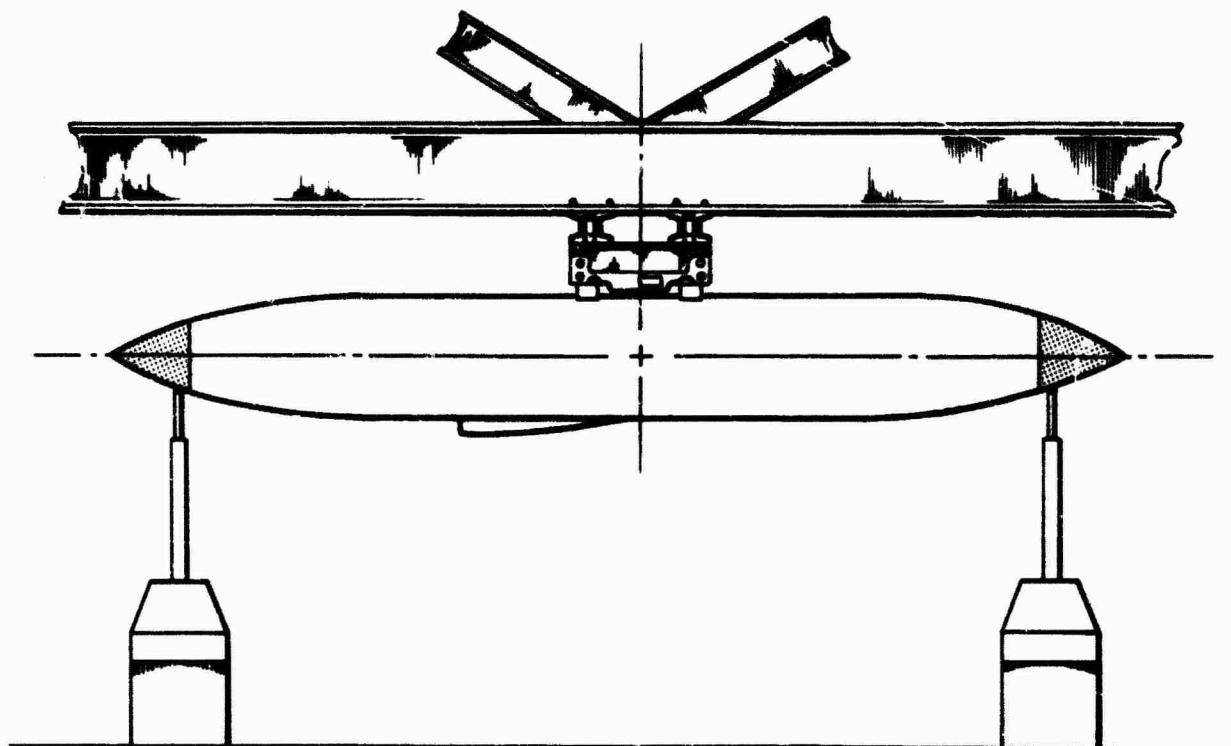


Fig.3 Test rig, excitation applied to pod ends

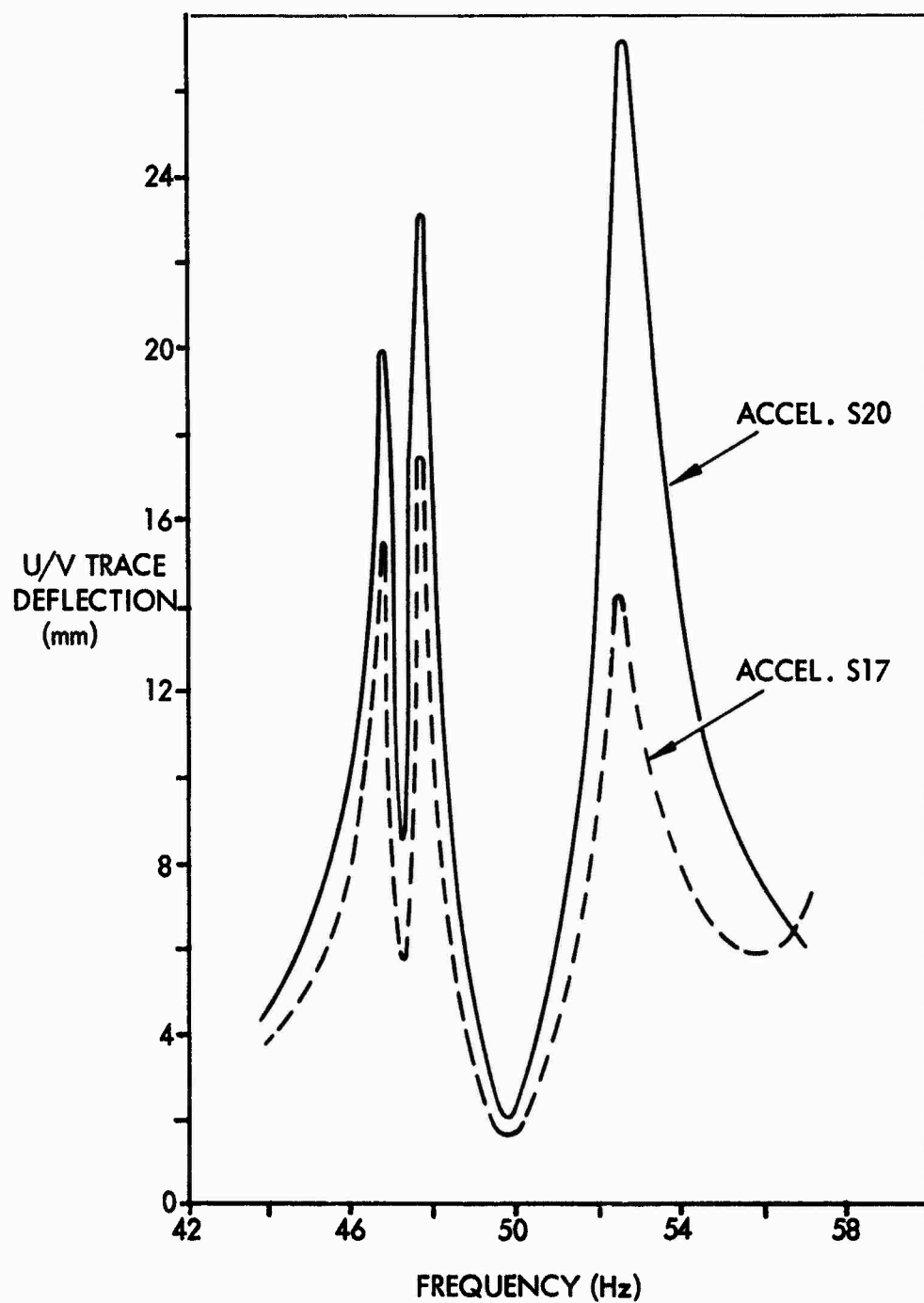


Fig.4 Suspension system A - vertical symmetric bending, excitation at nose and tail

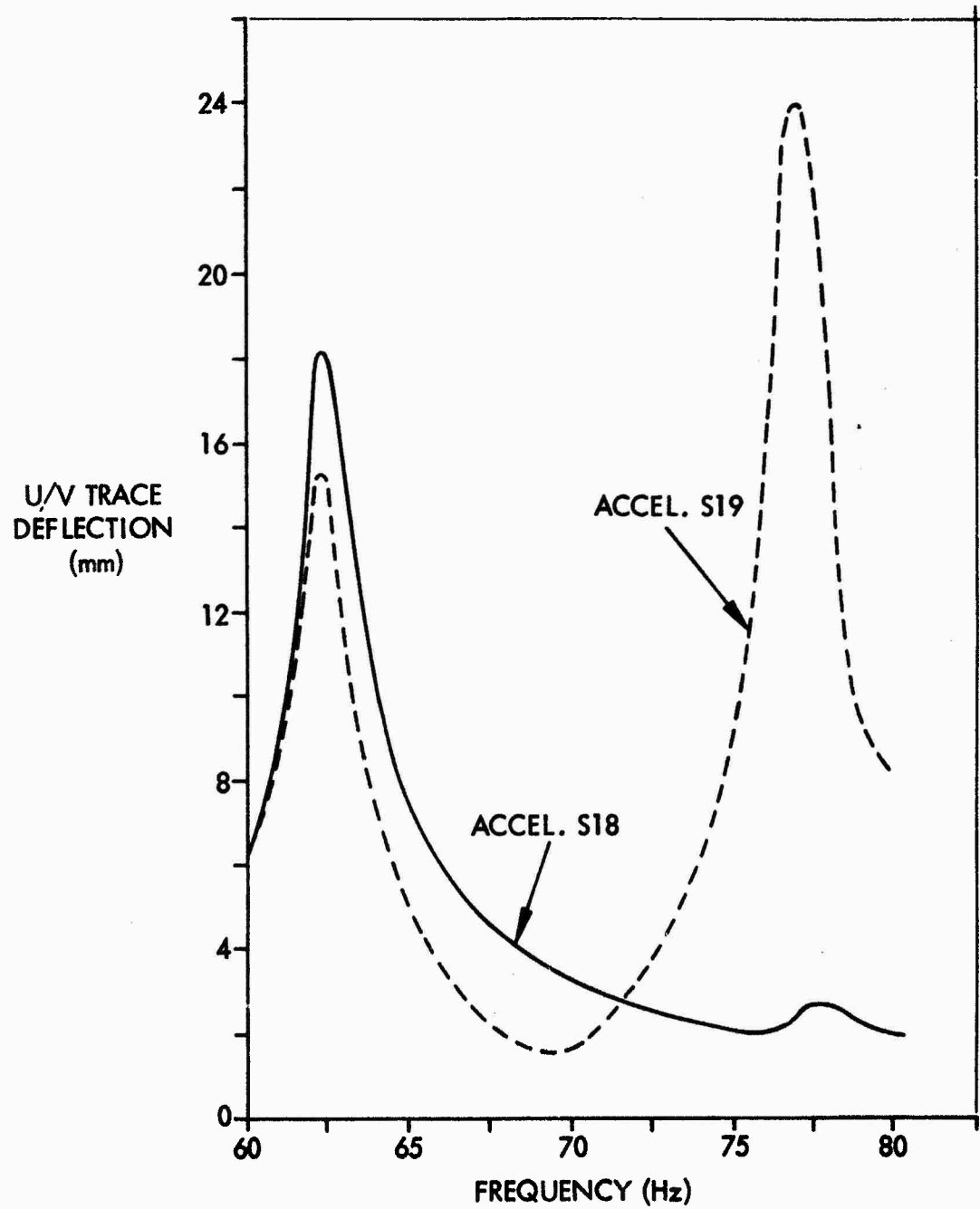


Fig.5 Suspension system A - Lateral symmetric bending, excitation at nose and tail

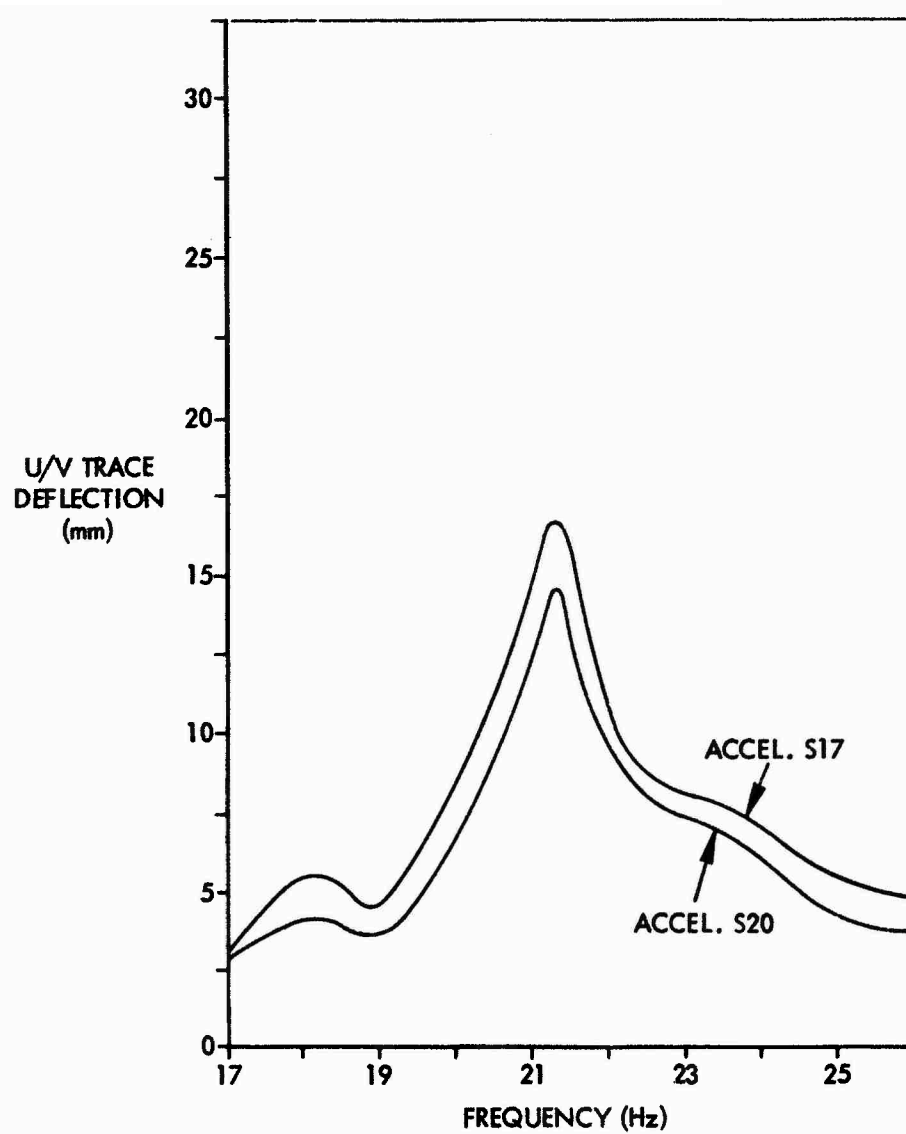


Fig.6 Suspension system A - pod pitch excitation at nose and tail

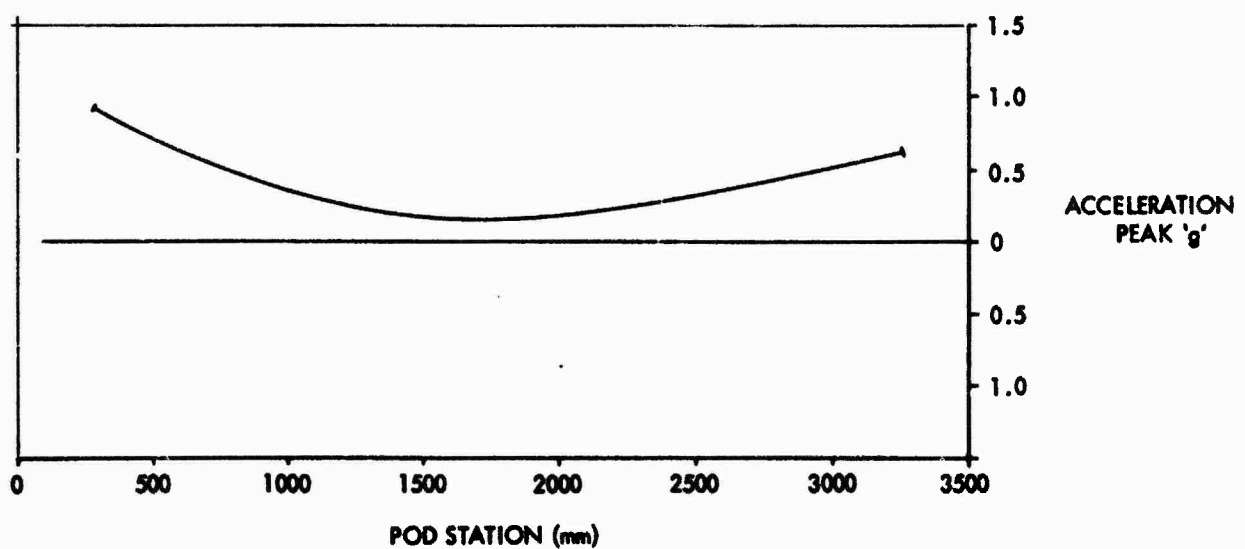


Fig.7 Suspension system A - vertical symmetric bending (46.6 Hz) excitation at nose and tail

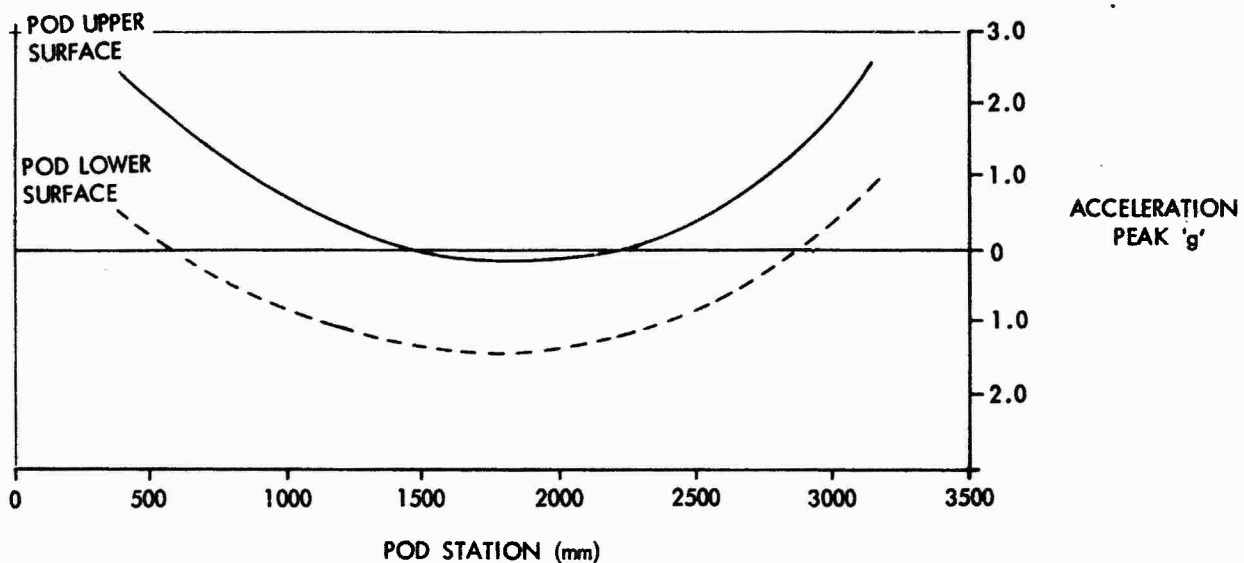


Fig.8 Suspension system A - Lateral symmetric bending (62.4 Hz) excitation at nose and tail

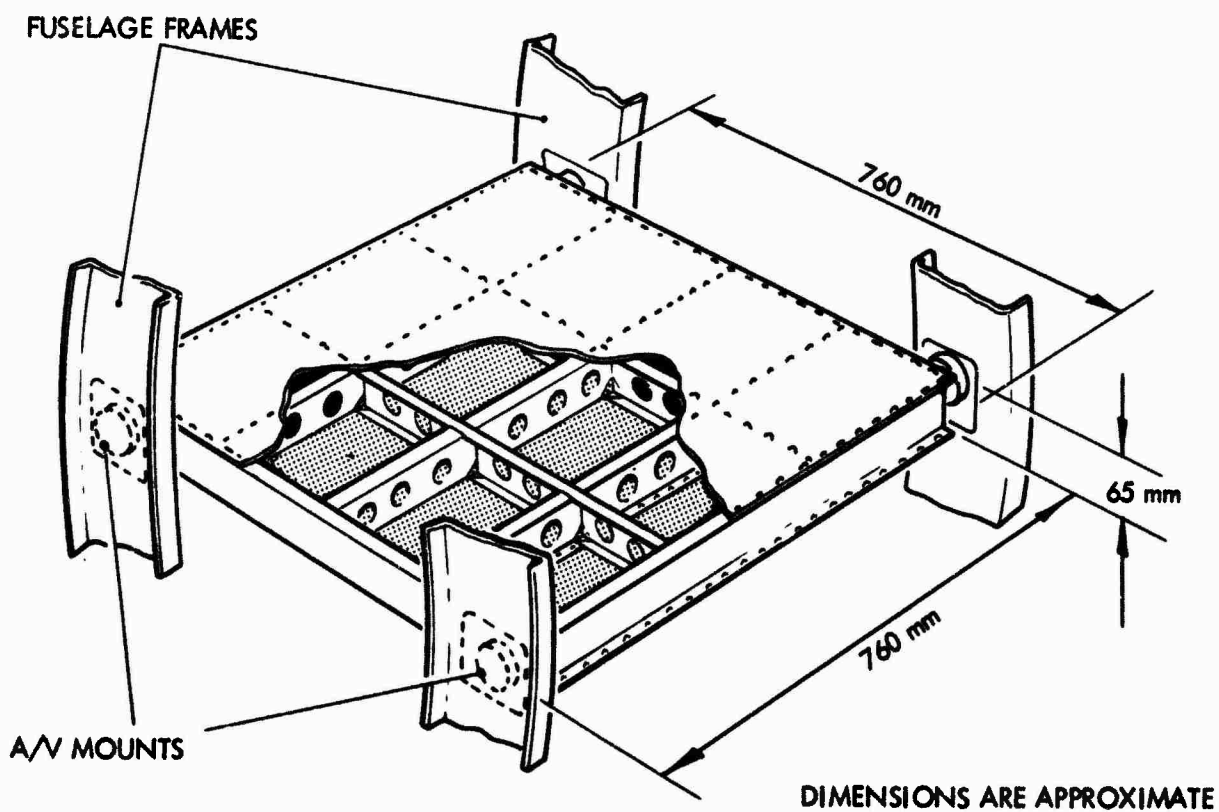


Fig.9 Avionic equipment shelf structure

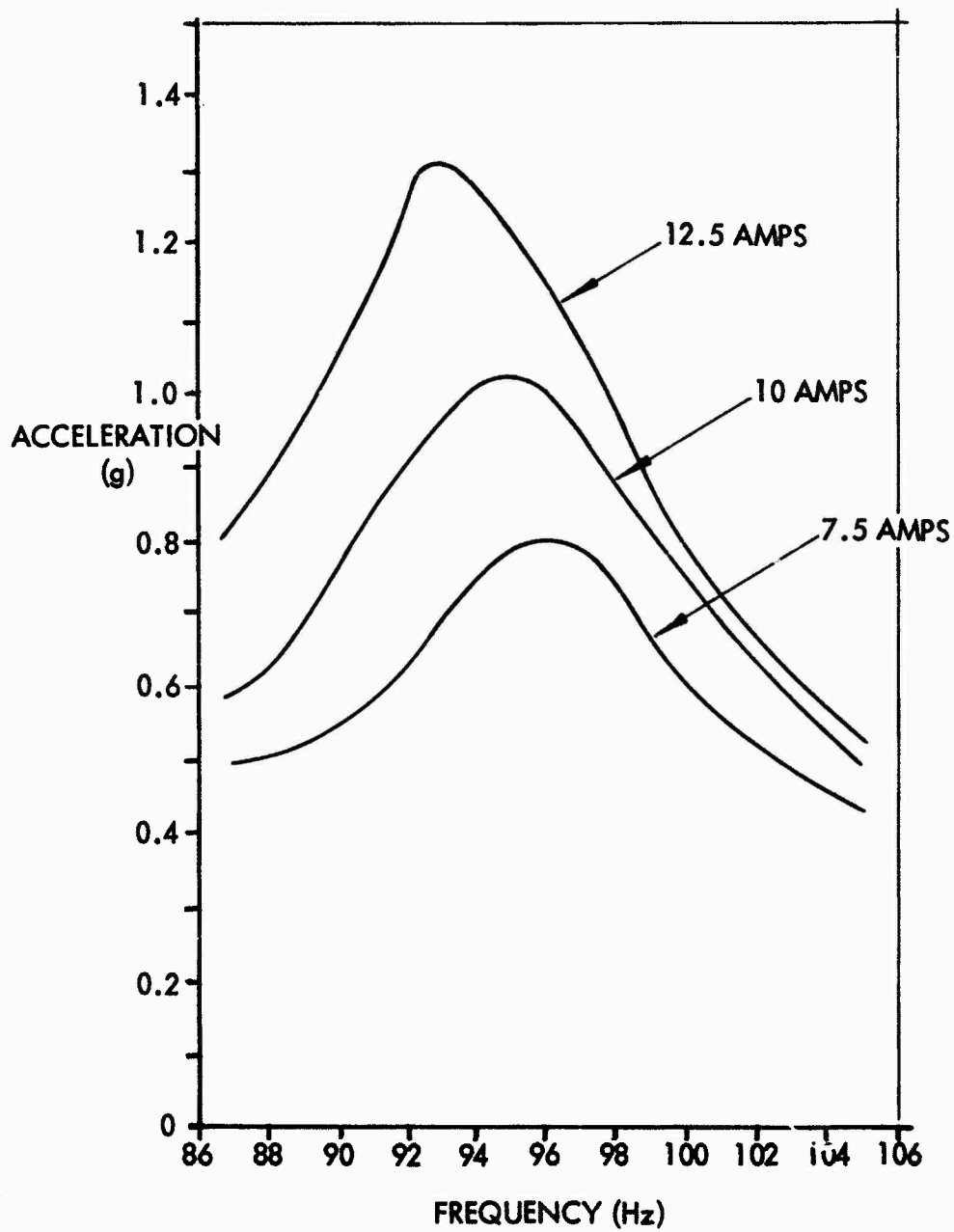


Fig.10 Avionic equipment shelf, accelerometer 13, response curves at three input levels

EFFECT OF STRUCTURAL DAMPING ON THE DYNAMIC RESPONSE OF SPACECRAFT

by

M. Degener
Institut für Aeroelastik
Deutsche Forschungs- und Versuchsanstalt für Luft- und Raumfahrt E. V.
Bunsenstraße 10, D-3400 Göttingen, Germany

SUMMARY

The magnitude of the dynamic response behaviour depends sensitively on the damping of a structure. In this paper the effect of structural damping on the dynamic response of spacecraft structures, especially satellites, is investigated. Special regard is given to the influence of intermodal damping coupling and of a non-linear damping behaviour.

Results of dynamic tests on satellite structures are studied, in order to get an insight into the general damping characteristics of spacecraft structures.

A method is presented to determine the dynamic response of a spacecraft structure, taking into account a non-linear damping behaviour, by means of a numerical, iterative procedure based on modal data.

LIST OF SYMBOLS

Scalars

d	damping coefficient
f	frequency
f_r	eigenfrequency
g	acceleration by gravity
$h(\tau)$	weighting function
j	imaginary unit
k	stiffness constant
m	discrete mass
q_r	generalized coordinate
t	time
u_b	foundation displacement
u_{r0}	reference amplitude
$x(t)$	input signal
$y(t)$	output signal
D_{rs}	generalized damping coefficient
$H(\omega)$	frequency response function
$ H(\omega) $	gain factor
K_{rr}	generalized stiffness
M_{rr}	generalized mass
P_r	element of vector \underline{P}
$X(\omega)$	Fourier transform of $x(t)$
$Y(\omega)$	Fourier transform of $y(t)$
ζ_r	modal damping factor
τ	time

$\varphi(\omega)$	phase factor
ω	circular frequency
ω_r	circular eigenfrequency

Vectors and Matrices

\underline{q}	vector of generalized coordinates
\underline{u}	vector of relative displacements
\underline{u}_a	vector of absolute displacements
\underline{L}	vector, defined by Eq. (12)
\underline{P}	vector, defined by Eq. (23)
\underline{Q}	generalized force vector
$\underline{X}(\omega)$	input vector
$\underline{Y}(\omega)$	output vector
$\underline{\Phi}_r$	normal mode shape
$\underline{0}$	null vector
\underline{A}	mass matrix
\underline{B}	damping matrix
\underline{C}	stiffness matrix
\underline{D}	generalized damping matrix
$\underline{H}(\omega)$	frequency response matrix
\underline{K}	generalized stiffness matrix
\underline{M}	generalized mass matrix
$\underline{\Phi}$	modal matrix

Indices

a	absolute
b	base
i, j	structural point indices
r, s	normal mode indices
0	amplitude
T	transposed
-1	inverse

Symbols

$\underline{\cdot}, \{ \}$	vector
$\underline{=}, []$	matrix
'	real part
"	imaginary part
\cdot	derivative with respect to time
$ $	absolute value

1. INTRODUCTION

Spacecraft structures are subjected to a lot of static and dynamic loads during launch and mission. It must be ensured that the dynamic response of the spacecraft to these loads will not lead to a damage of the structure or failure of any equipment units.

On the one hand this dynamic response is determined by the kind of exciting loads, e.g. the location, the magnitude or the frequency. On the other hand it is influenced by the dynamic characteristics of the structure itself. These are the mass distribution, the eigenfrequencies, the normal mode shapes and the damping. Especially the damping is a sensitive parameter for the magnitude of the dynamic response.

This paper intends to demonstrate the influence of the structural damping on the dynamic response of spacecraft structures.

After a brief review of the response properties of physical systems the determination of the dynamic response is demonstrated for the example of a satellite structure. The effect of damping coupling and damping non-linearity is discussed taking into account the results of dynamic tests on actual spacecraft structures. Finally, an iterative method for the performance of a non-linear dynamic response analysis is presented.

2. DYNAMIC RESPONSE PROPERTIES OF PHYSICAL SYSTEMS

In this chapter the basic relations of response properties of structural systems shall be described, as they are used later in this paper. For this purpose the structure is assumed as an ideal system, that means a linear system with constant parameters. The dynamic characteristics of such a system can be described by a weighting function $h(\tau)$, defined as the response of the system at any time to a unit impulse or Dirac delta input at a time τ before (Refs. 1, 2).

By means of this weighting function the output $y(t)$ of the system for any arbitrary input $x(t)$ is given by the convolution integral (Duhamel integral):

$$(1) \quad y(t) = \int_{-\infty}^{+\infty} h(\tau) x(t - \tau) d\tau \quad .$$

In the frequency domain the input and the output are described by their Fourier transforms:

$$(2a) \quad X(\omega) = \int_{-\infty}^{+\infty} x(t) e^{-j\omega t} dt \quad ,$$

$$(2b) \quad Y(\omega) = \int_{-\infty}^{+\infty} y(t) e^{-j\omega t} dt \quad .$$

By taking the Fourier transform of both sides of Eq. (1) the convolution integral reduces to simple algebraic expression:

$$(3) \quad Y(\omega) = H(\omega) X(\omega) \quad .$$

$H(\omega)$, which is the Fourier transform of the weighting function $h(\tau)$

$$(4) \quad H(\omega) = \int_{-\infty}^{+\infty} h(\tau) e^{-j\omega \tau} d\tau \quad ,$$

is called the frequency response function.

It describes the dynamic characteristics of the structural system in the frequency domain, while $h(\tau)$ describes them in the time domain. The relationship between the dynamic response of a structure and the excitation input is sketched in Figure 1 schematically.

The response of a structure to a dynamic input is determined by the frequency response function. Therefore the effect of structural characteristics (e.g. damping) on the dynamic response is equivalent to the effect of these characteristics on the frequency response function.

The frequency response function is generally a complex valued quantity, that can be written as a sum of a real and an imaginary part

$$(5) \quad H(\omega) = H'(\omega) + jH''(\omega)$$

or in terms of a magnitude and a phase angle

$$(6) \quad H(\omega) = |H(\omega)| e^{-j\phi(\omega)}$$

The absolute value

$$(7) \quad |H(\omega)| = \sqrt{H'^2(\omega) + H''^2(\omega)}$$

is called the gain factor or magnification function, while the phase angle

$$(8) \quad \phi(\omega) = \tan^{-1} \left(\frac{H''(\omega)}{H'(\omega)} \right)$$

is called the phase factor of the system.

A physical meaning of both values can be illustrated, if the input $x(t)$ is assumed to be a harmonic excitation with a circular frequency ω . Then the dynamic response of the system is harmonic, too, with the same frequency. As illustrated in Figure 2, in this case the gain factor $|H(\omega)|$ is the ratio of the output amplitude to the input amplitude, while the phase shift between input and output is equal to the phase factor $\phi(\omega)$.

The foregoing relationships were derived for a single input/single output system. For a multiple input/multiple output system Eq. (3) becomes:

$$(9) \quad Y_i(\omega) = \sum_j H_{ij}(\omega) X_j(\omega)$$

or in matrix notation

$$(10) \quad \underline{Y}(\omega) = \underline{H}(\omega) \underline{X}(\omega)$$

It should be noted, that the frequency response functions $H_{ij}(\omega)$ depend only on frequency and not on time or excitation level. If the system is non-linear, $\underline{H}(\omega)$ is also a function of the excitation input. This case will be discussed later in this paper.

3. FREQUENCY RESPONSE OF A SPACECRAFT STRUCTURE

The effect of structural damping on the dynamic response, which is equivalent to the effect on the frequency response functions $H_{ij}(\omega)$, shall be demonstrated for the example of satellite structures, which are excited at the base by the dynamic input of the launcher. This excitation results in a forced foundation motion input (s. Figure 3), as it is simulated experimentally in a shaker test.

Assuming structural linearity and viscous damping the equations of motion for such a system are

$$(11) \quad \underline{A} \ddot{\underline{u}}_a + \underline{B} \dot{\underline{u}} + \underline{C} \underline{u} = \underline{0}$$

\underline{A} , \underline{B} , \underline{C} are the mass matrix, damping matrix and stiffness matrix, respectively. \underline{u} is the displacement vector relative to the base of the structure, while \underline{u}_a is vector of the absolute displacements measured in a fixed coordinate system.

The difference vector of \underline{u}_a and \underline{u} is defined as

$$(12) \quad \underline{u}_a(t) - \underline{u}(t) = \underline{L} \underline{u}_b(t)$$

\underline{L} has unity elements for the structural degrees of freedom coinciding with the direction of excitation and zero elements for all others.

Introduction of Eq. (12) into Eq. (11) yields

$$(13) \quad \underline{A} \ddot{\underline{u}} + \underline{B} \dot{\underline{u}} + \underline{C} \underline{u} = -\underline{A} \underline{L} \ddot{\underline{u}}_b$$

Using modal coordinates q_r the deformation of the structure can be described by a sum of their normal mode shapes $\underline{\phi}_r$

$$(14) \quad \underline{u} = \underline{\phi}_1 q_1 + \underline{\phi}_2 q_2 + \underline{\phi}_3 q_3 + \dots = \underline{\phi} \underline{q}$$

After insertion of the above equation and premultiplication with the transposed of the modal matrix $\underline{\phi}^T$ Eq. (13) becomes:

(15)

$$\underline{M}\ddot{\underline{q}} + \underline{D}\dot{\underline{q}} + \underline{K}\underline{q} = \underline{Q}$$

with

$$\underline{M} = \underline{\Phi}^T \underline{A} \underline{\Phi} : \text{generalized mass matrix (diagonal),}$$

$$\underline{D} = \underline{\Phi}^T \underline{B} \underline{\Phi} : \text{generalized damping matrix (non-diagonal),}$$

$$\underline{K} = \underline{\Phi}^T \underline{C} \underline{\Phi} : \text{generalized stiffness matrix (diagonal),}$$

$$\underline{Q} = -\underline{\Phi}^T \underline{A} \underline{L} \ddot{u}_b : \text{generalized force vector.}$$

The matrices of the generalized masses and generalized stiffnesses are diagonal because of the orthogonality property of the normal modes. By the eigenfrequencies of the structure the following relation exists:

$$(16) \quad K_{rr} = \omega_r^2 M_{rr} = (2\pi f_r)^2 M_{rr}.$$

The generalized damping matrix is non-diagonal, in general. That means, that the normal modes are coupled by the damping of the structure.

With the modal characteristics f_r , Φ_r , M_{rr} , D_{rs} , which can be measured by means of a ground vibration test or modal survey test (Ref. 3), the frequency response can be determined, assuming a sinusoidal vibration input:

$$(17) \quad u_b = u_{b0} \sin \omega t.$$

Then the vibration response of the structure in generalized coordinates is

$$(18) \quad \underline{q} = \underline{q}'_0 \sin \omega t + \underline{q}''_0 \cos \omega t.$$

Introduction of Eqs. (17) and (18) into Eq. (15) and comparison of the coefficients of $\sin \omega t$ and $\cos \omega t$ yields the matrix equation:

$$(19) \quad \begin{bmatrix} \underline{K} - \underline{M}\omega^2 & -\underline{D}\omega \\ \underline{D}\omega & \underline{K} - \underline{M}\omega^2 \end{bmatrix} \begin{bmatrix} \underline{q}'_0 \\ \underline{q}''_0 \end{bmatrix} = \begin{bmatrix} \underline{\Phi}^T \underline{A} \underline{L} u_{b0} \omega^2 \\ \underline{0} \end{bmatrix}.$$

The unknown vectors \underline{q}'_0 and \underline{q}''_0 are given by the inverse of the matrix in the above equation

$$(20) \quad \begin{bmatrix} \underline{q}'_0 \\ \underline{q}''_0 \end{bmatrix} = \begin{bmatrix} \underline{K} - \underline{M}\omega^2 & -\underline{D}\omega \\ \underline{D}\omega & \underline{K} - \underline{M}\omega^2 \end{bmatrix}^{-1} \begin{bmatrix} \underline{\Phi}^T \underline{A} \underline{L} u_{b0} \omega^2 \\ \underline{0} \end{bmatrix}$$

and the dynamic response of the structure to the sinusoidal input is

$$(21) \quad \underline{u} = \underline{\Phi} \underline{q} = \underline{\Phi} \underline{q}'_0 \sin \omega t + \underline{\Phi} \underline{q}''_0 \cos \omega t.$$

The ratio of the output \underline{u} to the excitation u_b is the frequency response function $H(\omega)$. By means of $H(\omega)$ the dynamic response to an arbitrary time-dependent input can be determined.

The determination of the frequency response of a structure is a very time-consuming process, because the matrix in Eq. (20) has to be inverted for each exciting frequency ω . The investigations would be simplified essentially in case of modal damping, i.e. if the generalized damping matrix is diagonal, too. Then the elements of \underline{q}'_0 and \underline{q}''_0 in Eq. (19) are given by a set of decoupled equations

$$(22a) \quad (K_{rr} - M_{rr}\omega^2) q'_{r0} - D_{rr}\omega q''_{r0} = P_r \omega^2 u_{b0}$$

$$(22b) \quad D_{rr}\omega q'_{r0} + (K_{rr} - M_{rr}\omega^2) q''_{r0} = 0.$$

P_r is the r -th element of the vector

$$(23) \quad \underline{P} = \underline{\Phi}^T \underline{A} \underline{L}.$$

Eq. (22) can be solved for q'_{r0} and q''_{r0} :

$$(24a) \quad q'_{r0} = \frac{1 - (\omega/\omega_r)^2}{(1 - (\omega/\omega_r)^2)^2 + (2\zeta_r \omega/\omega_r)^2} \cdot \frac{P_r}{M_{rr}} \cdot \frac{\omega^2}{\omega_r^2} u_{b0},$$

$$(24b) \quad q''_{r0} = \frac{-2\zeta_r \omega/\omega_r}{(1 - (\omega/\omega_r)^2)^2 + (2\zeta_r \omega/\omega_r)^2} \cdot \frac{P_r}{M_{rr}} \cdot \frac{\omega^2}{\omega_r^2} u_{b0}.$$

The value P_r/M_{rr} is called the participation factor. ζ_r is the structural damping factor of the r -th normal mode

$$(25) \quad \zeta_r = \frac{D_{rr}}{2 M_{rr} \omega_r}$$

With the generalized coordinates the dynamic response \underline{u} of the structure is given and the frequency response functions can be calculated by dividing \underline{u} by u_b . The vector of the gain factors is

$$(26) \quad |\underline{H}(\omega)| = \sum_r \Phi_r \frac{P_r}{M_{rr}} \frac{\omega^2}{\omega_r^2} \frac{1}{\sqrt{(1 - (\omega/\omega_r)^2)^2 + (2\zeta_r \omega/\omega_r)^2}}$$

while the vector of the phase factors is

$$(27) \quad \underline{\varphi}(\omega) = \sum_r \Phi_r \tan^{-1} \left(- \frac{2\zeta_r \omega/\omega_r}{1 - (\omega/\omega_r)^2} \right)$$

It is evident, that neither the gain factors nor the phase factors are functions of the value of the input u_b , but only of the frequency of the excitation.

Eq. (26) shows, that the amplifications of the structure depend sensitively on the value of the structural damping factor ζ_r . Especially, if the exciting frequency is near to an eigenfrequency of the structure, then it is $\omega/\omega_r \approx 1$ and the amplification is approximately reciprocal to the damping factor. Therefore, the knowledge of the values of ζ_r is the most important factor in the determination of the dynamic response of the structure.

4. INFLUENCE OF DAMPING COUPLING

As it was shown in the last chapter, a diagonal generalized damping matrix does simplify the determination of the dynamic response essentially.

The most simple way to obtain such a diagonal matrix is by neglecting the off-diagonal values. The errors, which are involved by such a rough approximation, shall now be studied for a simple mathematical model and an actual satellite structure. By this means it will be possible to get an insight into the effect of damping coupling on the dynamic response.

4.1 SIMPLE MODEL

The simple mathematical model, which was used to study the effect of damping coupling, is shown in Figure 4. The modal characteristics of this model are given in this figure, too.

The model consists of five masses, which are connected by springs and dampers. The masses and spring constants are chosen so that there is almost a coincidence between the eigenfrequencies f_4 and f_5 , in order to investigate the effect of damping coupling in case of adjacent eigenfrequencies. The eigenvectors in the modal matrix $\underline{\Phi}$ are normalized so that the largest component has absolute value 1 cm.

In order to obtain large off-diagonal values in the generalized damping matrix, a strong local damper is placed between m_3 and m_4 . Consequently, many off-diagonal elements are of equal size or even greater than the appertaining diagonal elements, as can be seen from the generalized damping matrix \underline{D} in Figure 4. Among others the adjacent modes Φ_4 and Φ_5 are strongly coupled. The values of the modal damping factors have a realistic order of magnitude for spacecraft structures.

The model is excited by a foundation motion input $u_b(t)$. The frequency response functions for the five masses are plotted versus frequency in Figure 5 in linear scaling and in logarithmic scaling, respectively.

The plots show, that the differences are rather small. Especially, for the first three well separated eigenfrequencies the frequency response functions are nearly identical. Likewise, the influence of damping coupling can be neglected in the frequency ranges between the normal modes. Only in the case of adjacent eigenfrequencies there are some slight differences. Changes in damping configuration show the same effect.

Although this simple model cannot represent a complex spacecraft structure, it shows that the influence of damping coupling on dynamic response is not very significant in most cases. The results of a dynamic response analysis on an actual satellite structure shall confirm this.

4.2 SATELLITE STRUCTURE

The investigations were performed on the SMOP-satellite, a modern light weight structure, typical for communication satellites. This structure was developed by CONTRAVES at Zürich by order of the European Space Agency ESA for a Satellite Mass Optimization Programme (SMOP), which was part of the

The core structure of the SMOP-satellite was completed for dynamic testing with several mass dummies for equipment simulation. Figure 6 shows the overall dimensions of the structure, whose total mass was 720 kg.

Based on the results of a modal survey test (Ref. 6) a dynamic response analysis was performed (Refs. 7, 8). In the frequency range up to 120 Hz 35 normal modes were taken into consideration.

Similar to the foregoing chapter the analyses were performed with the complete generalized damping matrix as well as with a diagonalized damping matrix. For the first case a 70 times 70 matrix had to be inverted for each excitation frequency, as can be seen in Eq. (20). By using a diagonal generalized damping matrix the computing time (CPU-time) could be reduced to a fourth. Figures 7 and 8 show the results of these calculations for some structural points. Points No. 7 and 53 are upper platform points, while points No. 411 and 453 lie at the lower platform of the structure.

Again there are only slight differences between both frequency response functions in spite of large off-diagonal elements in the generalized damping matrix. The dynamic response of a structure can be approximated very well by using only the diagonal elements of the modal damping matrix. The influence of damping coupling on the dynamic response is rather small and can be neglected for most practical purposes. This effect, which was already described by other authors (Ref. 9), does simplify response investigations essentially.

It should be noted, that for purposes other than dynamic response (e. g. modal synthesis), damping coupling may be of greater importance and cannot be neglected.

5. DAMPING CHARACTERISTICS OF ACTUAL SPACECRAFT STRUCTURES

In this chapter the results of dynamic tests on several spacecraft structures will be analysed for their damping characteristics. The investigations include both shaker tests and modal survey tests. Comparing the test results of the different structures an amplitude dependent damping characteristic for spacecraft structures can be outlined.

5.1 SMOP-SATELLITE

In addition to modal survey test and dynamic response analysis a shaker test was performed on the SMOP-structure (Ref. 10). The structure was excited at its base with a constant acceleration amplitude. A typical result of this test is shown in Figure 9. Comparing it with the appertaining gain factor of the dynamic response analysis, which is also given in Figure 9, large discrepancies are recognizable. The dynamic amplifications differ very much, while the resonance frequencies are almost the same. This indicates, that the structural damping values are not constant but depend on the magnitude of the excitation. The response of the first axial mode, as to be seen in Figure 9, is about 3 g, while the acceleration of the same point was only 0.3 g in the modal survey test. Accordingly, the shaker test yielded higher amplifications, when the input level was reduced. The values of the structural damping factors ζ_r , measured in the modal survey test, lay between 0.5 % and 1 %, while the shaker test yielded values between 2 % and 3 %.

Comparing the results, it became evident, that the damping is not constant, but increases with an increase of the excitation. Consequently, the amplifications decrease with an increase of the excitation. Additionally, this non-linear damping characteristic is different for each mode. This is of course an important fact for dynamic response determination.

5.2 ITOS-SATELLITE

A modal survey test and a shaker test were performed on ITOS, a rectangular box-type satellite structure, too. The results are similar to those of the SMOP-structure. The modal survey test (Ref. 11) yielded damping values between 0.5 % and 2 %, but for some modes even much higher values were found.

In the shaker tests on ITOS (Refs. 12, 13) the input level was varied between 0.3 g and 2 g for damping investigations. It was found that the eigenfrequencies were almost independent from the excitation level, while the amplifications became smaller with greater input levels. On an average, an increase of the excitation by 60 % caused 20 % higher damping values.

5.3 GEOS-SATELLITE

The third spacecraft structure, whose test results shall be presented, is the GEOS satellite. The shaker test as well as the modal survey test yielded similar results concerning damping behaviour.

An example from the modal survey test (Ref. 14) is given in Figure 10. The response of a reference point is plotted versus force input for the first platform mode. The non-linear behaviour is evident. In general, damping values for ζ_r between 0.5 % and 2 % were measured for GEOS in the modal survey test.

The dependency between dynamic amplifications and acceleration input measured in the shaker test (Ref. 15) for the first lateral mode becomes obvious from Figure 11. For this mode the damping rises by 40 %, when the structure is excited with 0.5 g instead of 0.3 g. Similar results were obtained for other normal modes.

5.4 SUMMARY OF TEST RESULTS

There are much more spacecraft structures, of course, that have been tested with special regard to their damping behaviour, e.g. Refs. 16 and 17, but it would go beyond the scope of this paper to describe them all.

It can be stated however, that they have shown similar results as the above mentioned satellite structures. These can be summarized as follows:

- In general the damping of spacecraft structures is not constant, but increases with the dynamic input. Therefore a non-linear damping behaviour must be taken into account.
- This damping characteristic is different for each normal mode. It can be measured by means of a ground vibration test or modal survey test. In a shaker test the structure does not vibrate purely in its normal mode shapes, especially at higher modes.
- Typical damping values for spacecraft structures, especially satellites, are between 0.5 % and 5 %, but smaller or larger values are possible, too.

6. DYNAMIC RESPONSE IN CASE OF NON-LINEAR DAMPING

A method to determine the frequency response functions at the presence of a non-linear damping shall be presented now. The method is an iterative numerical approach. Because the influence of damping coupling on the dynamic response is rather small, as it was shown before, only a diagonal generalized damping matrix is taken into account for this approach.

Then the non-linear damping characteristic of the structure can be expressed by the structural damping factors as functions of appertaining reference displacements for each mode:

$$(28) \quad \zeta_r = \zeta_r(u_{r0}) \neq \text{const.}$$

The general characteristics of a linear and a non-linear damping behaviour are shown in Figure 12.

If the modal parameters, i.e. the eigenfrequencies, the normal mode shapes, the generalized masses and the amplitude-dependent damping factors are known, the frequency response functions for a certain input level can be determined iteratively as follows.

For an initial value of the exciting frequency ω the amplitudes of the real and imaginary parts of the generalized coordinates are calculated by Eq. (24). Hereby, arbitrary starting values are used for the structural damping factors ζ_r . By means of the generalized coordinates and the normal mode shapes the displacement vector \underline{u} of the structure can be evaluated from Eq. (14). With \underline{u} the displacements u_{r0} of the reference points are given, too, and new damping factors $\zeta_r(u_{r0})$ can be calculated for each mode.

In a second step the displacements are determined with these new damping factors. This iterative computing process is continued, until the damping factors do no longer change significantly. Then the gain factor and the phase factor of the frequency response function are calculated.

For the exciting frequency $\omega + \Delta\omega$ it is convenient to use the last damping factors as new starting values. In general, these starting values will be so close to the actual values, that only some or even no iterations are necessary. That means, that this iterative non-linear dynamic response analysis can be performed for a certain input level nearly as fast as in case of a linear damping behaviour, which is of course an important advantage of this method.

A non-linear dynamic response analysis, as described above, was performed on the SMOP-satellite structure with an assumed non-linear damping characteristic, because this had not been measured during the modal survey test. Comparing the results of the modal survey test and the shaker test the following damping characteristic seemed to be close to reality:

$$(29) \quad \zeta_r = 0.005 + 0.125 \frac{1}{\text{cm}} u_{r0} \quad .$$

This is illustrated in Figure 13. For simplicity this damping characteristic was assumed to be equal for all modes.

Some results of this analysis are given in Figures 14 and 15, respectively. Figure 13 shows the gain factor of a upper platform point (grid point No. 7), while Figure 15 shows it for a lower platform point (grid point No. 411). The results are presented for a base excitation in x-, y- and z-direction.

The figures show clearly the effect of non-linear damping increasing with the excitation input. In the frequency ranges remote from eigenfrequencies the influence of damping non-linearity is rather small, but in the neighbourhood of eigenfrequencies the dynamic amplifications decrease rapidly with increasing

excitation. This effect is verified by the results of the dynamic tests described in the last chapter.

7. CONCLUSIONS

In this paper the effect of structural damping on the dynamic response of spacecraft was investigated. Special topics were damping coupling and damping non-linearity.

The analytical investigations and the experimental results of dynamic tests on spacecraft structures have shown:

- The effect of damping coupling is rather small and can be neglected for most practical purposes. By this the determination of the dynamic response is simplified essentially.
- In general, the damping of spacecraft structures cannot be described by a constant damping coefficient, because damping increases with the excitation level. Therefore, a non-linear damping must be taken into account.
- The damping characteristic is different for each normal mode.

8. REFERENCES

- [1] BENDAT, J. S.
PIERSOL, A. G. Random Data: Analysis and Measurement Procedures.
New York, J. Wiley & Sons, 1971.
- [2] FÖRSCHING, H. W. Grundlagen der Aeroelastik.
Berlin/Heidelberg/New York, Springer-Verlag, 1974.
- [3] BREITBACH, E. A Semi-Automatic Modal-Survey Test Technique for Complex Aircraft
and Spacecraft Structures.
Proc. Third Testing Symposium, Frascati 22-26 October 1973,
ESRO SP-99, pp. 519-528.
- [4] SCHNEITER, H.
SCHIBLI, U.
WIJKER, J. J.
STROEVE, A. Development of a Mass Optimized European Communication Satellite
Structure.
Denver, Colorado, 27-29 May 1975,
AIAA Paper No. 75-783.
- [5] VILLALAZ, P. A.
SCHIBLI, U. SMOP II - Dynamic Analysis and Testing of a Mass-Optimized Satellite
Structure.
ESA SP-133 (1977) pp. 1-19.
- [6] BREITBACH, E.
DEGENER, M.
SIMM, H. -J. Modal Survey Test on the SMOP-Structure.
DFVLR-AVA-Report IB 253 - 75 C 16 (1975).
- [7] DEGENER, M. Dynamic Response Analysis on Spacecraft Structures Based on Modal
Survey Test Data Including Nonlinear Damping.
ESA SP-121 (1976) pp. 25-36.
- [8] DEGENER, M. Bestimmung der dynamischen Antwort von Raumfahrtstrukturen auf der
Grundlage eines Standschwingungsversuchs unter Berücksichtigung einer
nichtlinearen Dämpfung.
DLR-FB 77-17 (1977), (also published as ESA TT-431).
- [9] HASSELMANN, T. K. Modal Coupling in Lightly Damped Structures.
AIAA Journal, Vol. 14, No. 11, November 1976, pp. 1627-1628.
- [10] IABG/TRV Vibration Test on SMOP II.
Report No. 75-10-3136 (1975).
- [11] BREITBACH, E.
KIESSLING, F.
NIEDEBAL, N. Modal Survey Tests on the Spacecraft Structure ITOS RCA 1/69 701.
ESA CR-573 (1976).
- [12] LOUP, J. Recherche sur l'amortissement en vibration des structures de satellite,
Rapport d'essais.
ESRO CR-634 (1975).

- [13] LOUP, J. Recherche sur l'amortissement en vibration des structures de satellite, Rapport final. ESRO CR-633 (1975).
- [14] KIESSLING, F. Modal Survey Test on the Structural Model of the GEOS-Satellite. SIMM, H. -J. DFVLR-AVA Report IB 253 - 75 C 03 (1975).
- [15] DORNIER SYSTEM Input for GEOS Structure. Development Test Review, 1974.
- [16] GIRARD, A. Réponse harmonique d'une structure de satellite à une table vibrante. LOISEAU, H. L'Aéronautique et l'Astronautique, No. 52 (1975) pp. 49-56.
- [17] CARRINGTON, H. G. A Survey of Data on Damping in Spacecraft Structures, Final Report. OTTENS, H. H. ESRO CR-539 (1975).

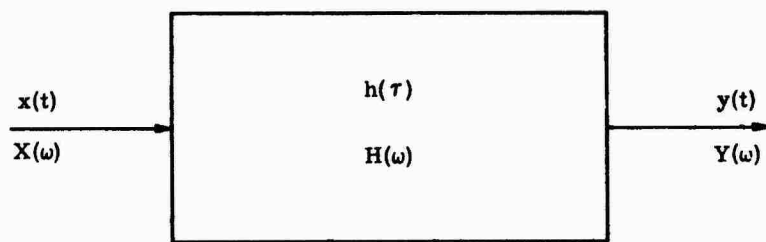


Figure 1: Input/Output-Model

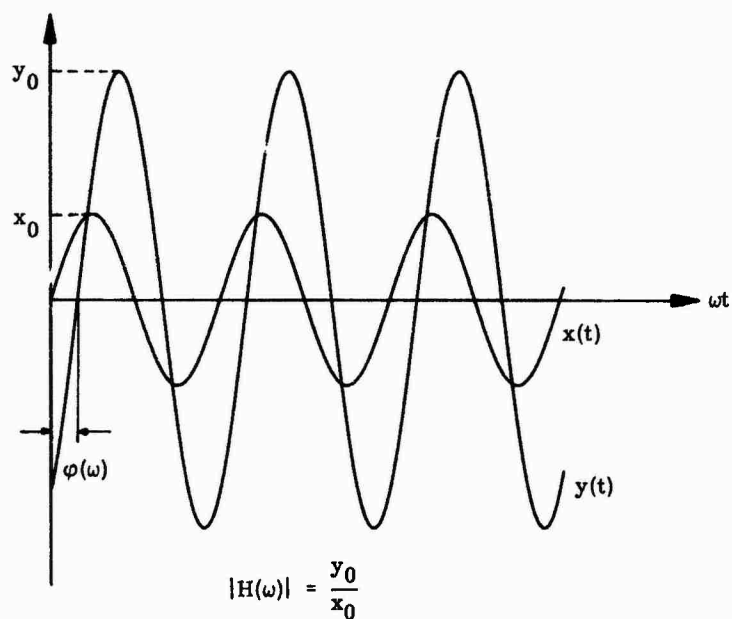


Figure 2: Gain Factor and Phase Factor

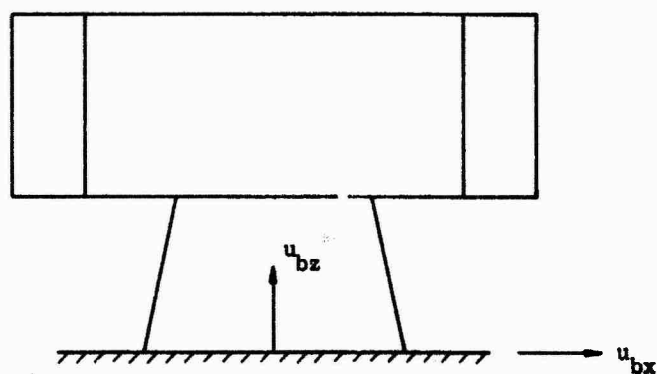
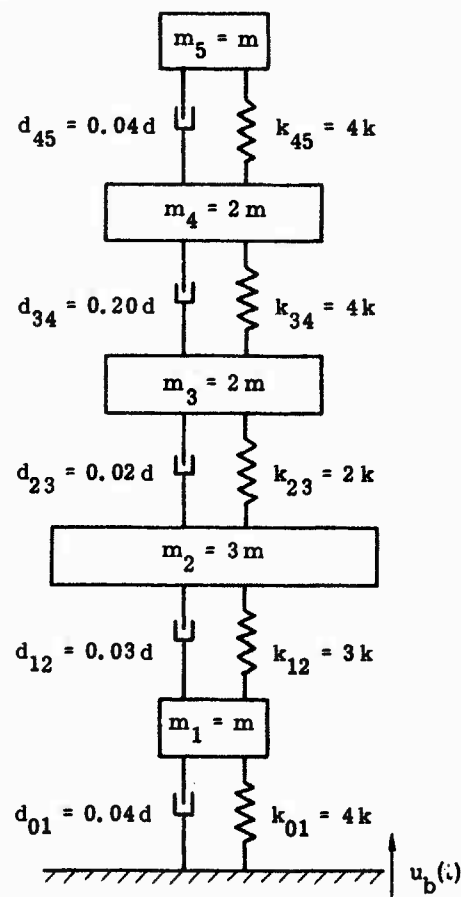


Figure 3: Satellite Structure with Foundation Motion Input



$$\frac{k}{m} = 1 \frac{\text{Rad}^2}{\text{sec}^2}$$

$$\frac{d}{\sqrt{mk}} = 1$$

Modal Characteristics:

Eigenfrequencies:

$$\begin{aligned} f_1 &= 0.06016 \text{ Hz} \\ f_2 &= 0.17125 \text{ Hz} \\ f_3 &= 0.29790 \text{ Hz} \\ f_4 &= 0.43032 \text{ Hz} \\ f_5 &= 0.43738 \text{ Hz} \end{aligned}$$

Matrix of Eigenvectors:

$$\underline{\Phi} = \begin{bmatrix} 0.2308 & 0.5135 & 0.2057 & -0.5923 & 1 \\ 0.5276 & 1 & 0.2398 & 0.0613 & -0.1840 \\ 0.8597 & -0.0070 & -0.9692 & 0.3698 & 0.1248 \\ 0.9643 & -0.5064 & 0.1241 & -0.8276 & -0.1920 \\ 1 & -0.7127 & 1 & 1 & 0.2162 \end{bmatrix} \text{ cm}$$

Generalized Masses:

$$\begin{aligned} M_{11} &= 5.2260 \text{ m cm}^2 \\ M_{22} &= 4.2846 \text{ m cm}^2 \\ M_{33} &= 3.1242 \text{ m cm}^2 \\ M_{44} &= 3.0054 \text{ m cm}^2 \\ M_{55} &= 1.2532 \text{ m cm}^2 \end{aligned}$$

Generalized Damping Matrix:

$$\underline{D} = \begin{bmatrix} 0.0092 & -0.0084 & 0.0183 & -0.0200 & -0.0053 \\ -0.0084 & 0.0895 & -0.0874 & 0.0957 & 0.0253 \\ 0.0183 & -0.0874 & 0.3007 & -0.2095 & -0.0554 \\ -0.0200 & 0.0957 & -0.2095 & 0.4491 & 0.0607 \\ -0.0053 & 0.0253 & -0.0554 & 0.0607 & 0.1107 \end{bmatrix} \text{ d cm}^2$$

Modal Damping Factors:

$$\begin{aligned} \zeta_1 &= 0.23\% \\ \zeta_2 &= 0.97\% \\ \zeta_3 &= 2.57\% \\ \zeta_4 &= 2.76\% \\ \zeta_5 &= 1.61\% \end{aligned}$$

Figure 4: Simple Mathematical Model

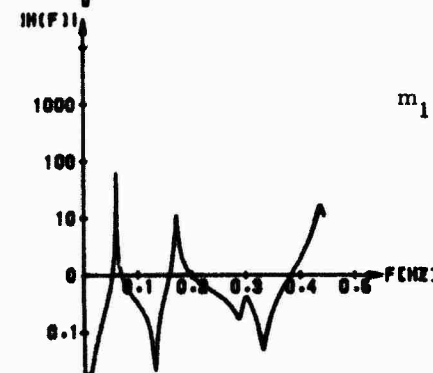
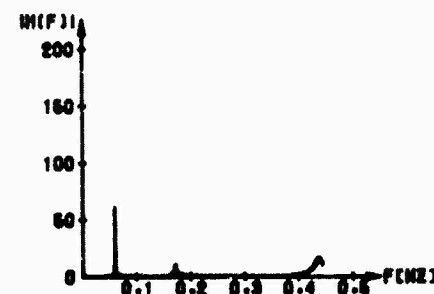
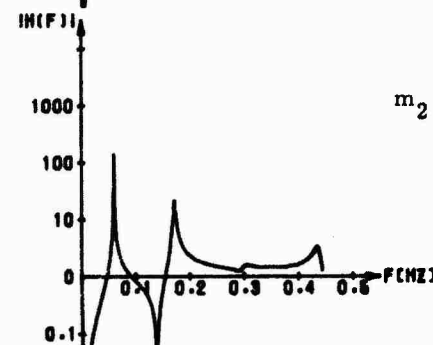
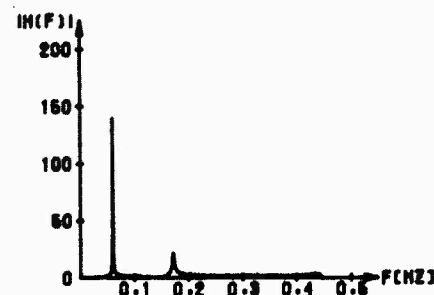
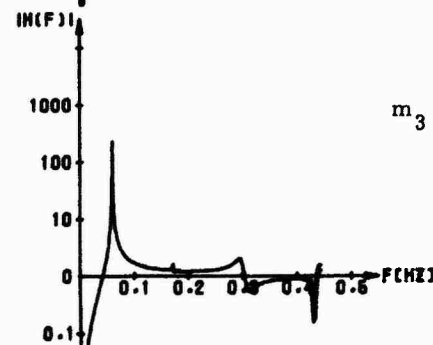
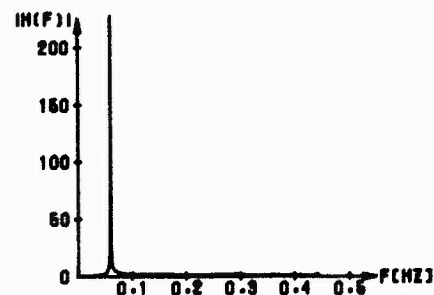
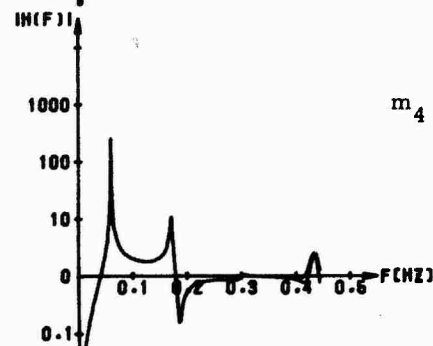
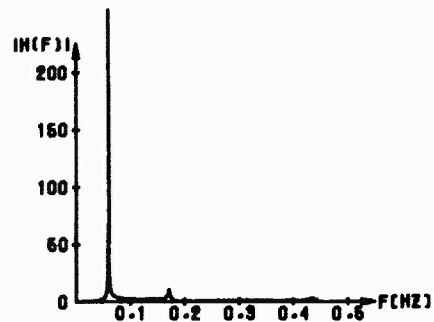
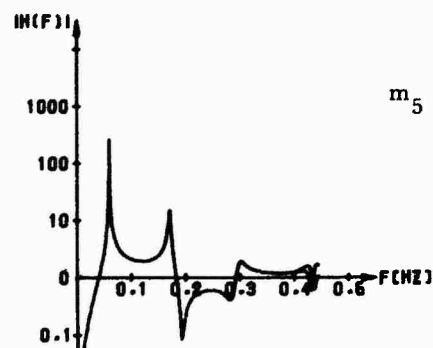
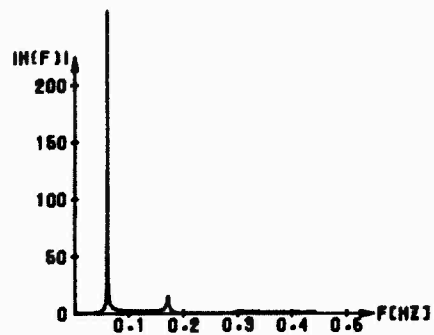


Figure 5: Dynamic Response of Simple Model in Case of Modal Damping and Damping Coupling

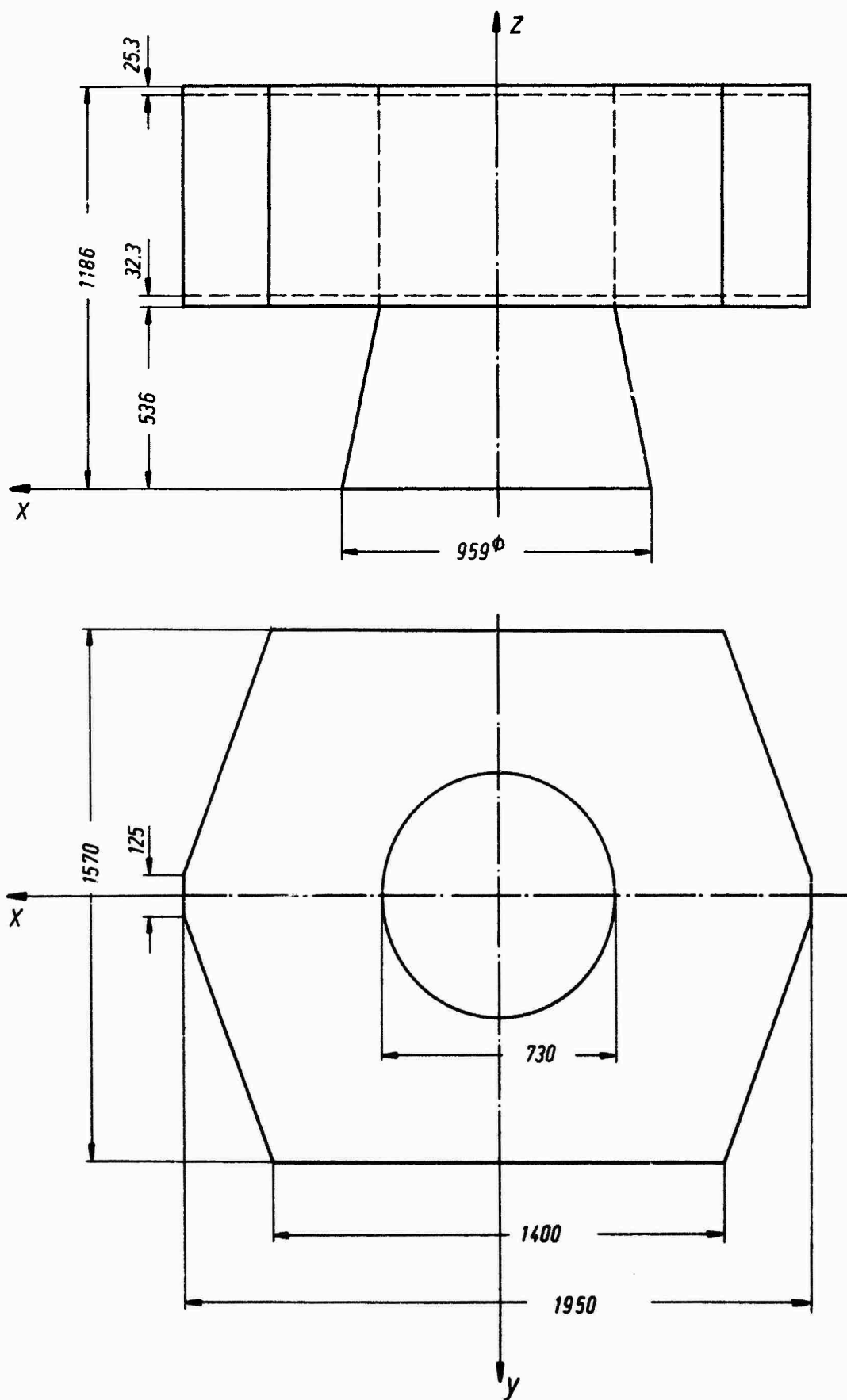


Figure 6: Dimensions of the SMOP Satellite Structure (in mm)

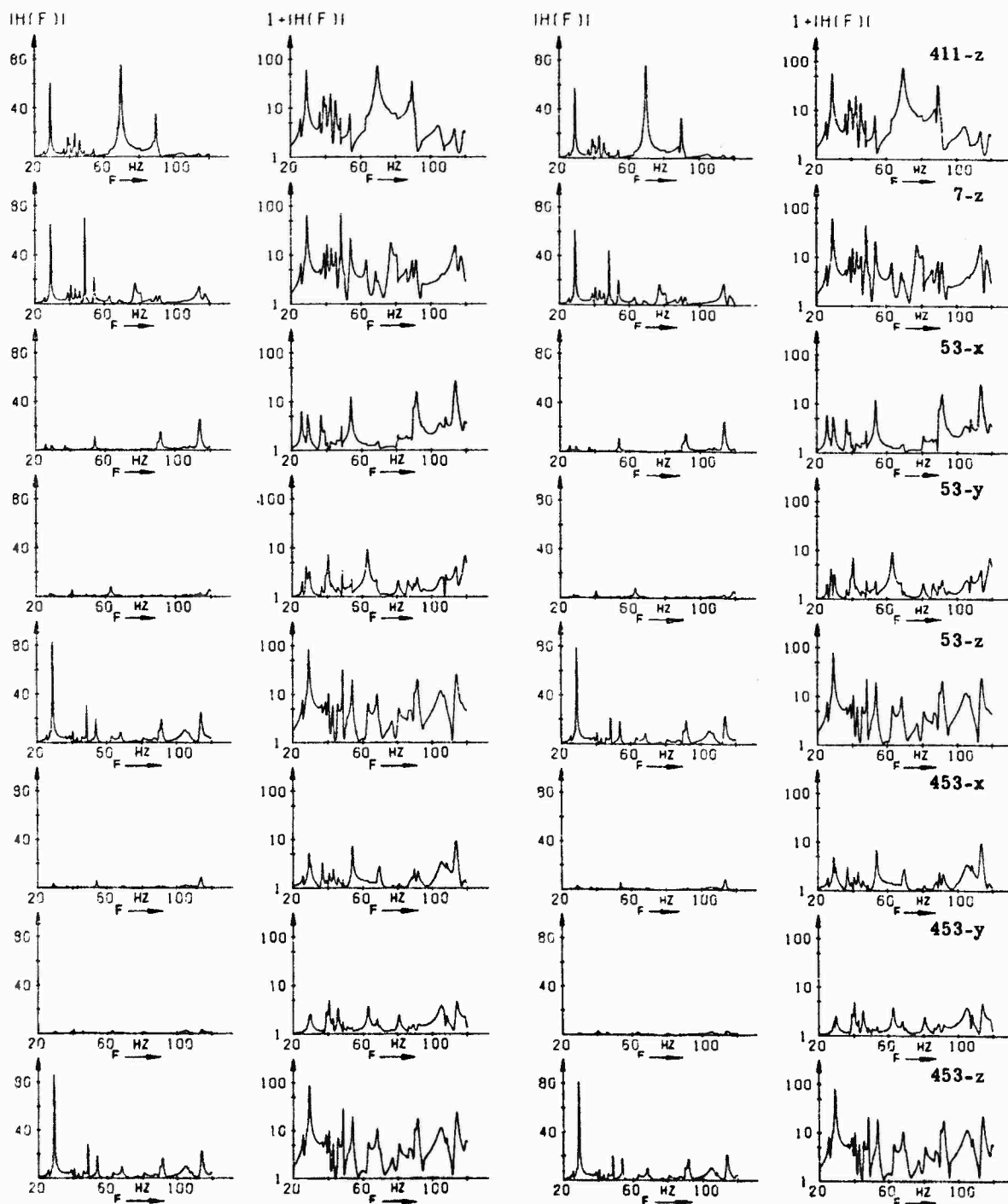
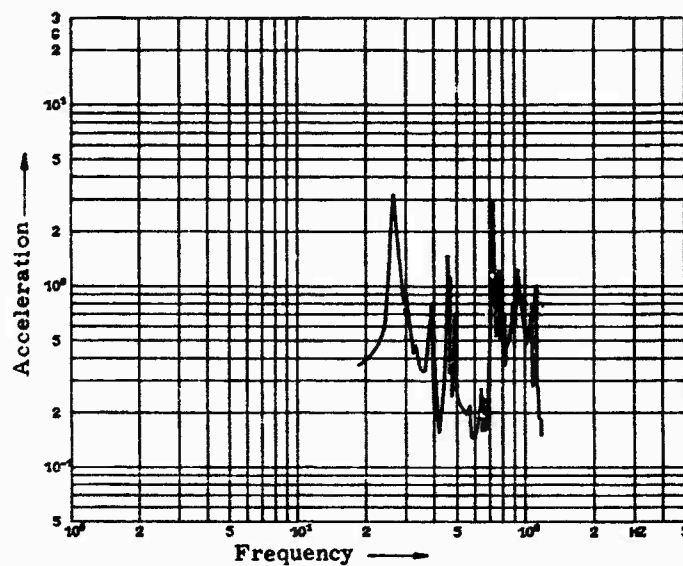
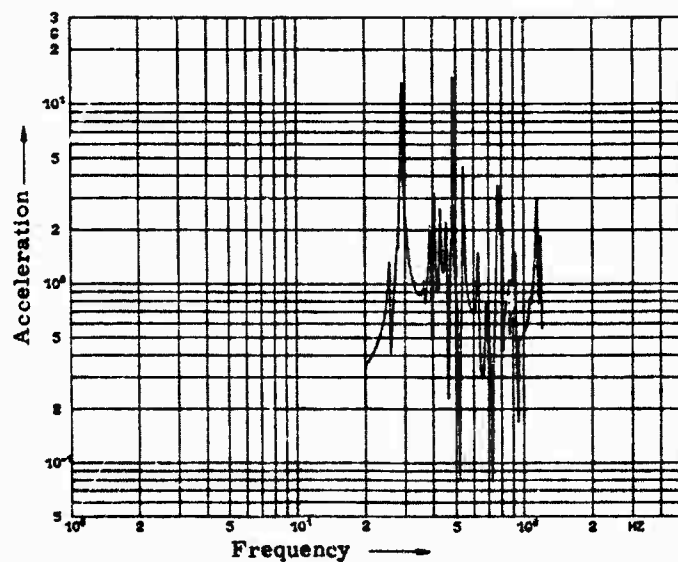


Figure 7: Dynamic Response of the SMOP-Structure to Axial Excitation in Case of Modal Damping

Figure 8: Dynamic Response of the SMOP-Structure to Axial Excitation in Case of Damping Coupling



Dynamic Response Measured in the Vibration Test
(Axial Excitation of 0.2 g; Grid Point No. 7)



Dynamic Response Calculated on Basis of
Modal Survey Test Data

Figure 9: Comparison of Calculated and Measured
Dynamic Responses of the SMOP-Structure

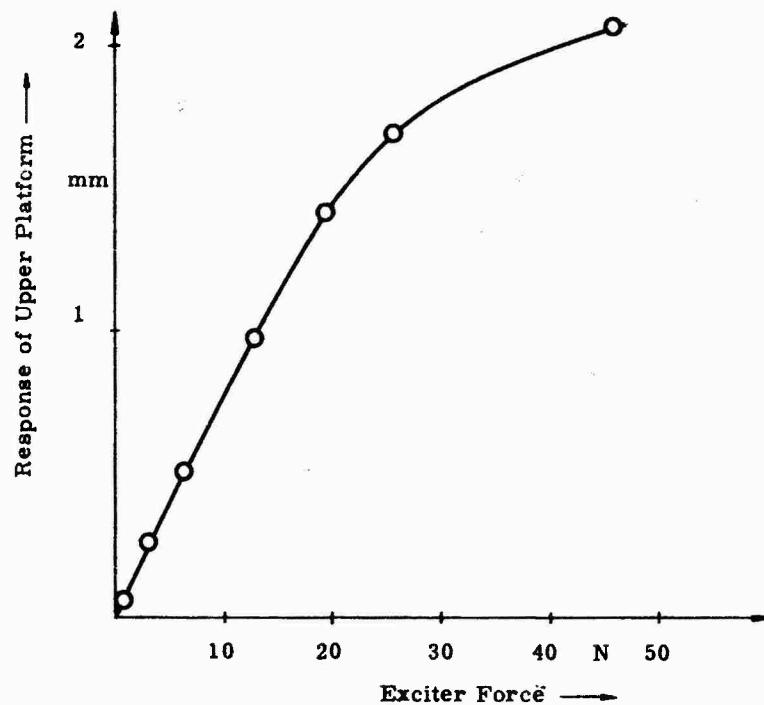


Figure 10: Non-linear Behaviour of the GEOS-Satellite
Measured in the Modal Survey Test

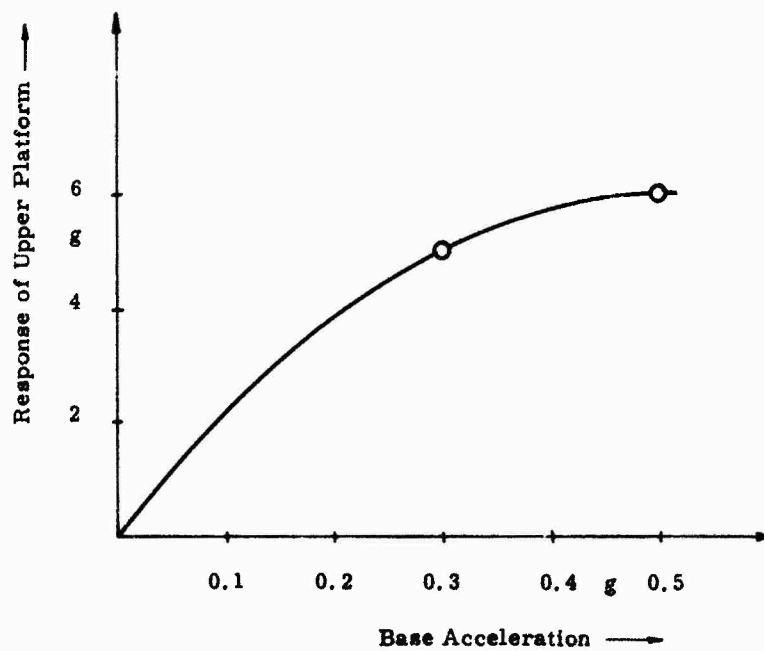


Figure 11: Non-linear Behaviour of the GEOS-Satellite
Measured in the Vibration Test

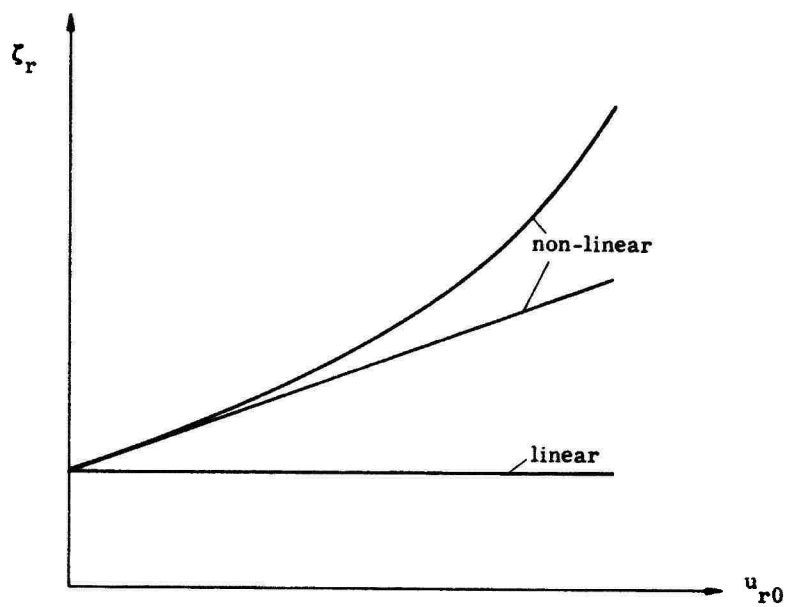


Figure 12: Structural Damping Characteristics

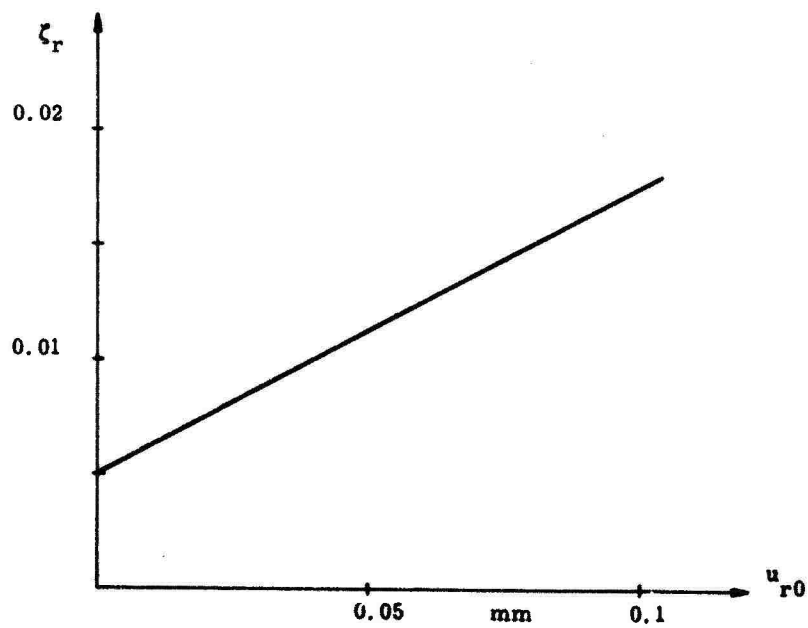


Figure 13: Assumed Non-linear Damping Characteristic for the SMOP-Structure

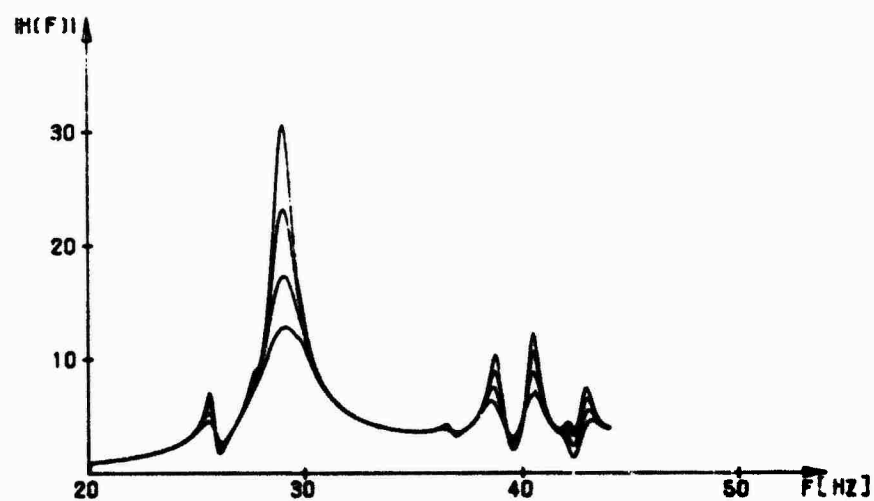
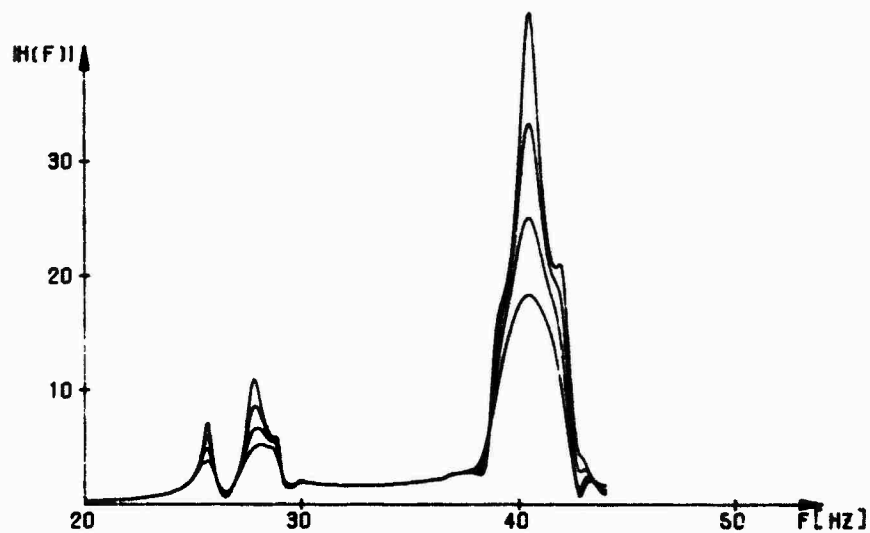
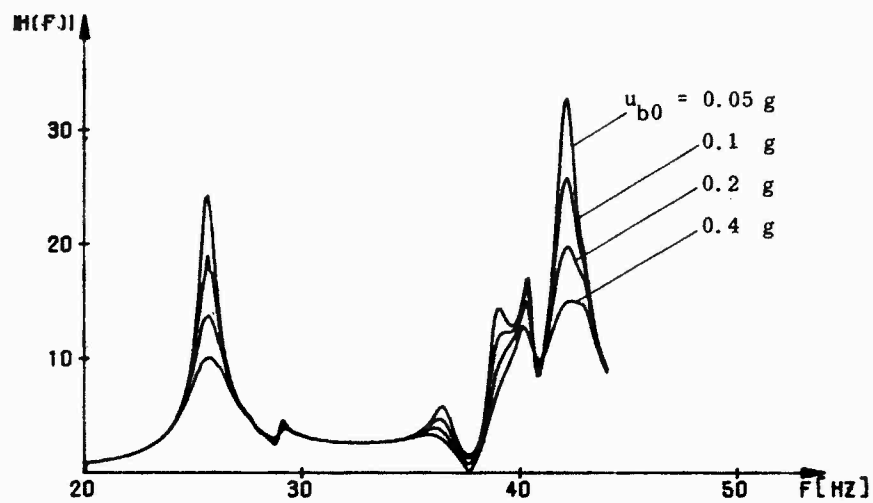


Figure 14: Non-linear Dynamic Response of the Upper Platform of the SMOP Satellite Structure to Base Excitation in x-, y- and z- Direction

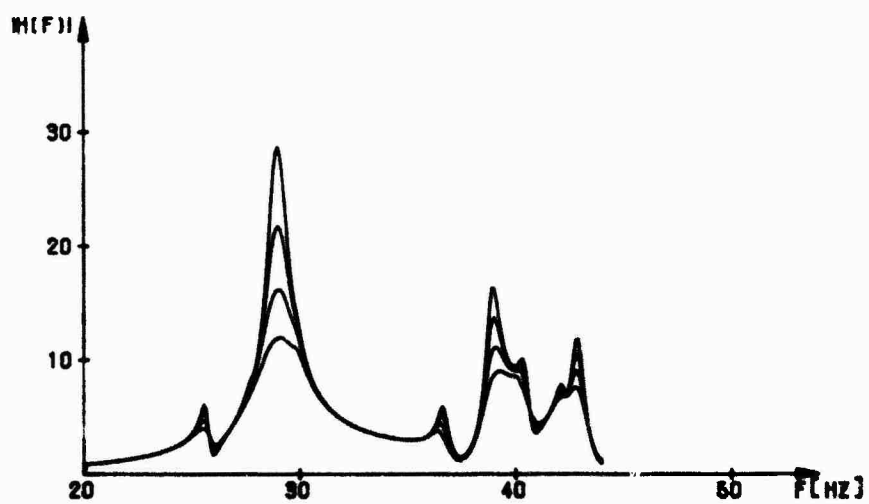
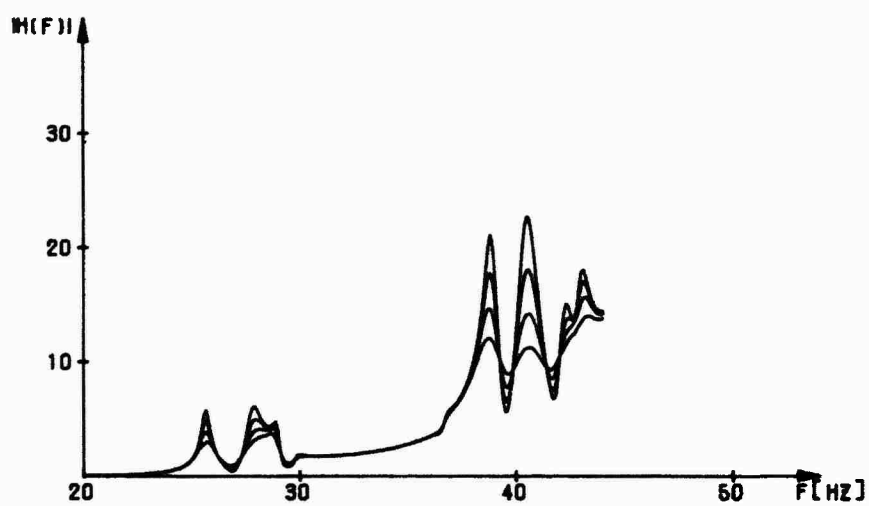
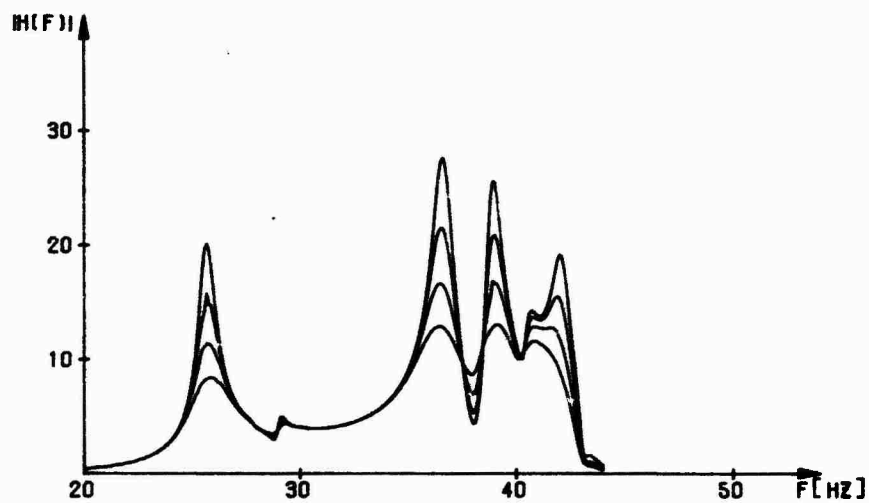


Figure 15: Non-linear Dynamic Response of the Lower Platform of the SMOP Satellite Structure to Base Excitation in x-, y- and z-Direction

by
B. K. Wada
Manager, Applied Mechanics Technology
D. T. DesForges
Engineer

Jet Propulsion Laboratory
California Institute of Technology
4800 Oak Grove Drive
Pasadena, California 91103 USA

SUMMARY

Damping plays a significant role in the prediction of spacecraft structural responses and loads, which in turn influence the structural design. In this study, the methods used by the aerospace community to incorporate damping in the structural analysis are summarized. A discussion of experiences and procedures relating to damping for recent spacecraft is presented. Methods for modal testing and experimental determination of damping, the use of discrete dampers and other topics are treated briefly. Lastly, a collection of damping data for recent spacecraft and related hardware is provided in the appendix.

INTRODUCTION

A study has been conducted recently to determine how the concept of damping has been treated in the analysis and design of spacecraft in the U.S., and to present available damping data for recent spacecraft and other flight hardware. The information contained herein is the result of experiences at the Jet Propulsion Laboratory and discussions with representatives from the U.S. aerospace industry.

The discussions here are limited to damping considerations which influence the spacecraft structural design in the low frequency regime, i.e., that frequency range in which analytically derived eigenvalues and eigenvectors are considered representative of the structural dynamic behavior, and in which they can be verified by experimental techniques such as modal testing [1-3].

A discussion relating how damping has been treated in structural analysis historically precedes a summary of experiences from recent spacecraft. Other factors relating to damping such as experimental determination of damping values and recent trends in modal testing are described briefly. The appendix presents a compendium of experimentally observed damping values for a number of spacecraft and related hardware.

BACKGROUND

Since the beginning of the U.S. space program, the increasing complexity of spacecraft structures, the development of digital computers, and the development of finite element computer programs (and matrix methods in general) have resulted in the discretization of continuous structures into lumped parameter systems, yielding the fundamental structural dynamics problem

$$M\ddot{x} + C\dot{x} + Kx = f(t), \quad (1)$$

in which x is the vector of discrete coordinates,
 $f(t)$ is the vector of forcing functions, and

M , C , K are the system mass, damping, and stiffness matrices, assembled from the individual matrices of structural finite elements.

The mass and stiffness characteristics of a structural element can be derived fairly accurately by analytical means or simple experiments. Initial attempts to experimentally determine the individual elements of the damping matrix for various structural configurations proved difficult because of uncontrollable factors such as manufacturing variability and hardware tolerances. Thus, efforts to determine directly the elements of the structural damping matrix were largely discontinued. When discrete damping devices were incorporated into the spacecraft design, thorough experimental determination of the element characteristics were necessary to include their effects in the structural analysis.

As the matrices of equation (1) became larger, and the coordinates became more highly coupled, the direct solution of the equations of motion became prohibitively time-consuming and expensive. Since structural integrity in the low frequency regime is normally the prime design concern, the approximation resulting from representing equation (1) with a small set of generalized coordinates, a small set of eigenvectors as

distributed coordinates, is often both adequate and appropriate. Such a transformation substantially reduces the problem size, and, with the proper assumptions about the damping matrix, C, the resulting equations of motion are uncoupled. Using the eigenvectors of the undamped free vibration problem, i.e.,

$$M\ddot{x} + Kx = 0 \quad (2)$$

Caughey [4,5] showed that if C were proportional to some power expansion of M or K, the equations of motion of the damped vibration problem would be uncoupled. Substituting into equation (1) the transformation

$$x = \phi q, \quad (3)$$

where ϕ is the matrix of the eigenvectors (mode shapes) of equation (2) and q is the vector of time dependent generalized coordinates, and pre-multiplying by the transpose of ϕ results in the modal equations of motion

$$\bar{M} \ddot{q} + \bar{C} \dot{q} + \bar{K} q = \phi^T f(t) \quad (4)$$

in which \bar{M} , \bar{C} , and \bar{K} are the diagonal generalized mass, damping, and stiffness matrices. If the eigenvectors of equation (2) are normalized such that the generalized mass matrix becomes an identity matrix, and the assumption of modal (viscous) damping is introduced, the equation of motion for the i th generalized coordinate in equation (4) becomes

$$\ddot{q}_i + 2\zeta_i \omega_i \dot{q}_i + \omega_i^2 q_i = Q_i \quad (5)$$

where ζ_i is the modal damping ratio for mode i ,

ω_i is the i^{th} modal frequency, and

Q_i is the i^{th} modal generalized force

The approximations involved in recording equation (5) were well within the level of solution accuracy attainable for spacecraft structures which did not have discrete dampers or applied damping materials. Also, the modal damping ratio defined in this manner can be determined easily using the modal testing and data reduction techniques which have been developed in the aerospace community. Although modal damping values obtained through testing vary with different types of structures, frequency, and mode shape, and can be nonlinear with amplitude, conservative estimates of modal damping can often be provided to both analyst and designer, based on past experiences from testing of similar structures.

As an alternative to the assumption of modal damping, the equations of motion (1) can be uncoupled without restrictions on the damping matrix, C, other than that it be symmetric, by selecting a different set of generalized coordinates, as described by Foss [6]. Equation (1) is re-formulated in first order form

$$A\dot{\eta} + B\eta = F(t), \quad (6)$$

in which

$$A = \begin{bmatrix} 0 & M \\ M & C \end{bmatrix} \quad B = \begin{bmatrix} -M & 0 \\ 0 & K \end{bmatrix} \quad \eta = \begin{bmatrix} \dot{x} \\ x \end{bmatrix} \quad F(t) = \begin{bmatrix} 0 \\ f(t) \end{bmatrix} \quad (7)$$

the complex eigenvalue problem is solved, orthogonality conditions for the eigenvectors are imposed, and the resulting modal equations are uncoupled in terms of the generalized modal displacements. At the time Foss developed this method, response analysis software utilizing complex modes was not generally available, and verification of complex eigenvalues and eigenvectors through testing was beyond the state-of-the-art. Even today the use of complex modes and frequencies in spacecraft response analysis is limited; the assumption of modal damping and the use of the normal modes obtained from the undamped free vibration problem are prevalent in the industry, because of the simplicity in the problem formulation, ease of verification by modal test, and the reasonable accuracy of analysis results.

DAMPING IN COMPONENT MODE SYNTHESIS

As the matrices in equation (1) became even larger due to increased complexity of spacecraft structures and their finite element representations, solutions to the eigenvalue problem of equation (2) became more costly. Hurty [7] introduced the method of component mode synthesis, in which the structure is sub-divided into components or sub-systems as shown in Figure 1. The modal characteristics of the total structure are synthesized from the modal characteristics of the individual components. Thus, a number of small eigenvalue problems are solved; the number of degrees-of-freedom in each component is reduced by selecting a smaller number of displacement functions (mode shapes).

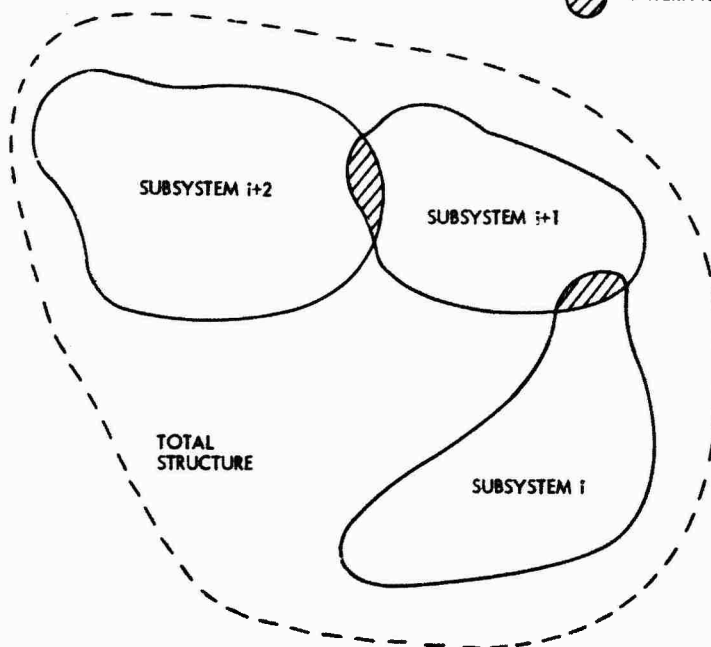


Figure 1. Idealization for Component Mode Synthesis

An apparent advantage of the approach is that modal damping values could be estimated and confirmed by testing for smaller subsets of the total structure. Theoretically, the structure could be divided into structural subsets for which the same type or level of damping behavior was expected, or for which damping values were available from previous spacecraft, subject, of course, to the restrictions imposed by analysis software, the desire to minimize the number of retained degrees-of-freedom, and ease of experimental verification.

The equations of motion for unconnected components in terms of the discrete physical coordinates are identical to equation (1). To derive the reduced set of modal equations for the total structural system, three transformations are necessary. The first relates the component discrete coordinates to the generalized coordinates of the normal modes and other displacement functions for a particular component as in equation (3). The second transformation is required to introduce compatibility at the interfaces of connected components, and the final transformation involves the normal modes of the total system. Thus, for each component, repeating equation (3),

$$x = \Phi q, \quad (8)$$

and, combining the remaining two transformations,

$$q = \Gamma \Psi \eta \quad (9)$$

in which Γ is a rectangular matrix defining the required inter-component displacement compatibility,

Ψ is the matrix of system normal mode shapes, and

η is the vector of time-dependent system modal coordinates.

If the system mode shapes are normalized to yield a generalized mass matrix which is an identity matrix, the system modal equations of motion become

$$I\ddot{\eta} + C'\dot{\eta} + \Omega^2\eta = f'(t) \quad (10)$$

where $D^T \Phi^T M \Phi D = I$

$$D^T \Phi^T C \Phi D = C'$$

$$D^T \Phi^T K \Phi D = \Omega^2$$

$$D = \Gamma \Psi$$

(11)

Ω^2 is a diagonal matrix whose elements are the squares of the undamped natural frequencies of the system, and C' is the system modal damping matrix which is generally a full matrix.

One of the central issues in the component mode synthesis method is the determination of the elements of C' . If the off-diagonal elements of C' are neglected, as they often are to simplify structural dynamic analysis, the diagonal elements can be written

$$C'_{ii} = 2\zeta_i \omega_i \quad (12)$$

where ζ_i is the fraction of critical damping for the i^{th} system mode. The system modal damping ratios could be determined from modal testing of the entire structure, but often such full-scale testing occurs just prior to flight; the only data available to the analyst may be from prior component testing.

A number of techniques for synthesizing the system modal damping matrix C' have been developed with the assumption that the modal damping matrices of individual components are available from component testing or can be estimated to a reasonable accuracy. However, damping values associated with displacement functions other than component normal modes (e.g., static, attachment, rigid degrees-of-freedom) can only be estimated since experimental methods for their determination do not exist.

Kana and Huzar [8], extending earlier work by Chang [9], investigated the validity of relating the energy dissipated by damping in component vibration to the peak kinetic energy in a system mode for a given modal displacement. They derived system modal damping ratios proportional to the ratio of the sum of the component dissipation energies to the total system kinetic energy for particular modes. The test articles included discrete dampers and were intended to simulate the Shuttle Orbiter and booster. Both were tested as individual components and as a coupled system. The system modal damping ratios predicted from the component tests using their empirical law were within 10 percent to 20 percent error of those obtained from the coupled system test.

Approaches similar to this, utilizing some measure of the participation of component modes in the overall system modes via an energy expression, have been used popularly for quite some time. Such methods normally result in a diagonal system modal damping matrix, neglecting any off-diagonal damping coupling terms which may exist. There is some measure of justification for neglecting the off-diagonal terms. If the system modes are well-spaced in frequency, the energy that may be transferred between two adjacent modes through damping will be small, and hence the off-diagonal terms of the system damping matrix associated with these modes will be small. Also, if component modal damping ratios are not known accurately, or, in the absence of component test data, have been assigned rather arbitrarily, the increase in analytical complexity necessitated by retention of inaccurate off-diagonal terms in the system damping matrix may not be warranted.

In determining the modal damping values of a component from modal test and applying the results to the analysis, a complication can arise related to the boundary conditions imposed on the structural component. Components may be tested or analyzed with boundaries which are fixed, free, or with boundary conditions somewhere in between these extremes. For free boundaries, component modes consist of both rigid body modes and normal modes, while in the case of fixed boundaries, constraint modes are also included. The constraint modes define the structural motion at the interfaces of adjacent components and are typically specified in terms of static displacement functions. In either case, representation of damping near the component interfaces is bound to be poor, according to Hasselman [10]. For free boundaries, a large number of component modes are required to adequately represent the true strain energy distribution near the boundaries in the system modes, and most probably the dissipative behavior also. When static displacement functions are used for the constraint modes in the case of fixed interfaces, damping information is lacking for them, thus leading to inadequate representation of damping for the system modes. The use of component interfaces having artificial mass loading can alleviate the difficulty to some extent, as discussed by Goldenberg and Shapiro [11].

Hasselman [10] has developed an approach for synthesizing the system modal damping matrix from component test data which uses full (rather than diagonal) component modal damping matrices. His argument is that since most structures are in fact lightly damped, the undamped normal modes typically used in analysis are close relatives to the actual damped modes measured during test, with differences being attributed to minor variations in phase. And with the test equipment available today, these small phase variations are measurable, and can potentially provide more information about structural damping than simple decay data. Pursuing this thought, he develops a first-order perturbation algorithm using measured frequency response functions to refine the measured component modes and to derive the elements of the full component modal damping matrices, which in turn are combined as in equation (11) to yield the system modal damping matrix. Although the method has shown promise in its application to experimental data from early Space Shuttle model tests performed at Langley Research Center, it has not been used in industry as yet.

EXPERIENCES FROM RECENT SPACECRAFT

Some of the experiences gained from recent spacecraft in the determination and use of damping in analysis are summarized here to illustrate some of the considerations which have influenced spacecraft structural analysis and design.

For the structural dynamic analysis of the Viking spacecraft as for others, the spacecraft was subdivided into various components as described previously. Estimates of the overall system modal damping ratios were obtained by establishing the kinetic energy contributions of the various component modes to the kinetic energy of a given system mode. The system modal damping ratio was thus a weighted sum of the component modal damping ratios, each weighted by its kinetic energy fraction.

Typically, when a spacecraft model is delivered to the launch vehicle contractor for a coupled spacecraft/launch vehicle loads analysis, the modal damping values to be used for the coupled system modes are derived from the individual spacecraft and launch vehicle modal damping matrices or are specified based on available flight data or engineering judgment. For payloads utilizing the Titan launch vehicle, the uncoupled, diagonal spacecraft and Titan modal damping matrices are pre- and post-multiplied by the coupled system modal matrix to obtain a non-diagonal system modal damping matrix, the off-diagonal terms of which are eliminated for the loads analysis. In contrast, the current procedure for transient loads analysis for Space Shuttle payloads is to assign a modal damping value of one percent of critical for all payload modes. Similarly, for the HEAO A and B spacecraft, one percent of critical damping was assigned to all spacecraft/launch vehicle modes in the loads analysis. For the loads analysis of the tele-operator spacecraft, modal damping values of 0.5 percent were assigned to all system modes. At Goddard Space Flight Center, the general procedure is to assign one percent of critical modal damping for all loads analysis. If, at the time of the verification loads analysis (which occurs after the spacecraft modal test), loads problems with payloads are anticipated, damping values obtained from the modal test are incorporated into the loads analysis. For the Delta launch vehicle, a value of 1.5 percent of critical damping is assumed for all coupled system modes. Modal and response data measured in-flight have provided a sound basis for this value. Use of this constant value for all modes is felt to yield slightly conservative results, since certain local modes may exhibit higher damping values.

Although the influence of damping for highly transient events such as liftoff may be minimal, it can be significant for other flight events such as POGO. For the first flight of the Titan/Centaur a Viking dynamic simulator was flown [12]. The Viking dynamic simulator was composed of several interconnected subsystems with appropriate mass and stiffness properties to simulate accurately the fundamental lateral, longitudinal, and torsional modes of the Viking spacecraft. Damping was not simulated. In the loads analysis, use of the damping values shown in Figure 2 for the coupled system modes predicted a stable POGO response. However, during flight, telemetered data indicated that the system

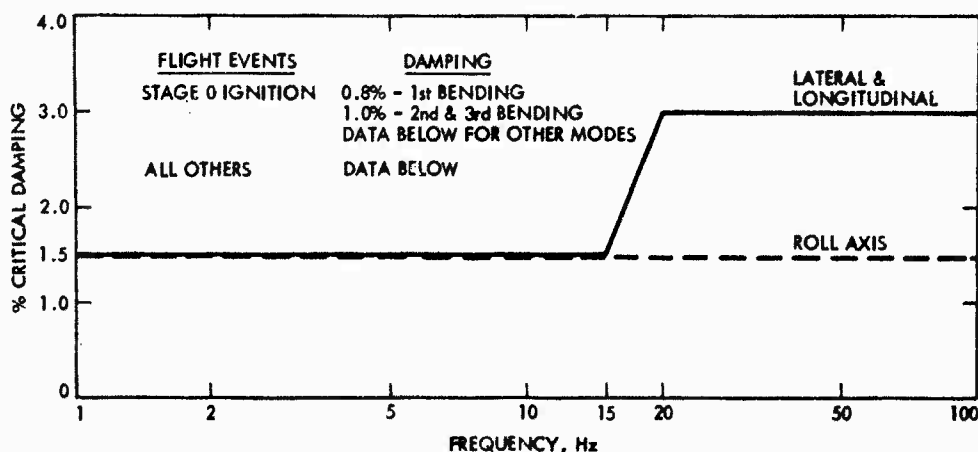


Figure 2. Damping Schedule for Titar Launch Vehicle

was on the verge of POGO instability; subsequent incorporation of the damping data from flight into the analysis revealed a very low margin of safety for non-occurrence of POGO.

The ultimate verification of the overall coupled loads analysis process is the comparison of available flight data with predicted results. On Viking [13 - 15] an excellent set of flight instrumentation [16, 17] was employed, extensive analyses were performed to predict responses, a good analytical model (verified by test) was available, a flight-verified model of the launch vehicle for certain flight events was available, and a collection of computer software which had been verified by repeated use on previous flight programs was used. Since most of the events analyzed were transient in nature, the responses were not as dependent on damping as they would have been were a steady-state sine input used. Figures 3 and 4 illustrate the excellent correlation between flight and analysis for both Viking [18] and Voyager [19] for a typical flight event. The analysis did include allowances for flight-to-flight scatter.

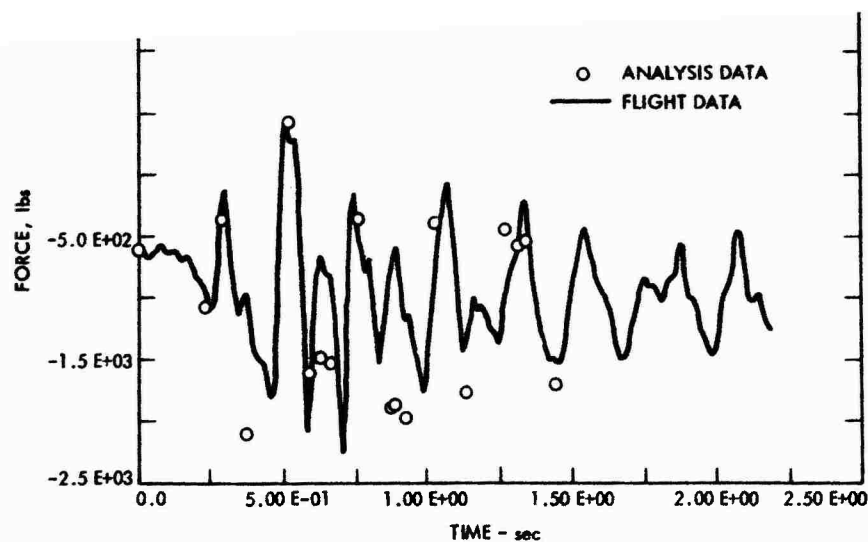


Figure 3. Viking Flight/Analysis Correlation - Typical Member Load

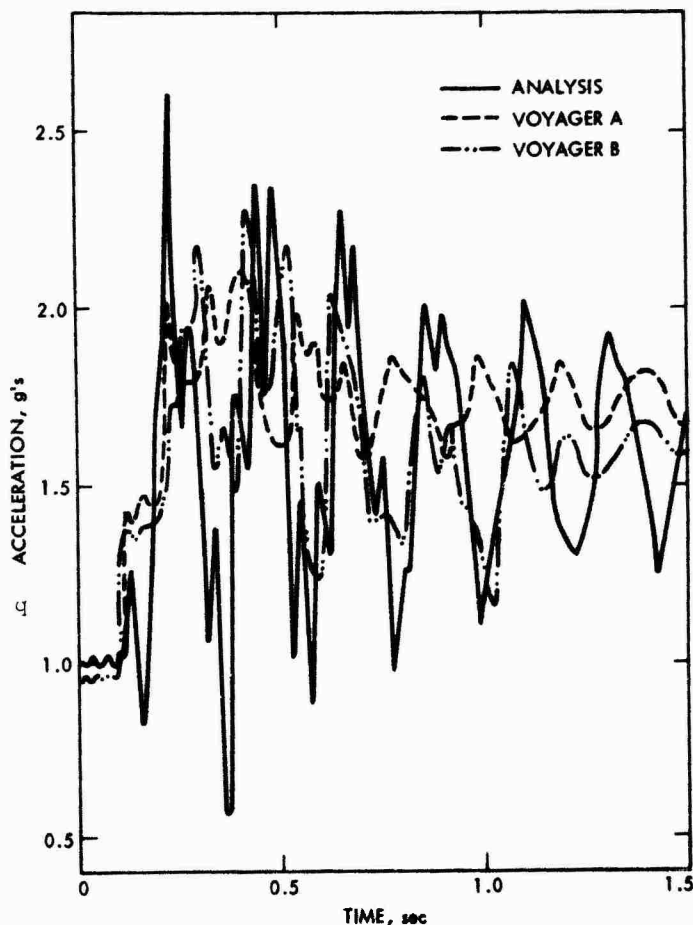


Figure 4. Voyager Flight/Analysis Correlation - Interface Acceleration

OTHER CONSIDERATIONS

Modal Test/Data Reduction

In the past few years, the options available for the modal testing of spacecraft structures have expanded, owing to the advances in test control hardware and data reduction software as well as the use of single-point random and transient excitations. The Voyager spacecraft was tested using conventional multi-point sine dwell (MPSD) excitation and single-point random excitation to provide a basis for comparison of these two modal testing approaches. In a study exploring cost reduction of dynamic testing through the use of simpler test procedures and more rapid data reduction methods, Hanks et al [20] used the Voyager test data to assess the relative merits of four different test/data reduction combinations for obtaining modal information. The approach for reducing the sine dwell data is outlined in [1]. The single-point random test data were analyzed using two different curve-fitting approaches (in the frequency domain) (SPR-1, SPR-2) and a time domain method (ITD) developed by Ibrahim [21, 22]. The results for the modal frequencies and damping ratios for all four methods shown in Tables 1 and 2 indicate considerable variations between methods in many instances. Also, the MPSD approach can result in missing modes, particularly those involving remote components.

Test Article

Another factor which must be considered in estimating damping values for analysis is the test article from which such estimates are derived. Often tests are performed on engineering models or dynamic simulators, rather than on flight hardware. In such cases, mass and stiffness distributions can be matched fairly accurately to the flight article to yield the correct eigenvalues and eigenvectors. However, the representation of damping in such structures may be inadequate. Wiring harness, electronic equipment and mounting hardware, and other items which do not add to the structural integrity of the spacecraft can contribute directly to the damping in the structure, suggesting that judgment must be exercised in estimating flight vehicle

Table 1. Voyager Modal Frequencies - Hz

Mode No.	MPSD	SPR-1	SPR-2	ITD	Mode Description
1	10.5-10.7	10.92	10.97	10.95	1st Bending, Y
2	10.9-11.3	11.29	11.19	11.19	1st Bending, X
3	17.1-17.2	17.25	17.18	17.25	1st Torsion
4	20.8		21.50	21.80	RTG
5				23.12	2nd Torsion + LECP
6	22.6-23.5	23.37	23.25	23.30	2nd Torsion
7				24.10	2nd Torsion + Magnetometer
8	25.4-26.2			25.13	2nd Bending, X
9	26.5-27.2	26.21	26.42	26.05	2nd Bending, Y
10	27.3		27.97	27.81	Scan Platform, Axial
11			30.83	30.92	Antenna, Z
12	31.1	30.81	31.57	31.56	3rd Bending Y, + Antenna
13			32.80	32.50	3rd Bending X
14				32.98	3rd Torsion
15				33.96	LECP, RTG Torsion
16				34.74	Scan Platform, X
17	35.2			35.94	RTG, X
18			37.09	36.81	Science Appendage, X
19			38.70	38.75	Science, Appendage, X, Antenna
20				39.14	Science Appendage, X, Z Rotation
21	39.6-40.3	40.04	39.90	40.24	Science Appendage, X
22			40.77	40.64	Science Appendage, X
23		42.13	42.20	42.21	Antenna Rotation, X
24				44.59	Tank Rot., Science Appendage
25		44.80	44.80	44.80	Hydrazine Tank Rotation
26	46.3		45.60	45.65	1st Axial
27				48.04	Tank, Appendage
28	52.9			50.69	RTG, Scan Platform, Z

damping if damping values have been measured on an engineering model. Also, the amplitude level at which tests are conducted can influence the magnitude of the observed damping. The damping is the result of many complex mechanisms in addition to material damping such as slippage and friction in joints. At lower amplitudes, the damping may result primarily from internal material damping, while at higher amplitudes, the contributions of joint friction and slippage and even air damping may be significant. Further, the variation of damping with amplitude may not be linear so that caution should be used in extrapolating damping values to account for different amplitude levels in analysis.

Discrete Dampers

When discrete linear or non-linear damping elements exist in the structure, they are typically isolated into subsystems for the analysis. The discrete dampers' characteristics are modeled in detail as functions of acceleration, velocity, displacement, temperature or other relevant parameters. The displacement functions for the other subsystems are chosen in the normal manner of component mode synthesis, and the equations of motion can be re-formulated as in equations (6) and (7). Any nonlinear damping functions can be represented as forcing functions on the right-hand side of equation (7). The equations can then be solved via analog simulation or with special purpose digital computer programs. Gayman [23] developed an orifice damper to attenuate solar panel vibrations on the Ranger spacecraft, and achieved good correlation between analysis predictions and measured responses during testing and flight.

Table 2. Voyager Modal Damping - C/C_c

Mode No.	MPSD	SPR-1	SPR-2	ITD
1	0.012-0.015	0.013	0.020	0.016
2	0.012-0.015	0.024	0.019	0.069
3	0.026-0.031	0.027	0.033	0.024
4	0.027-0.032		0.030	0.031
5				0.002
6	0.015-0.023	0.023	0.025	0.024
7				0.021
8	0.015-0.018			0.092
9	0.011-0.028	0.016	0.018	0.100
10	0.013-0.014		0.019	0.062
11			0.028	0.019
12	Poor Wave Form	0.029	0.025	0.021
13			0.034	0.036
14				0.030
15				0.024
16				0.023
17	0.018-0.022			0.070
18			0.026	0.022
19			0.040	0.029
20				0.047
21	0.011-0.016	0.016	0.030	0.023
22			0.017	0.012
23		0.003	0.002	0.001
24				0.012
25	0.026-0.036	0.008	0.008	0.009
26	0.026-0.036		0.010	0.018
27				0.024
28	0.012			

Air Damping

Studies have been performed to evaluate the influence of air on the total damping exhibited in a vibrating structure. Stephens and Scavallo [24] investigated the effects of air damping on simple beam-plate models and achieved good correlation with Stoke's theory. But little has been done to assess the impact of air damping on modal damping values obtained from full-scale spacecraft modal or vibration tests. Recently, Boeing Aerospace Company performed structural damping tests for graphite/epoxy members of a metering truss for the Space Telescope in air and vacuum to determine the significance of air damping. Their results indicated that air damping for the graphite/epoxy tube specimen was negligible. General Electric Company has tested a flexible roll-up solar array (approximately 250 ft²) in both air and vacuum and found considerable differences in damping values, at least in the first mode; the resonance was at about 0.25 Hz with 0.10 fraction of critical damping in air, 0.004 in vacuum. A rather complete discussion of the damping properties of materials in air can be found in Lazan [25].

Estimation of Payload Response

Normally for determination of design loads, damping information is required to estimate the payload response in a loads analysis. A technique for estimating preliminary design loads which has been used in the past and is currently being updated by detailed analysis, test, and flight measurements is to estimate the spacecraft response as a function of its effective mass, using curves such as those in Figure 5, which have been evolving for the past 10 years. Responses thus obtained should yield fairly conservative loads estimates for preliminary design purposes.

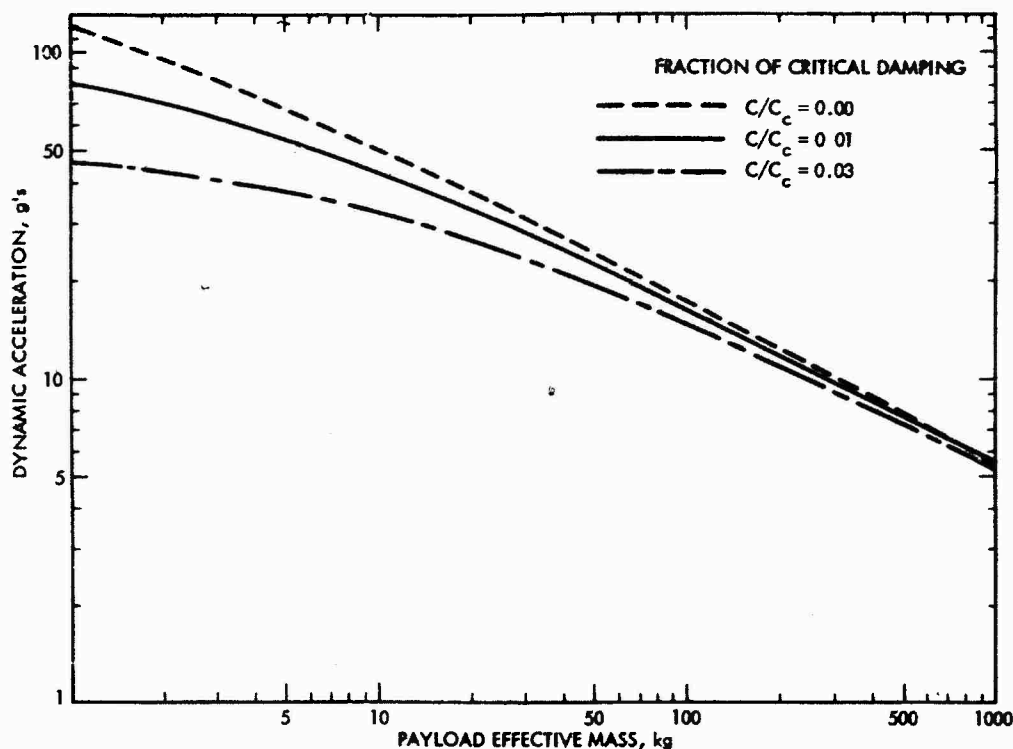


Figure 5. Estimation of STS Payload Dynamic Response

CONCLUSIONS

For current spacecraft (excluding large space structures) being boosted on expendable launch vehicles or to be boosted on the Space Shuttle, the current methods used to predict damping appear to be adequate. Furthermore, new techniques to improve prediction methods do not appear to be forthcoming, although improvements in modal testing and data reduction methods are providing more and better refined data with which to estimate damping. Good engineering judgment and design practice are required to estimate damping values, incorporate dampers into the spacecraft design where appropriate, and to properly use the realistic forcing functions for design. A document that collects experimental damping data on real flight hardware and characterizes them with some significant parameter, that collects different methodologies used to estimate system damping from subsystem damping values, and that clearly identifies the approximations made by the various approaches is certainly of value.

For future large space structures, more accurate methods of analysis and test will be required to verify the dynamic behavior of subsystems. Confidence in individual subsystems must be obtained to assure Project Managers that small errors within a subsystem do not propagate when large non-testable (on Earth) structures are created. As the analysis and test become more sophisticated methods of formulating and handling damping must improve. Experimental programs must be established to estimate changes in the damping characteristics of materials used for large space structures. However, in the end, evaluation of damping will be at best a scientific estimate.

REFERENCES

1. Leppert, E. L., Lee, S. H., Day, F. D., Chapman, C. P., and Wada, B. K., "Comparison of Modal Test Results: Multipoint Sine Versus Single-Point Random," SAE Paper No. 760879, San Diego, CA, November 29 - December 2, 1976.
2. Wada, B. K., "Modal Test: Measurement and Analysis Requirements," SAE Paper No. 751066, Los Angeles, CA, November 17-20, 1975.
3. Mustain, R. W., "Survey of Modal Vibration Test/Analysis Techniques," SAE Paper No. 760870, San Diego, CA, November 29 - December 2, 1976.
4. Caughey, T. K., "Classical Normal Modes in Damped Linear Dynamic Systems," Journal of Applied Mechanics, Vol. 27, June, 1960, pp. 269-271.
5. Caughey, T. K., and O'Kelley, M. E. J., "Classical Normal Modes in Damped Linear Dynamic Systems," Journal of Applied Mechanics, Vol. 32, September, 1968, pp. 583-588.
6. Foss, K. A., "Coordinates Which Uncouple the Equations of Motion of Damped Linear Dynamic Solutions," Journal of Applied Mechanics, Vol. 25, September, 1958, pp. 361-364.

7. Hurty, W. C., "Dynamic Analyses of Structural Systems by Component Mode Synthesis," Technical Report 32-530, January 1964, Jet Propulsion Laboratory, Pasadena, CA. Also AIAA Journal, Vol. 3, No. 4, pp. 678-685, 1965.
8. Kana, D. D., and Huzar, S., "Synthesis of Shuttle Vehicle Damping Using Substructure Test Results," J. Spacecraft and Rockets, Vol. 10, No. 12, pp. 790-797, 1973.
9. Chang, C., "Damping in Multi-Beam Vibration Analyses, Part I, Analytical Methods," Lockheed Missiles and Space Company, Huntsville Research and Engineering Center, Technical Memorandum, TM54/20-2, August, 1964.
10. Hasselman, T. K., "Damping Synthesis from Substructure Tests," AIAA Journal, Vol. 14, No. 10, pp. 1409-1418, 1976.
11. Goldenberg, S. and Shapiro, M., "Study of Modal Coupling Procedures for the Shuttle," Grumman Aerospace Corporation, NASA CR-112242, 1972.
12. Leondis, A., "Viking Dynamic Simulator - Vibrating Testing and Analysis Modeling," The Shock and Vibration Bulletin, 45th Shock & Vibration Symposium, October, 1974, Dayton, OH.
13. Wada, B. K., "Viking Orbiter - Dynamics Overview," The Shock and Vibration Bulletin, Bulletin 44, Part 2, August, 1974, pp. 25-39.
14. Snyder, R. E., "Viking Spacecraft Dynamic Overview," The Shock & Vibration Bulletin, Bulletin 44, Part 2, August, 1974.
15. Pohlen, J., "Viking Capsule Lander - Dynamic Overview," The Shock & Vibration Bulletin, Bulletin 44, Part 2, August, 1974.
16. Day, F. D. and Wada, B. K., "Unique Flight Instrumentation/Data Reduction Techniques Employed on the Viking Dynamic Simulator," 45th Shock & Vibration Symposium, Dayton, OH, October, 1974.
17. Day, F. D., and Wada, B. K., "Strain Gaged Struts and Data Reduction Techniques to Maximize Quality Data from Spacecraft Flight Measurements," 21st International Instrument Symposium, ISA, Philadelphia, PA, May, 1975.
18. Garba, J. A., private communication, Jet Propulsion Laboratory, Pasadena, California.
19. Chen, J. C., Garba, J. A., Day, F. D., "Voyager Design and Flight Loads Comparison, AIAA Journal of Spacecraft and Rockets," Vol. 16, No. 1, Jan., 1979, pp. 27-34.
20. Hanks, B., Ibrahim, S. R., Miserentino, R., Lee, S., Wada, B. K., "Comparison of Modal Test Methods on the Voyager Payload," SAE Paper No. 781044, San Diego, CA., November, 1978.
21. Ibrahim, S. R., Mikulcik, E. C., "A Method for the Direct Identification of Vibration Parameters from the Free Response," The Shock and Vibration Bulletin, Bulletin 47, Part 4, September, 1977.
22. Ibrahim, S. R., "The Use of Random Decrement Technique for Identification of Structural Modes of Vibrations," Proceedings of the AIAA 18th Structures and Structural Dynamics and Materials Conference, March, 1977.
23. Gayman, W. M., private communication, Jet Propulsion Laboratory, Pasadena, California.
24. Stephens, D. G., Scavullo, M. A., "Effect of Pressure Environment on the Damping of Vibrating Structures," paper presented at the 34th Symposium on Shock, Vibration, and Associated Environments, Monterey, California, October 13-15, 1964.
25. Lazan, B., Damping of Materials and Members in Structural Mechanics, Pergamon Press, 1968.

ACKNOWLEDGEMENTS

The authors wish to acknowledge the cooperation of several U.S. aerospace industry representatives in providing much of the spacecraft damping data appearing herein. Carl Schultz, Robert Hull, and Bob Berry of Martin Marietta Aerospace Company for the data on Titan, Skylab, and SCATHA. Reggie Jones and Bob Zuziak of Hughes Aircraft Company who supplied data for many Hughes-built spacecraft as well as the European spacecraft. Tom Golden of Boeing Aerospace Company for the information on the Space Telescope metering truss. Don Wade of Johnson Space Center, Joe Yahata of Rockwell International, Claude Green and Larry Kiefling of Marshall Space Flight Center, Joe Young of Goddard Space Flight Center, Bob Freeland of the Jet Propulsion Laboratory, Des Pengelley, Bill Kittle, and Ted Sitek of General Dynamics, Convair Division, and Clyde Stahle of General Electric Company for sharing their experiences and information relating to damping for various payloads and launch vehicles.

This study was supported by NASA-OAST under the direct cognizance of Mr. R. Goetz, and represents the results of one phase of research carried out at the Jet Propulsion Laboratory, California Institute of Technology, under Contract No. NAS 7-100; sponsored by the National Aeronautics and Space Administration.

APPENDIX

A number of studies have been performed in the past few years to collect and summarize damping data for spacecraft and launch vehicles. Data thus collected can aid in determining appropriate damping estimates for use in structural dynamic analysis. Damping data for a number of recent spacecraft and other space hardware are provided here for information.

Hughes Aircraft Company performed an in-house study in 1978 to determine spacecraft damping values for in-orbit configurations. Their primary concern was to establish the amount of structural damping that could be associated with the bearing assembly joining the spun and despun portions of an orbiting dual-spin spacecraft. Most of the Hughes-built spacecraft to date have been spin-stabilized, consisting of a spinning cylindrical section and a despun platform or antenna farm, and have been used as communications satellites, providing overseas television and telephony. Only a limited amount of data applicable to in-orbit spacecraft damping is available, although a large amount of information exists from ground vibration and modal testing. Table A-1 summarizes the in-orbit damping information Hughes obtained for an Intelsat IV spacecraft, utilizing telemetry data from an accelerometer mounted on the spinning motor.

As a part of the Hughes study, damping data for a number of Hughes spacecraft as well as others were collected from the results of ground vibration (sinusoidal and random excitation) and modal survey tests. Very little of this data is applicable to the prediction of spacecraft damping in orbit since most tests are conducted in air and excitation levels (for vibration tests) probably exceed the level of in-orbit disturbances; however, the data does provide an illustration of the range of damping values that can be expected in ground testing of typical spacecraft structures.

Figure A-1 summarizes modal damping values obtained for the Intelsat IV-A spacecraft during both random and sinusoidal excitation vibration tests, at two different input amplitude levels. The plotted values are based upon transfer functions between various accelerometers and strain gages on the spacecraft and the spacecraft base. Clearly, there is considerable variation in damping with input amplitude, and some frequency shifting of the resonances at the higher input amplitudes as might be expected, but no simple damping/amplitude relationship is discernible. Tables A-2, A-3, and A-4 list modal damping values determined for three other Hughes spacecraft in modal survey tests, using low level sinusoidal excitation. Each of these spacecraft has a large cylindrical rotor, as those of the Intelsat IV-A series.

In a Fokker report, "A Survey on Damping in Spacecraft Structures," published in 1973 under contract from ESRO, damping data for five European spacecraft are summarized. The five spacecraft, ANU, TDI, COS B, ESRO IV, and PICO, were tested with varying levels of sinusoidal base excitation. Figures A-2 through A-6 clearly show increased damping with increased input amplitude, and a trend towards lower damping at higher frequencies. Three of these spacecraft were of the spin-stabilized cylinder/platform type, and all are much less massive than most of the Hughes spacecraft.

SCATHA (Spacecraft Charging At High Altitude) is an experimental satellite designed to study the buildup of static electric charges on spacecraft surfaces in high synchronous orbits. The spacecraft is a spin-stabilized cylinder with extendible booms, having a total mass of approximately 655 kg. A modal survey was performed for SCATHA with the damping values of Table A-5 determined by the logarithmic decrement method from transient decay data. Individual modal surveys were conducted for the graphite/epoxy booms; modal damping ranged from 2.1-4.5 percent of critical.

The SEASAT spacecraft was built to provide radiometric information about ocean surfaces. The long, slender spacecraft was composed of an Agena stage with deployable solar arrays, an equipment module support mast, and a deployable rectangular antenna. Table A-6 summarizes the results of the modal survey test; the deployable structures were not included in the test article, but their masses were simulated.

The Ranger series of spacecraft provided much information about the lunar surface in the mid-1960's. These spacecraft were built-up conical structures with deployable solar panels. Table A-7 displays the modal frequencies and damping values obtained for the Ranger III structural test model (less solar panels).

Extensive dynamic testing was performed for SKYLAB, the largest orbiting U.S. spacecraft structure to date. After a modal survey of the SKYLAB orbital configuration, modal damping values were determined from measured decay transients. The measured modes ranged in frequency from 1.31 Hz to 17.02 Hz, with damping varying from 0.008 to 0.048 fraction of critical. Four different data reduction methods were used to determine damping: the least-squares iterative approach of Wilcox and Crawford (NASA TN D-4503), a least-squares third order polynomial fit, logarithmic decrement, and the modal velocity method. The results shown in Table A-8 reveal fairly good correspondence between the Wilcox-Crawford and logarithmic decrement methods, and some considerable variations between the modal velocity method and the others at the higher frequencies.

Another large piece of space hardware for which modal damping data is available is the liquid oxygen tank of the STS External Tank (ET LOX Tank). Marshall Space Flight Center performed both multiple point sine dwell and single point random modal tests on the tank, for the liftoff condition. A portion of the results are displayed in Figure A-7.

G-13

Fewer data points exist for the multiple point sine test because there was apparently insufficient testing time to excite all of the shell modes which were uncovered in the single point random test. A detailed description of the test article, testing and data reduction procedures, and more complete results can be found in a paper by G. D. Johnston, H. M. Hammac, and A. D. Coleman, "A Comparison of Test Techniques Used During Modal Testing of ET LOX Tank," presented at the Payload Flight Loads Prediction Methodology Workshop, Marshall Space Flight Center, November 14-15, 1978.

A final item of space hardware which may be useful in assessing the damping characteristics of large, lightweight structures is the metering truss for the Space Telescope built by the Boeing Aerospace Company. Structural motion of the truss can contribute to jitter in the telescope images. This structure is a cylindrical truss roughly 3 meters in diameter and 7 meters long, constructed with graphite/epoxy tubes. Boeing has conducted tests specifically to determine the amount of structural damping (2x equivalent viscous damping) inherent in the truss for very low amplitudes of motion. The test results shown in Table A-9 reveal fairly low levels of damping at all resonances. The experimentally-derived damping values were subsequently incorporated into the dynamic analysis to assess the impact of truss vibration on image motion.

Table A-1. Intelsat IV In-Orbit Damping

Frequency, Hz	Viscous Damping, % Critical	Remarks
1.85	0.17	In-orbit damping; first antenna bending
7.0	0.74	In-orbit damping; second antenna bending
24.0	0.80	In-orbit damping
60.0	0.80	In-orbit damping
76.0	1.20	In-orbit damping
98.0	1.00	In-orbit damping
100.0	1.70	In-orbit damping
125.0	0.68	In-orbit damping
135.0	0.70	In-orbit damping
195.0	0.80	In-orbit damping

Table A-2. Hughes Spacecraft Modal Damping

Frequency, Hz	Viscous Damping, % Critical	Frequency, Hz	Viscous Damping, % Critical
9.01	0.67	30.0	0.66
9.11	0.45	31.04	0.41
10.1	0.99	32.10	0.44
10.53	0.60	34.34	0.87
15.79	0.92	35.15	0.40
16.78	0.70	36.83	0.81
17.02	0.83	37.13	0.76
17.19	0.79	37.52	0.14
17.30	1.1	40.31	1.07
17.59	1.23	40.77	1.20
19.94	0.31	42.34	1.14
20.66	0.78	44.88	1.22
21.79	0.34	45.24	1.10
21.91	0.95	46.44	1.10
23.42	0.57	47.91	1.06
26.06	2.23		

Table A-3. Hughes Spacecraft Modal Damping

Frequency, Hz	Viscous Damping, % Critical	Frequency, Hz	Viscous Damping, % Critical
5.89	0.50	23.15	1.0
6.72	1.50	25.21	1.0
9.47	1.0	26.66	0.50
10.9	0.50	31.14	1.0
13.76	0.50	31.20	1.0
14.72	0.50	33.94	1.0
15.31	0.50	35.44	1.5
18.33	1.0	37.55	2.0
21.58	2.0	40.15	1.5
21.96	1.0		

Table A-4. Hughes Spacecraft Modal Damping

Frequency, Hz	Viscous Damping, % Critical	Frequency, Hz	Viscous Damping, % Critical
7.95	3.8	30.36	1.0
8.05	1.6	33.37	1.5
18.94	2.3	34.47	1.4
22.32	3.5	38.22	2.0
23.97	4.4	39.89	1.2
24.24	2.9	42.49	1.6
25.92	2.2	43.58	1.9
26.61	2.3	46.88	3.6
29.20	1.5		

Table A-5. SCATHA Modal Damping

Frequency, Hz	Viscous Damping, % Critical	Mode Description
14.1	1.16	First bending
14.8	0.92	First bending
27.3	1.43	Mast bending
29.8	0.57	Mast bending
30.9	2.20	Torsion
32.6	0.77	Mast bending
34.3	0.63	Mast bending
42.6	1.76	First longitudinal

Table A-6. SEASAT Modal Damping

Frequency, Hz	Viscous Damping, % Critical	Mode Description
3.76-3.78	0.68-0.93	First bending
4.19-4.21	0.28-0.30	First bending
11.99-12.09	0.23-0.26	Combined torsion/bending
13.78-13.81	0.34-0.38	Local bending
14.76	0.24-0.30	Second bending
16.94-17.01	0.35-0.36	Second bending

Table A-7. Ranger III STM Modal Damping

Frequency, Hz	Viscous Damping, % Critical	Mode Description
28.4	0.78	First bending
30.7	0.45	First bending
67.0	0.80	Second bending
70.2	0.74	Second bending
94.5	1.00	Torsion

Table A-8. SKYLAB Modal Damping

Frequency, Hz	Modal Damping Ratio, Fraction of Critical, Mean \pm Standard Deviation			
	Wilcox-Crawford	Polynomial Fit	Log. Decrement	Modal Velocity
1.31	0.048	0.042	0.049	0.015
1.43	0.011 \pm 0.008	0.024	0.017 \pm 0.003	0.023
1.66	0.025 \pm 0.006	0.014 \pm 0.008	0.027 \pm 0.008	0.025
1.72	0.027 \pm 0.009	0.040 \pm 0.019	0.028 \pm 0.006	0.020
2.51	0.030 \pm 0.007	0.058 \pm 0.025	0.050 \pm 0.007	0.026
3.06	0.020 \pm 0.002	0.022 \pm 0.007	0.020 \pm 0.001	0.015
4.10	0.017	0.027	0.017	0.010
4.50	0.032 \pm 0.009	0.019 \pm 0.003	-	0.030
4.55	0.030 \pm 0.009	0.013	0.021 \pm 0.003	0.026
5.03	0.040 \pm 0.008	0.034 \pm 0.029	0.041 \pm 0.010	0.034
5.86	0.010 \pm 0.001	0.013 \pm 0.001	0.010 \pm 0.000	0.011
6.25	0.027 \pm 0.005	0.018 \pm 0.006	0.027 \pm 0.008	0.015
6.36	0.013 \pm 0.001	0.014 \pm 0.007	0.014 \pm 0.001	0.015
6.73	0.010 \pm 0.001	0.013 \pm 0.003	0.010 \pm 0.003	0.010
8.85	0.008 \pm 0.001	0.008 \pm 0.002	0.008 \pm 0.001	0.009
11.59	Not available	0.010 \pm 0.005	0.010 \pm 0.004	0.021
12.65	Not available	0.009 \pm 0.004	0.013 \pm 0.003	0.001
12.87	Not available	0.024 \pm 0.004	0.015 \pm 0.002	0.022
13.30	Not available	0.019	0.012	0.014
13.68	Not available	0.008	0.009	0.046
15.40	Not available	0.016 \pm 0.002	0.008 \pm 0.001	0.028
15.78	Not available	0.019 \pm 0.006	0.017 \pm 0.004	0.026
16.20	Not available	0.038	0.012	0.076
17.02	Not available	0.013 \pm 0.007	0.010 \pm 0.003	0.018

Table A-9. Space Telescope Metering Truss Structural Damping

Frequency, Hz	Structural Damping, % Critical	Mode Description
16.6	0.40	First bending
28.1	0.65-0.87	First longitudinal
39.5	0.58	Second bending
50.9	0.32-0.40	Torsion
79.9	0.57-0.64	Forced lateral excitation
106.0	0.66-0.76	Forced lateral excitation

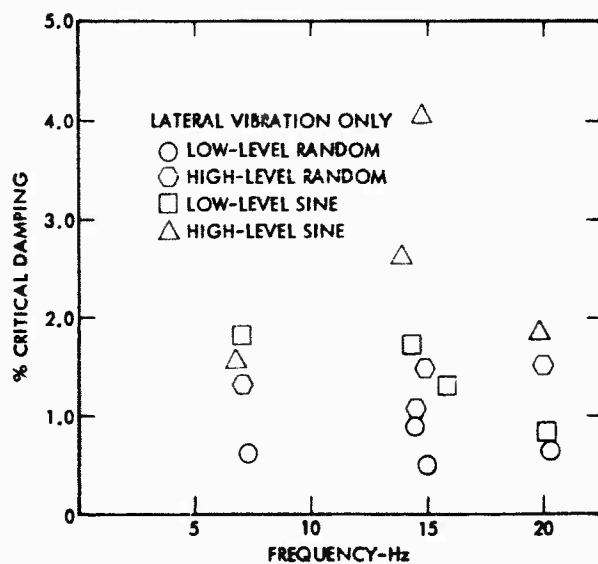


Figure A-1. Intelsat IV-A Modal Damping

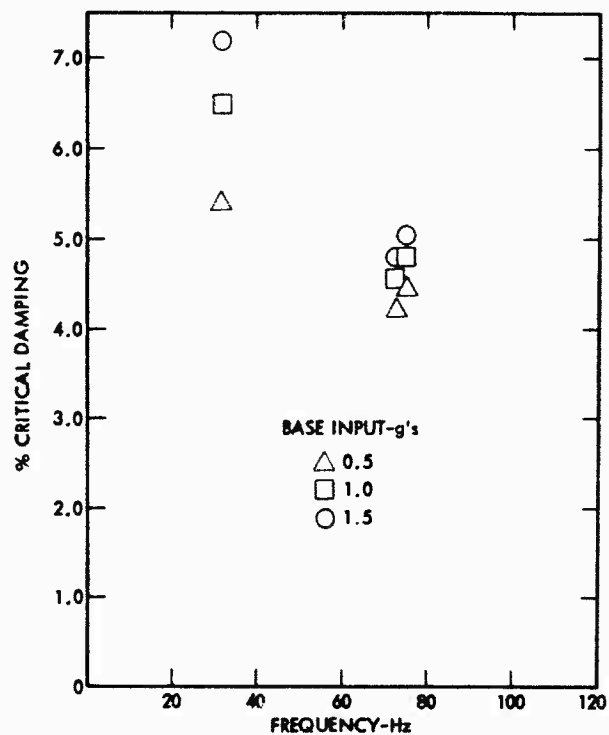


Figure A-3. TDI Modal Damping

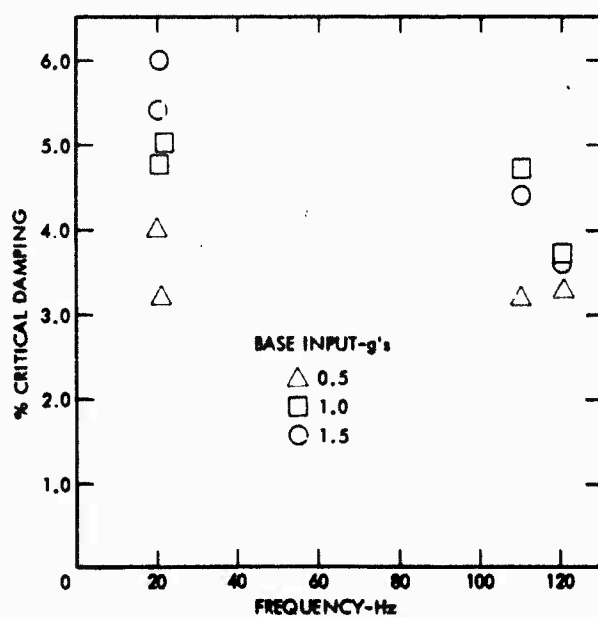


Figure A-2. ANS Modal Damping

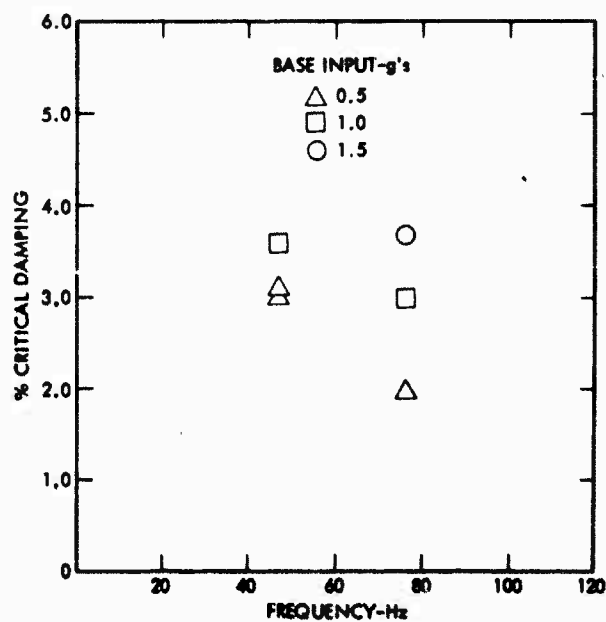


Figure A-4. COS B Modal Damping

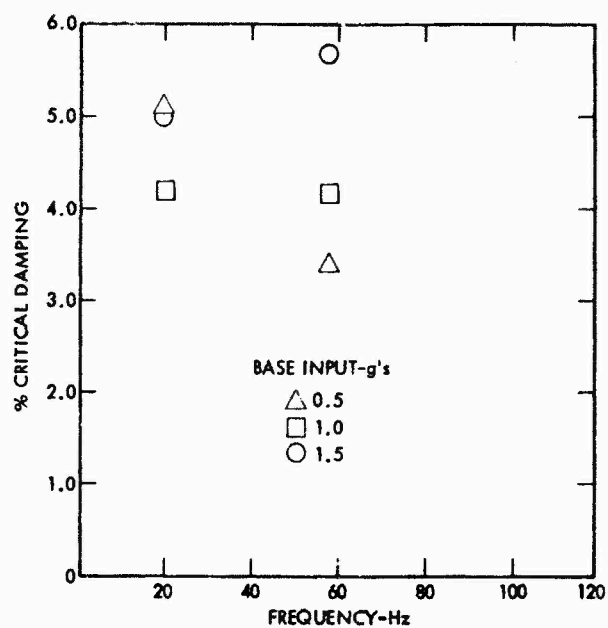


Figure A-5. ESRO IV Modal Damping

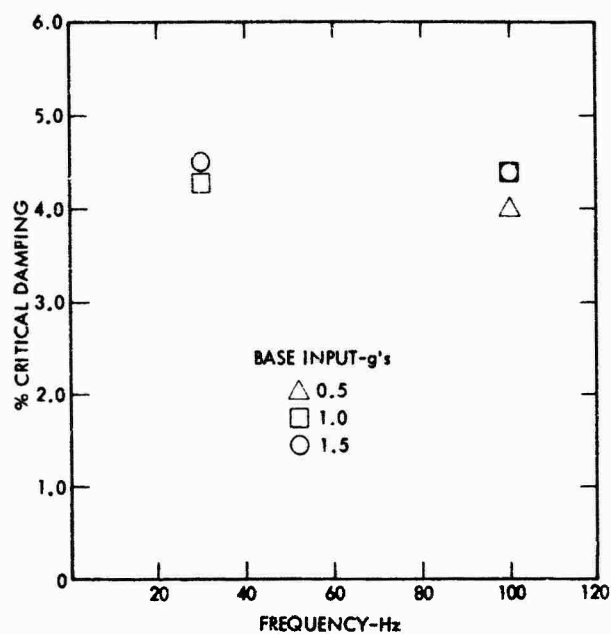


Figure A-6. HEOS Modal Damping

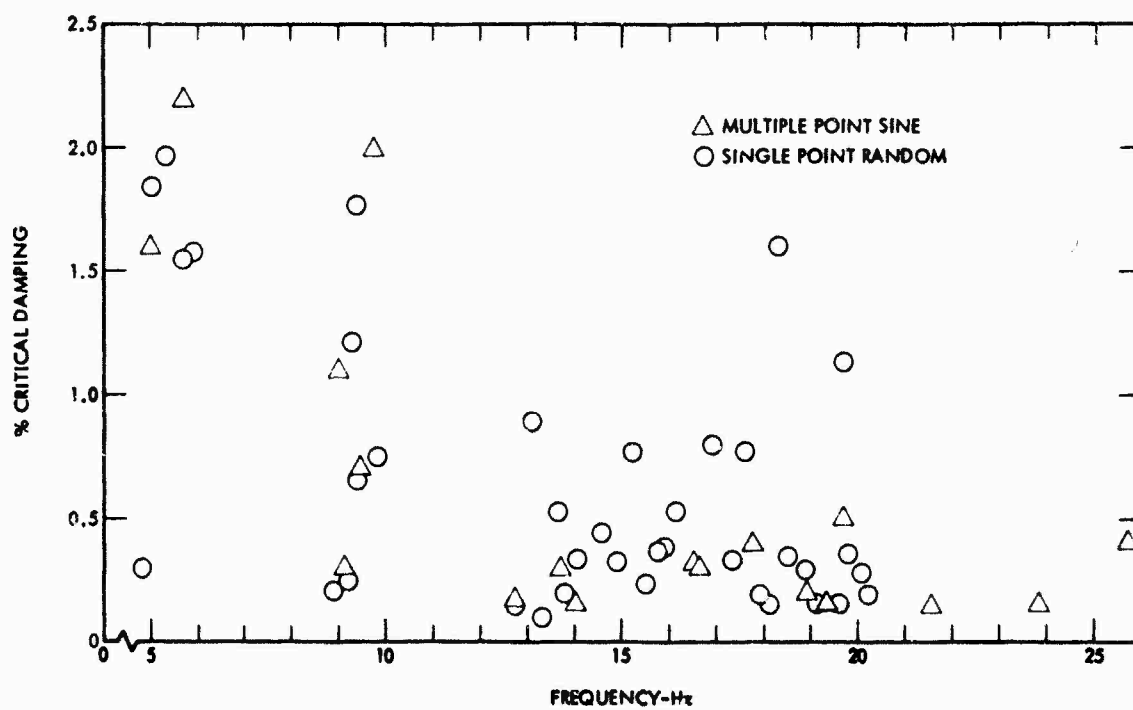


Figure A-7. ET LOX Tank Modal Damping

VIBRATION DAMPING ON SAN MARCO SATELLITES

RESULTS AND COMMENTS

Prof. Carlo Arduini - Ing. Alessandro Agneni

Scuola d'Ingegneria Aerospaziale

Università degli Studi di Roma

Via Eudossiana, 18

ROMA

ItaliaSUMMARY

This paper is a survey of the damping data from the dynamic tests of the San Marco structures.

The behavior of the damping data obtained by the half power method, is generally consistent with other sources of the literature on the subject.

The typical trend of the damping coefficient to decrease with frequency is confirmed. On the contrary there is no clear evidence of significant variations with the input level. This feature is also discussed in the frame of a review of the limits of the half power method.

SYMBOLS

- d_1 difference, in mm, between 10 Hz and the lowest frequency of the bandwidth
- d_2 difference, in mm, between 10 Hz and the highest frequency of the bandwidth
- d_p distance between 10 Hz and the peak frequency
- g gravity acceleration
- f frequency
- A complex amplification factor
- A_k complex amplification factor for the k^{th} node
- D differential operator
- F driving force
- F_c Coulomb damping force
- R_s scale factor of the logarithmic paper
- α coefficient of non linear restoring force
- $\bar{\alpha}$ coefficient of non linear damping term
- δ bandwidth
- ζ damping factor
- ω angular frequency
- ω_0 natural angular frequency

1. INTRODUCTION

1.1 The data presented in this paper concern the dynamic tests carried out on San Marco I and San Marco "C" satellites (Ref. 1-8).

The two satellites, although different in their dimensions were rather similar in their architecture.

They essentially appeared as two spheres whose internal elements were supported by two circular plates welded to a central cylinder, the ends of which were connected to the rims of the plates by means of struts (Fig. 1). All the components of the satellites were welded and the boxes were screw joined.

The light outer shell elements were riveted. The structure was rather heavy compared with other space structures. Some of the packages inside had intrinsic damping capacity (masses imbedded in plastic matrix).

1.2 In tables I and II are shown the acceleration levels to which the two above said satellites were subjected on a MB C125 vibration exciter.

The accelerometers used were the Endevco (models 2221 and 2227) and the monoaxial Bruel-Kjaer (model 4331), whose outputs, amplified by five charge amplifiers Endevco (model 2768), were recorded by means of either galvanometer amplifiers (Honeywell Visicorder) or magnetic tape recorders Honeywell LAR-7400.

The analysis of these records were carried out by an automatic wave analyser Honeywell (model 9051).

2. THE HALF-POWER METHOD (OR BAND-WIDTH METHOD)

2.1 Damping factors were obtained using the half-power method.

As known, it consists in the determination of those frequencies at which the response is reduced to $(1/2)^{1/2}$ times the maximum, i.e. those frequencies for which the power is half the power at resonance. Conceptually the method is based on the idea that in the neighborhood of a resonance peak the system behaves as a single linear spring-mass oscillator. The validity of this scheme will be discussed later.

Because of the wide range of frequencies, in this case 10 ± 2000 Hz, the outputs from accelerometers were directly plotted on logarithmic paper; this fact gives rise to some difficulties of reading among frequency values; in order to calculate the damping factor, the following formula was used:

$$1) \quad \zeta = \frac{1}{2} \left\{ e^{\frac{\ln 10}{R_s} (d_2 - d_p)} - e^{\frac{\ln 10}{R_s} (d_1 - d_p)} \right\}$$

where

- R_s is the scale factor, depending on the type of logarithmic paper used, that is the distance between 10 Hz and 100 Hz expressed in millimeters;
- d_p is the distance, in mm, from 10 Hz to the peak frequency;
- d_1 and d_2 are respectively the lowest and the highest distance from the point corresponding to 10 Hz and those ones for which the power is half.

For very narrow peaks may be better to calculate the damping factor by means of the band-width δ (all so measured in mm); expanding the exponentials in Eq. (1) up to the first order terms, we obtain:

$$2) \quad \zeta = k \delta$$

where $k = (0.5/R_s) \ln 10$.

2.2 Equation (1) is derived from a single degree of freedom linear oscillator mode' forced by sinusoidal input. In its derivation terms of order ζ^2 are neglected, within same accuracy the natural frequency may be confused with the peak frequency. The order of magnitude of all these uncertainties is usually below 10% in our case.

2.3 Question arises about the limit of validity of the single degree of freedom linear forced oscillator scheme. The points to discuss are:

- i) the fact that the actual structure is generally a multiple degree of freedom complex structure;
- ii) that non linearities are generally present;
- iii) that the forcing term is non sinusoidal, due to the finite frequency sweep rate and to the acceleration changes.

2.3.1 The solving equation of a n degrees of freedom linear system is of the type:

$$3) \quad D_1 \cdot D_2 \cdots D_n(x) = D_k(F)$$

where $D_1 \cdot D_2 \cdots D_n$ is the multiple differential operator "product" of the

$$4) \quad D_i = \frac{d^2}{dt^2} + 2\omega_i \zeta_i \frac{d}{dt} + \omega_i^2$$

where the ω_i , ζ_i are the natural undamped frequency and the modal damping factor of the i -th mode.

$D_k(F)$ is a differential operator of order lower than $2n$, different node (k) to node.

When a sinusoidal input $e^{i\omega t}$ is applied to the system, the D_k results in a polynomial $p_k(\omega)$ of the frequency; complex amplification factor is given at the k -th node by:

$$5) \quad A_k(\omega) = \frac{p_k(\omega)}{\prod_r [(\omega_r^2 - \omega^2) + 2i\omega_r \zeta_r \omega]}$$

The amplification factor for a single degree of freedom in the r -th mode is now:

$$6) \quad A(\omega) = \frac{1}{[(\omega_r^2 - \omega^2) + 2i\omega_r \zeta_r \omega]}$$

so that

$$7) \quad \begin{cases} A_k(\omega) = \alpha_k(\omega) A(\omega) \\ \alpha_k(\omega) = \frac{p_k(\omega)}{\prod_{z \neq r} [(\omega_z^2 - \omega^2) + 2i\omega_z \zeta_z \omega]} \end{cases}$$

In the application of the half power method to complex structures it is assumed that the variation of A_k in the vicinity of the r -th mode resonance peak is given substantially by the $A(\omega)$, while α_k is almost constant. Now:

$$8) \quad \begin{aligned} \frac{dA_k}{A_k} &= \frac{d\alpha_k}{\alpha_k} + \frac{dA}{A} = \\ &= \frac{dp_k}{p_k} - \sum_{h \neq r} \frac{(2i\omega_h \zeta_h - 2\omega) d\omega}{(\omega_h^2 - \omega^2) + 2i\omega_h \zeta_h \omega} - \frac{(2i\omega_r \zeta_r - 2\omega) d\omega}{(\omega_r^2 - \omega^2) + 2i\omega_r \zeta_r \omega} \end{aligned}$$

If δ is the bandwidth at the half power condition the max deviation of dA_k/A_k from its assumed value dA/A is therefore:

$$9) \quad \left[\frac{A}{dA} \frac{d\alpha_k}{\alpha_k} \right]_{\max} = \frac{2\omega_r \zeta_r}{i + \zeta_r} \left[-\frac{1}{\delta} \frac{dp_k}{p_k} + \sum_{h \neq r} \frac{i\omega_h \zeta_h - \omega_r}{(\omega_h^2 - \omega_r^2) + 2i\omega_h \zeta_h \omega_r} \right]$$

Assumed $\delta = 2\omega_r \zeta_r$ (from the half power method) the necessary conditions for the validity of the method are:

$$10) \quad \begin{cases} \zeta_r \ll \frac{\omega_h^2 - \omega_r^2}{2\omega_r^2} \\ \frac{dp_k}{p_k} \ll 1 \end{cases} \quad \text{for every } h \neq r$$

The first condition requires well separated peaks and small dampings. This is not however sufficient, since the second condition requires the constancy of the node function p_k , and very little can be said in general on this.

An "a posteriori" partial verification can be given by the independence of the ζ_r computations from node to node; Tables III and IV give some of our results.

The p_k in fact is the only node dependent factor in the computation.

A better "a posteriori" check can be the comparison of the A_k and A profile, or better of their derivatives. Fig. 2 gives an idea of the situation.

The experimental data have been previously filtered (see next paragraph), the definition of the derivative reduces to the two average values at the right and left of the peak. A detailed comparison is therefore impossible. It is seen however that the slope of the A curve (computed from the half power ζ value) in correspondence of the half power points fits very well the actual slope.

Among the masses and elasticities to consider in the system it is necessary to include also the shaker.

The interference of the shaker with the test specimen is discussed at length in Ref. 10, including non linear interactions. As a matter of fact we found problems of this probable origin in the analysis of a resonance peak at about 18 Hz. In addition the probable effect of the shaker "electric" resonance toward 170 Hz is visible in the form of an increased scatter in Fig. 5a.

2.3.2 The second very important point is the effect of the non linearities. The presence of these latter is evidenced by the data.

The data exhibit in fact:

- i) a not negligible content of out-of-frequency response;
- ii) appreciable unsymmetries in the peak shape, with the high frequency side steeper than the other.

The presence of non-linearities deeply impacts at the root of the problem since question arises on the actual possibility of representing a non linear phenomena by a parameter (the damping factor) of intrinsic linear meaning.

This is however still possible in the case where the only non linearity is concentrated in the elastic term while the damping is still linear. As a check of the situation consider the computed case of Fig. 3 where the effect of a non linearity $\omega^2 = \omega_0(1 + \alpha x^2)$ on a system linearly damped with $\zeta = 0.10$ is plotted for $\omega_0 = 628.32 \text{ (sec}^{-1}\text{)}$ and $\alpha = 5.75 \cdot 10^6 \text{ (m}^{-2}\text{)}$.

It is easily seen that, although the shape of the amplification factor is badly distorted by the non linearity, the half power method still results in rather good evaluation of ζ (≈ 0.11 against the 0.10 nominal value).

Note however that if it was hoped, by using the evaluated value of ζ , to estimate the actual behavior

of the system with the linear model, this hope is completely illusory.

Fig. 3 shows also in fact how is different the response of the linear system, and how in particular the max linear level is much higher than the non linear one for the same ζ .

Let us check now the situation for a non linear damping by the example:

$$11) \quad \ddot{x} + 2\zeta\omega_0(1 + \bar{\alpha}x^2)\dot{x} + \omega_0^2 x = F e^{i\omega t}$$

for small $\bar{\alpha}$ a simple iterative procedure gives the first order solution:

$$12) \quad x = A F e^{i\omega t} - \frac{2i\zeta\omega_0\bar{\alpha}\omega(FA)^3 e^{3i\omega t}}{(\omega_0^2 - 9\omega^2) + 6i\zeta\omega_0\omega}$$

where A is the amplification factor of the linear system.

It is seen that the in-frequency response is not altered with respect to the linear case; therefore the evaluation of the base value of ζ is possible using filtered data in order to eliminate the out of frequency $e^{3i\omega t}$ term.

The discussion is thus shifted on the more general topic of the out of frequency terms and their filtering. Responses at different frequencies from the fundamental input frequency are the results of various phenomena, as transients, input defects and non linearities. Filtering of these terms is a relatively easy job and is usually done on the spacecraft test results especially at low frequency.

The effect of filtering in this San Marco data is shown in Fig. 5 a) and Fig. 5 b) where the ζ values corresponding to unfiltered (a) and filtered (b) data are presented.

It is apparent the noticeable reduction in the data scatter due to the filtering. The effect of filtering should be higher at higher input levels, due to the larger importance of the non linearity in this condition. This is not however easily verified in the presented data.

2.3.3 This preliminary examination of the limits of our damping evaluations concludes with the consideration of the effects of Coulomb-type damping; this consists in a constant F_c damping force, independent from the oscillation level or velocity but changing its sign at each velocity zero.

This damping mechanism approximates the joints dry friction effect. Its presence is highly probable in screw joined parts; it produces a typical unsymmetric shape of the response peaks; the presence of this feature in the vibration data can be attributed to this cause as well as (and may be more probable) to other non linearities.

Fig. 4 shows single degree of freedom response curves for a given linear damping plus variable amount of Coulomb damping (represented by the (F_c/F) ratio between the damping force and the excitation amplitude F) (Ref. 11).

The damping factors derived from these curves by the half power method have practically no relationship with the given ζ value.

In addition they have little relationship with the value of the response peak.

If the evaluation of this peak is made using the computed ζ values and the linear model, responses much higher than the real ones are in fact obtained.

3. RESULTS

The San Marco results are presented in Fig. 5 a), 5 b) and 6. Each of the point of the plots has been deduced from a set of data similar to those of tables III and IV.

The bulk of the results refers to the frequency range 50-500 Hz. Fig. 5 a) shows all the data obtained from the filtered inputs as a function of frequency in the said range.

The points have been fitted by a decreasing function of the frequency (shown by the continuous line in the figure).

The σ of the fitting is 1,6%, to be compared to damping values from 14% down to 3,5%.

This kind of consistency can be considered satisfactory, taking into account all the uncertainties of the method described previously and the fact that the points refer to four different structures and seven independent tests at various g levels, ranging from 1.5 up to 21 g 's.

Consequence of this situation is of course that we are not able to evidence in the San Marco structures differences in damping which could be attributed to different construction details. Moreover it is also impossible to detect a clear dependence of the damping from the vibration level. Although other authors (Ref. 9) claim the existence and the experimental proof of this dependence, we should not to be exceedingly surprised of our result, if we rely on the model of eq. (11) and (12).

In fact it is seen from this model that the half power method is able to detect only the base value of ζ corresponding to the very small oscillation amplitudes. All the ζ increase at higher amplitudes goes in the higher harmonics which are eliminated by the filtering.

Fig. 5 b) shows ζ values computed in the range 50-2000 Hz from unfiltered data. The large scatter of these data from 50 to 500 Hz has still been discussed and is for sure due to the out of frequency components of the output, which garble the simple scheme of our ζ computation. Neither the separation of the points according the different structures nor according the different g levels is able to clarify the

situation.

In the high frequency range from 500 up to 2000 Hz the scatter of the unfiltered data is appreciably less. This testifies of a reduced importance of the out of frequency terms at high frequency (see also again the model of eq. 12).

A handfitting of the data with a continuous curve has been attempted and shown by a continuous line in the figure. According to what has been said this fitting should deserve some credit at least at high frequency.

Fig. 6 is the synthesis of all the previously described results. A solid line represents the average of the ζ from filtered data, the more reliable of our data. A dotted line represents the average of the unfiltered data. This curve runs a little higher than the previous one, more or less parallel. (So the average effect of the out of frequency terms is an overestimate of the ζ factor, due to the widening of the peak width, uncompensated by the peak level increase). This curve should therefore provide an upper limit for ζ at the high frequency, and may also suggest the possible extrapolation of the filtered curve toward this region.

4. CONCLUSIONS

The results of Fig. 6 prove the characteristic decrease of the damping factor with the frequency and provide also quantitative estimate of the ζ for San Marco type structures.

The frequency decreasing feature confirms the results of Ref. 9. The absolute values of the damping at low frequency are higher with respect to the quoted reference. This fact should be attributed mainly to the structural differences (rather than to the higher vibration levels, that, according our results should have minor influence).

The San Marco spacecrafts are in fact rather bulky, and some of the packages (the battery packages) could have exerted a very effective damping action at low frequency.

The given results have to be considered in the frame of the discussion of paragraph 2: it has been in fact once again confirmed that reasonably accurate data can be obtained also by the simple method here used and starting from data not particularly suited for this computation.

It has also been shown however that the meaning and the usefulness of these data have still to be fully understood and that special experimental work would be highly advisable in the area of non linearity and non linear damping models.

TABLE I

SAN MARCO I

Vibration axis	Range of frequency (Hz)	Test duration (min.)	Acceleration (g)
x	10 ÷ 60	1.66	0.9
and	60 ÷ 500	1.66	2.1
y	500 ÷ 2000	1.00	4.2
z	10 ÷ 50	1.66	2.3
	50 ÷ 500	1.66	10.7
	500 ÷ 2000	1.00	21.0

TABLE II

SAN MARCO "C"

Vibration axis	Range of frequency (Hz)	Test duration (oct./min.)	Acceleration (g)
x	10 ÷ 150	2	1.5
and	150 ÷ 400	2	3.0
y	400 ÷ 2000	2	7.5
z	10 ÷ 53	2	(12 inch/sec)
	53 ÷ 100	2	10
	100 ÷ 2000	2	7.5

TABLE III

SAN MARCO "C" (STRUCTURAL MODEL)

y axis Acc. No.	Unfiltered data f (Hz)	Input acceleration 3 g ζ
4	180	0.05677
5	180	0.04036
6	180	0.07354
7	180	0.06640
9	135	0.05382
10	175	0.05241
11	180	0.02712
12	175	0.04958
13	180	0.05311
15	180	0.06741
17	180	0.06015

$$\bar{f} = 179.5$$

$$\bar{\zeta} = 0.0537$$

$$q_b = 0.012$$

TABLE IV

SAN MARCO "C" (STRUCTURAL MODEL)

z axis Acc. No.	Filtered data f (Hz)	input acceleration 10 g ζ
2	78.5	0.14717
3	73.0	0.25504
8	78.3	0.20071
14	75.7	0.20584
16	80.0	0.20416
20	71.3	0.23440
21	73.6	0.21610
22	76.0	0.22696

$$\bar{f} = 75.8$$

$$\bar{\zeta} = 0.2113$$

$$\sigma_{\zeta} = 0.029$$

REFERENCES

- 1) G. Ravelli, U. Ponzi, C. Arduini, M. Di Ruscio
San Marco C-2 Payload Description Document
Centro Ricerche Aerospaziali, November 1973
- 2) U. Ponzi, C. Arduini
The Structural Configuration of the San Marco Satellite
Sciences et Industries Spatiales Vol. 2 N. 9-10, pag. 55-59, 1966.
- 3) U. Ponzi, C. Arduini, G. Ravelli
Environmental Test Specifications for San Marco B Satellite
Centro Ricerche Aerospaziali, May 1966.
- 4) U. Ponzi, C. Arduini, G. Ravelli
Environmental Test Specifications and Test Procedure for San Marco Scout 1 Satellite
Centro Ricerche Aerospaziali, August 1964.
- 5) U. Ponzi, R. Ferroni
Vibration Tests of the San Marco D Structural Model
Centro Ricerche Aerospaziali, Rep. V040, March 1969.
- 6) U. Ponzi, R. Ferroni, G. Morelli
Vibration Tests of the San Marco C Prototype Model
Centro Ricerche Aerospaziali, Rep. V049, July 1969.
- 7) U. Ponzi, R. Ferroni
Vibration Tests of San Marco C F.U.1 and F.U.2
Centro Ricerche Aerospaziali, Rep. V059, January 1971.
- 8) U. Ponzi, R. Ferroni
Vibration Tests of the San Marco C2 F.U.
Centro Ricerche Aerospaziali, Rep. V090, January 1974.
- 9) A Survey of Data on Damping in Spacecraft Structures
Fokker VFW B.V Space Division. ESAO CR(p) 539.
- 10) U. Ponzi, R. Ferroni, G. Morelli
Problemi di Interazione nelle Prove di Vibrazione delle Strutture Aerospaziali
L'Aerotecnica Missili e Spazio N. 5, 1974.
- 11) J.P. Den Hartog
Forced Vibrations with Combined Coulomb and Viscous Friction
Trans. ASME, 1931 Vol. 53.
- 12) J.J. Stoker
Non Linear Vibrations in Mechanical and Electrical Systems
Interscience Publ., New York-London 1954.

- 13) W. Thomson
Vibration Theory and Application
G. Allen and Unwin Ltd., London 1971.
- 14) A. Worthing, J. Geffner
Elaborazione dei Dati Sperimentali
Casa Ed. Ambrosiana, Milano 1965.
- 15) J. Topping
Errors of Observation and their Treatment
Chapman and Hall Ltd., London 1961.
- 16) P. Santini, A. Castellani, A. Nappi
An Introduction to the Problem of Dynamic Structural Damping
AGARD R 663, September 1977.

ACKNOWLEDGEMENT

The authors wish to thank Prof. U. Ponzi for the suggestions and useful discussions on the subject of this paper.

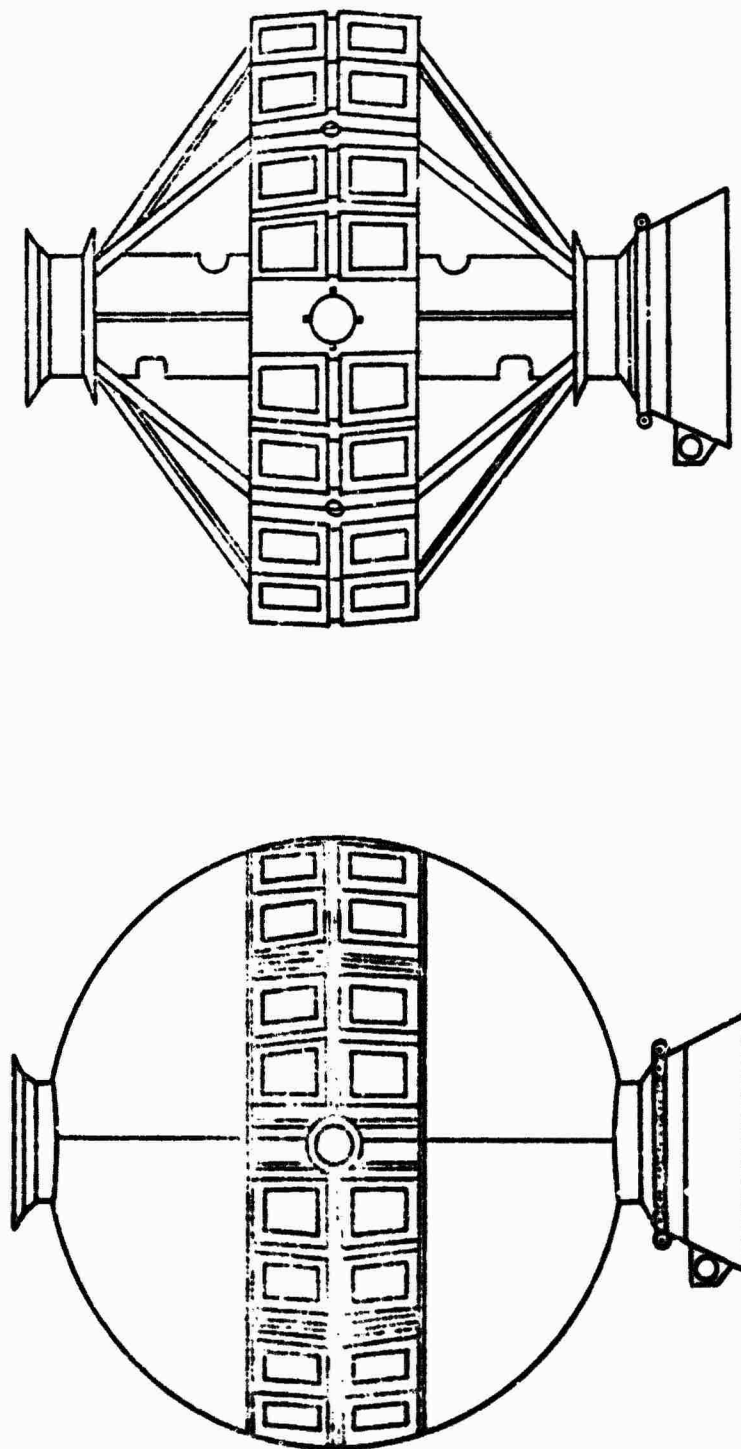


Fig. 1 - *S. Marco Structure* (Schematic)

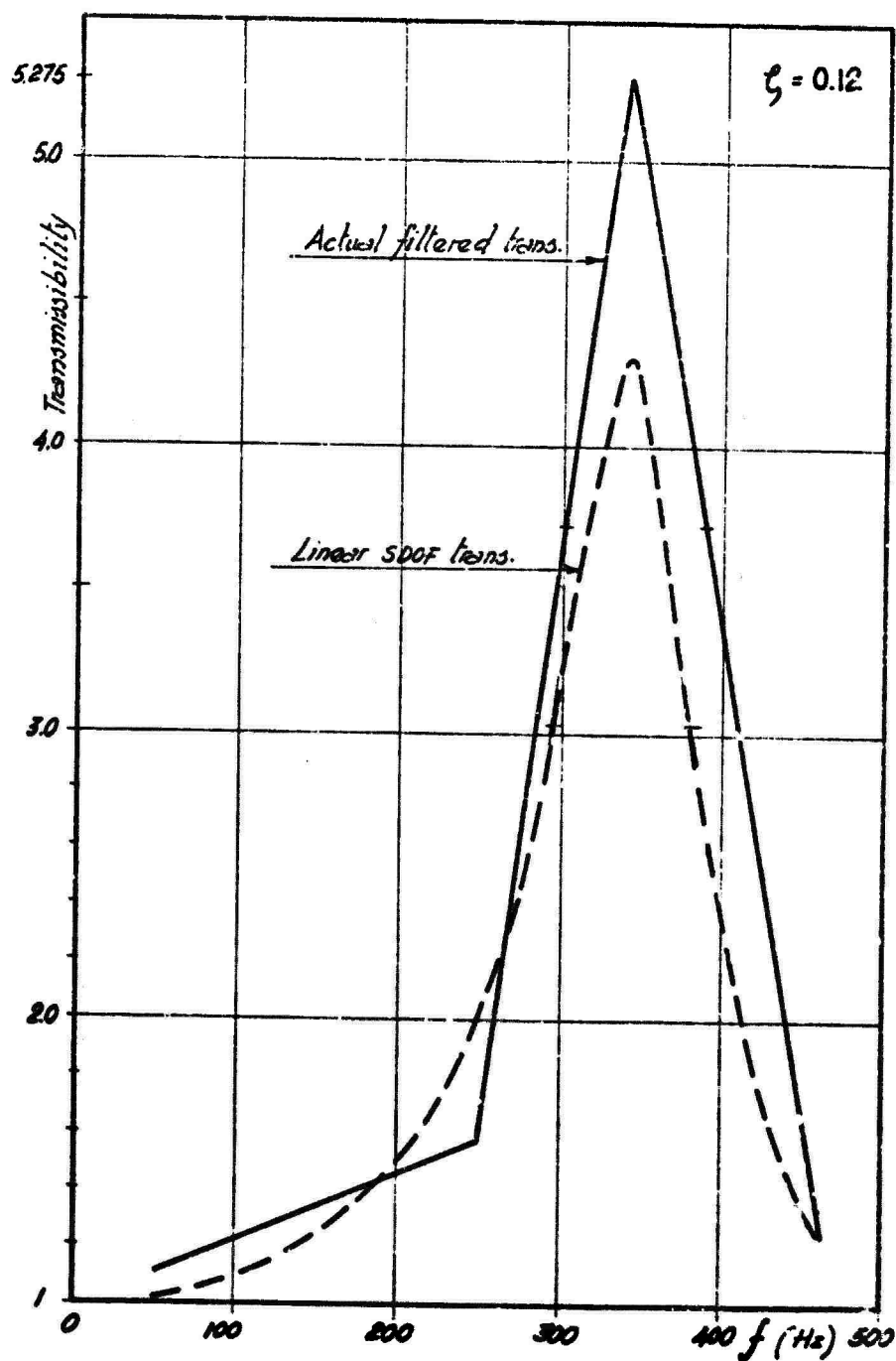


Fig. 2 - S. Marco I Z axis - Bottom shelf
filtered data

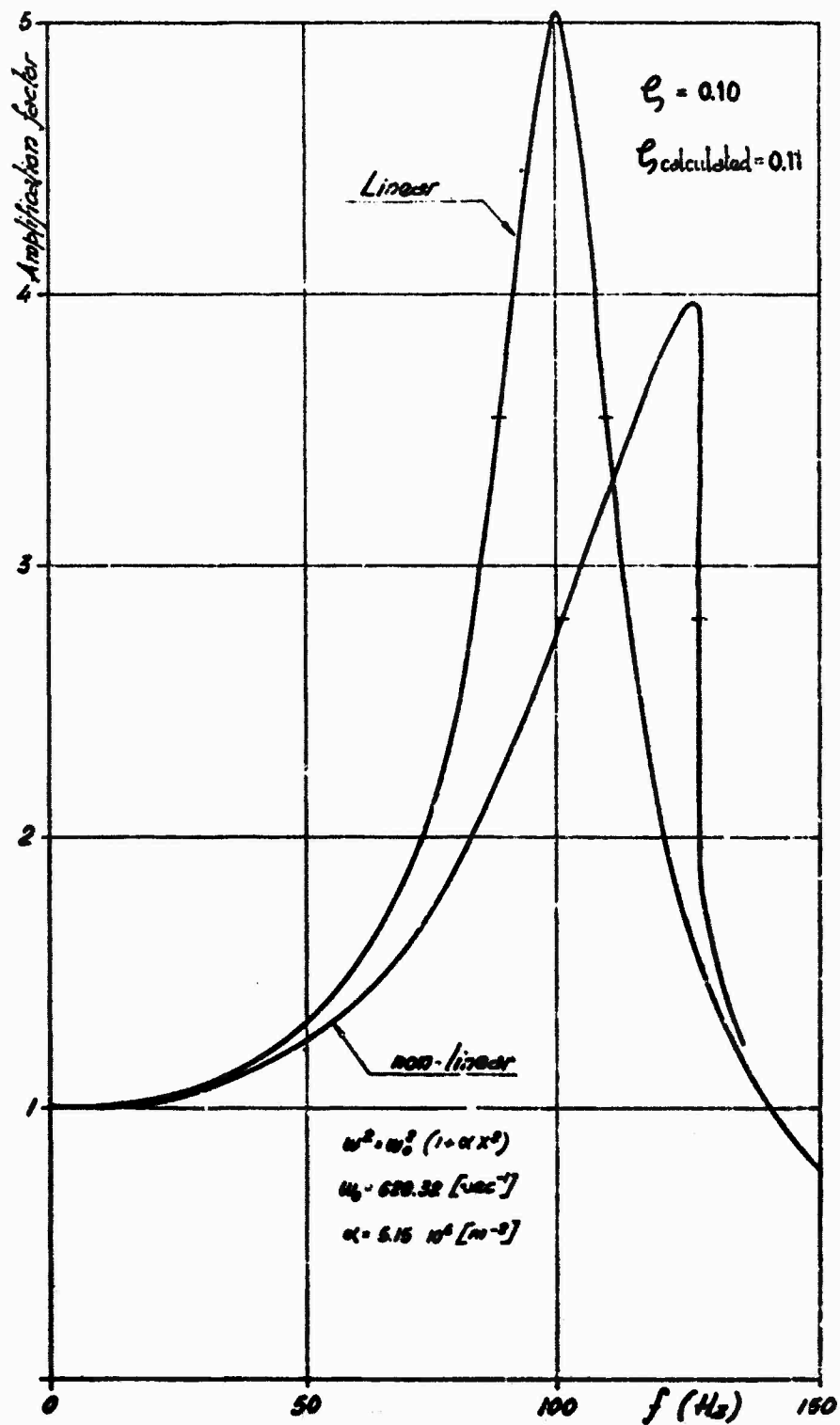


Fig. 3 - SDOF response - Linear damping on non linear elastic system.

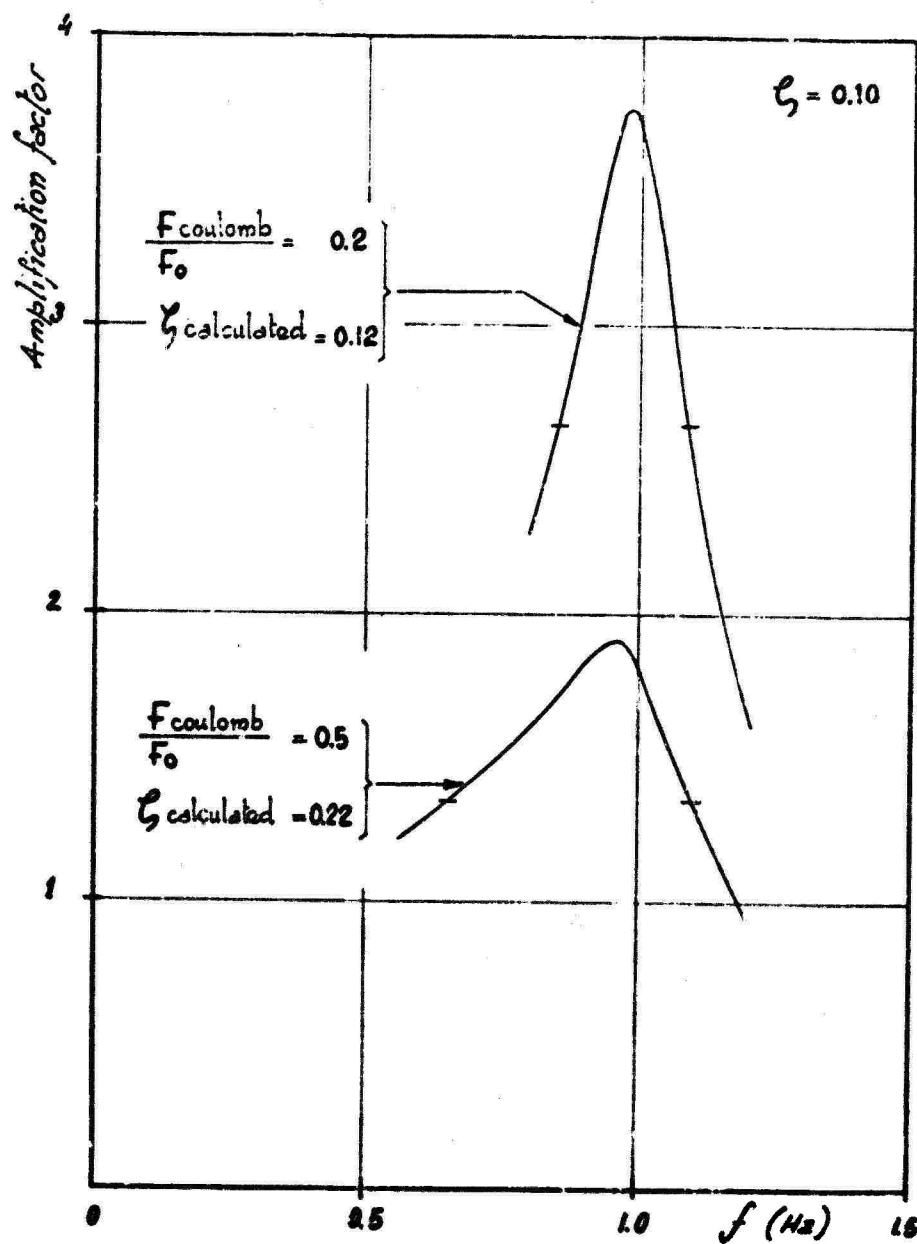


Fig. 4 - Response of a SDOF system with viscous and Coulomb damping

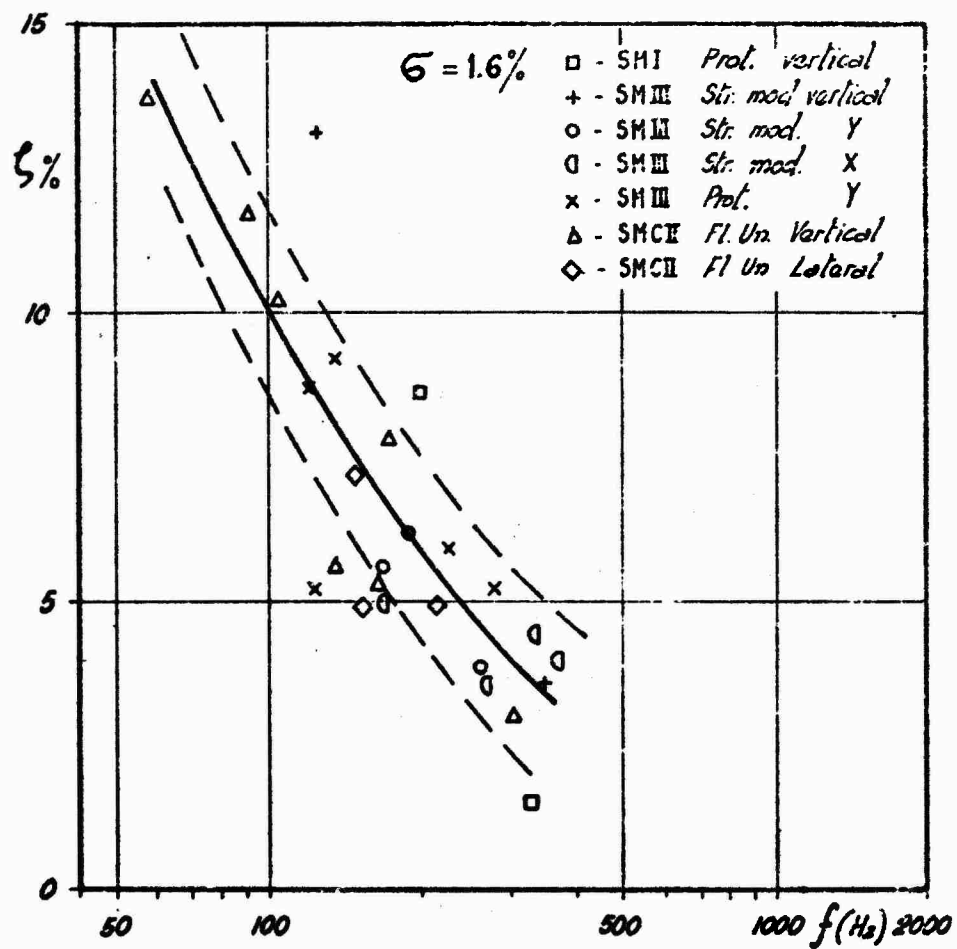


Fig. 5 a - S. Marco Damping factors
Filter. data

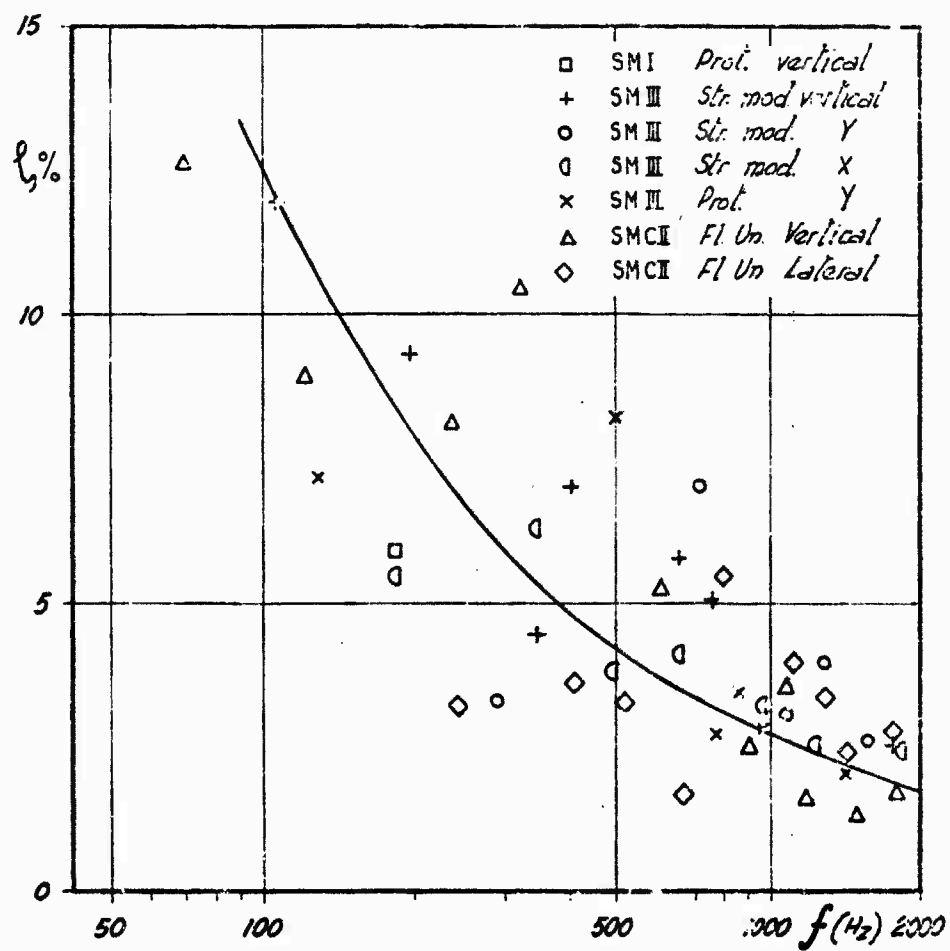


Fig. 5 b - S. Marco Damping factors
Unfilter. data

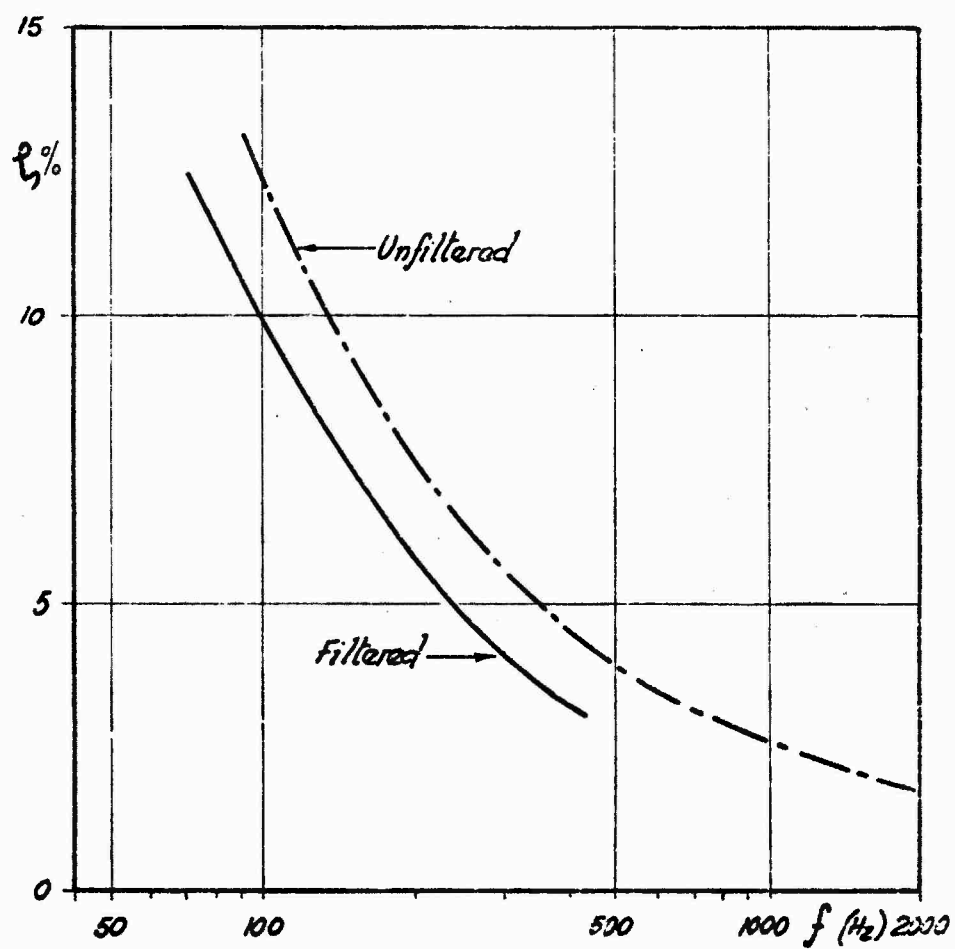


Fig. 6 - S. Marco Damping factors

DAMPING PROBLEMS IN ACOUSTIC FATIGUE

by

Vittorio Giavotto, Marco Borri
Istituto di Ingegneria Aerospaziale del Politecnico di Milano, Italy

Giorgio Cavallini
Istituto di Aeronautica dell'Università di Pisa, Italy

1. FOREWORD

The high degree of reliability required for aerospace structures, today is obtained with drastic reduction in the allowable stress levels.

In fact, the structures subjected to acoustic excitation must inevitably work in resonance, where the response is ruled by damping parameters, which are not adequately known.

This is the main cause that forces high safety margins to be adopted, and that leads to a design that may be exceedingly heavy.

This paper discusses and evaluates the impact of the present lack of knowledge about damping on fatigue design of wide-band noise excited structures.

The need is emphasized for models to be used as effective tools, and capable to estimate damping effects with a higher degree of accuracy; the aim should be to obtain at least the same level of accuracy as the other relevant parameters.

The achievement of this result must necessarily be gradual, requiring at first a certain amount of ingenuity in designing simple experiments to improve the state of the knowledge, without losing contact with the actual needs of designers.

2. THE PART PLAYED BY DAMPING IN ACOUSTIC FATIGUE PHENOMENON

The need for a detailed analysis of the damping of the structural components of aerospace vehicles springs from two fundamental considerations. The first is the impact which, as far as present and future vehicles are concerned, acoustic fatigue phenomena have on the life of the structure as a result of the even increasing extent of the causes producing these phenomena, the power of the propulsion system in particular, and therefore the noise thus creates, and the speed of the vehicle; as is well known, the damping is the main parameter for establishing the stress level for a given value of the exciting force. The second consideration concerns the need to design structures which must meet durability and safety requirements. These requirements demand, respectively, that the nucleation of a defect caused by fatigue stresses, and therefore by those stresses due to acoustic loads, should be sufficiently unlikely in the life of the vehicle and that, if however a defect appears or is present in the structure from the beginning, this should not grow over a given period and eventually lead to catastrophic failure. To meet these requirements in the course of designing a vehicle, as far as the acoustic load is concerned, is a very difficult problem, given present level of acoustic loads and the knowledge we possess concerning the phenomenon of acoustic fatigue.

As was pointed out in a previous paper, /1/, in which a rough estimate was made of available data, /2/, the experimental values of the stress are widely scattered around the corresponding values which can be calculated with a design procedure.

For this design procedure reference can be made to the procedure suggested in the ESDU, /3/. Use of a different procedure can lead to rather different results, but cannot change the meaning of these observations.

The ratio between the experimental values of the stresses due to acoustic loads and the corresponding values thus calculated is considered to have a lognormal distribution with $\sigma(\log s_{RMS} - \log \bar{s}_{RMS}) = .14$.

On the basis of this consideration, in the design of the structure in relation to the problem of acoustic fatigue, it is advisable to consider the calculation of s_{RMS} as a process which provides an estimate of a statistical nature of the real value of the stresses.

The calculated value of s_{RMS} must then be compared with the value of the fatigue strength S_{RMS} of the structure for this type of stresses. Reference is made for this to the $S_{RMS} - N_R$ data of the ESDU, /4/, obtained for totally representative conditions of the phenomenon under discussion. Obviously, even s_{RMS} must be considered as a quantity characterized by random nature.

For data concerning riveted skin specimens in particular, s_{RMS} can be considered to have a lognormal distribution with $\sigma(s_{RMS}) = .09$ around the s_{RMS} mean value corresponding to 50% of survival probability, in the whole field of N_R relative to this subject.

The difference between $\log s_{RMS}$ and $\log \bar{s}_{RMS}$ is still a random function with normal distribution and:

$$\sigma(\log s_{RMS} - \log \bar{s}_{RMS}) = \sqrt{\sigma^2(\log S_{RMS}) + \sigma^2(\log s_{RMS})} \approx .166 \quad (1)$$

We can now bring in the requirement of the durability of the vehicle with the condition that

during the planned life no cracks appear in the structure with an established probability.

In reference to an assigned value of a 99.9% probability of there being no cracks, in (1) we have, /5/, that the difference $(\log \bar{S}_{RMS} - \log \bar{s}_{RMS})$ must be:

$$(\log \bar{S}_{RMS} - \log \bar{s}_{RMS}) = 3.09 \sqrt{\sigma^2(\log S_{RMS}) + \sigma^2(\log s_{RMS})} \quad (2)$$

It follows that mean fatigue strength \bar{S}_{RMS} must be about four times greater than the calculated \bar{s}_{RMS} value of the acoustic stresses. This condition is much heavier than the similar condition imposed on the stresses originated by other loads.

Since N_f is very high for acoustic load phenomena, for example $N_f = 10^7$, \bar{S}_{RMS} is in the range of 16 MN/m² and the calculated \bar{s}_{RMS} stress levels therefore have to be extremely low.

A similar situation, and even heavier, occurs when we want to introduce safety requirement for the structure, this being designed with damage tolerance characteristics. To cut a long story extremely short, it must be ensured that a crack which may have nucleated or which may have been presented in the structure since the beginning, does not grow at such a rate that it takes on critical dimensions in an inspection period.

In /1/ there is a discussion of the problem of the evaluation of the reliability of the growth time of the damage from the initial to the critical size. The problem is a complex one but a simple analysis can, however, provide certain indicative results. It is assumed that the only variables with statistical characteristics are the level of the acoustic stresses and the crack propagation rate of the material used. The other quantities needed to calculate the growth time, which can be expressed by N number of cycles, are considered deterministic variables, for example the initial and final sizes of the crack.

If the calculation is made by means of the integration of a propagation law using the value of the stress intensity factor K_{RMS} referred to the stresses S_{RMS} such as $da/dN =$

m_1
 $= C_1 K_{RMS}$, the calculated values of \bar{N} must be considered the mean value of a random variable depending upon scatter on the calculated level of the acoustic stresses, previously examined, and upon scatter on the characteristics of the propagation rate. This data is obtained by considering the C_1 constant of the propagation law as lognormal distributed around an mean value with $\sigma(\log C_1) = .15$. From the expression of N obtained from the integration of the propagation law, it transpires that N has lognormal distribution with $\sigma(\log N) = \sqrt{\sigma^2(\log C_1) + m_1^2 \sigma^2(\log s_{RMS})} = .446$, if $m_1 = 3$.

If we want to determine the inspection period characterized by a extremely slight probability that, in this period, the crack grows until it reaches critical size, the mean value \bar{N} calculated with respect to the value of $\sigma(\log N)$ must be reduced.

The $\sigma(\log N)$ is extremely high because of the already considerable value of the $\sigma(\log s_{RMS})$ which, in this case, is amplified by the m_1 coefficient of the propagation law which is around 2.5 - 3. Therefore the safety coefficient which must be applied to the calculated value of the inspection period, is, for acoustic loads, much greater than the one usually used in the case of other kinds of loads.

This makes it necessary to inspect the structures very frequently or to keep the stress level of acoustic loading very low.

The observation which have been made so far indicate how the aim of ensuring the structures have adequate levels of durability and safety, is made very difficult to reach because the scatter which affects the fatigue behaviour in the nucleation and propagation phases and, above all, the calculated stress level in the case of acoustic loads.

Therefore, if we go on to examine the causes of the wide scatter on the evaluation of the stresses, it may be observed that in the entire s_{RMS} calculation procedure, the main source of scatter is the highly random nature of the evaluation on the damping value δ , and on structural damping in particular.

The proof of what has been stated here, is to be found in the experimental data concerning structural damping given in /6/. These have a lognormal distribution with $\sigma(\log \delta) = .24$ around the mean value $\bar{\delta}$, which is used in calculating the stress levels. Since the standard deviation of the experimental values of the s_{RMS} around the calculated value is $\sigma(\log s_{RMS}) = .14$, and since the value of s_{RMS} is a function of $(1/\delta)^{1/2}$, it can be concluded that almost all the scatter on s_{RMS} is introduced by the scatter existing on the value of the structural damping.

In these conditions, if the acoustic loads takes the level of the corresponding stresses to values which are no longer negligible, and if we want to reach adequate durability and safety values in the structure, two possibilities are open to us. The first is the introduction of a damping treatment which leads to a increase in total damping in such way that the stress levels are still very low: this possibility has been fully explored over the last ten years, /7/, but may not always be practicable or, at least, easily practicable for the operations and involves it increase in weight.

The second possibility can therefore be followed which consists in the improvement of our knowledge of structural damping. An eventual improvement in this field may lead to the reduction of the considerable scatter which, at present, we are obliged to associate with the forecast of the stress level. This possibility, therefore, up to a point can lead to the structure being able to stand higher acoustic loads, while still maintaining adequate durability and safety features. It should, however, be noted that this improvement must be accompanied by a corresponding improvement in the fatigue behaviour of the structures, otherwise the efforts made to widen our knowledge of the characteristics of the damping will be useless, since the design of the structure is also considerably influenced by the scatter on the calculated values of the fatigue strength and crack propagation rate. A second important reason for not neglecting the improvement of our knowledge of fatigue behaviour is the interdependence which in any case exist, for the riveted structures, between this characteristics and the damping value which develops in the riveted joints.

A sudden decrease in fatigue strength due to the fretting phenomenon can be linked to the higher damping values.

3. DAMPING MECHANISM

Generally the heading of damping is used to collect the effects of all the dissipative phenomena which are not so important and so well known to deserve a special treatment.

For instance the aerodynamic forces acting on a wing oscillating in flight at low frequencies may have a very large dissipating effect, but they use to have a special treatment, i.e. they are treated just as aerodynamic forces, and their effect is not included in damping.

So the damping of an aircraft structure results from the superimposition of several effects, having very different natures and very different causes, but whose magnitude is such that they can be all represented with a single model.

In fact when the damping is relatively high, as in the case where dampers or special damping materials are used, the main damping effects are usually well known, and minor damping effects can be neglected. But in the most interesting cases only minor damping effects are active and yet cannot be neglected because they have a fundamental function, e.g. in determining response amplitude at resonance.

In the latter cases the damping forces acting on an oscillating structure are relatively small compared with elastic and inertia forces, so that their short-time effect could be neglected, but their long-time or secular effect causes energy flows which are responsible of the energy distribution within the structure and between the latter and its surrounding. Then the dynamic behaviour of the structure can be adequately described by a certain number of undamped natural modes, i.e. by a certain number of uncoupled oscillators^(*); the energy flows between the oscillators and towards the surrounding are controlled by damping. Such energy flows are slow, in the sense that, for instance in one cycle, the energy flowed by damping is very little compared with the energy flowed from kinetic to potential and viceversa.

If it is so any damping model can be adequate as long as it is capable of a correct evaluation of the energies exchanged in one cycle.

Hence also the linear viscous damping model, which is the simplest model available and which surely can be used with any available computational procedure, could be suitable, even if the actual dissipation processes are far more complicated.

Then for a moderately damped structure with reference to a certain number of natural modes, the generalized damping forces could be represented as linear functions of the time derivatives of the modal coordinates, through an appropriate damping matrix. So the real problem is to know the terms of such a matrix with a reasonable accuracy, and possibly to know how they depend on frequency. But since the response of any natural mode is significant only around its resonance, the terms of the damping matrix could also be considered non frequency-dependent, having the value corresponding to the relevant resonance frequency. Likewise the coupling terms (off-diagonal terms) could be considered non-null only for the couples of modes having frequencies not too far off.

So what would be really useful for the structure analyst, once he has found a good modal description of the structure, is a method for making a good estimate of the damping matrix.

The most significant damping processes are commonly described as:

- material damping, - joint damping, - acoustic radiation damping.

Material damping is mainly due to hysteresis and to viscosity in the material. It is very low for the usual metallic structural materials; it may be slightly higher for composites, and much higher for special damping materials. When the latter are not present, and other damping processes are active, materials damping generally can be neglected.

Joint damping is basically due to the sliding that may take place between some surfaces in the joints. Such sliding causes friction forces to build up, that in general can be considered as Coulomb forces. Joint damping is definitely more significant than material damping, but unfortunately it is much more difficult to specify, because it is likely to depend also on the particular type of joint. Moreover for a structure containing joints, this kind of damping must depend also on the extension of the joints and on the amount of their sliding in each vibration mode.

So it is possible that two modes having close frequencies but very different shapes have very different damping coefficients.

The acoustic radiation damping is generally the most significant part of the damping, but also the most difficult to be characterized. In fact acoustic damping is a very simple model for a very complex reality, which actually is the interaction between the structure and one or more fluids.

Acoustic radiation has been deeply investigated by very valuable scientists; for instance we know that radiation in an open space is very different from radiation in a closed cavity, and that radiation efficiency /8,9/ is strongly dependent on the velocity of the bending waves. So it seems reasonable that the coefficients of such damping depend also on such velocity and on extension and shape of the radiating surfaces.

The many investigations and studies /10,11/ done on damping processes up to now, have given some deeper insight into the mechanism of damping, but unfortunately a very little help to the knowledge of damping coefficients.

In fact it seems that a wide gap exists between the needs of the structural analysts and designers and the results obtained by the researchers. The designers need a reasonable evaluation of the response of their structural design, for instance under wide band acoustic excitation, and the analysts, to produce such evaluations need some reasonable figure to put into their viscous damping models.

(*) In some cases structure dynamics is more conveniently described in terms of travelling waves; as far as the following discussion is concerned such also travelling waves can be considered as independent oscillators exchanging energy through damping.

All that is available now, are experimental values of the damping ratio plotted vs. frequency for certain classes of structural components, /6/ (see Fig.3).

Such plots have the very discouraging aspect of clouds of points, without any significant correlation with frequency.

About the same kind of situation would occur if one pretends to plot the drag coefficients of different bodies, with different angles of attack, only vs. velocity.

Incidentally the scatter of such plots would have about the same value, around one decade, of the plots of damping ratios.

So it seems evident that mode frequency alone is not enough to obtain a reasonable correlation of the damping ratios, and that something better is needed.

An investigation is now carried on by the authors of this paper, based on relatively simple experiments and on sound reasoning, to ascertain if it is possible to find a better way for correlating experimental damping data, taking into account some other variables.

Some preliminary results of this research are summarized in the following section; further results are expected in the near future.

4. EXPERIMENTAL DAMPING DATA

A first series of measurements has been accomplished on a corrugation stiffened panel, having the corrugation profile depicted in figure 1, and a square plan form with a side length of 588 mm. between the supports. The aim of such experiments was to investigate if for a single panel, tested with a single methodology, a significant correlation exists between modal damping ratio and modal frequency.

The panel was excited sinusoidally by means of a small electro-magnetic exciter; the frequency sweep and the analysis of panel response were both performed automatically by Spectrum Analyzer HP 3580 A; panel frequency response was recorded on an X-Y pen recorder. Figure 2 reports a typical frequency response recording. It must be noted that above 1200 Hz the recording appears to be flat because both the transducer and the exciter employed have a very sharp attenuation above such frequency.

Below 1200 Hz the panel response shows several resonance peaks; some of them are very sharp and clean and some other show mode intermixing.

To evaluate modal damping coefficient, the resonance peaks were analyzed in detail by zooming on the frequency axis; some improvement in mode separation was also obtained by searching the best position for the exciter and the transducer.

From such resonance peaks damping ratios were evaluated by means of a modified half-power method, and a single-mode identification technique.

The two methods gave very close results, which could be considered fairly accurate, and that do not show any significant correlation with frequency.

Some of these results are plotted in figure 3 /12/, compared with the data of ESDU /6/, for Flat Skin and Stringers Panels in the same frequency band. The values measured for the panel of figure 1 fall in the same range of ESDU data, with a slightly smaller scatter.

Another series of measures were taken from a panel stiffened by 2 stringers, Figure 4. Such panel was one of a group of 10 panels fatigue-tested in the Acoustic Fatigue Plant at Centro Ricerche FIAT /13/.

The panel was pre-stressed and subjected to wide-band acoustic excitation in the progressive wave chamber; the output of 17 strain gage bridges (shown in Figure 4), and of 5 microphones placed at a distance of about 100 mm. from the panel surface were recorded on an analog magnetic tape.

Subsequently such analog recordings were converted into digital, and processed in a large computer by means of a Time Series Analysis Program. The analog signals were sampled with a rate of 8000 points/sec., and the average was taken from 5 transforms.

Some of the transfer functions computed are reported in figures 5, 6 and 7, corresponding respectively to the output of bridges 5, 8 and 13.

Such transfer functions show two prevailing mode groups, one around 470 Hz and the other around 630 Hz. Previous analyzes /14/, carried out both with computational procedures and resonance tests showed that the first mode group concerns mainly stringer deflection, with out significant panel bending, while the second involves significant panel bending.

Modal damping and frequencies were then obtained with a modal identification techniques, based upon a Difference Formula, using single degree of freedom model /15/.

A large scatter could be expected in damping results, due to the fact that single degree of freedom model may be very poor where modal frequencies are very close together.

For any resonance peak modal damping has been computed from right and left differences, and when these two gave very different results, the corresponding value was rejected.

The values returned are shown in Figure 8.

The scatter, sensibly coming also from the identification procedure, is rather large, but has the same order of magnitude as the data published by ESDU (Fig.3). Moreover the points on Figure 8 fall in the same range of ESDU data.

If this rough correspondence may confirm the reliability of the procedures employed, on the other hand it confirms also that even for a single panel with a high modal density no significant correlation can be found between damping ratio and frequency, and so the problem of finding a better correlation for experimental data remains open.

The data, shown in Fig.8, point out the need of a separated investigation for the different mechanisms of damping.

This survey must be firstly performed on very simple structures, where the different mechanisms and the relative influence of the principal parameters characterizing the phenomenon, e.g. the mode shape of the structure in resonance, can be separately evaluated.

In this way only we are allowed to hope to realize something about a set of experimental data like those of Fig.8 and, first of all, to be able to forecast the damping value with a better accuracy than that we now get.

For these reasons, some tests were performed and are still running to investigate one of the most important sources of damping, the friction forces in riveted joints.

The primary purpose is the evaluation of the damping of joints of different configuration and a measure of the scatter on the damping value connected with the fabrication techniques of specimens nominally identical to each other.

The tests were performed on simple specimens, but further tests are planned on more complex structures with the aim of checking the possibility of employing the results gained with simple specimens even for the more complex ones.

The specimen tested is shown in Fig.9.

It is a one stiffener riveted panel made of 2024-T3.

The tests were run on an electrodynamic shaker; the damping measuring technique is based on the analysis of the response bandwidth of the structure about the resonance condition.

As response signal, the strain in one or more places, of the specimen as obtained by strain-gauges, was employed.

All the experimental points of the response curve were used to evaluate the damping value. A particular way of computing was adopted as it allows a very accurate measure of the damping.

As the target of this first batch of tests is the analysis and the evaluation of the damping mechanisms related to the friction forces in riveted joints, we had to eliminate or separately measure the damping due to other sources. Among these they are the internal damping of the material, the damping for the specimen constraint, the acoustic damping due to the sound radiation from the specimen and the damping arising from "air-pumping" phenomenon.

The last of the said sources of damping are eliminated as the tests are carried on in air-vacuum; particularly the tests are performed at different degree of vacuum to point out the trend of the influence of air and to obtain data for absolute vacuum by extrapolating this trend as, with the present vacuum plant, it's not possible to reach air-vacuum over a fixed limit.

The internal damping of the material and that due to the friction forces in the constraint are, on the contrary, evaluated through "ad hoc" tests, the results of which are shown in Fig.10 as function of vacuum degree.

Further tests were carried out on these panels to get an estimate of the random error which may be made in the experimental method, particularly that one due to different in the reality, even if nominally identical mounting procedures and data collection techniques. This scatter is added to the one, from the different building process, which is the only one we have to evaluate.

Therefore it's necessary for us to estimate the former in order to subtract it from the lump sum measured from stiffened panel tests.

An unstiffened identical panel was so tested repetitively six times.

The results distribution on normal probability paper is shown in Fig.11. The estimated standard deviation typical of the employed test procedure is $\sigma = .045$ while the coefficient of variation amount to $v = .02$.

The data of the damping of six nominally identical stiffened specimens, the configuration of which is reported in Fig. 9, are shown in Fig.10. Vs. the particular vacuum degree used in the test.

As damping value, the mean value of the six specimens was used; also the calculated standard deviation refers to this value, to give an estimate of the scatter. The data were collected for three typical vibration mode shapes of the stringer in the stiffened panels: bending, torsional and local.

Some basic remarks can be drawn from this results.

The vibration mode shape is a main parameter of the damping mechanism in dry-riveted joints; the highest damping values concern the bending mode.

The data for the internal damping and for the specimen constraint damping are obtained at frequencies of the same order than the ones related to stiffened specimens data and we can directly subtract the internal damping value from these latter.

Kept in mind the relation between damping and mode shape, we can understand the trend of data shown in Fig.8, which refers to multi-stiffened panels, where, at any given frequency, each stringer can develop a different mode shape.

The acoustic damping influence is not relevant; but this conclusion may be not true at high vacuum degree which we could not still reach.

About the standard deviation of the data, we can remark now much it greater is, in each case respect with the values obtained from the 6 tests on the same unstiffened specimen. The difference between them provides an estimate of the scatter which is brought in by the fabrication techniques, nominally identical, but as a matter of fact different from each other.

Again the scatter of the bending mode is noticed to be the largest; the reason, explaining this behaviour, may be searched for in the development, at all the rivet sites, of much stronger friction forces than for the other modes.

The above remarks have only a preliminar character, in that on the basis of the few collected data we can only develop qualitative judgements. Nevertheless through some further tests, performed in an improved plant test and by a more accurate test procedure, we can forecast that a comprehensive understanding of the mechanism of this particular damping may be achieved, and data are collected, which can be employed in the design of this structure too.

5. CONCLUSIONS

The importance of a more accurate knowledge of the damping value has been pointed out; without it a guarantee of the usual levels in the durability and safety of structures operating in a acoustic fatigue environment, is very hard to assess, unless they are subjected to particular damping treatments.

Different mechanism developing some damping have been considered, the results of tests on

stiffened panels, typical of aerospace structures, have been shown.

The picture, coming from these, is very discouraging and a time more make us understood the difficulties the designer encounters in front of this problem.

A program of tests has been launched with the aim to clarify the damping phenomenon in the riveted joint and possibly to evaluate the damping, through a batch of more accurate data.

The first tests performed on a one stringer stiffened panel have shown the strong influence of the vibration mode on the damping value.

6. REFERENCES

- 1 - BORRI M.,CAVALLINI G. Acoustic Fatigue Assessment in the Design of Aerospace Vehicles. 11th ICAS Congress,Lisbon,September 1978.
- 2 - E.S.D.U. Stress Response to Acoustic Loading. Acoustic Fatigue Sub-Series, Vol.3,1972.
- 3 - E.S.D.U. The Estimation of R.M.S. Stress in Stiffened Skin Panels Subjected to Random Acoustic Loading. Acoustic Fatigue Sub-Series,Vol.3,1972.
- 4 - E.S.D.U. Endurance Under Acoustic Loading. Acoustic Fatigue Sub-Series,Vol.1, 1972.
- 5 - KECEGIOLU D. Fundamentals of Mechanical Reliability Theory and Applications to Vibroacoustic Failures. Reliability Design for Vibroacoustic Environments, AMD,Vol.9,ASME,1974.
- 6 - E.S.D.U. Damping in Acoustically Excited Structures. Acoustic Fatigue Sub-Series,Vol.3,1972.
- 7 - Conference on Aerospace Polymeric Viscoelastic Damping Technology for the 1980'S. Dayton, February 1978, AFFDL - TM-78-78-FBA.
- 8 - SMITH P.W.,LYON R.H. Sound and Structural Vibration. NASA CR 160.
- 9 - MAIDANAK G.,KERWIN E.M. Response of Ribbed Panels to Reverberant Acoustic Fields. J.Acoust. Soc. AM,34,6,809 (1962).
- 10 - MEAD D.J. The Damping of jet Excited Structures. Noise and Acoustic Fatigue in Aeronautics, Wiley 1968,Ch.18.
- 11 - JONES D.I.G. Two Decades of Progress in Damping Technology. Aircr.Eng.,Vol.51,n.1, pp.9-14,1979.
- 12 - BORRI M.,MERLINI T., PUCINELLI L.,SALVIONI L. Contribution to the Evaluation of the Dynamic Response Under Acoustic Load. Convegno A.I.F.A.
- 13 - SELVAGGI P.LOREA A. Acoustic Fatigue Test on the VFW-Fokker VAK 191B Structural Component. AGARD CP 113,1972.
- 14 - MERLINI T.,SALVIONI L. Oscillazioni proprie di un pannello irrigidito. Rilievo sperimentale e analisi alle striscie finite. L'Aerotecnica Missili e Spazio, 1979.
- 15 - RICHARDSON M. Modal Analysis Using Digital Test Systems. The Shock and Vibration Inform. Center, N.R.L.,Washington.

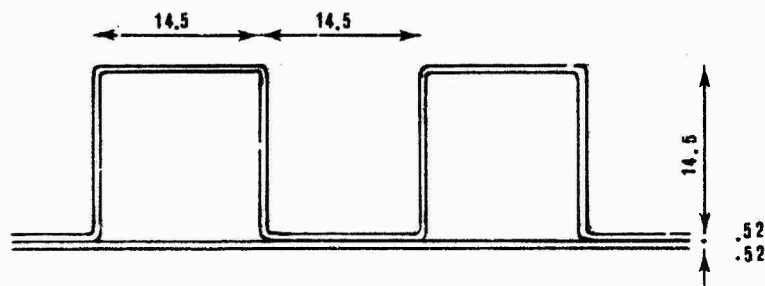


Fig. 1 - Corrugation profile of the panel tested in resonance.

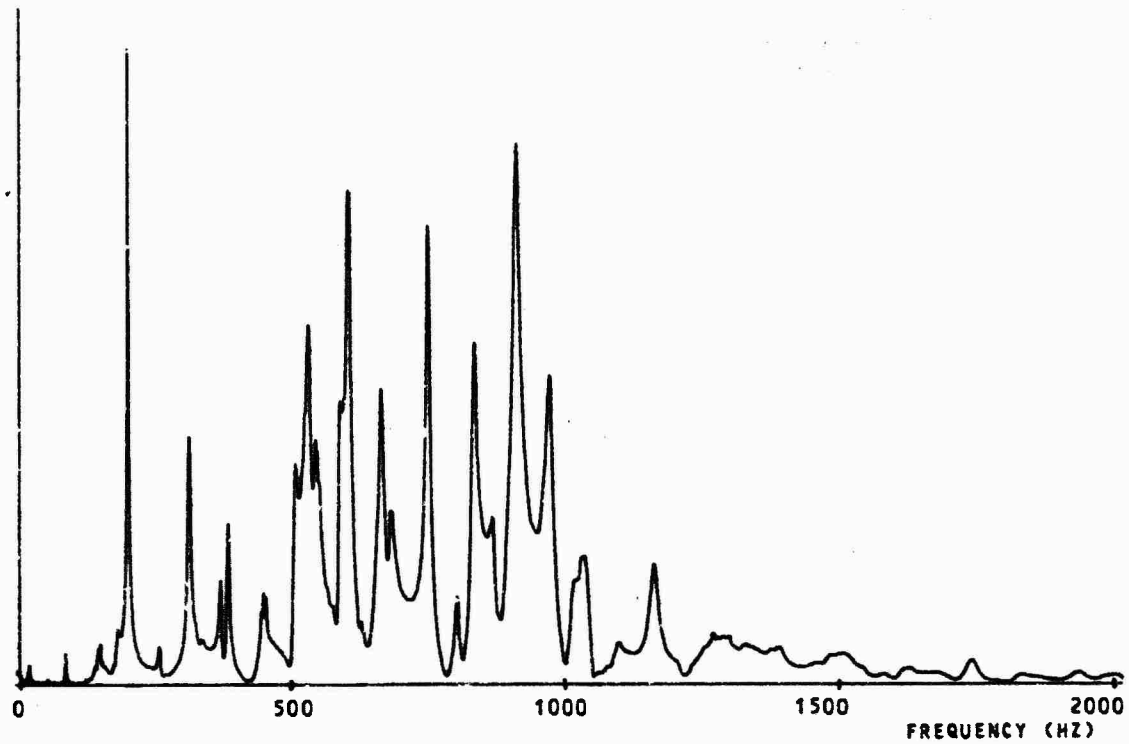


Fig. 2 - Frequency response of the panel in Fig. 1.

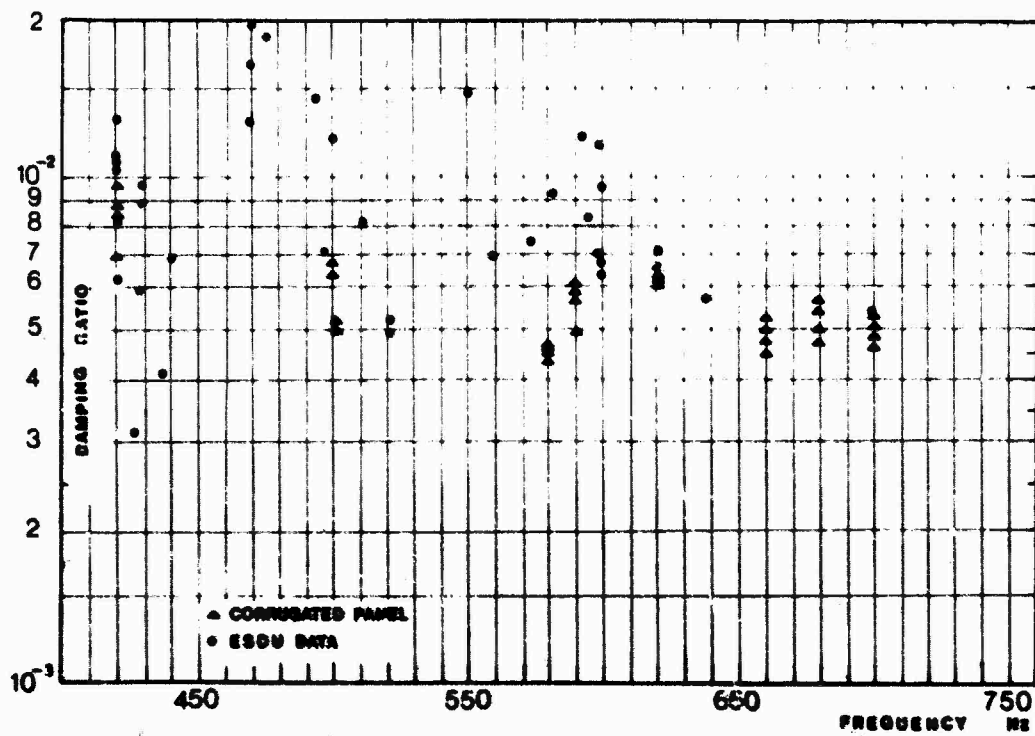


Fig. 3 - Comparison of experimental damping data with ESDU figures.

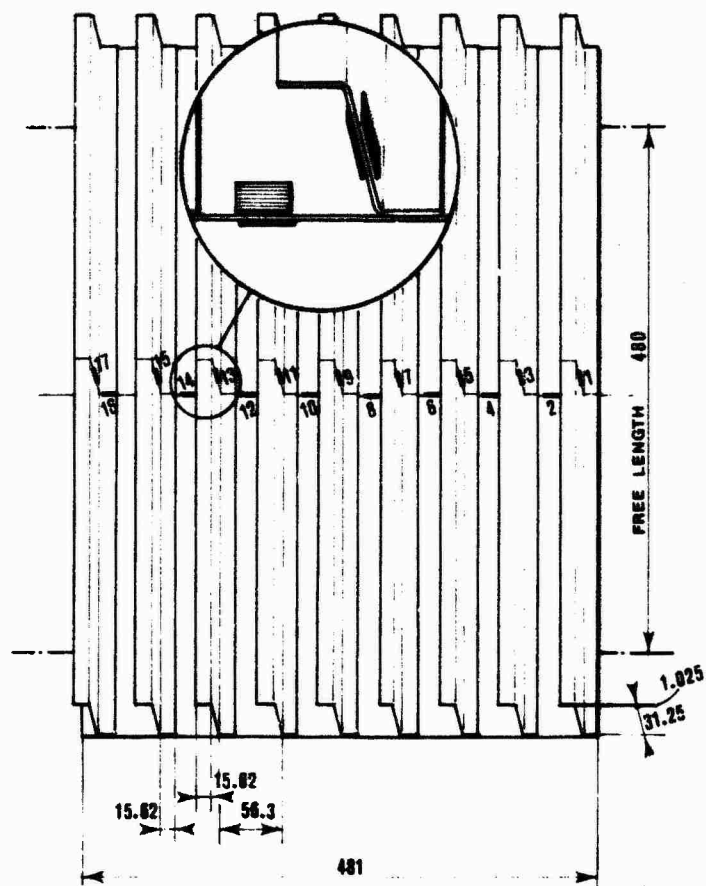


Fig. 4 - Strain-gauged stiffened panel tested in acoustic fatigue plant.

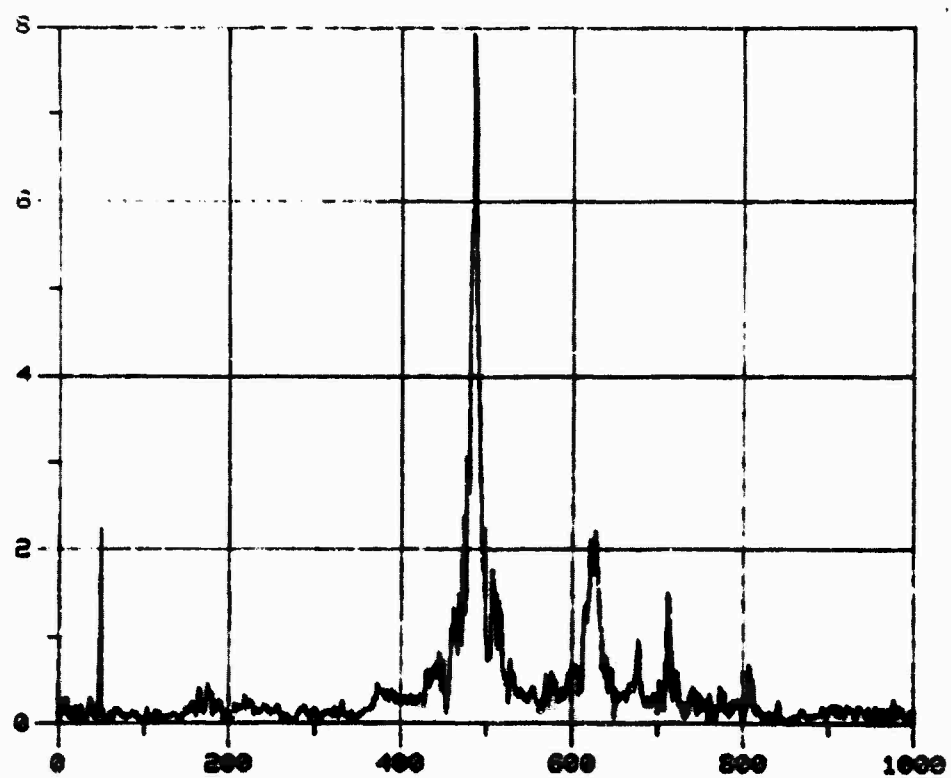


Fig. 5 - Panel of figure 4: transfer function of bridge n. 5.

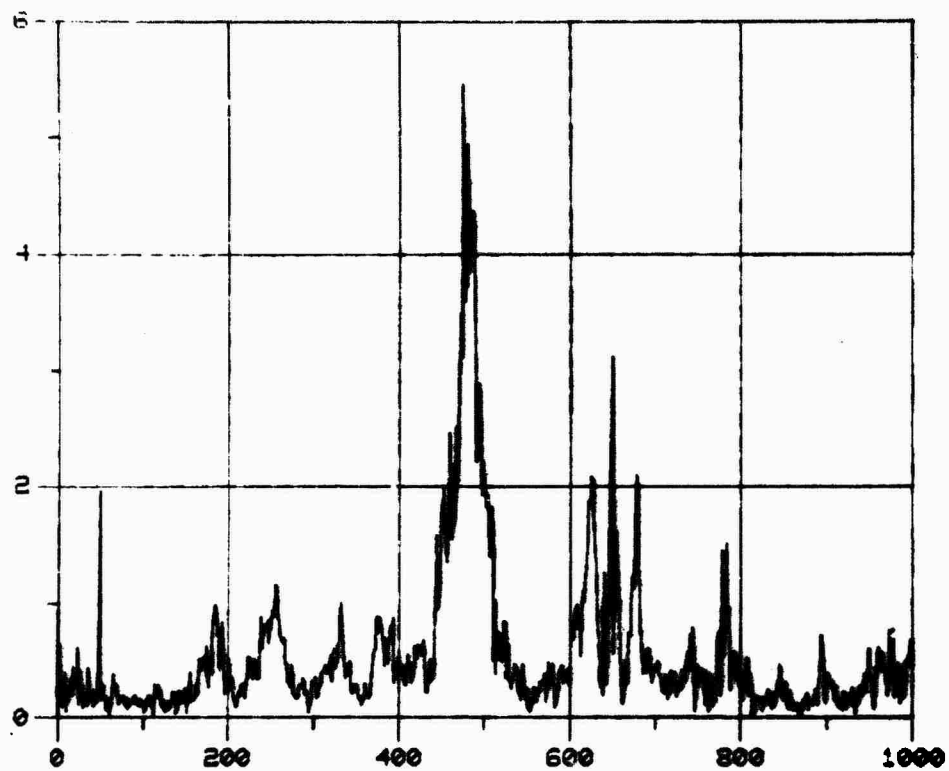


Fig. 6 - Panel of figure 4: transfer function of bridge n. 8 .

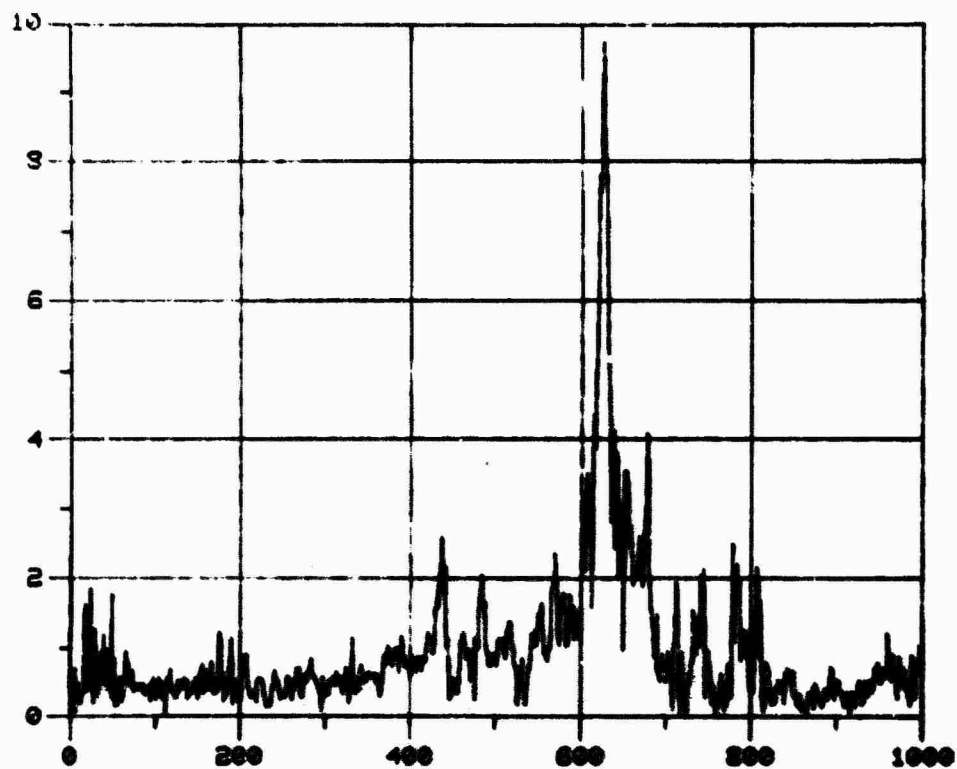


Fig. 7 - Panel of figure 4: transfer function of bridge n. 13.

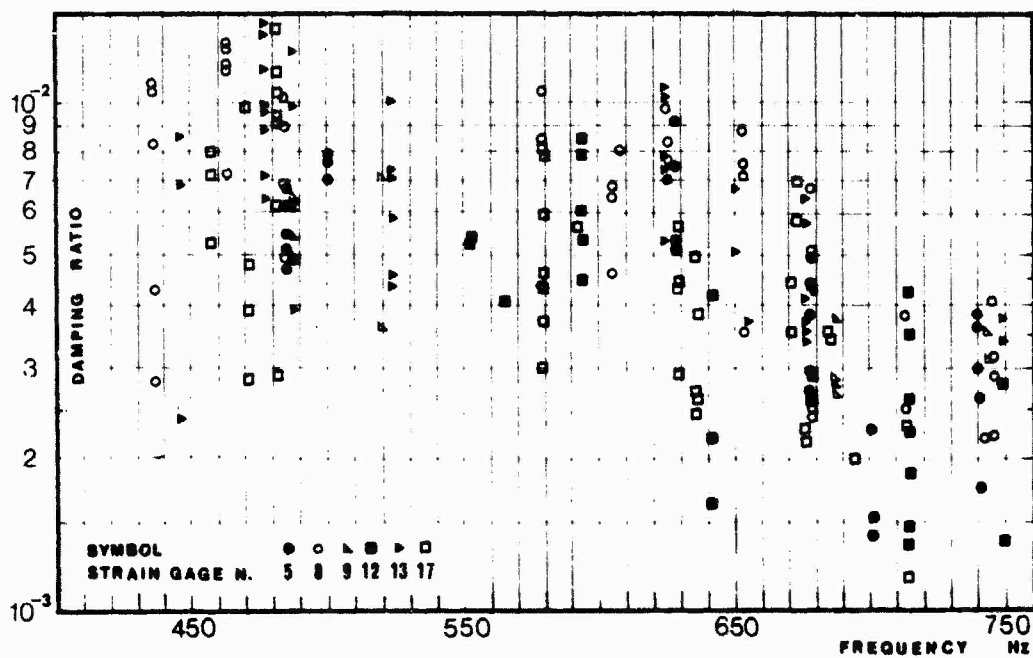


Fig. 8 - Damping data from strain gage bridge output.

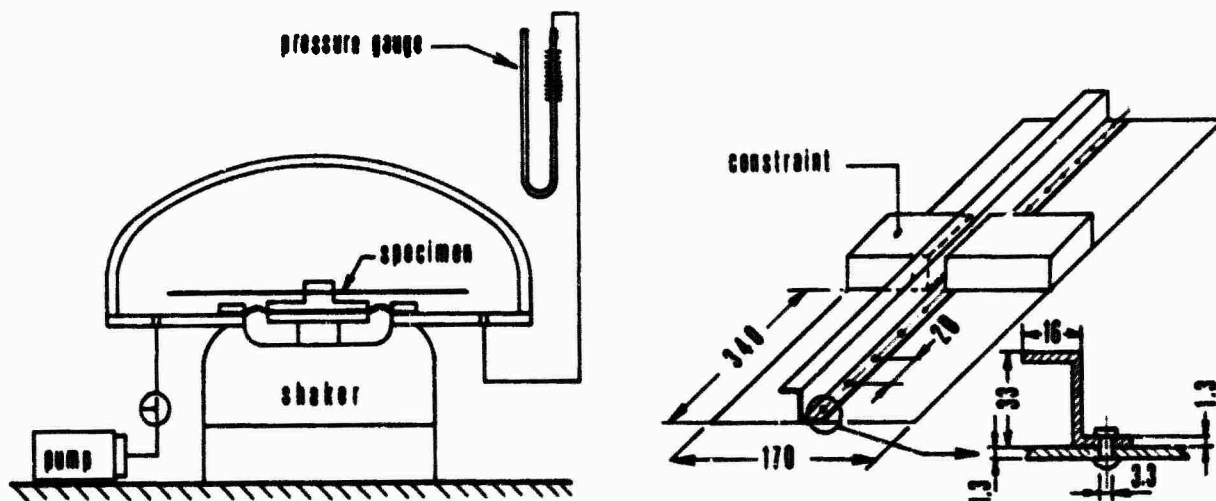


Fig. 9 - Apparatus and specimen for damping tests.

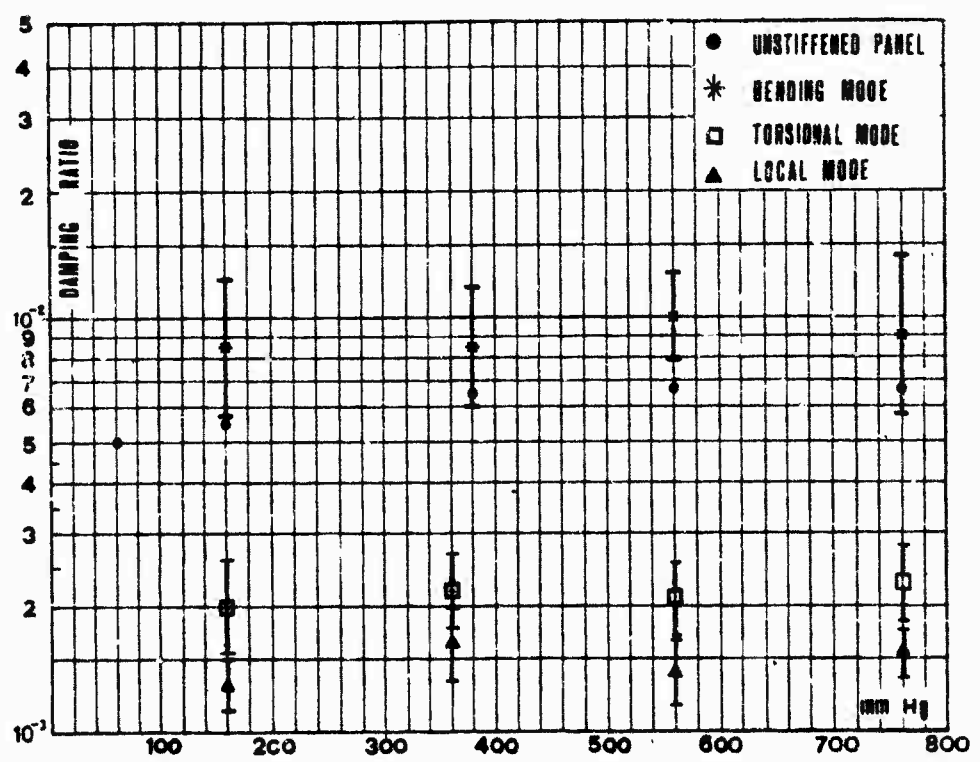


Fig. 10 - Damping data Vs. vacuum degree.

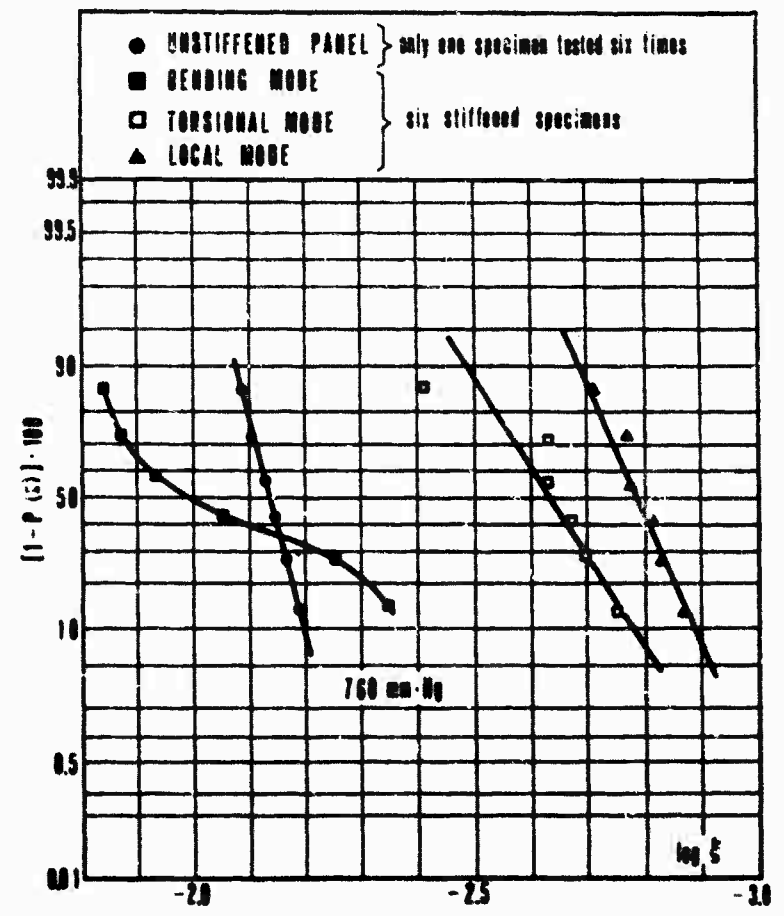


Fig. 11 - Probability distribution of the damping data.

DYNAMIC DAMPING INVESTIGATIONS
ON COMPOSITES

by

H. Georgi

Institut für Bauweisen- und Konstruktionsforschung
Deutsche Forschungs- und Versuchsanstalt
für Luft- und Raumfahrt E.V.
7 Stuttgart 80, Pfaffenwaldring 38-40, Germany

ABSTRACT

Characteristic regularities and data from a series of damping measurements on fibre reinforced composite materials and structures are presented. Experiments were carried out mainly on natural frequencies of lateral vibrations in free decay and forced excitation.

Tests included composite materials (with reinforcement by boron-, carbon-, glass- and synthetic fibres), structural components (sandwich and I-beams); composite structures (wing box, rotor blades). Experimental parameters considered were: amplitude, temperature, vibration mode, frequency, air pressure, aspect ratio, fibre orientation.

Dynamic response properties of several composites are compared by means of a simple linear oscillation model with spring, mass and damping values corresponding with the composite data.

The structural damping of a wing box and a wind turbine blade is compared with the damping of the respective structural element (beam, sandwich).

Numerical extrapolations of the damping behaviour of beams differing from experimental configurations are discussed (fibre orientation, air pressure, aspect ratio).

1. INTRODUCTION AND ACTIVITIES

An accelerating application of fibre reinforced materials and structures can presently be observed, due to the advantages of high strength-to-weight and stiffness-to-weight ratios and the tailorability of strength and damping properties. Weight savings up to 40 % at equalising production costs compared to metal structures are anticipated. Composite technologies already dominate in special ranges of aircraft design and have displaced metal or fabric constructions, e.g. in the fields of sailplanes or helicopter and wind turbine rotor blades.

Therefore, the knowledge of composite damping behaviour becomes increasingly more important. As a rule, experience with damping characteristics of metal structures should not be transferred simply to composite structures, as damping influencing parameters are of different importance and additional effects enter the problem. Too, there is a basic difference in the design of metal and composite structures, though aimed at the same purposes.

Today, there is only poor experience with optimizing vibration properties by prescribed damping behaviour. Only few quantitative recommendations can be given to the benefits relative to economy and endurance of a structure resulting from an improved stress history by best-fit damping characteristics.

In practice, often only fragmentary knowledge of qualitative and quantitative damping properties of composite materials and structures is encountered. Some reasons are:

- The large number of different generally unseparable influence parameters on damping.
- Interaction of usually nonlinear damping mechanisms.
- Extensive test requirements.
- Difficulties in theoretical and semi-empirical treatment of damping.
- Uncertainty in transmitting damping data to different elements, structures or vibration conditions.
- Coupling of stiffness and damping qualities, generally with primary importance of stiffness behaviour.

In Table I several influence parameters are grouped into three main categories, some could be subdivided, though. By this the complexity of distinct damping investigations becomes apparent. The interaction of these parameters results, as a rule, in a complicated nonlinear damping behaviour of oscillating systems rendering system characteristics normally impossible to be solved analytically.

With more simple configurations, mechanisms are predominating sometimes which enable a theoretical approach [1]. The viscoelastic case with quadratic damping and elliptical hysteresis loop is solvable by complex notation and may be represented by net models. However, at engineering stress levels those models often use to fail even with simple composite geometries.

In the near future, experimental damping investigation will be prevailing, accompanied by the attempt to extrapolate numerically the damping data gained from simple elements to more complicated structures. Those methods will become more important, as large structures often are inconvenient for direct damping measurements. Recent results in predicting damping of structures based on numerical superposition of substructure test results are promising [2 to 5].

Activities

Our own damping investigations are mainly directed towards contribution to the following problems:

- Qualitative and quantitative determination of damping properties of composite beams with boron, carbon, glass and synthetic fibres in epoxy, and boron fibres in aluminum matrices (BFRP, CFRP, GFRP, SFRP, B/Al).
- Comparison of damping data of different composites including stiffness properties.
- Damping of structural elements made of the above mentioned composites (Sandwich and I-beams).
- Damping of composite structures (wing box, helicopter and wind turbine rotor blades) and comparison to damping of elements and beams.
- Discussion of a semiempirical approach to damping qualities of composite beams with changed configurational and operational conditions, e.g. influence of laminae orientation angle, reduced air pressure, aspect ratio.

2. COMPOSITE DAMPING AT SMALL AMPLITUDES

Two different regimes of vibration amplitudes have been tested:

- o small amplitudes up to 5 μ m at free-free vibrations
- o Large amplitudes at cantilever mounting (> 5 mm).

Test equipment

For small amplitude damping measurements industrial serial devices are available. The "Elastomat 1.024" (produced by Dr. Förster, Reutlingen, Germany) was employed here, Fig. 1.

The composite test body is supported by thin metallic threads in its nodal points and excited electromagnetically by means of small metal plates bonded to its ends. The advantages of this equipment are:

-elimination of disturbances by support and energy input, - quick damping measurements, - simple locating of natural frequencies and automatic frequency control, - different methods for damping measurements (free amplitude decay, half bandwidth and phase change methods). Drawbacks are: - measurement of small amplitudes only ($< 5 \mu$), - no direct information about loss energy and amplitude, - lowest frequency 300 Hz, - free decay method applied here is inadequate to nonquadratic damping.

The damping temperature dependence in the range of -100 to $+100$ $^{\circ}\text{C}$ was determined in specially equipped temperature chambers at longitudinal and lateral vibrations.

Matrix damping

The damping and stiffness properties of composites are strongly affected by the characteristic qualities of the matrix material applied. For an average epoxy resin system the typical damping, stiffness, and temperature behaviour is plotted in Fig. 2. The logarithmic decrement Δ increases with mode number n and is lower in transversal than in longitudinal vibration at the same mode. Double symbols indicate the scatter of test results from several beams.

Different parameters produce the increase of damping with higher vibration modes: - changed shear to bending stress ratio at decreasing effective beam slenderness, - transition to deformation at transverse contraction restraint.

A damping peak is observed near 0 $^{\circ}\text{C}$, with a maximum slope between 20 to 40 $^{\circ}\text{C}$. Again, damping increases with mode number. In the temperature range considered the Young's modulus increases by a factor of 2.

Composite materials damping

Typical damping and stiffness characteristics depending on vibration mode, laminae orientation angle and temperature are illustrated for BFRP- and CFRP-beams in Figs. 3 and 4; dimensions and processing procedures are listed in App. I. Further data on other composite materials are given in [7 and 8] with identical tendencies.

Qualitative conclusions for damping behaviour are:

- o Damping increases with mode number.
- o Maximum damping occurs at lamina orientation angles between $\pm 60^{\circ}$ and $\pm 67,5^{\circ}$.
- o Temperature dependence of damping follows the trend of the resin but without reaching its maximal values. The influence of the matrix increases with growing fibre orientation angle.

The damping properties with respect to α agree with measurements of other authors, e.g. [9]. Though the multilayer laminate may possibly show orthotropic behaviour it must be considered as composed of per se anisotropic laminae with an essential part of matrix shear damping. This effect should render maximum damping at $\alpha = \pm 45^{\circ}$. This expected result could not be verified by measurements. Therefore, we can assume a more complex stress state as usually expected.

Additionally, Figs. 3 and 4 show the stiffness behaviour: - no uniform tendencies with mode number, - strong decrease at low α with minimum at $\alpha \approx \pm 70^{\circ}$, - less dependence on temperature than the matrix material.

Further parameter studies deal with the influence of - beam support, - attached metal plates, - slenderness, - frequency, etc. [6]. At similar test conditions the maximum scatter of damping values was in a range of $\pm 5\%$, never exceeded $\pm 10\%$.

Comparison of modern composite materials

Damping properties of composite materials should not be compared without taking into account their stiffness qualities. Each term of the complex stiffness or compliance matrices of a harmonically oscillating body includes in the imaginary part a more or less prominent damping value. The real part of the elastic coefficients decides upon the stiffness and resonant frequencies. Thus, a material with high stiffness but with relatively little damping may return to the undisturbed initial state faster than a material with contrary characteristics, as the damping mechanism is acting more frequently per time unit. This aspect postulates not only high stiffness but also high damping capacity for optimum vibration characteristics. However, stiffness and damping of composites are approximately in a reversed proportion.

In Table II values for the logarithmic decrements of damping Δ , stiffness, frequency and density are given for some composite materials in the sequence of damping magnitude. Data hold for free-free lateral vibration in fundamental mode and have been converted to the same geometrical configurations. The reciprocity of stiffness and damping becomes evident. As stiffness qualities of structures often are of primary importance, the margin of damping optimization is left relatively small and often not at all taken advantage of.

To compare the dynamic behaviour the composite data of Table II have been transmitted to a linear oscillator with constant coefficients, so that a Hooke-spring simulates frequency and stiffness and a Newton dashpot the viscous damping, the mass being equal to the beam mass. Different excitation functions were chosen: - free decay at the same initial displacement or the same deflecting force, - and Dirac- and heaviside-functions because they enable simple mathematical treatment via Laplace transformation [10]. These excitations are idealised equivalencies for important service conditions encountered in aero/space structures, e.g. load jettisoning, landing impact, gusts, control deflections, etc.

Fig. 5 demonstrates the time histories of the amplitude envelope for free decay at constant initial deflection (above) and constant static deflection force (below). Notice the fact that at the same initial amplitudes for all materials considered, an amplitude decay to e.g. 10 % is reached by SFRP first and last by B/AI, i.e. not in the sequence of damping magnitude.

For equal deflection forces the sequence is changed again on account of the different initial amplitudes. The dynamic response of step or impulse functions is plotted in Fig. 6 and again the sequence is altered.

These examples indicate that for practically occurring excitation forces different requirements are relevant in reference to damping/stiffness properties. Therefore, according to the time history of the load functions during the life span of a structure, the best-fit material has to be selected by a careful analytical comparison to reach the best compromise.

3. COMPOSITE DAMPING AT LARGE AMPLITUDES

Damping measurements at large amplitudes require usually more effort, as clamping and vibration excitation devices have to be adjusted to the test body.

Test equipment

A clamping device with gripping pressure definable by four pressure gauges was developed and engaged, Fig. 7. The shown mechanical release mechanism for free amplitude decay had to be replaced by an electro-magnetic release set for bending flexible beams in order to achieve clean amplitude envelopes. Besides the location of the deflection pin on the beam its rapid removal for initiating bending vibrations was essential for exact damping measurements.

For nonlinear damping behaviour, oscillator records gained from strain gages turned out to be unsuitable for damping determination because of inaccuracy of visual readings. Therefore, the damped vibration process was stored by means of an IBM 1130 computer. The oscillation was partitioned into 5400 points per run with a maximum resolution of 512 digits for vibration amplitudes. Up to 30 oscillation periods (number depends on frequency) were stored, from which successive amplitudes were taken to determine the log. decrement.

Some difficulties arose from the more or less pronounced anisotropy of elastic properties met with composites, rendering a small unsteadiness in amplitude decay, nearly invisible in amplitude vs. time plots, but leaving substantial distortion in damping curves. Therefore, the measured amplitude envelopes have been softened by regression with a third degree exponential function

$$A = A_0 \exp[at + bt^2 + ct^3]$$

In many cases an approximation of the amplitude envelope by appropriate selection of 4 equidistant amplitudes was successful and rendered the same result as the described regression procedure.

At least threefold repetition of each measurement was carried out with generally less than 5 % scatter in damping values. As a rule, the amplitude envelope is a rather complicated mixed function, especially with friction influence prevailing [11]. The transient initial oscillation range was eliminated by a time-delayed entrance to the vibration. Fig. 8 illustrates schematically the methods employed with damping measurements at large amplitudes in free decay.

Clamping influence

To establish large amplitudes, clamping devices are necessary which are known to contribute to damping on account of friction losses. Fig. 9 shows the influence of the cantilever mounting for unidirectional GFRP beams. Log. decrement Δ_g here was determined from oscillator records over 5 vibration periods as a function of gripping force. The curve below demonstrates less increase in damping at low forces than expected; at clamping pressures $> 30 \text{ N/mm}^2$ damping remains constant. If the friction area is increased by a slot in the clamping region, a damping increment up to 100 % can be observed (upper curve), but it will drop again to the original value at high clamping pressure. Those measurements indicated possible changes in damping and vibration behaviour of structural components due to attrition in joints during service life, e.g. in composite helicopter rotor blades.

If the artificial slot is regarded as a delamination area this can lead to the trial of detecting damages by damping measurements. Tests carried out on this problem were successful only if a considerable loss of energy by friction in the damage area occurred, i.e. delaminations should be localised away from nodal lines and be in regions with strong shear deformations during vibration. Thus, the slot being in the free end of the tested cantilever beam did not noticeably change frequency and damping.

Similar tests with the "Elastomat" with locally enlarged or reduced cross sections of beams by attached lashings or milled grooves rendered the same trends [6]. Therefore, damage detection by damping measurements at present is yet in an impracticable phase.

CFRP cross-ply laminates

Damping dependence on amplitude is demonstrated in Figs. 10 - 12 for a CFRP laminated flat beam at cantilever lateral vibration in fundamental mode and free air; beams tested had 0° , $\pm 22.5^\circ$, $\pm 45^\circ$, $\pm 67.5^\circ$, and $\pm 90^\circ$ laminae orientation angles.

Fig. 10 indicates an enormous influence of vibration amplitude on damping, compared to which the laminae orientation angle influence is relatively small at constant amplitude. At growing amplitudes damping reaches to a multiple of small amplitude damping. Near zero amplitude damping was found by extrapolating the measured values; values include inherent material and clamping damping. The latter could

not be specified closer with the available test device. Dotted lines show the characteristic curves for Young's modulus and frequency. By plotting damping vs. maximum bending stress another characteristic can be observed due to the widely differing bending stiffness at different orientation angles, Fig. 11. Whereas damping peaks at constant amplitudes occur at $\alpha \approx \pm 45^\circ$, peaks are now shifted to $\alpha \approx \pm 67,5^\circ$ and slopes are remarkably steeper. Stresses are still left in the elastic range. The large increase of damping with rising stress level and orientation angles becomes particularly evident from Fig. 12, showing the reciprocal tendency mentioned with respect to Young's modulus in Fig. 10.

Air pressure

From the steep increase in damping with amplitude - even at small stress levels - it can be concluded that the moved air volume, acting as external damper, accounts for this fact, more than the increasing ratio of bending and shear stresses. This has been verified by tests at reduced air pressure in a vacuum chamber, Fig. 13. At high vacuum a nearly linear damping behaviour ($n = 2$ in Table I) can be assumed for the tested composite beams. Up to date, only few test data on damping influence of air pressure are available, especially concerning composites, though for space structures knowledge of damping properties in vacuum is indispensable.

To reduce test expenses the question arises how to evaluate air damping theoretically and/or empirically. Velocity-proportional and velocity-squared air drag damping is treated in [12, 13]. However, from insteedy wing aerodynamics we know about the rather complicated relationship between aerodynamic coefficients and frequency, amplitude, aspect ratio, Reynold's number etc.; that leaves the problem unsolved even for simple cases. Tubes in transverse flow (Karman's vortex street) can be treated theoretically [14], but for transversely vibrating beams with nonuniform velocity distribution no numerical method is available.

From Fig. 13 a nearly linear dependence of air damping on air pressure or air density seems to be derivable. To substantiate this presumption we checked if a linear extrapolation from normal pressure would render adequate damping values for reduced air pressure. The result is plotted in Fig. 14 for CFRP 0° ; for other laminae orientations the same tendency became apparent.

From the fat line, representing regressed measurement data for 760 mm Hg, damping at reduced air pressure was approximated by

$$\Delta_p \approx \frac{p}{760} [\Delta_{760} - \Delta_i] + \Delta_i$$

with Δ_i internal damping, approximated by graphical extrapolation. Comparing correlating curves for the same aspect ratio ($\lambda/\lambda_0 = 1$) it becomes obvious, that linear extrapolation (\square) renders slightly higher damping values than measurements (\bullet), and percentage error increases with decreasing air pressure.

Air damping additionally depends on aspect ratio (width/length), as the amount of moved air mass which flows around the beam edges during vibration becomes smaller with increasing beam width. If there is one value from damping measurements at a reduced aspect ratio and normal air pressure (\oplus), the influence of beam width on damping can be included in the above mentioned linear approximation for pressure reduction:

$$\Delta_{\lambda,p} \approx \frac{p}{p_0} [\Delta_{p_0} K - \Delta_i \{1 - \frac{p_0}{p}\}]$$

where

$$K = \frac{1}{\Delta_{\lambda_0}} \left[\Delta_{\lambda_1} + \frac{\Delta_{\lambda_0} - \Delta_{\lambda_1}}{\lambda_0 - \lambda_1} \{\lambda - \lambda_1\} \right]$$

This simple relation applied to aspect ratios $\lambda_1/\lambda_0 = 2/3$ and $1/3$ is plotted in Fig. 14, too, showing the possibility of evaluating damping at variable pressure and beam width from one curve and an additional point at reduced width, all taken at 760 TORR.

For information, examples are given in Fig. 14 for measured amplitude decays and damping values resulting therefrom (zig-zag lines, nonregressed data, Δ , \diamond). These unsteady lines do not represent scattering due to inaccuracy of measurements and are reproducible; they are caused by the fact that even simple composite beam configurations must not give "clean" amplitude decay.

Frequency

The frequency is not affected strongly by decrease of damping during amplitude decay or by reduction of air pressure. For 0° -CFRP frequency increases by only 0,5 % in the amplitude range from 120 to 12 mm and only by 2,5 % at pressure reduction from 760 to 50 mm Hg.

Frequency range was extended to the fourfold of the initial value by shortening the free length of the beams. With growing frequency an increase in damping was observed, Fig. 15, though not visibly affected by aspect ratio. The per cent increase of damping with frequency is essential, especially at large amplitudes and low air pressure.

Obviously, the slope of damping curves remains nearly unchanged by pressure reduction; therefore, the damping increase can be assumed predominately to be a frequency effect, while the influence of frequency-dependent insteady aerodynamic forces is small in the frequency range considered. Further investigations are required in respect to the different clamping conditions, too.

4. DAMPING OF COMPOSITE STRUCTURAL ELEMENTS

Most treatises published on experimental and theoretical handling of the damping behaviour of composite structural elements are directed mainly towards sandwich beams with aluminum core and composite facings [15 to 18]. Other publications deal with metal beams with covering or embedded composite layers or bonded metal beams [19 to 21]. Systematic research data concerning the regularities of damping behaviour of modern composite structural elements are not available.

A teamwork with VFW-Fokker rendered damping data for I-beams (composed of two aluminum U-profiles partly with CFRP facings bonded on) and for sandwich beams with aluminum honeycomb cores and aluminum or CFRP/BFRP hybrid composite facings [22, 23], Figs. 16 and 17.

The damping measurements were carried out at small amplitudes in free-free lateral vibrations and consecutive resonant frequencies and show these characteristic trends:

- o Damping increases in the sequence (Fig. 16):
I-beam; I-beam with composite layers; Al-sandwich; sandwich with 0° -CFRP/ 30° -BFRP-facings; sandwich with 0° -CFRP-facings; sandwich with 90° -CFRP/ 50° -BFRP-facings; sandwich with 45° -CFRP-facings.
- o A remarkably unsteady damping curve with increasing natural frequencies is observed on sandwich beams only.

Additionally, the damping data of isolated 0° - and 45° -CFRP-facings are plotted. The graph offers an insight into the damping characteristics of special composite structural elements of different configurations.

Again, the temperature dependency of damping is typically influenced by the matrix behavior, though there is some unsteadiness especially at higher lamina orientation angles, Fig. 17.

5. DAMPING OF LOAD-BEARING COMPOSITE STRUCTURES

Composite technology for load carrying aero/space structures is still in an accelerating development phase. In the fields of sailplanes and rotor blades composite techniques are state of art, but without rendering sufficient data on damping up to date.

Wing box

An experimental wing box developed together with the Dornier Company for loading tests of composite wing structures was also tested to measure damping properties. The box is a fulldepth honeycomb sandwich configuration with aluminum honeycomb core and hybrid composite facings of several 0° -CFRP- and $\pm 30^\circ$ -BFRP-laminae (App. I). GFRP-U-spars were used on both sides to close the box. The joints for load introduction on both ends were made of aluminum and titanium components.

The equipment for free decay testing consisted of a rigid clamping device and a mechanical release set; deflection was achieved hydraulically, Fig. 18.

Test objective was to expand the measurements at small amplitudes, carried out at DFVLR-AVA-Göttingen, to large amplitudes on the identical box. Further the damping of the wing box should be compared to the damping behaviour of the elements (sandwich, facings). Results are plotted in Fig. 19a vs. a reduced amplitude (vibration amplitude/free length) which seemed to be a reasonable parameter. To find a parameter for comparing the damping of different elements and structures proved to be a precarious problem, as data differ in dimensions, frequencies, mass and stiffness distributions and stresses. Amplitude and stress per se are unsuitable for damping comparison.

As evident from Fig. 19a, comparing the damping of different but similar configurations seems to be difficult, but not impossible. Related to the damping of facings and sandwich beams, the wing box damping (★) is expected to be between the values for 0° - and 45° - sandwich beams (◇). However, less damping of the wing box was measured, accidentally close to CFRP- 0° -facings.

By adding tip masses to the free end of the wing box, damping changes as indicated in the small diagram of Fig. 19a. Assuming, the aluminum tip end in the box (mass ≈ 1 kg) would be removed, a damping increase of about 20 % would occur, rendering approximately the same damping as the 0° -sandwich beam (★).

Added tip masses decrease frequencies, but mode shapes are deformed, too. To assure that stress distributions are kept invariant over the test structure, the box frequencies were reduced by attaching distributed adequate additional masses to the box surface [24]. Fig. 19b shows the results of the free-free fundamental bending mode at small amplitudes and demonstrates the damping dependence on frequency of this composite structure.

Assembled structures often cannot be changed afterwards. Therefore, further measurements should be carried out in order to provide damping data for an empirical or numerical approach to the damping behaviour of composite structures from component damping. Thus prescribed damping properties could be considered in the design phase already.

Composite rotary wing blade structures

The advantages of composite technology application to helicopter rotor blades and blades of wind energy turbines have already been recognised since two decades. Blades have been developed to full operational safety to date. Rotor design was essentially simplified by the omission of flap and lag hinges, the functions of which were replaced by the inherent elasticity of composite blades.

One of the activities of our DFVLR-Institute concerns the development of wind energy converters. The rotor blades are designed as composite structures. With a GFRP-blade of a 10 KW turbine damping tests were carried out, Fig. 20.

The methods of free amplitude decay and of forced vibrations by electrodynamic excitation in the lower bending modes have been applied to a cantilever mounted blade of 5,5 m length. At forced vibrations two cases are distinguished: constant energy input at different vibration modes and, on the other hand, constant tip amplitudes for all modes tested.

Fig. 21 shows the results up to the fifth mode. For free decay in fundamental mode the typical damping dependence on amplitude is observed again, chiefly due to air damping (1). At forced bending vibrations caused by harmonic excitation at constant energy input, for all the modes a considerable amplitude - and damping - decrease up to mode IV becomes apparent; for the subsequent mode damping increases again (2). Curve (3) demonstrates damping decrease vs. resonant frequencies at constant energy input.

Vice versa, if the tip amplitudes for all modes are kept constant by increasing the energy input (curve (4) for tip amplitudes ± 15 mm), there is a damping decrease by 25 % between modes I and II and afterwards a weak increase in damping. From this we can conclude a strong influence of air damping, especially at the fundamental bending mode. Concerning higher modes, we cannot distinguish by now between the decreasing share of air damping and the increasing share due to higher shear/bending stress ratios in resulting damping increase.

The intersection of curves (1) and (2) proves the damping values from free decay and from half-bandwidth-method to be in good agreement.

Damping of the same GFRP-blade is compared to the damping of conventional metal helicopter rotor blades [29] in Fig. 22. The values for free decay in fundamental bending mode are plotted vs. amplitude/free length ratios. Profile sections indicate essential differences in structural design of composite blades. A higher damping capacity of the composite blade compared to metal blades is observed. Of course, from tests on simple beams no direct conclusion can be drawn to the blade damping.

6. SEMI-EMPIRICAL DAMPING EVALUATION OF CROSS-PLY LAMINATES

Description of method

Mathematical formulation of the damping of composite structures is usually coupled with enormous difficulties. Therefore, experimental determination of damping of composite structures will prevail in the next future. For simple composite beams and specimens, a numerical treatment of damping is difficult, too, because of the uncertainties in interpreting the applied methods. On the other hand, series of measurement covering all influence parameters are time-consuming and expensive. So the requirement for methods to extrapolate damping values to differing configurations is of great interest. As shown above, evaluation of damping data for altered air pressures and aspect ratios can supply satisfactory results.

The following method deals with the predictability of damping characteristics of composite beams, composed of laminae with varying symmetrical lamina orientation angles. Availability of representative data of distinct beams is presumed.

For unidirectional symmetrically arranged laminae orthotropic stiffness behaviour often can be assumed approximately. Formulae for moduli and damping are given in Table III. Eq. (1) describes the motion of a thin orthotropic plate in lateral vibration [26]. Symbols are: w deflection, t time, ρ density, s thickness, b_{ik}^k bending stiffnesses of complex orthotropic stiffness matrix, x longitudinal, y lateral coordinates.

For the geometrical dimensions of the beams considered, the wave length of the coupled transverse resonant vibration in y-direction is much longer than the wave length in x-direction λ_B . If beam width b is smaller than $\lambda_B/2$ - and this condition holds for the beams regarded - the vibration in y-direction may be neglected. Thus eq. (1) becomes uncoupled to pure lateral vibration in x-direction, eq. (2). Eq. (3) represents the general solution for a free-free beam in lateral vibration with linear damping (A_n, C_n are constants, η_n damping factor, ω_n circular natural frequency, τ_n roots of frequency equation $\cos \tau_n L + \cosh \tau_n L = 1$, n mode).

After separating the real and imaginary parts, solutions of eq. (2) by eq. (3) render the storage and loss functions eq. (4), where I is the axial inertia moment, F the cross section. At damping factors < 0.1 , eq. (5) is valid for the n^{th} values of natural frequency, eq. (6) for the damping factor, and eq. (7) for the log. decrement. The complex longitudinal stiffness b_{11}^k is replaced by the longitudinal stiffness a_{11}^k , according to $b_{11}^k = s^3 \cdot a_{11}^k/12$. As indicated by eq. (10) in Table IV, a_{11}^k is composed of storage stiffness a_{11}^s and of loss stiffness a_{11}^v . The loss factor d_{11} is defined by the ratio a_{11}^v/a_{11}^s .

If transverse beam contraction is not restrained, then $a_{11}^s = E_{11} \frac{A}{L}$; the dynamic modulus in bending is given by eqs. (4) and (5) from measured resonant frequencies. This holds for thin beams in pure bending, as long as the empirical value $s < \lambda_B/2\pi$ is not exceeded. Corresponding evaluation of shear strain influence and deformation of the beam cross section (for isotropy) proved eq. (4) and (5) to be employable [27] for the beams considered.

Beam slenderness L/b should be > 5 to assure unrestrained transverse contraction of the beam. If this ratio is related to the nodal distances in the different modes, then at $n = 2$ already transverse contraction restraint should occur, for beam dimensions with $L = 150$ mm and $b = 15$ mm, for example. An increase in stiffness and a decrease in damping due to this effect was not observed, however.

Evaluation of modulus and damping

The orthotropic stiffness matrix (Table IV) contains 4 independent elastic constants. Provided that measurements carried out on 0° - and 90° -beams rendered uncoupled compliances a_{11}^{s*}, a_{22}^{s*} and loss factors d_{11}^*, d_{22}^* , there were left only two unknown coefficients in the equations of polar transformation for the rotated compliances: transverse contraction term a_{12}^{k*} and shear compliance a_{33}^{k*} (eq. 9).

For GFRP laminates it has been proved that, for uniaxial loading, determination of diagonal coefficients in the compliance matrix for the main directions of orthotropy is sufficient, i.e. omitting a_{12}^{k*} leads to an error smaller than 10 %, thus being in the scatter of measurement accuracy [9].

Now, if another pair of frequency and damping data of a third arbitrary lamina orientation is available, shear compliance a_{33}^{k*} can be calculated from transformations eq. (9) for $a_{12}^{k*} = 0$ (e.g. for $\alpha = \pm 45^\circ$ see eq. (11)). For all residual orientation angles $\pm \alpha$ the coefficients of the compliance diagonal matrix, respectively by inversion the complex stiffness matrix, can be calculated now.

Fig. 23 shows the results thus derived from measurement data on $0^\circ, 45^\circ$ and 90° -beams. Hatched areas indicate the difference between measurements and numerical approach. The applied evaluation method delivered an acceptable agreement of numerical and test data for GFRP- and CFRP-beams. For BFRP, results are diverging in the range $\pm \alpha < 40^\circ$. Caused by the inherent anisotropy of BFRP, due to the rather large fiber diameters, there may be an unneglectable influence of term a_{12}^{k*} . Thus, shear modulus $G = 1/a_{33}^{s*}$ should be taken only as rough approximation.

7. SUMMARY

Damping behaviour of modern composite materials is governed by characteristic regularities, qualitatively valid for the entire material category. Air damping and test body configuration have a great influence on damping, especially at large amplitude vibration. Comparison of damping capacities of different configurations and materials should include stiffness properties.

Prediction of structural damping of composed systems based on damping measurements of simpler, but similar configurations seems to be possible (e.g. wing box). Damping of more complex structures (e.g. rotor blades) at present cannot be derived from simple element damping.

A numerical approach to damping characteristics of flat beams at modified conditions is practicable, but sometimes with unsatisfactory accuracy (air pressure, aspect ratio, lamina orientation).

Future damping activities on composites should be directed towards problems as:

- further investigations on regularities and relationships of damping behaviour of structural elements and structures made of them, - improvement and development of numerical approach to damping behaviour, - systematic completion of experimental damping data, - influence of composite structures damping characteristics with respect to economy and life endurance, - damping behaviour of composites under environmental conditions, e.g. space environment.

8. REFERENCES

1. Ruzicka, J.E. (Ed.), Structural Damping, Pergamon Press, Dec. 1959
2. Santini, P., Castellani, A., Nappi, A., An Introduction to the Problem of Dynamic Structural Damping, AGARD Rep. No. 663, 1978.
3. Kana, D.D., Huzar, S., Synthesis of Shuttle Vehicle Damping Using Substructure Test Results. J. Spacecraft Vol. 10, No. 12, Dez. 1973.
4. Kana, D.D., Unruh, J.F., Substructure Energy Method for Predicting of Space Shuttle Mode Damping. J. Spacecraft Vol. 12, No. 5, May 1975.
5. Hasselmann, T.K., Damping Synthesis from Substructure Tests. AIAA-Journal, Vol. 14, No. 10, Oct. 1976.
6. Georgi, H., Dämpfungseigenschaften von faserverstärkten Verbundwerkstoffen und Composite-Strukturen, Vortrag Nr. 19 AVK 14. Off. Jahrestagung, Freudenstadt 4.-6.10.1977.
7. Georgi, H., Dämpfungsmessungen an Hybridproben. DFVLR - WB-BK 454 74/5, 1974.
8. Georgi, H., Untersuchung des Werkstoffdämpfungsverhaltens an Faserverbund- und Metallwerkstoffen. DFVLR WB-BK IB 454/74/2, 1974.
9. Ghosh, S.K., Kehl, K., Versuchstechnische Bestimmung des Dämpfungsverhaltens orthotroper GFK-Schichtlamine. Institut für Luft- und Raumfahrt, TU Berlin, ILR Mitt. 35 (1976).
10. Georgi, H., Schwingungsverhalten linear gedämpfter Schwinger mit den Eigenschaften faserverstärkter Kunststoffe. DFVLR WB-BK IB 78/10, 1978.
11. Dahl, P.R., Solid Friction Damping of Mechanical Vibrations. AIAA-Journal, Vol. 14, No. 12, Dec. 1976.
12. Baker, W.E., Woolam, W.E., Young, D., Air and Internal Damping of thin Cantilever Beams. Int. J. Mech. Sci., Pergamon Press Ltd. 1967, Vol. 9 pp. 743 - 766.
13. Adams, R.D., Bacon, D.G.C., Measurement of the Flexural Damping Capacity and Dynamic Young's Modulus of Metals and Reinforced Plastics. J. Phys. D: Appl. Phys. Vol. 6, 1973.
14. Fürsching, H., Grundlagen der Aeroelastik. Springer-Verlag, 1974.
15. Di Taranto, R.A., Natural Frequencies and Damping Capabilities of Laminated Beams. MEL R.u.D. Rep. 295/66.
16. Lazan, B.J., Keler, L., Damping and Fatigue Properties of Sandwich Configurations in Flexure. ASD Tech. Rep. 61-646, 1961.

17. Bert, C.W., Wilkins, D.J., Crisman, W.C., Damping in Sandwich Beams with Shear Flexible Cores, Transactions of the ASME, Nov. 1967.
18. Socvere, J., Dynamic Properties of Graphite Fiber Honeycomb Panels. AIAA paper No. 73/326.
19. Oberst, H., Frankenfeld, K., Über die Dämpfung der Biegeschwingungen dünner Bleche durch festhaftende Beläge. Akustische Beihefte, Acustica Heft 4, 1952.
20. Yin, T.P., Kelly, T.J., Barry, J.E., A Quantitative Evaluation of Constrained Layer Damping. Transact. of the ASME, Paper No. 67 - Vibr. 26, 1967.
21. Lindholm, U.S., Yeakley, L.M. Studies of Interface Damping. Southwest Res. Inst., Oct. 1969, Houston.
22. Georgi, H., Dämpfungseigenschaften von Sandwichstäben. DFVLR WB-BK IB 454/75/8, 1975.
23. Borgwardt, C., Experimentelle Bestimmung der Dämpfung von Hybridverbundwerkstoffen. VFW-Fokker Ber. Ek. 414-04-1977.
24. Ludwig, D., Dämpfungsuntersuchungen an einem Holmkasten in Faser-Hybrid-Bauweise. DFVLR IB 253-77 C 03, 1977.
25. Baker, W.E., Inherent Vibration Damping of Helicopter Blades. Southwest Res. Inst. San Antonio, May 1969.
26. Wiedemann, J., Berechnung und Modellierung des Dämpfungsverhaltens orthotroper Schichtlamine. Vortrag Nr. 5, AVK 13. Off. Jahrestagung, Freudenstadt 5.-7.10.1976.
27. Huang, T.C., The Effect of Rotatory Inertia and of Shear Deformation on the Frequency and Normal Mode Equations of Uniform Beams with Simple End Conditions. J. Appl. Mech., Vol. 28 (1961), p. 579.

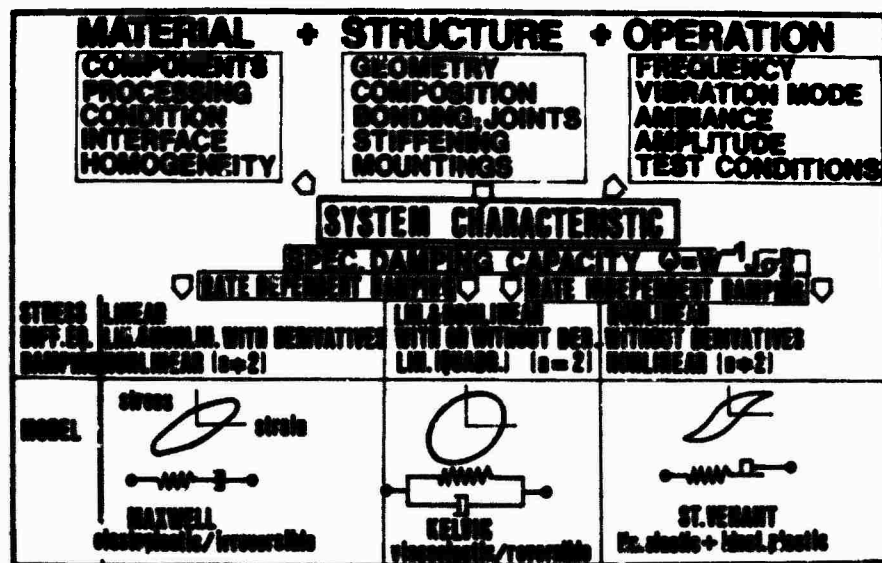


Table 1 : Characteristics of Composite damping

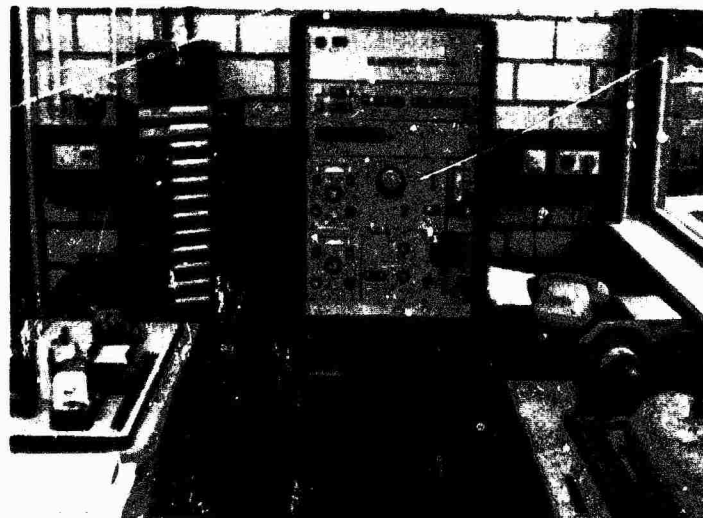
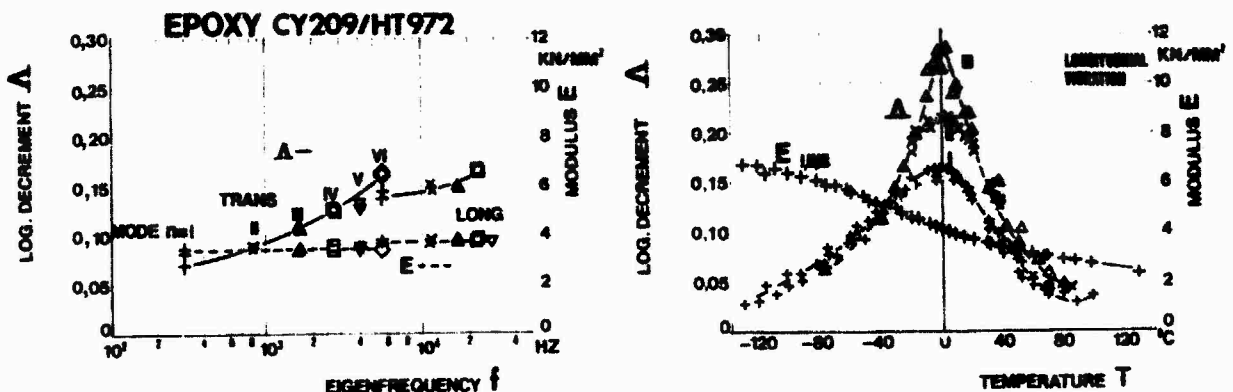


Fig. 1 : Test equipment "Förster ELASTOMAT 1.024" for small vibration amplitudes



Figs. 2A and 2B : Logarithmic decrement of matrix damping and Young's modulus vs. natural frequencies and temperature

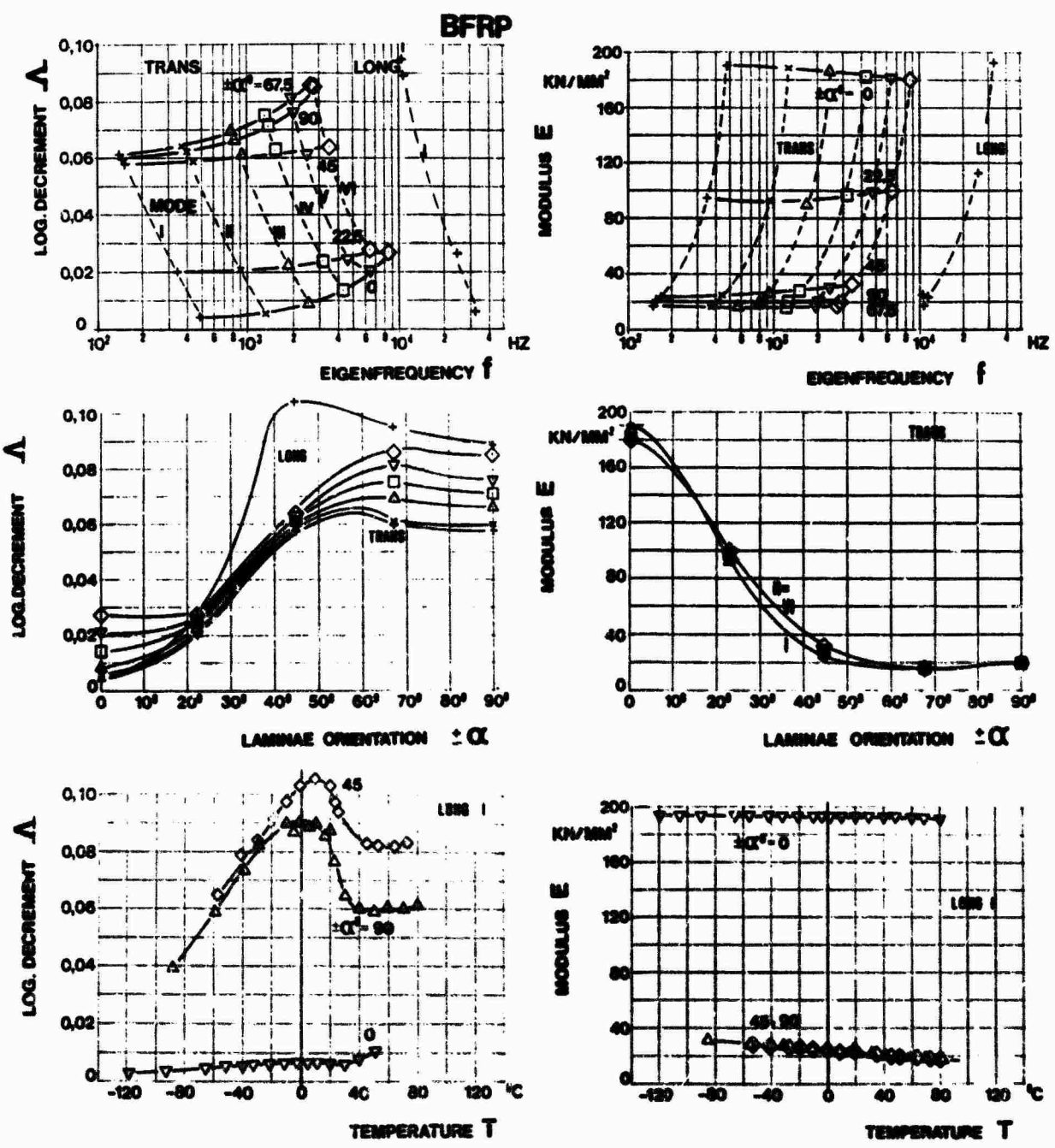


Fig. 3 : Characteristic damping and stiffness behaviour of boron fibre reinforced plastics

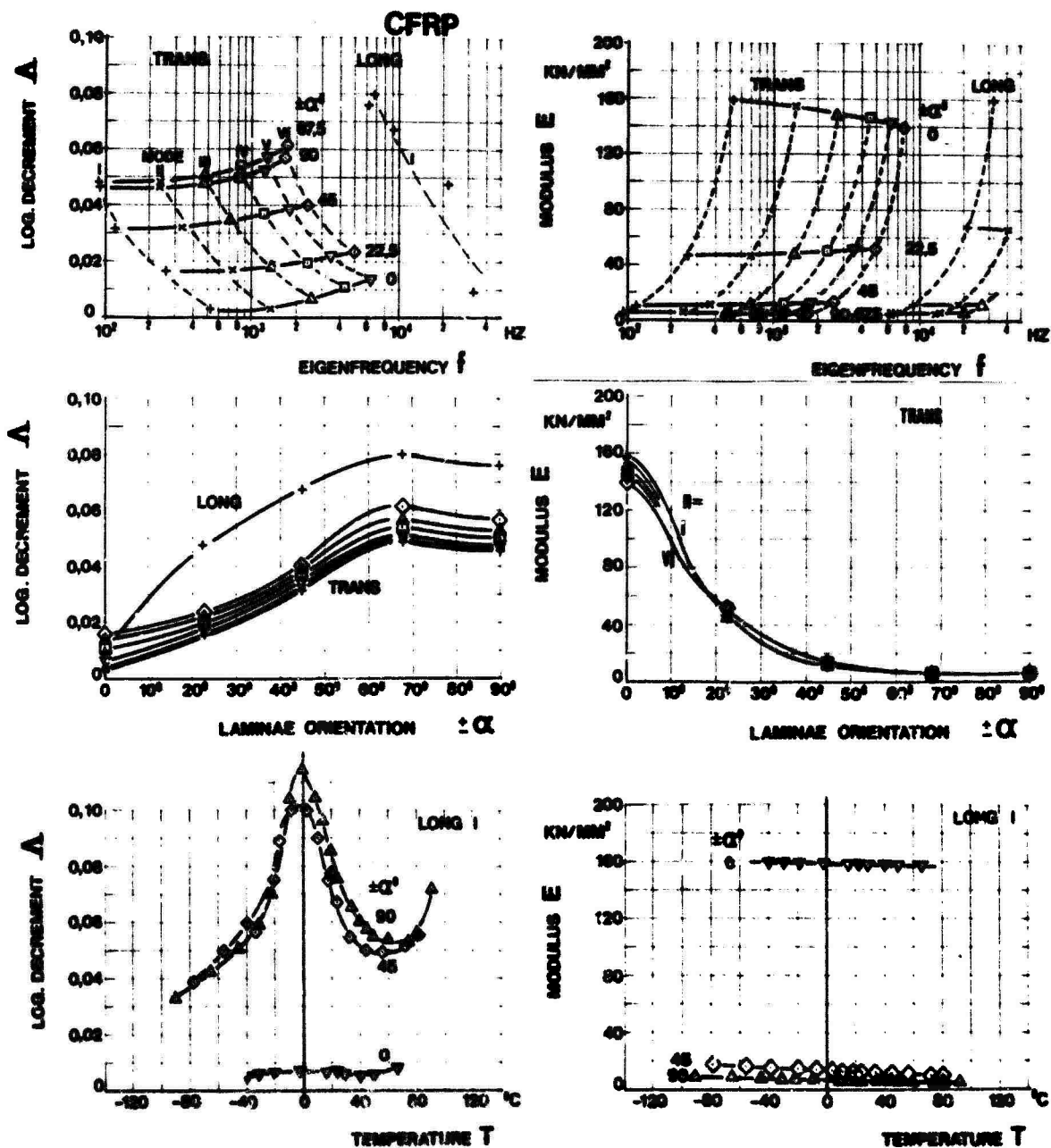


Fig. 4 : Damping and stiffness behaviour of carbon fibre reinforced plastics

10

ELASTICITY 1.024
LATERAL FUNDAMENTAL MODE
AMPLITUDE $< 5 \mu$
FREQUENCY 10 ± 0.1

MATERIAL	LOG DECREMENT Δ	MODULUS E (KN/MM ²)	FREQUENCY (Hz)	DENSITY (g/cm ³)
CFRP	0.0130	3.6	1.00	1.200 $\times 10^{-3}$
SPF	0.0100	22	4.50	1.224
CFRP/SPF	0.0097	97	9.30	1.102
SPF	0.0091	16	4.50	2.000
SPF	0.0088	130	10.02	2.000
CFP	0.0086	100	10.30	1.000
SPF/AL	0.0080	230	9.80	2.001
AL	0.0081	99	8.00	2.000

Table II: Test data at small amplitudes. Lateral fundamental mode.

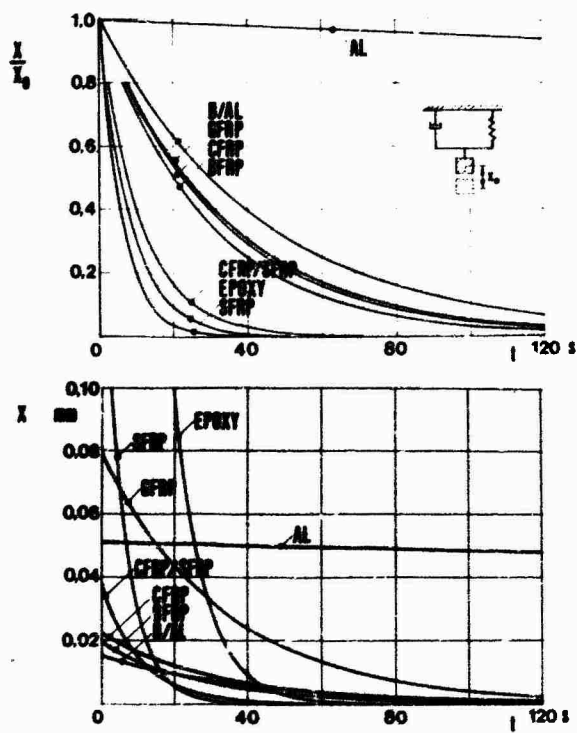


Fig. 5 : Amplitude envelopes at constant initial deflection (above) and const. deflection force (10^{-2} N, below)

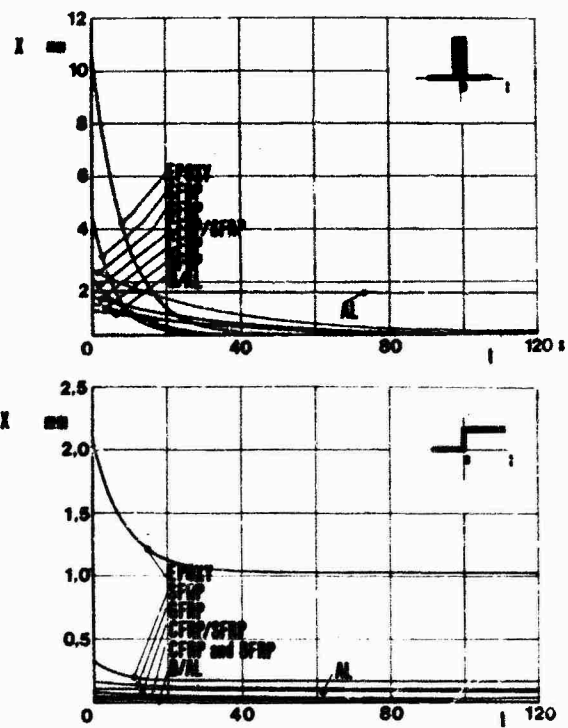


Fig. 6 : Amplitude envelopes at constant impulse excitation (10^{-2} Ns, above) and const. step function (10^{-2} N, below)

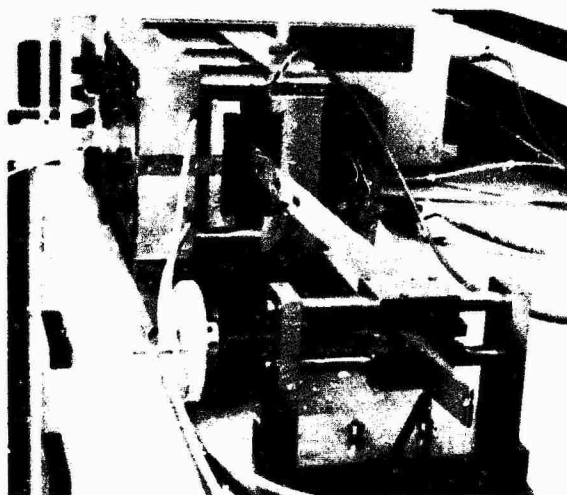


Fig. 7 : Test equipment for large amplitudes.

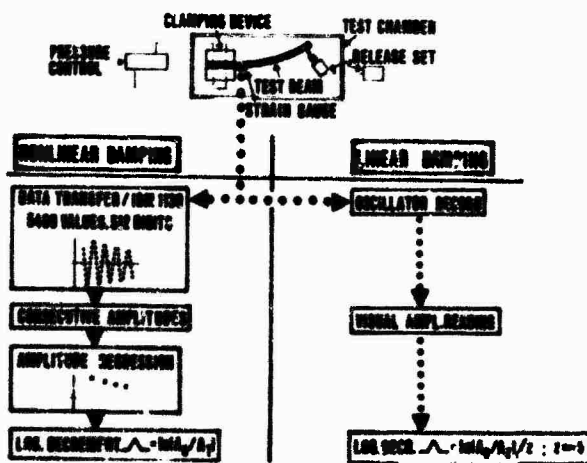


Fig. 8 : Test methods employed at free decay.

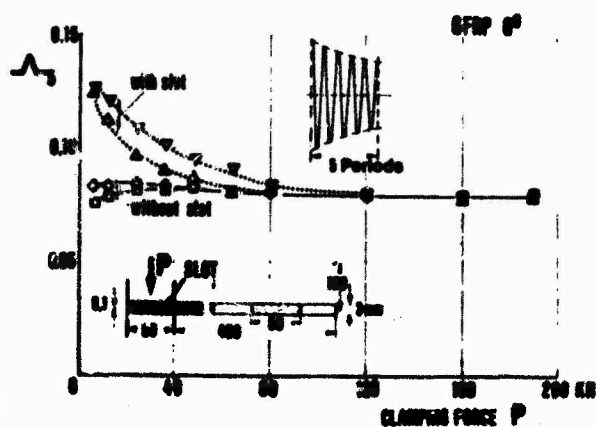


Fig. 9 : Friction in clamping device.

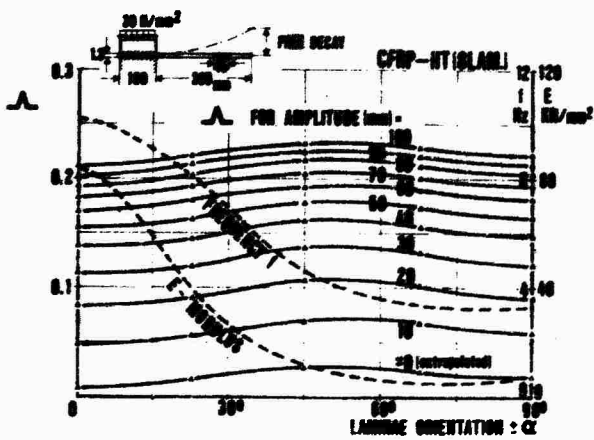


Fig. 10 : Effect of amplitude and laminae orientation

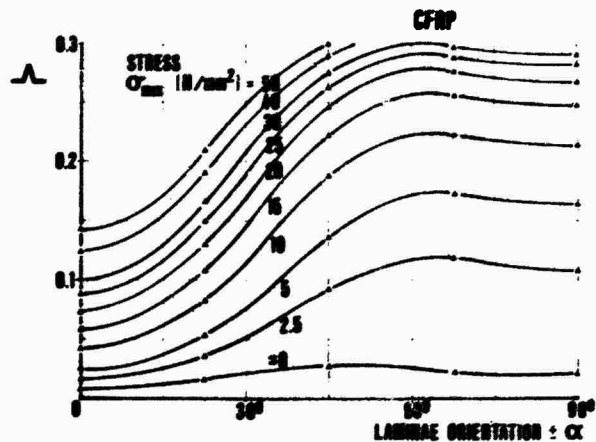


Fig. 11 : Effect of stress amplitude and laminae orientation

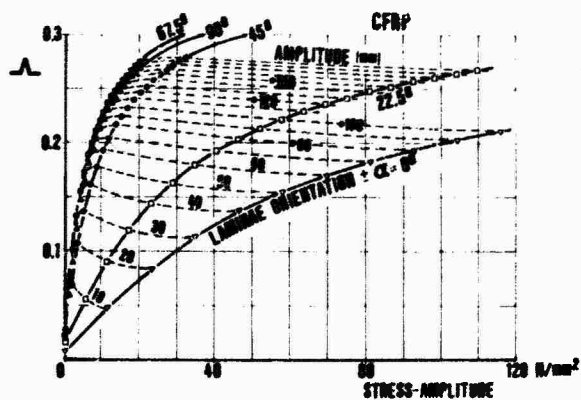


Fig. 12 : Log. decrement versus stress amplitude

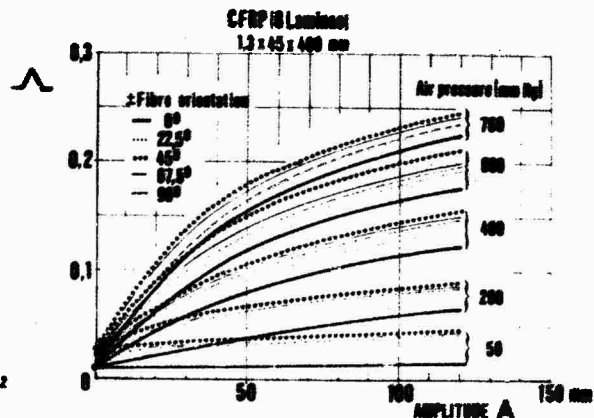


Fig. 13 : Effect of air pressure and laminae orientation

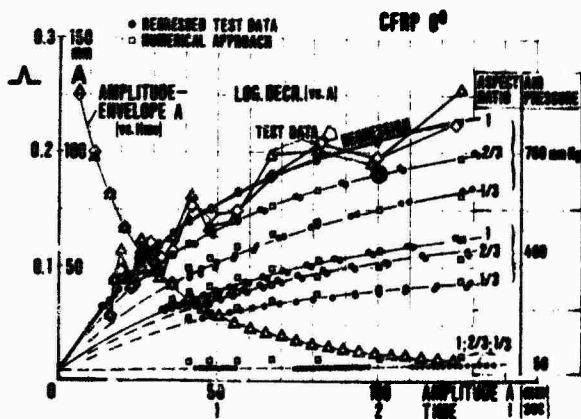


Fig. 14 : Numerical approach to reduction of air pressure and beam width

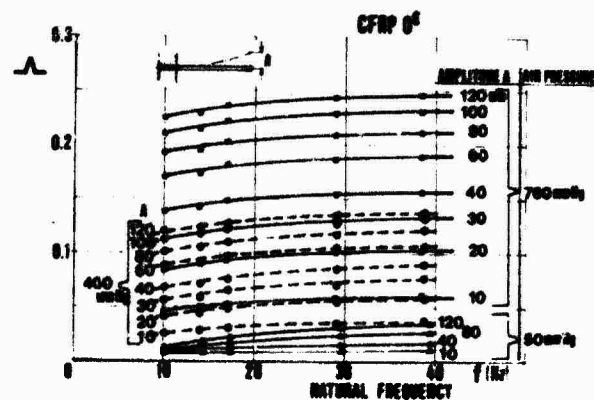
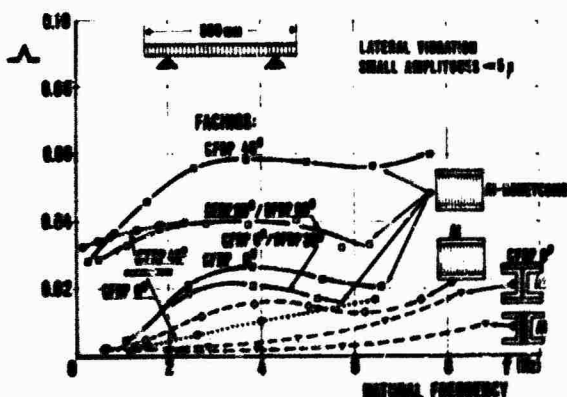


Fig. 15 : Effect of frequency



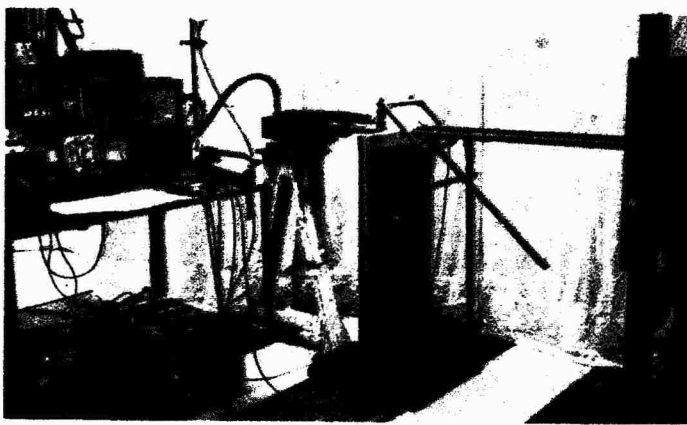


Fig. 18 : Wing box.
Test equipment.

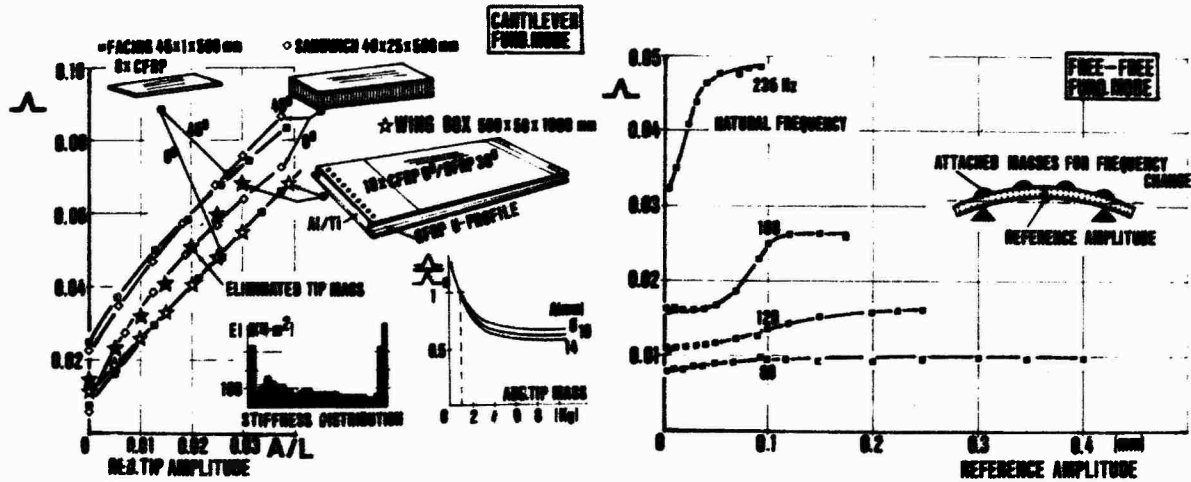


Fig. 19A : Damping of a wing box compared to structural elements.

Fig. 19B : Wing box damping. Effect of natural frequency (DFVLR/AVA)

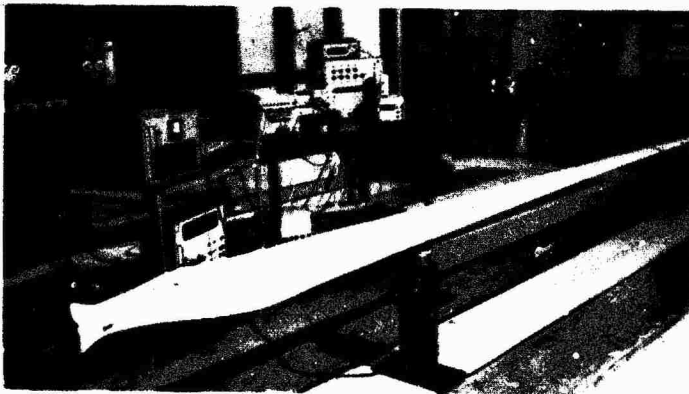


Fig. 20 : Forced vibration of a GFRP wind turbine blade.

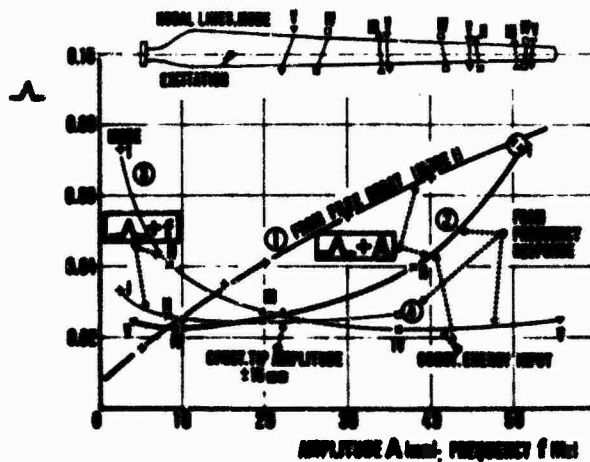


Fig. 21 : Damping of a GFRP wind turbine blade.

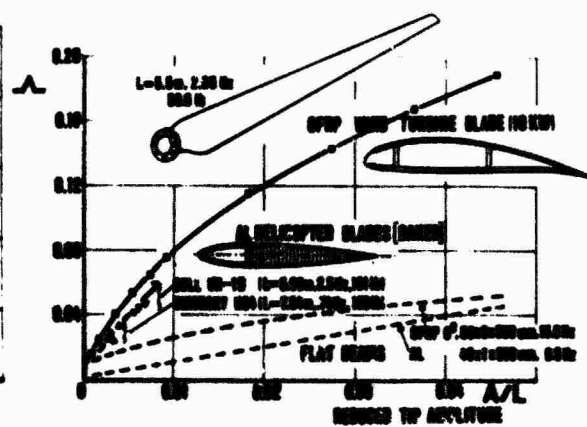


Fig. 22 : Damping of GFRP and metal rotor blades.

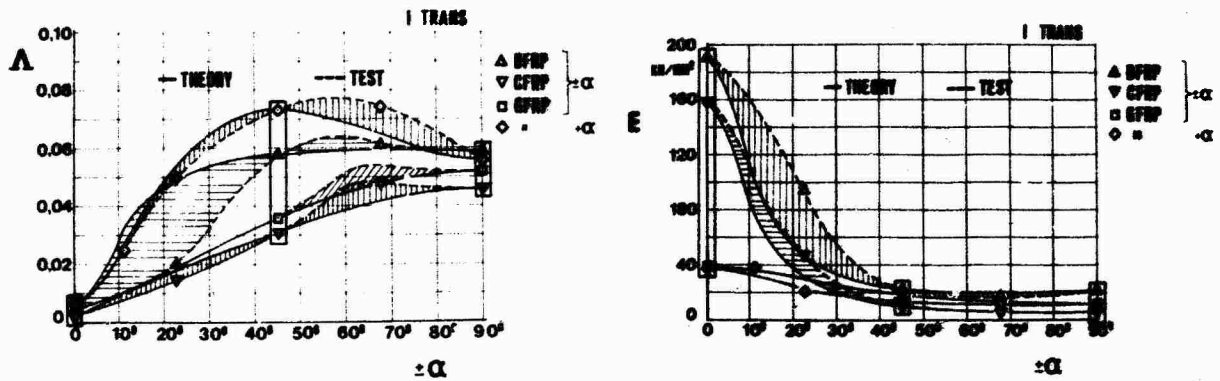


Fig. 23 : Comparison of theory and test results of flat beams.
Log. decrement and Young's modulus of cross-ply laminates.

$$-\frac{\partial^2 w}{\partial t^2} = \frac{1}{\rho s} \left[b_{11} \frac{\partial^4 w}{\partial x^4} + 2(b_{12} + 2b_{33}) \frac{\partial^4 w}{\partial x^2 \partial y^2} + b_{22} \frac{\partial^4 w}{\partial y^4} \right] \quad \text{DIFF. EQ. PLATE} \quad (1)$$

$$-\frac{\partial^2 w}{\partial t^2} = \frac{1}{\rho s} \cdot b_{11} \frac{\partial^4 w}{\partial x^4} ; \quad b < \lambda_B/2 \quad \text{DIFF. EQ. BEAM} \quad (2)$$

$$w(x,t) = A_n e^{-\gamma_n t} e^{i\omega_n t} [C_n (\cos \alpha_n x + \cosh \alpha_n x) + \sin \alpha_n x + \sinh \alpha_n x] \quad \text{SOLUTION} \quad \Delta \quad (3)$$

$$S_n = \frac{b_{11} \alpha_n^4}{\rho s} \quad \text{STORAGE FUNCTION} \quad V_n = \frac{b_{11} \alpha_n^4}{\rho s} \quad \text{LOSS FUNCTION} \quad (4)$$

$$\omega_n^2 = (S_n - \sqrt{S_n^2 - V_n^2})/2 = S_n \quad \text{NATURAL FREQUENCY} \quad (5)$$

$$\eta_n^2 = (S_n - \sqrt{S_n^2 - V_n^2})/2 = V_n^2/4S_n \quad \text{DAMPING FACTOR} \quad (6)$$

$$\Lambda_n = 2\pi \eta_n / \omega_n = \pi V_n / (S_n - \sqrt{S_n^2 - V_n^2}) \quad \text{LOG. DECREMENT} \quad (7)$$

Table III : Lateral vibration of plates and flat beams.

$$\hat{d} = \begin{bmatrix} \hat{d}_{11} & \hat{d}_{12} & 0 \\ \hat{d}_{12} & \hat{d}_{22} & 0 \\ 0 & 0 & \hat{d}_{33} \end{bmatrix} ; \quad \hat{d} = \begin{bmatrix} E_1/(1-\nu_1\nu_2) & \nu_1 E_1/(1-\nu_1\nu_2) & 0 \\ \nu_2 E_1/(1-\nu_1\nu_2) & E_2/(1-\nu_1\nu_2) & 0 \\ 0 & 0 & G_{12} \end{bmatrix} \quad (8)$$

COMPLEX ORTHOTROPIC STIFFNESS

REAL PART

COMPLIANCE POLAR TRANSFORMATION

$$\begin{aligned} \hat{d}_{11}^* &= \hat{d}_{11}^* \cdot \hat{d}_{22}^* \cos 2\alpha + \hat{d}_{33}^* \cos 4\alpha ; & \hat{d}_1^* &= (\hat{d}_{11}^* + \hat{d}_{22}^*)/3 + (\hat{d}_{11}^* - \hat{d}_{22}^*)/4 \\ \hat{d}_{22}^* &= \hat{d}_{11}^* \cdot \hat{d}_{22}^* \cos 2\alpha + \hat{d}_{33}^* \cos 4\alpha ; & \hat{d}_2^* &= (\hat{d}_{11}^* - \hat{d}_{22}^*)/2 \\ \hat{d}_{12}^* &= \hat{d}_{12}^* - \hat{d}_{33}^* \cos 4\alpha ; & \hat{d}_3^* &= (\hat{d}_{11}^* + \hat{d}_{22}^*)/8 - (\hat{d}_{11}^* - \hat{d}_{22}^*)/4 \\ \hat{d}_{33}^* &= \hat{d}_{33}^* - 4\hat{d}_{33}^* \cos 4\alpha ; & \hat{d}_4^* &= (\hat{d}_{11}^* - \hat{d}_{22}^*)/8 + (6\hat{d}_{12}^* - \hat{d}_{33}^*)/8 \\ & & \hat{d}_5^* &= (\hat{d}_{11}^* + \hat{d}_{22}^*)/2 - (\hat{d}_{11}^* - \hat{d}_{22}^*)/2 \end{aligned} \quad (9)$$

STRESS/STRAIN/DAMPING RELATIONS

$$\hat{d} = \hat{d}^* \hat{d} ; \quad \hat{d} = \hat{d} + i\hat{d} = \hat{d}(1 + i\hat{d}) \quad (10)$$

$$\hat{d} = \hat{d}^* \hat{d} ; \quad \hat{d} = \hat{d}^* \hat{d} = \hat{d}^* \hat{d} (1 + i\hat{d}) \quad (11)$$


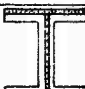

$$\alpha = \pm 45^\circ, \quad \hat{d}_{12}^* \rightarrow \hat{d}_{12}^* - \hat{d}_{11}^* - \hat{d}_{22}^* ; \quad E_1 = 1/\hat{d}_{11}^* ; \quad \Lambda_1 = \pi \cdot \hat{d}_{11}^* \quad (11)$$

Table IV : Orthotropic stiffness matrix. Compliance polar transformation.

FLAT BEAMS

Fig./ Table	Material/ Fibre	Layers	Orient. [°]	Matrix	Fibre [Vol.-%]	Dim. [mm]
2	Resin	-	-	CY 209/ HT 972	-	10 x 3 x 150
3	BFRP " " " "	8 8 8 8 8	0° ± 22,5° ± 45° ± 67,5° ± 90°	Epoxy " " " "	55 %	15 x 1 x 150
4	CFRP-HM " " " "	4 4 4 4 4	0° ± 22,5° ± 45° ± 67,5° ± 90°	CODE 64 " " " "	50 %	15 x 1 x 150
5, 6	A1 6061	-	-	-	-	15 x 1 x 150
T II	GFRP	-	0°	LY 556/ HZ 978	60 %	10 x 1 x 200
	SFRP (Kevlar 49)	4	0°	EHG 250-65-50	55 %	10 x 1 x 150
	Hybrid: CFRP-HM SFRP (PRD)	1 2	0° 0°	CY 209/ HT 972	50 %	10 x 1 x 150
	B/A1: B9 4 C	25	0°	A1 6061	57 %	10 x 3 x 200
9	GFRP	-	0°	Epicate 162, Laromin C 260	58 %	50 x 3 x 500
10-15	CFRP-HT " " " " "	8 8 8 8 8	0° ± 22,5° ± 45° ± 67,5° ± 90°	CIBA 920 F " " " "	51 % - 56 %	45 x 1 x 500

I-BEAMS, SANDWICH-BEAMS, WING BOX (Figs. 16, 17, 19)

Form	Core	Composite Facings					Adhesive	Dim. [mm]
		Material	Layers	Orient. [°]	Thickness [mm]	Matrix		
	1 Al-U 3.1354.6 (2 mm)	-	-	-	-	-	FM 123.5	30 x 32 x 500
	2 "	CFRP-HM	-	0°	1	CODE 64	"	30 x 34 x 500
	3 Al 5056 3/16-20	A13.1354.5	-	-	1	-	AF 126-2.06	40 x 22 x 500
	4 "	CFRP-HM -HT	2 2	0° 0°	1,1	CODE 64	FM 123.5	"
	5 "	CFRP-HT	4	+ 45°	0,9	"	"	"
	6 "	Hybrid: CFRP-HT BFRP CFRP-HT BFRP CFRP-HT	3 2 1 ^{*)} 2 3	0° ± 30° 0° ± 30° 0°	1,45 (1,3)	DX 210/ BF 3	AF 126-2.06	40 x 25 x 500
	7 "	Hybrid: CFRP-HT BFRP CFRP-HT BFRP CFRP-HT	3 2 1 ^{*)} 2 3	90° ± 60° 90° ± 60° 90°	"	"	"	"
	*) in one facing only							
	8	centre section corresponds to 6 ; additional layers at the box ends; Al/Ti-joints; GFRP-U-Profiles at both sides.						500 x 50 x 1000
wing box								

VISCOELASTIC DAMPING IN USAF APPLICATIONS

by

D.I.G. Jones and J.P. Henderson
Air Force Materials Laboratory, (AFML/LLN)
Wright-Patterson AFB, OHIO 45433

and

L.C. Rogers
Air Force Flight Dynamics Laboratory
Wright-Patterson AFB, OHIO 45433

SUMMARY

The possibilities for developing new vibration control techniques based on the energy dissipation characteristics of viscoelastic damping materials emerged with the development of synthetic rubber during World War II. These new materials have created an entire industry for the production of an almost endless variety of chemical substances having both rubber like properties and high energy dissipation capability under cyclic strain. USAF interest in these materials for purposes of vibration control began about the time the B-52 began to experience sonic fatigue. Since that time, the technology has developed greatly with improvements occurring in the areas of materials, design concepts and application methods. The aim of this paper is to describe some aspects of the development and utilization of viscoelastic damping technology for vibration control in the United States Air Force.

NOMENCLATURE

E	Young's modulus
E_D^*	complex Young's modulus of damping material
E_1	Young's modulus of base plate or beam
E_3	Young's modulus of constraining layer
E_c^*	complex Young's modulus of shear damping layer
G_2^*	complex shear modulus of shear damping layer
g, g_N	shear parameters
H_1	thickness of base plate or beam
H_2	thickness of shear damping layer
H_3	thickness of constraining layer
l	length of beam
l_e	effective length
T	temperature
N	number of layer pairs in treatment
$\eta, \eta_D, \eta_2, \eta_3$	loss factors
ζ_n	nth eigenvalue
α_T	shift parameter

1. INTRODUCTION

A large variety of aerospace systems being developed for USAF operational needs in the future, as well as many of those in the current inventory, will strongly utilize damping technology for vibration control. Figure 1 illustrates some of these actual or potential application areas, as well as the technology base which will support the efforts. The aim of this paper is to describe some of these applications in more detail, along with recent advances in the technology base (materials, characterization, design) which make possible the achievement of future successful applications.

Let us first look at where these needs arose. In the remote past, vibration of machinery has occurred from time to time, but has usually involved a single fixed frequency of excitation, low stresses and relatively unexacting performance requirements. In today's aerospace systems, on the other hand, we invariably find the opposite to be true; excitation is broad-band random or arises from harmonic loads which change in frequency during operation of the system, so that resonance cannot be avoided; stresses are often high, and performance requirements are invariably exacting. In these

circumstances, damping has a vital role to play in almost every case - sometimes alone, most often in conjunction with other related measures. In large flexible spacecraft structures, for example, active control techniques will be used to move the systems in response to commands and to control some of the resulting jitter, but the extremely exacting requirements for positional stability will require passive damping to supplement the active controls, especially when very high modal densities are encountered. In jet engines, many of the stationary components are subjected to very high levels of combined static stress (often from thermal gradients) and dynamic stress (from resonance), and damping has often emerged as the most cost effective approach toward reducing replacement and repair costs, as well as sometimes arresting crack growth completely in situations where critical crack lengths exist, beyond which point catastrophic failure can occur. Some of these applications will be described in this paper. Other areas such as printed circuit boards, aircraft avionics and equipment support structures will also be discussed.

2. TECHNOLOGY BASE

2.1. Summary

Referring once more to Figure 1, we see that the windows for advantageous application of damping technology in the United States Air Force, for vibration control in large space vehicles, jet engines, aircraft avionics, aircraft structure, and equipment support structures are approached through a three-level technology base. This technology base requires, and has, a capability for (i) production of damping materials; (ii) characterizing, measuring and standardizing the damping properties of these materials and (iii) designing and creating damping configurations for specific components in their operational environment.

The area of damping material production is heavily influenced by the civilian automotive industry, since it is the largest single market for the materials manufacturers. The USAF, as a far smaller customer, utilizes materials originally developed for automotive or related purposes, as well as creating a requirement for smaller quantities of more exotic materials, usually at higher costs.

As far as the design and production of damped components is concerned, a number of specific technological areas are of interest to the USAF. Some of these areas include (i) the complex modulus representation of viscoelastic damping material behavior under harmonic excitation; (ii) the reduced-frequency concept (Ferry¹ et al) and the newly developed reduced-temperature nomogram²; (iii) the equations of Ross, Kerwin and Ungar³ and of Oberst⁴ for predicting the complex flexural stiffness of free and constrained layer treatments on various structures, as well as more recent work in these areas; (iv) the continuing process of measuring the damping properties of elastomers⁵ and enamels⁶, including the study of the effects of composition changes and (v) finite element analysis⁷ and transfer matrix⁸ analysis of damped structure response. We shall now discuss some of these areas.

2.2. Modeling of viscoelastic material behavior

It is well known and generally accepted that when a specimen of a linear viscoelastic material is harmonically strained at a single, specific frequency, the corresponding stress also varies harmonically with a phase difference between the stress-time and strain-time signals. It is further generally known and accepted that the corresponding locus of stress against strain under harmonically varying excitation is an elliptical, or nearly elliptical, loop⁹, and that if the strain varies as $\exp(i\omega t)$, then the stress varies as $\exp(i\omega t + \phi)$ where:

$$\sigma = E^* e^{i\phi} \epsilon = E' (1 + i\eta) \epsilon = (E' + iE'') \epsilon \quad (1)$$

This equivalence can also be expressed as:

$$\sigma = E' \epsilon + \frac{E'' \eta}{|\omega|} \frac{d\epsilon}{dt} \quad (2)$$

which is a form usable whether or not we use the complex representation $\epsilon_0 \exp(i\omega t)$ for the strain $\epsilon(t)$. However, it is not directly usable when $\epsilon(t)$ is not a cyclic, harmonic, function of time, and this has led to many questions regarding the complete generality of the complex modulus approach and a search for alternative approaches. These questions have not yet been fully resolved, but this should not prevent us from working in the frequency domain, where much of our modern testing capability lies.

Other ways of representing the stress-strain relationship for linear viscoelastic materials are used, but we feel that the complex modulus approach is by far the simplest, especially since for real materials the properties are very highly dependent on frequency and temperature, and hence the need to track only two physical quantities, namely E' and η (or E' and E'') is very useful. Because of the very large number of materials which must be characterized in order to be available to designers and other users, for practical application, this is extremely important. The work involved in data reduction is enormous and every possible valid simplification must be used to cope with what would otherwise be an "information explosion".

Once one has, by some test method or another, measured the modulus and loss factor of a given damping material sample, the data generated will generally consist of a limited, discrete, set of points in the frequency-temperature domain, as illustrated in Figure 2. Only by exploiting a fundamental relationship between the frequency and temperature variables can one collapse all the data onto a single variable, namely the reduced-frequency $f a_T$ of Ferry et al, where f is the frequency and a_T is a function of temperature alone for each specific damping material. This is the well known temperature-frequency principle. This technique is often used in the Air Force for data reduction, display, standardization, transmittal and storage. In fact, it has been taken even further through the use of "reduced-temperature" nomogram² as illustrated in Figure 3. With the aid of this concept, we have been able to rationally characterize a very large number of elastomeric and other damping materials, including acrylic adhesives, silicone polymers, synthetic rubber, natural rubber, neoprene and many glasses and enamels. These form the basis of a technology which can be used to effectively control vibrational response in many structures at temperature ranging from -10°C to $+1100^\circ\text{C}$. Some typical measured material properties are shown in Figures 4 and 5.

2.3. Measurement of damping material properties

Many methods have been used, with varying degrees of success, to measure the dynamic mechanical properties of viscoelastic materials, including mechanical impedance^{10,11}, resonance¹², impact¹³, and vibrating beam techniques¹⁴⁻¹⁶. At the present time, the vibrating beam techniques are being used by the Air Force and a high level of reliability has been achieved within the inherent limits of such methods. The outcome of these measurement activities will be a series of nomograms describing the damping properties of a large number of commercial and generic materials, which will be usable by designers, researchers and experimentalists in the near future. Furthermore, significant efforts are now being made to develop a U.S. Standard^{17,18}, and eventually an International Standard, on measurement of dynamic properties of damping materials. Figure 6 shows some typical beam geometries.

2.4. Design of damping treatments

Most damping treatments used at the present time consist of one or more layers of viscoelastic material bonded between one or more metallic or other stiff structural members. Figure 7 illustrates some of the concepts available. The simplest known basis for analysis of all such treatments is the well known set of equations due to Ross, Kerwin and Ungar³ for the effective flexural rigidity of a three element sandwich beam or plate, illustrated in Figure 7:

$$E^*I = \frac{E_1 H_1^3}{12} + E^* H_2 \left(\frac{H_2^2}{12} + H_{21}^2 \right) + E_3 H_3 \left(\frac{H_3^2}{12} + \frac{g^* E_1 H_1 H_{31}^2}{E_1 H_1 + g^* (E_1 H_1 + E_3 H_3)} \right) \\ - E_2^* H_2 H_{31} \left(\frac{E_1 H_1 \left[\frac{H_{21}}{2} + \frac{H_2}{12} \right] + 2g^* E_3 H_3 H_{21}}{E_1 H_1 + g^* (E_1 H_1 + E_3 H_3)} \right)$$

where $H_{31} = \frac{H_1 + H_3 + H_2}{2}$

$$H_{21} = \frac{H_1 + H_2}{2}$$

$$E^* = E(1 + i\eta)$$

$$E_2^* = E_2(1 + i\eta_2)$$

$$g^* = g(1 + i\eta_2)$$

$$g = \frac{G_2}{E_3 H_3 H_2} \left(\frac{l}{n\pi} \right)^2$$

The equations were derived many years ago but they still remain one of the most useful sets of equations for predicting damping treatment behavior. If we neglect the flexural rigidity of the middle layer and assume that the sandwich is symmetric these equations reduce to the much simpler form:

$$E^*I = \frac{E_1 H_1^3}{6} + \frac{g^* H_{31}^2 E_1 H_1}{1 + 2g^*}$$

For this symmetric sandwich configuration, these equations can be inverted very readily to derive the shear modulus G_2 and the loss factor η_2 of the middle layer from observed resonant frequencies and modal damping. The equations in this particular form depend heavily on the assumption that the beam behaves as a pinned-pinned beam of length l ,

and for other boundary conditions some level of approximation must be introduced. This is usually done by defining an effective length l_e where

$$l_e = l\pi/\xi_n$$

where ξ_n is the n^{th} eigenvalue. This approach works very well indeed for most classical boundary conditions, except for those which deviate most markedly from the pinned-pinned shape, such as the fundamental mode of a clamped-free beam.

For multiple sandwich layers, the equations can be used, in succession, for each group of layers, starting at the outermost sandwich as illustrated in Figure 8. Having found E^*I for that sandwich, one can use it as an effective constraining layer having a complex E^* and create the next sandwich, and so on until all the layers have been accounted for. In this way, one can allow for different damping materials in different layers, and hence design a treatment for specific damping capability over a selected temperature range in a given mode. Calculator and computer programs have been developed to perform these calculations, given the physical dimensions and complex modulus properties of the selected materials.

Figure 9 shows a typical computer plot of modal damping versus temperature for a constrained layer treatment on a beam.¹⁹ The effects of temperature and constraining layer thickness are clearly seen. For each specific damping material, the peak damping and the corresponding temperature depend on the adhesive thickness and the constraining layer thickness. Figure 10 shows the result of varying these parameters. The corresponding (η, T) points form what is referred to as a "carpet plot", which is a very useful way of allowing a designer to select a treatment before concluding more detailed analysis.

For structures with non-classical boundary conditions, or consisting of many beam-like or plate-like segments jointed together, as in a typical aerospace structure, damping treatments might normally be applied only to parts of the structure. It is then much more difficult to predict the effect of the treatments on modal response and damping, and the "equivalent free layer" treatment approach^{20,21} comes into its own. The usual approach here is to analytically or experimentally treat each multiple layer damping configuration as if it were homogeneous, having equivalent uniform complex modulus properties which depend only on a new shear parameter $g_N = g/N$, where N is the number of layer pairs, and the thickness ratio H_1/H_2 .

Needless to say, many variations on this approach are possible, and different materials can be used in each layer, for example to broaden the effective temperature range of the treatment. The most important thing to recognize is that these methods and equations are currently being used for the design of damping treatments for a wide variety of specific applications i.e. the aim is design, not research. The approximations and simplifications involved, while by no means essential if one wishes to seek exact answers, do serve to make the analyses readily amenable to calculator and computer programming. This is important even today, if only because of economic factors.

Other important damping treatments which are sometimes more useful than the layered damping treatments, particularly where high vibration amplitudes occur without correspondingly high surface strains, include the tuned damped vibration absorber and dissipative linkages. Many geometric configurations have been developed and some will be discussed in the applications.

2.5. Current Technological Problems

While many theoretical problems remain to be solved in damped vibration analysis, the problems of most concern to the United States Air Force are those involved with the practical application of damping treatments in operational and planned systems. Quite simply, the most important such problems appear to be the following:

- (i) Need for damping materials data base
- (ii) Need for improved techniques for protecting treatments in severe environments
- (iii) Reduction of manufacturing and application costs
- (iv) Need for more advanced design techniques for structures with additive or integral damping (laminates)
- (v) Need for technology transfer to industry
- (vi) Need for effective damping materials for the temperature range 200°C to 450°C and for temperature below -70°C

Some of these problems have been discussed in the literature²²⁻²⁴.

3. APPLICATIONS

3.1. Summary

Now that a rational technological base for characterizing and measuring damping material behavior and for damping treatment design is available and becoming more widely known, efforts to utilize such materials for vibration and noise control in diverse areas are increasing in number and level of success.

Areas where greatest gains are being made at the present time include jet engine stationary components, equipment support structures, circuit boards and avionics and some of these will be discussed presently. Areas where strong future gains are possible, but cannot be readily capitalized on yet because of some gaps in the technology base, include large flexible spacecraft structures and rotating jet engine components. In the case of spacecraft, the low frequencies, the space environment (vacuum, radiation, wide temperature range) and the large size of some planned structures will demand that further efforts be made to seek more practical design configurations (than those in current usage), and to seek an appropriate role for passive damping in relation to active control and to produce materials or configurations appropriate for the environment.

In the case of rotating engine components, efforts are needed to produce and characterize appropriate materials and design concepts for use in the high temperature/high g-load environment and to develop prediction procedures to determine effect of damping configuration on dynamic stress levels. Such approaches include the utilization of glass or enamel coatings in dovetails and enhanced slip at such interfaces. In both these cases, new dovetail designs may eventually evolve to take advantage of the possibilities and minimize the problems. Some of the possibilities have been discussed briefly in the literature.^{25,26}

3.2. Jet Engines

Most successful applications of damping technology in jet engines, up to the present time, have utilized polymeric damping materials on non-rotating components at temperatures below 400°C (750°F).

3.2.1 Inlet guide vane damping wrap

A bonded vibration damping wrap, consisting of multiple layers of damping adhesives, separated by constraining layers of aluminum foil, has been successfully applied to the inlet guide vanes (IGV) of TF-30 engines²⁷ used in the F-111, and shown in Figure 11. This wrap has been extensively tested in both test cells and in service experience over a 3 year period. It has been shown to be an effective solution to a high maintenance cost situation, and is presently being applied on a production basis during engine overhaul. Major cost savings are expected. The high maintenance costs were due to repair and refurbishment of vanes which had cracked after a short time in service (sometimes less than 50 hours). Cracking was found to be due to high cycle fatigue (HCF) caused by the resonant vibration of the vanes, excited by pressure.

Since the environment of the inlet guide vanes is very severe because of inlet air flow and a wide range of operating temperatures, the design of this damping treatment involved the application of advanced bonding technology along with modern vibration damping technology. The details of the design of the damping wrap are shown in Figure 12. Materials and thicknesses were chosen to produce the required damping for the temperatures, resonant frequencies, and wavelengths expected in service. Two different viscoelastic adhesives (2 layers of 3M-ISD 830 on the convex side, 2 layers of 3M-ISD 112 on the concave side) are used to obtain the desired modal damping as a function of temperature. The bar graph in Figure 13 shows percent of time versus total inlet air temperature for service conditions of the F-111 aircraft from a statistical analysis of data recorded during 1500 hours of operation²⁷. Based on these data the damping treatment was designed to be effective in a temperature range from 0°F to 125°F. This range accounts for 98 percent of engine operation and the most significant damage accumulation. Occasional excursions to higher and lower temperatures, due to infrequent flight conditions, are not important from a fatigue damage accumulation standpoint, but were considered in determining durability of the damping treatment. Furthermore, the design of the treatment was specifically selected for high damping in the modes occurring at about 3000 and 4000 Hz since the highest vibratory stresses were associated with these modes. The damping of the fourth torsional mode of a single wrapped vane, measured in a fixture under laboratory conditions²⁷ is shown in Figure 13 as a function of temperature. The entire damping wrap is carefully assembled in a manner which minimizes volatiles and entrapped air so as to enhance wrap durability. Finally the wrap is bonded to the titanium surface of the inlet guide vane using a structural adhesive (AF 453 epoxy manufactured by 3M), which is cured under temperature and pressure in an autoclave.

Stress on inlet guide vanes with and without the damper wrap installed indicate that vibratory stresses have been lowered to a level to preclude HCF cracking. In addition, other system integration parameters such as effects on engine performance, distortion tolerance, anti-icing effectiveness, and wrap durability have been carefully assessed and found to be acceptable. Field service experience over a three year period has substantiated these findings. The cost savings resulting from applying this damping wrap to Air Force TF-30 engine is expected to exceed \$13 million in the first five years. Investigations are presently underway to extend this type of damping concept to similar problems in other engines.

3.2.2. Inlet extension damping

Another multilayer viscoelastic damping treatment has been successfully designed and tested, on the inlet extension of the TF-41 engine in the A-7D aircraft²⁸. This inlet extension, shown in Figure 14, is a truncated cone of sheet steel, approximately 20 cm (8 in) wide, with flanges welded on each end. In its original configuration, the extension was coated with a layer of fiberglass and epoxy, about 1 cm thick, to stiffen the structure and minimize high cycle fatigue during engine operation. In service,

however, the fiberglass became an expensive item to maintain and repair. Local disbands in the fiberglass resulted in burned spots, caused in turn by frictional heating in the severe vibration environment. The burned spots then led to reduced local stiffness which resulted in fatigue cracks in the steel. Repair and replacement of the fiberglass coating was time consuming and expensive.

Damping was required in several modes of vibration in the frequency range 2000 to 3500 Hz and over the temperature range -54°C (-65°F) to 107°C (225°F). Since the selection of damping materials and the geometric configuration of the damping treatment affect both the peak loss factor and the temperature at which it occurs, a computer program was used to optimize these design parameters in conjunction with the Ross, Kerwin, Ungar equations. The results of this optimization identified two separate multilayer damping treatments, utilizing commercially available damping materials, which were equally suitable for this application. Both treatments use a moderately high temperature shear type damping adhesive to produce one damping peak near 80°C (175°F) and a lower temperature shear damping adhesive to give another damping peak near 27°C (80°F), applied on top of the higher temperature treatment. The two aluminum constraining layers were 0.254 mm (0.01 in) thick. One treatment used 3M company materials, namely a 0.025 mm (0.001 in) thick layer of 3M-ISD-110 high temperature damping material and a 0.051 mm (0.002 in) thick layer of 3M-ISD-112 mid temperature damping adhesive. The other treatment utilized Soundcoat Company materials, and was designated Soundfoil 10N2-10D2, having both damping material layers 0.051 mm (0.002 in) thick. As of the present time, the 3M treatment has been tested for over 1000 hours in a test cell with no apparent degradation. Similar tests have commenced on the Soundfoil treatment, but only a few hours have been accumulated as of this time, with no degradation.

After laboratory verification of the treatment designs had been completed, instrumented runs in an engine test cell were conducted, under heated ram inlet conditions, so as to simulate flight conditions associated with maximum vibration levels. Figure 15 shows a comparison of acceleration levels on a standard fiberglass coated case with those measured on a damped case (3M treatment), under the same operating conditions and accelerometer position. Maximum accelerations on the standard case were in excess of 3000 g's, as compared with about 500 g's for the damped case. Subsequent tests, conducted after 1000 hours of operation, confirm these results.

3.2.3. Vitreous enamel applications at high temperature

Vitreous enamels have shown promise as damping materials for stationary engine components operating at temperatures in excess of 400°C (752°F). Various enamels have been demonstrated on engine components such as an exhaust duct for a helicopter³⁰, an augmentor mixer, an augmentor liner, an afterburner liner and various sheet metal fairings in the turbine sections of jet engines. In each application, it was necessary to not only match the damping peak to the environmental temperature and frequency of the engine component, but also to match the thermal expansion and adhesion characteristics of the enamel and the alloy being coated. Further to this, long term durability of the enamels in the thermal, chemical and airflow environment of the engine must be carefully considered. Each of these aspects are being investigated at the Air Force Materials Laboratory, under several programs. The projected payoff will be a major improvement of the durability of high temperature, non-rotating, engine components. In addition to this, research efforts have been initiated to determine the feasibility of using these materials to control the vibrations of rotating components such as high temperature compressor and turbine blades.

3.3. Avionics

3.3.1 Circuit Boards

Criteria and methodology are well established [31] for vibration control of circuit boards using conventional approaches. Circuit board and electronic chassis applications using viscoelastic materials date back to the early 1960's [32,33]. Table 1 lists some concepts for damping of circuit boards using viscoelastic materials.

Figure 16 shows a self-adhesive constrained layer damping treatment installed [34]. A reduction of first mode motion in the range of 50-67% was required. The maximum total thickness permissible was 2.03MM (.080 inches) to allow for card removal and manufacturing tolerances to prevent interference with adjacent cards. The treatment design chosen was 1.524MM (.060 in.) of the 3M Company ISD 112 with .508MM (.020 in.) scotch-ply fiber-glass as a constraining layer. It is peelable at -40°C (-40°F) to allow circuit maintenance and repair. Response of a typical board with and without damping is shown in Figure 17. Reduction in maximum response was about 75% in the first mode, 50% in the second and less in the higher modes at room temperature. Analysis indicated that the response would be adequately reduced at temperature expected in operation and the treatment was placed in service.

Another application [35] used damping to control resonant response to vibration. As a consequence, design criteria were imposed to limit the maximum dynamic amplification factor of the panel under shaker excitation to 6 while providing a 150 Hz minimum resonant frequency. The original design consisted of a 2.286 MM (0.090 in.) aluminum plate with a stiffening rib. The rib was removed and low density foam was bonded to the plate with holes to bridge over the relays. This maintained enough shear stiffness to minimize shear deflections and provided an offset "spaced" distance to maximize straining of the viscoelastic material which was applied as a free layer.

The damping and resonant frequency met the design criteria. In another application³⁵ two similar boards which were so densely packed with electronic parts that no path was available to install damping material. The board boundary conditions were altered to accomplish damping. To do this, a mid-span support was removed from both ends of the frame and the damping material was bonded on the now free edges, using one board as the constraining layer for the other. The strip was approximately 6.35 MM (1/4 in.) wide. The narrow constrained strips were placed so that they were deformed by the fundamental mode in the region of maximum curvature.

An integrally damped circuit board design [35] has been used for a high vibration environment. Connector rocking, which could break glass bodied parts or fatigue lead wires mounted nearby, is controlled by bonding the connector to the constraining layer of strips of damping material. Free edge modes are controlled by the damped sandwich finger and the edge strip. Other modes are controlled by the center constrained layer strip. The relative sizes of the damping materials, constraining layers, and board are determined by analysis. This integral design approach includes provisions for the damping treatment from design inception, permitting a more effective treatment and greatly enhancing reliability.

On boards in a moderate environment, one strip is often sufficient to adequately control vibration response. For example, a strip having 5% of the board width is often adequate. Epoxy-glass is a suitable constraining layer. The strips can be more effective when aluminum or high modulus graphite-epoxy constraining layers are used, permitting a smaller width and thickness. However, care must be taken to avoid excessive stiffening.

It should be noted that the dynamic modulus of the viscoelastic material employed dominates the configuration of the damping treatment. The "soft" or low modulus viscoelastic material lends itself to the full coverage laminate, which inherently damps all plate-type modes but complicates maintenance or repair. The "stiff" or higher modulus viscoelastic material requires somewhat more sophistication in design and is more suited to the strip. A concept which should be mentioned here is the staggered platelet rib [36] (or Stegosaurus, the dinosaur). The base of the row of platelets is bonded to the circuit board and the viscoelastic is placed at the tip of the platelets to kinematically magnify deformations or, equivalently, "space" the viscoelastic material away from the neutral axis.

An interesting approach [37] is one which used the tendency of viscoelastic foam to return to its original dimensions to install the viscoelastic material. The 12.7 MM (0.5 in.) thick 110 kg/m³ (7 lb/ft³) nonburning, closed cell foam is compressed to as thin as .508 MM (.020 in.) and placed between circuit boards. The foam expands and conforms around components to flushfit the board. Local modes of the components on their lead wires as well as the plate type modes of the circuit board are damped. The damping mechanism probably involves both extensional and shear deformation type energy dissipation. The modal loss factor is improved by as much as an order of magnitude. Obviously, this type of installation could have a large effect on temperature distributions. A somewhat related concept [38] makes use of a silicone rubber, in particulate form, poured loose into the unoccupied volume in electronic gear.

Another design concept for damping of a stack of circuit boards is illustrated in Figure 18. Rigid posts support and connect the circuit boards at the corners while a viscoelastic link connects adjacent boards at the midpoint of a free edge. This arrangement is effective in damping the fundamental mode because of the large amplitudes at the connection of the link. There exists an optimum dynamic stiffness for the link; too little resistance would not provide significant damping and too much resistance would serve to restrict motion, and therefore, to not introduce damping. This concept has proven effective and has been incorporated into a number of spacecraft equipment items.

A rather obvious concept is to use a laminated metal sandwich for the heat transfer plate which conducts the heat to the guides and the connector, when such a plate is used because of the board power consumption level. A thin layer of soft viscoelastic material would be required, and probably would not significantly affect the thermal distribution.

3.3.2 Other Avionics

A UHF antenna [39,40] had been failing due to vibration induced, high cycle fatigue on the F100 aircraft. The excitation was broad band random and the damage was induced by resonant response of a single mode. The high strains were in the bend radius, and the center part of the antenna (i.e., the electrical connector and adjacent link) moved predominantly as a rigid body; thus, a tuned viscoelastic damper was designed to reduce the response. Vibrational energy dissipated in the form of heat caused the temperature of the viscoelastic material to rise but this effect was accounted for in design and test and the duration of the excitation was short enough for repeated use of the damper to be possible. Subsequent to initial test failures, an additive constrained layer damping treatment was applied to several B-1 antennas which were to be located in the aft fuselage [40] where they would be subjected to a high noise environment. Several large, flat, thin panels were included in the antenna configurations. Maximum spectrum level stress reduction exceeded an order of magnitude in laboratory testing and the damping treatments were incorporated into the aircraft antenna designs.

The feasibility of damping doubly curved gimbal "rings" has been demonstrated [35] for the Charles Stark Draper Laboratory. The standard gimbal had heavy rings and extra

material thickness for strength and stiffness. The damping approach is shown in Figure 19. Excess material was removed so that the structure could be more easily damped. The constrained layer treatment restored much of the original stiffness, but the damped gimbal weighed 30% less than the baseline gimbal. With a natural frequency of 114 Hz and a maximum response magnification of 8, the damped design was satisfactory.

Work is continuing to complete the feasibility study on three gimbal rings in the presence of the flight temperature gradients. This treatment is used in combination with Draper developed interfacial damping and a viscoelastic device in the intergimbal bearing assemblies.

During vehicle vibration testing the response of a reaction wheel and of the S-band antenna and K-band feed were controlled by the addition of damping [35]. The reaction wheel and a maximum response magnification of 34 and the S-band response magnification was 44. These levels were discovered early in the vibration test and would, if not corrected, have seriously threatened the structural integrity of the equipment and structure during the expected launch environment. In both cases, treatments were designed and installed before the completion of the test, avoiding damage and expensive additional testing. The maximum reaction wheel response magnification was reduced to 4.5 by the introduction of a strut composed of two metal angle bars connected by a pad of damping material in direct shear. The maximum S-band/antenna feed response magnification was reduced to 10.9 by the addition of a plate-like connection between the three S-band support tubes and a flange in the feed horns. This placed the damping material in direct shear between the flange plate connected to the support rods.

An acoustic attenuating enclosure container developed for the NASA Goddard Space Flight Center to demonstrate the feasibility of space shuttle payload acoustic covers has a double wall construction [35,42]. The cylinder body is composed of two 508 MM (0.020 in.) thick aluminum sheets with a core of damping material.

The end bulkheads consist of a flat disk and a shallow cone of aluminum connected by wedges of damping material. Parametric variations were made to determine the amount of area coverage by the GE SMRD (for Structures and Materials Research Department, General Electric Company) damping material, the thickness needed to obtain a suitably stiff composite crosssection and a low surface density. The high composite stiffness allowed the lightweight cylinder to be effective in reducing the noise transmission into the container at the lower frequencies. The overall noise reduction was 20 dB with a fiberglass reverberant liner blanket included and 12 dB without the blanket. The high damping controlled noise transmission in the mid-frequency range when the enclosure began resonating. At higher frequencies the noise transmission was reduced by the "mass law" primarily, but damping is of value at the high frequencies, also.

3.4. Equipment Support Structure

In the preceding discussion of circuit boards and avionics, the fragile item itself was damped to control its response to a given environmental vibration. Often however the equipment support structure itself transmits the vibrational energy, and its resonances contribute to the severity of the environment. In these instances, the environmental vibration may be abated by damping the resonances of the equipment support structure.

A damped bracket for a camera was developed for the NASA Goddard Space Flight Center to be used on the International Ultraviolet Explorer. The camera is bolted to the inner frame at three points. The inner frame is supported by metal "dog-legs" which eliminate hysteretic misalignment while providing flexibility in all directions. The inner frame is redundantly connected to the channel-shaped constraining shells via six blocks of damping material which are strained by any of the six rigid body modes of the camera. The redundant path through the damping material also provides a large fraction of the total stiffness. This design protects the camera from high frequencies (to which an internal part is sensitive) by isolation. The bracket resonances are well damped as can be seen in Table 2, which show results of hard mounted bracket/camera testing. This design was analyzed by finite element methods with adequate success. The natural frequency was within 10 percent of the prediction and the isolation characteristic satisfactorily matched. Beginning at 650 Hz, camera elastic modes were isolated well enough to protect the internal parts of the camera. Response magnification was also satisfactorily predicted. The undamped bracket had maximum response magnifications of 10 to 20 various frequencies and had no clear isolation characteristic.

The test of an Interim Upper Stage (IUS) equipment shelf is described in Figure 20. Some test results are described in Tables 3 and 4. Kinematically, lateral vibration of the deck strut causes vibration of the equipment deck. The damping treatment tested included a viscoelastic link to the strut. A more effective damping treatment would be a constrained layer laminated design for the strut as shown.

Figure 21 presents response acceleration power spectra for acoustic excitation of the test article. The RMS response and the high level were reduced except for a peak at about 100 Hz. Modal survey data was not available in sufficient detail to define this mode. Tables 3 and 4 compare RMS and peak results.

In spacecraft equipment mounting structure such as bulkheads and panels, heat transfer through the structure is typically a major design requirement. The design concepts shown in Figure 22, have excellent thermal conductivity and damping. The honeycomb sandwich may be brazed to the face sheets to improve the heat transfer while the damping is provided by a thin layer of a suitably chosen viscoelastic material. The layer of viscoelastic material is a few thousandths of an inch thick and, therefore, does not seriously degrade the thermal path. Alternatively, as also shown, the constraining material may be some type of stiffener.

3.5. Other Aeronautical Structures

In several cases, multiple constrained layers of elastomeric damping materials have been applied to existing Air Force structures, either to increase service life or to reduce noise. For example, sonic fatigue was a primary design consideration for the aft fuselage of the B-1 aircraft. The Air Force Materials Laboratory investigated the possibility of applying damping to the skin and supporting structure of an aft fuel tank in the B-1 aircraft with a view to increasing the sonic fatigue life^{44,45}. The environment of this structure presented several formidable challenges to a designer of damped systems, including (i) anticipated structural temperature near to 150°C (302°F) during take-off; (ii) sound pressure levels anticipated at one time to be as high as 173 dbA and (iii) a requirement that the treatment be unaffected by long term exposure to aircraft fuel. Although this particular application was never introduced into practice, the investigation did serve as a basis for later design efforts⁴¹ and contributed to the development of digital Fast Fourier Transform test techniques for aiding design of damped systems.

Fatigue cracks in secondary structure can frequently be prevented or minimized through the application of additive damping. An example of such an application was the multiple layer treatment developed for application to the leading edge of the F-15 rudder. This treatment not only prevented initiation of new cracks, but also stopped the propagation of existing ones⁴⁶. In another application, a multiple constrained layer treatment was used to extend the service life of the SUU-41 weapons dispenser⁴⁷.

Multiple constrained layer treatments have also been shown to be effective for noise control. Such additive damping was used to reduce helicopter cabin noise caused by the resonant response of the skin-stringer type fuselage structure⁴⁸. This type of damping is presently being used on a routine basis during the construction of new helicopters in the U.S.A.

4. SUMMARY AND CONCLUSIONS

In this paper, we have given a very brief survey of some of the applications of damping technology in the United States Air Force, for vibration control, as well as the possibilities for application of this emerging technology in the future. It is evident that benefits resulting from reduction of maintenance costs in widely used systems are very high and, furthermore, that the payoff in improved performance and maintainability of new vibration-critical systems, such as large flexible spacecraft structures, digital electronics systems and rotating jet engine components, could be even greater.

References

1. J.D. Ferry, E.R. Fitzgerald, L.D. Grandine, Jr., and M.L. Williams, "Temperature Dependence of Dynamic Properties of Elastomers; Relaxation Distributions", Industrial and Engineering Chemistry, 44, pp. 703-706, 1952.
2. D.I.G. Jones, "A Reduced-temperature Nomogram for Characterization of Damping Material Behavior", Shock and Vibration Bulletin 48, Part 2, pp. 13-22, 1978.
3. D. Ross, E.E. Ungar and E.M. Kerwin, Jr., "Damping of Plate Flexural Vibrations by Means of Viscoelastic Laminates", Structural Damping, ed., J.E. Ruziska, Proc. ASME Colloq., 1959.
4. H. Oberst, "Über die Dämpfung Biegeschwingungen Dünner Bleche Durch fest Haftende Balage", Acustica (Akustische Beihefte) 4, 181-194, 1952.
5. L.C. Rogers (ed), Proc. Conference on Aerospace Polymeric Viscoelastic Damping Technology for the 1980's, AFFDL-TM-78-78-FBA, 1978.
6. G. Graves, C.M. Cannon, C. Pantana, R. Goodman and S. Hilton, "On Tailoring a Family of Enamels for High Temperature Vibration Control", Proc 15th Annual Meeting of Soc. Engineering Science. (SES), Gainesville, Florida, December 1978.
7. P. Trompette, M. Paulard, M. Lallane, D.I.G. Jones and M.L. Parin, "Prediction of Modal Damping of Jet Engine Stator Vanes Using Finite Element Techniques", ASME Paper 76-GT-60, 1976.
8. Y.K. Lin, "Free Vibrations of Continuous Skin-stringer Panels", J. Applied Mechanics, Vol. 27, No. 4, pp. 669-676, 1960.

9. E.O. Lazan, Damping of Materials and Members in Damped Mechanical Systems, Pergamon Press, Oxford, 1968.
10. J.L. Edwards and D.R. Hicks, "Useful Range of a Mechanical Impedance Technique for Measurement of Dynamic Properties of Materials", JASA, 52, pp. 1052-1056, 1976.
11. Anon, "Notice de presentation du "Viscoelasticimètre", available from Metravib, 24 bis chemin des Mouilles, 69130 Ecully, France.
12. C.M. Cannon, A.D. Nashif and D.I.G. Jones, "Damping Measurements on Soft Viscoelastic Materials Using a Tuned Damper Technique", Shock and Vibration Bulletin 38, pp. 151-165, 1968.
13. D.I.G. Jones, "Low Cost Measurement of Material Damping Behavior", paper presented at 49th Shock and Vibration Symposium, Washington, D.C., 1978.
14. A.D. Nashif, "New Method for Determining Damping Properties of Viscoelastic Materials", Shock and Vibration Bulletin 36, Part 4, pp. 37-47, 1967.
15. D.I.G. Jones, "Temperature-frequency Dependence of Dynamic Properties of Damping Materials", J. Sound and Vibration 33(4), pp. 451-470, 1974.
16. D.I.G. Jones and J.P. Henderson, "Specification of Damping Material Performance", Shock and Vibration Bulletin 48, Part 2, pp. 1-11, 1978.
17. ASTM Committee E-33 on Environmental Acoustics, Task Group E-33 03-M, Test Method for Damping Materials.
18. ANSI Committee S2 on Mechanical Shock and Vibration, Task Group S2-73, Damping Properties of Materials.
19. L.C. Rogers and A.D. Nashif, "Computerized Processing and Empirical Representation of Viscoelastic Material Property Data and Preliminary Constrained Layer Damping Treatment Design", Shock and Vibration Bulletin 48, Part 2, pp. 23-37, 1978.
20. D.I.G. Jones, "Damping of Stiffened Plates by Multiple Layer Treatments", J. Sound and Vibration 35(3), pp. 417-427, 1974.
21. D.I.G. Jones, "Design of Constrained Layer Treatments for Broad Temperature Damping", Shock and Vibration Bulletin 44, Part 5, pp. 1-12, 1974.
22. P. Santini, "Current Problems in the Area of Dynamic Damping", in AGARD-R-663, An introduction to the problems of dynamic structural damping, 1978.
23. A. Castellani and A. Nappi, "Some Aspects of Dynamic Structural Damping Prediction", in AGARD-R-663, 1978.
24. J.E. Ruzicka (ed.), Structural Damping, American Society of Mechanical Engineers, New York, N.Y. 1959.
25. A.V. Srinivasan (ed), Structural Dynamic Aspects of Bladed Disk Assemblies, ASME Publication-papers presented at Winter Annual Meeting, New York, December 1976.
26. D.I.G. Jones and A. Muszyńska, "Design of Turbine Blades for Effective Slip Damping at High Rotational Speeds", to be published in Shock and Vibration Bulletin 49, 1979.
27. J.P. Henderson, M.L. Parin, L.C. Rogers and D.B. Paul, "Engine Evaluation of a Vibration Damping Treatment for Inlet Guide Vanes", ASME Paper 79-GT-163, 1979.
28. L.C. Rogers and M.L. Parin, "A Thoroughly Engineered Application of Damping Technology to Jet Engine Inlet Guide Vanes", in AFFDL-TM-78-78-FBA, 1978.
29. M.L. Drake and J.D. Sharp, "An example of Additive Damping as a Cost Saving Alternative to Redesign", ASME Paper 77-WA/GT-2, ASME Winter Annual Meeting, November 1977.
30. J.J. deFelice and A.D. Nashif, "Damping of an Engine Exhaust Stack", Shock and Vibration Bulletin 48, Part 2, pp. 75-84, 1978.
31. D.S. Steinberg, Vibration Analysis for Electronic Equipment, John Wiley and Sons Inc., New York 19.
32. T.J. Loftus and L.J. Schwemmer, Constrained Layer Damping Applied to Printed Circuit Boards, American Society of Mechanical Engineers, Paper No. 61-WA-309, 1961.
33. J.E. Ruzicka, D. Ross and R.S. Gilfoy, "Application of Modern Vibration Control Techniques in Electronics Packaging and Production", Proc. of the National Electronic Packaging and Production Conference, June 1963.
34. R.N. Hancock and J.A. Hutchinson, Damping for Enhanced Reliability in Vibroacoustic Environments, in AFFDL-TN-78-78-FBA, 1978.

35. J.M. Medaglia and C.V. Stahle, SMRD Damping Applications, in AFFDL-TM-78-78-FBA, 1978.
36. B.M. Patel, G.E. Warnaka & D.J. Mead, "New Structural Damping Technique for Vibration Control", Shock and Vibration Bulletin 48, Part 2, pp. 39-52, 1978.
37. E.H. Berger, "Selected E-A-R Damping Materials and Applications", in AFFDL-TM-78-78-FBA.
38. R.R. Palmisano and D.W. Neily, Particulate Silicone Rubber; An effective, removable, encapsulant for electronic Packaging, Harry Diamond Laboratories, Shock and Vibration Bulletin 46, pp. 277-284, 1976.
39. C.M. Cannon, "Example of the Use of Additive Elastomeric Damping Treatments to Control Vibration Problems in Air Force Systems", in AFFDL-TM-78-78-FBA, 1978.
40. D.I.G. Jones et al, "Development of a Tuned Damper to Reduce Vibration Damage in an Aircraft Radar Antenna", Air Force Materials Laboratory Report No. AFML-TR-67-307, 1967.
41. A.G. Tipton, Viscoelastic Damping Applications B-1 Aircraft, in AFFDL-TM-78-78-FBA.
42. M. Ferrante, C.V. Stahle and F.J. On, "Feasibility Study of an Acoustic Cover for Shuttle Payloads", Shock and Vibration Bulletin 46, Part 2, pp. 209-228, 1976.
43. D. Muth, The Boeing Company, Private Communication.
44. M.L. Drake and J.P. Henderson, "An Investigation of the Response of a Damped Structure Using Digital Techniques", Shock and Vibration Bulletin 45, Part 5, 1975.
45. J.P. Henderson and M.L. Drake, "Investigation of the Effects of Damping Treatments on the Response of Heated Aircraft Fuselage Structure", Proc. Noisexpo 76, March 1976.
46. J.D. Sharp and M.L. Drake, "Elimination of a Resonant Fatigue Problem for High Maintenance Benefits", ASME Paper 77-DET-135, Chicago, Sept. 1977.
47. D.I.G. Jones, J.P. Henderson and A.D. Nashif, "Reduction of Vibration in Aerospace Structures by Additive Damping", Shock and Vibration Bulletin 40, Part 5, 1970.
48. J.P. Henderson and A.D. Nashif, "Reduction of Interior Cabin Noise Levels in a Helicopter Through Additive Damping", Shock and Vibration Bulletin 44, Part 5, 1974.

TABLE 1

VISCOELASTIC DAMPING CONCEPTS FOR CIRCUIT BOARDS

INTEGRAL CONSTRAINED LAYER³²
 ADDITIVE CONSTRAINED LAYER³⁴
 CONSTRAINED LAYER STRIP³⁵
 SPACED FREE LAYER STRIP³⁵
 PLATELET RIB (STEGOSAURUS³⁶)
 UNBONDED FOAM LAMINATE³⁷
 PARTICULATE FOAM PACKING³⁸
 LINK
 LAMINATED METAL HEAT TRANSFER PLATE
 HIGH LOSS MATRIX MATERIAL
 UNBONDED FOAM POST

Table 2 Camera Bracket G_{rms} Response

TEST INPUT AXIS					
X		Y		Z	
UNDAMPED	DAMPED	UNDAMPED	DAMPED	UNDAMPED	DAMPED
4.1	1.94	1.2	0.17	1.34	1.41
4.2	0.81	8.8	3.53	1.56	1.38
8.8	1.76	2.83	0.6	4.52	4.38

(0.005 G^2/Hz ; 3.15 G_{rms} input) Maximum Camera
 Random Response Reduced by 2.5

TABLE 3

IUS TEST RESULTS - RMS

ACCELEROMETER LOCATION	ACCELEROMETER DIRECTION	BASELINE	GRMS	RATIO
			DAMPED	
3 lb BOX	OUTER	14.5	11.5	.79
	RING	--	9.0	--
	VERTICAL			
MID SPAN	RADIAL	11.25	8.5	.76
	VERTICAL	17.5	12.2	.70
20 lb Box	RADIAL	7.0	5.4	.77
	VERTICAL	10.5	6.75	.64
Outer Deck Ring	RADIAL	10.5	7.25	.69
	VERTICAL	14.0	9.5	.68
Deck Strut	RADIAL	30.	9.54	.32

TABLE 4

IUS TEST RESULTS-PEAKS

SPECTRAL PEAKS - G^2/Hz

ACCELEROMETER	FREQ HZ	BASELINE DAMPED RATIO		
3 lb BOX VERTICAL	190	.96	.47	.44
	280	.4	.13	.33
	350	.23	.092	.40
	900	.38	.15	.39
20 lb BOX VERTICAL	200	.125	.095	.76
	220	.18	.12	.67
	340	.34	.18	.53
	1100	.23	.038	.17
DECK STRUT RADIAL	255	2.25	.31	.14
	340	9.0	.43	.048
	1000	.43	.06	.14

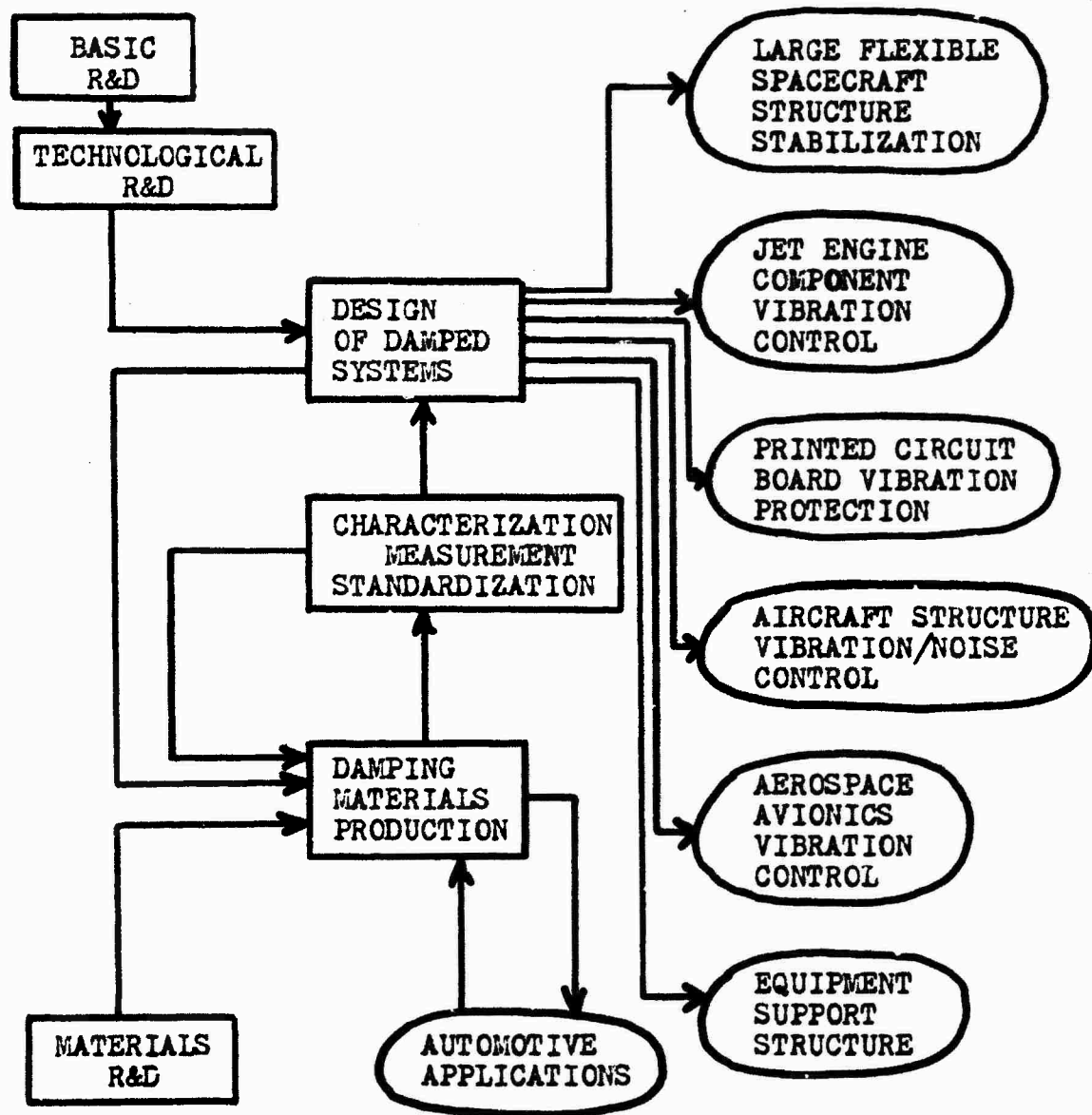


Figure 1. Damping technology and applications

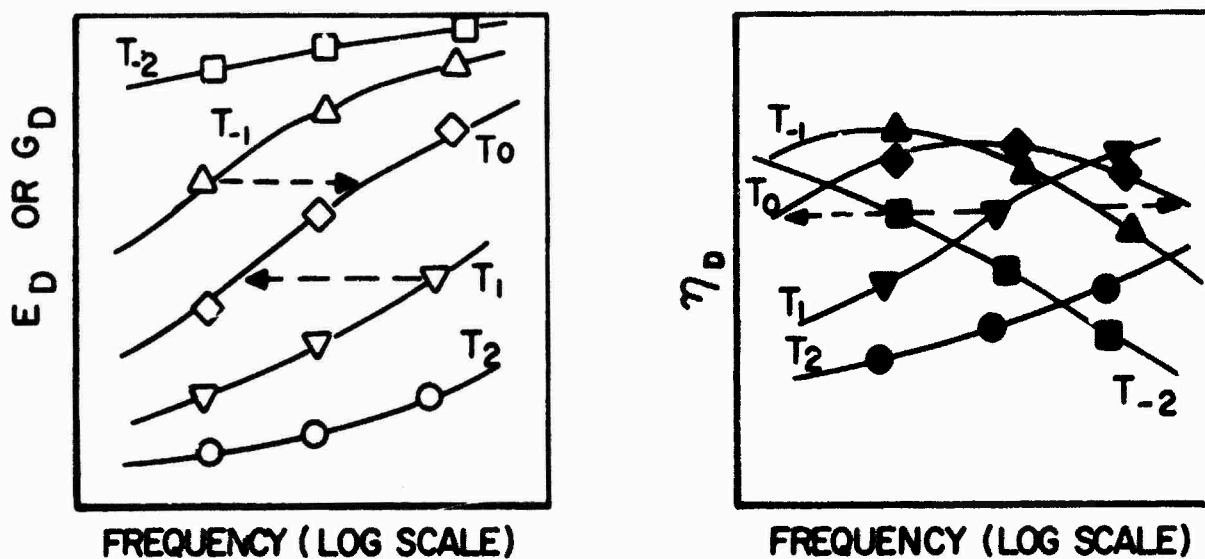


Figure 2. Effect of frequency and temperature on complex moduli

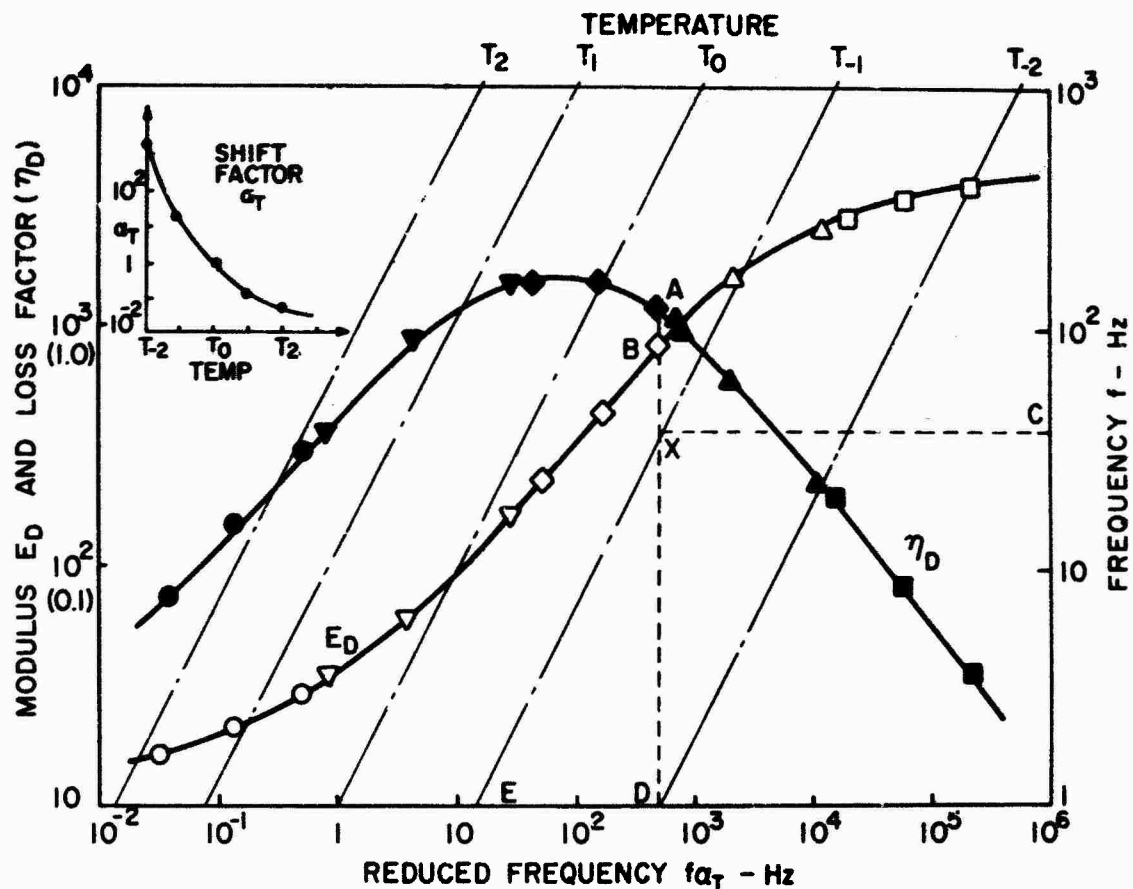


Figure 3. Reduced temperature nomogram

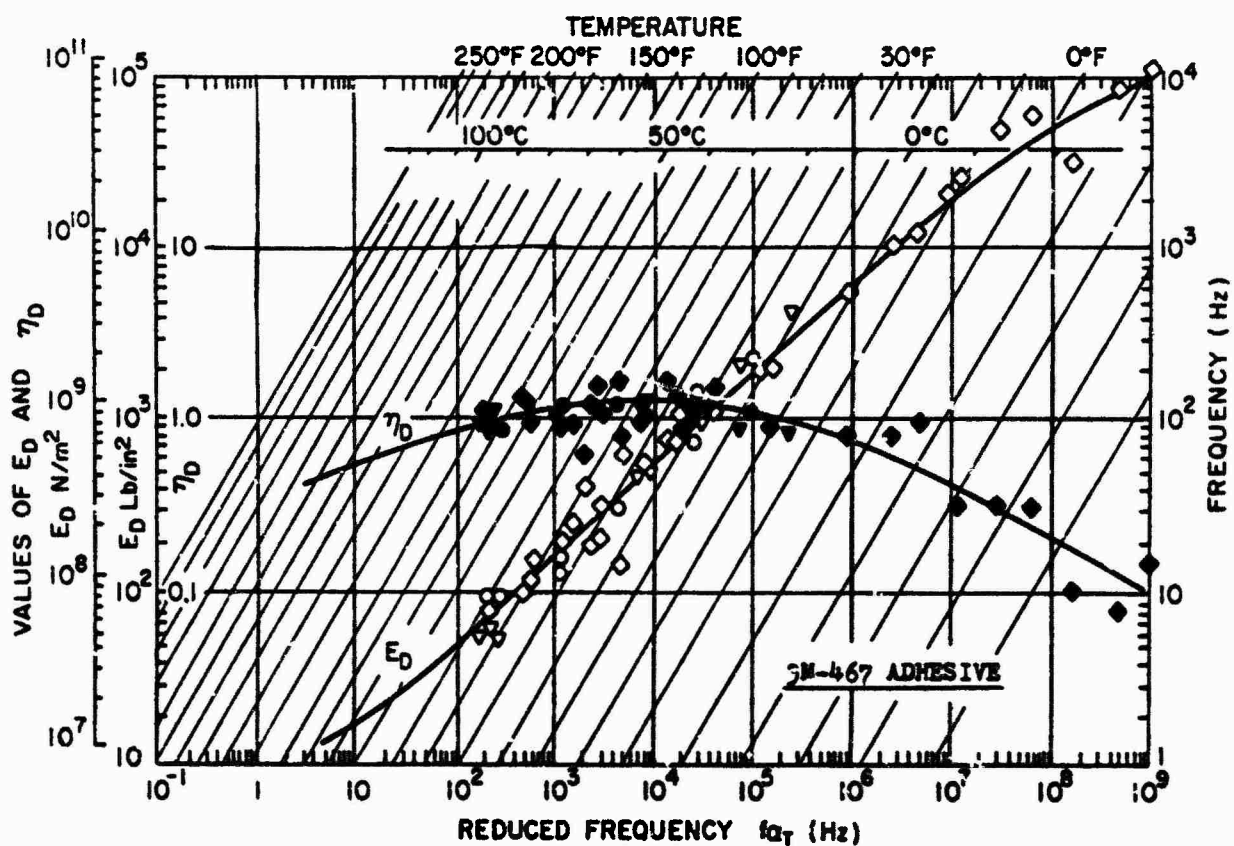


Figure 4. Reduced temperature nomogram for acrylic adhesive

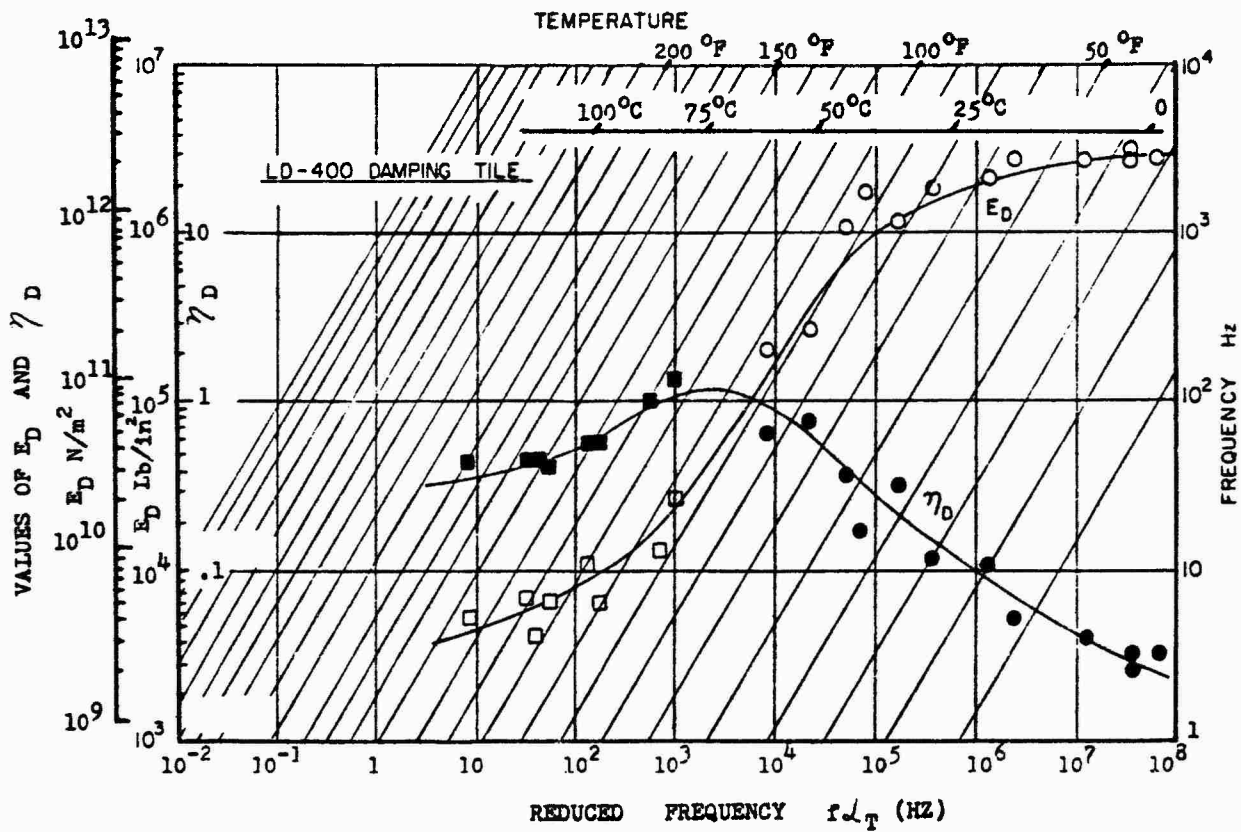


Figure 5. Reduced temperature nomogram for damping tile

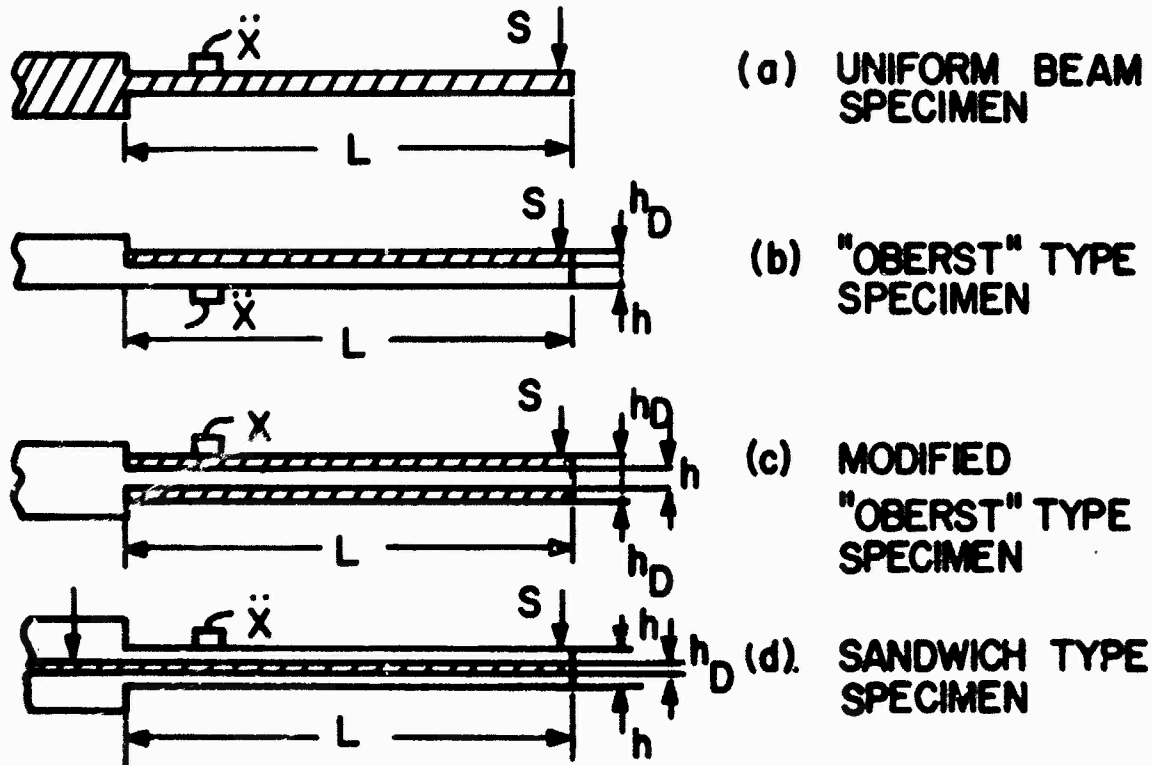
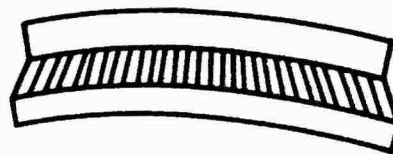


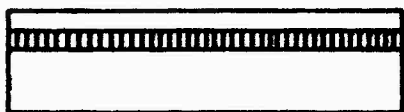
Figure 6. Beam geometries for damping material testing



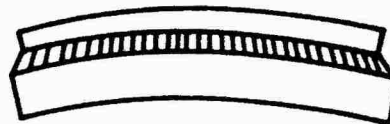
UNDEFORMED "SANDWICH"



DEFORMED "SANDWICH"



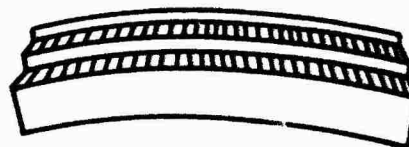
UNDEFORMED "DAMPING TAPE"



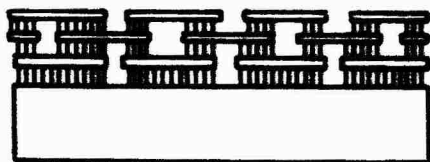
DEFORMED "DAMPING TAPE"



UNDEFORMED
"MULTIPLE DAMPING TAPE"



DEFORMED
"MULTIPLE DAMPING TAPE"



UNDEFORMED
"CUT" TREATMENT



DEFORMED
"CUT" TREATMENT

Figure 7. Damping treatments

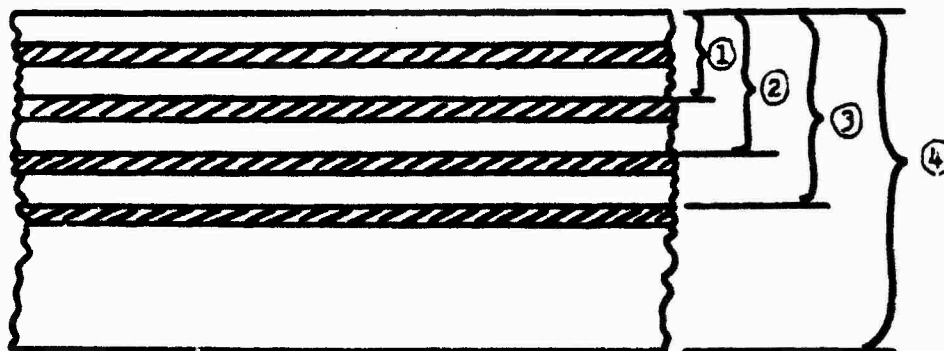


Figure 8. Multiple constrained layer treatments

BASE STRUCTURE MODE: MATL: N467-125F
 FREQ = 200. HZ MATL No. = 1
 H1 = .0313CM (.032IN) CONSTRAINING LAYER
 E1 = .6895E11 N/M2 (.1000E8 LB/IN2) E3 = .6895E11 N/M2 (.1000E8 LB/IN2)
 L = 9.592CM (3.776IN)

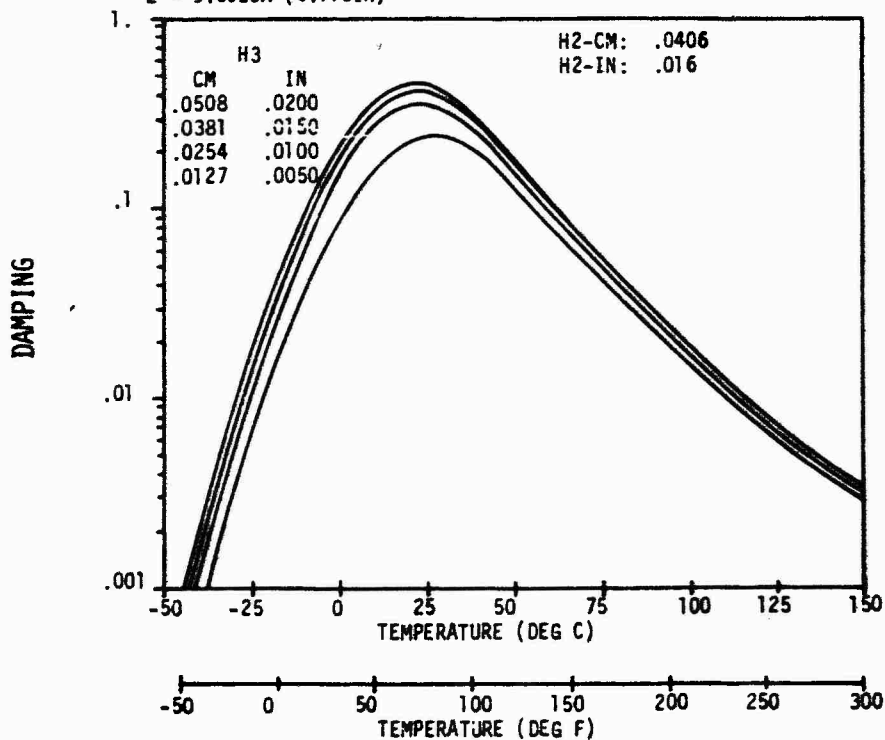


Figure 9. Effect of temperature and constraining layer thickness on modal damping

BASE STRUCTURE MODE: MATL: N467-125F
 FREQ = 200. HZ MATL No. = 1
 H1 = .0813CM (.032IN) CONSTRAINING LAYER
 E1 = .6895E11 N/M2 (.1000E8 LB/IN2) E3 = .6895E11 N/M2 (.1000E8 LB/IN2)
 L = 9.592CM

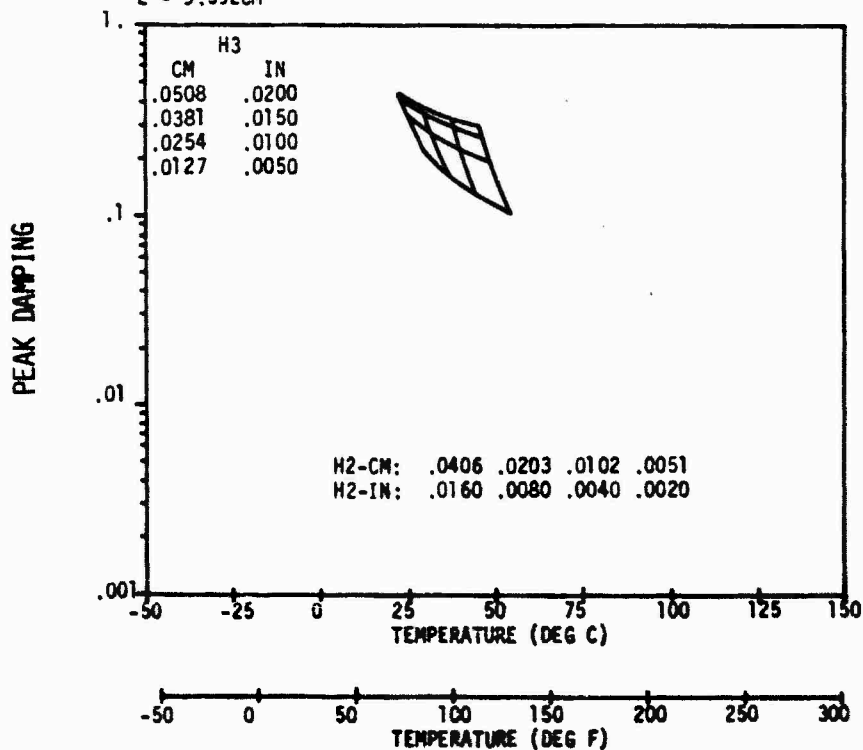
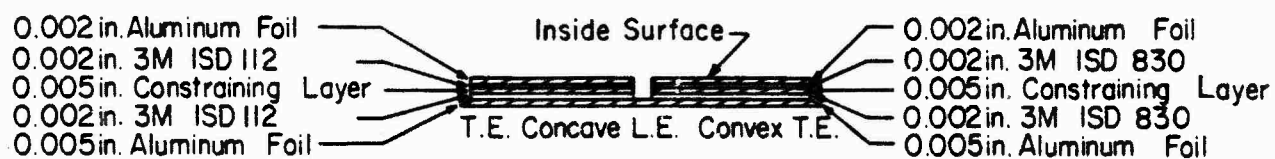


Figure 10. Carpet plot



Figure 11. Damping treatment on inlet guide vanes



All Dimensions in Inches

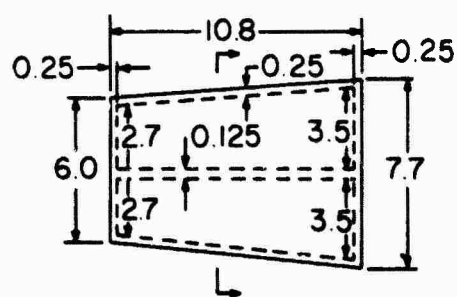


Figure 12. Damping treatment geometry

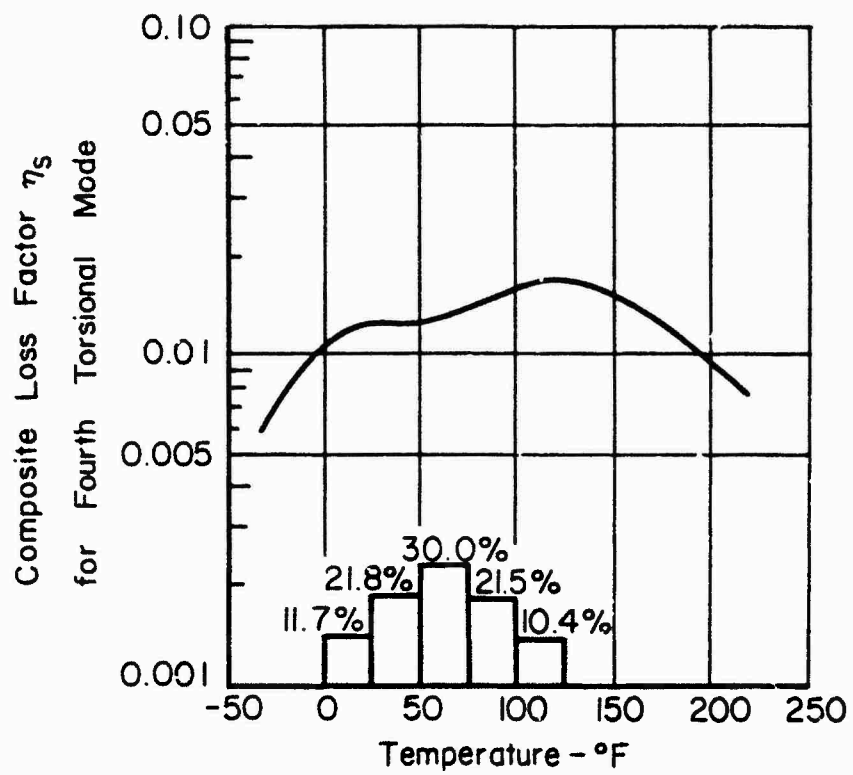
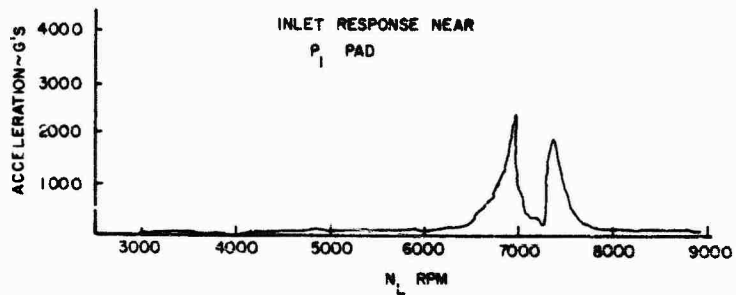
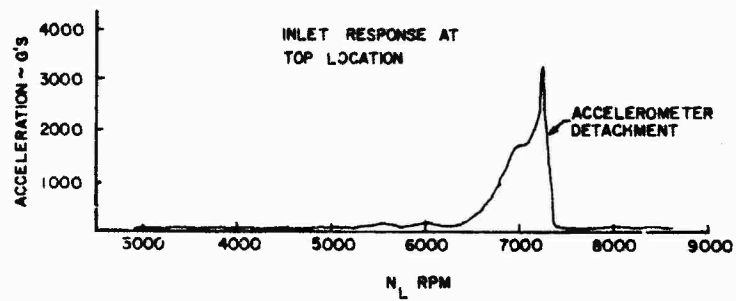


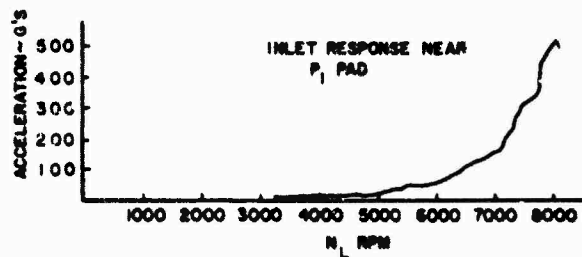
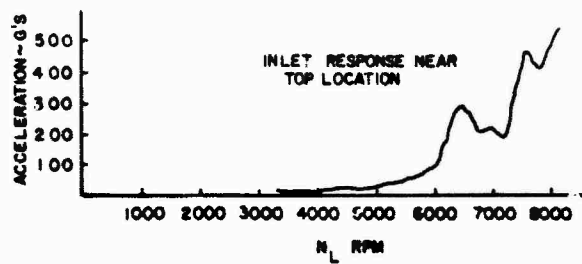
Figure 13. Modal damping versus temperature



Figure 14. Damping on inlet extension



(a)



(b)

Figure 15. Effect of damping on accelerations of inlet extension;
(a) undamped; (b) damped

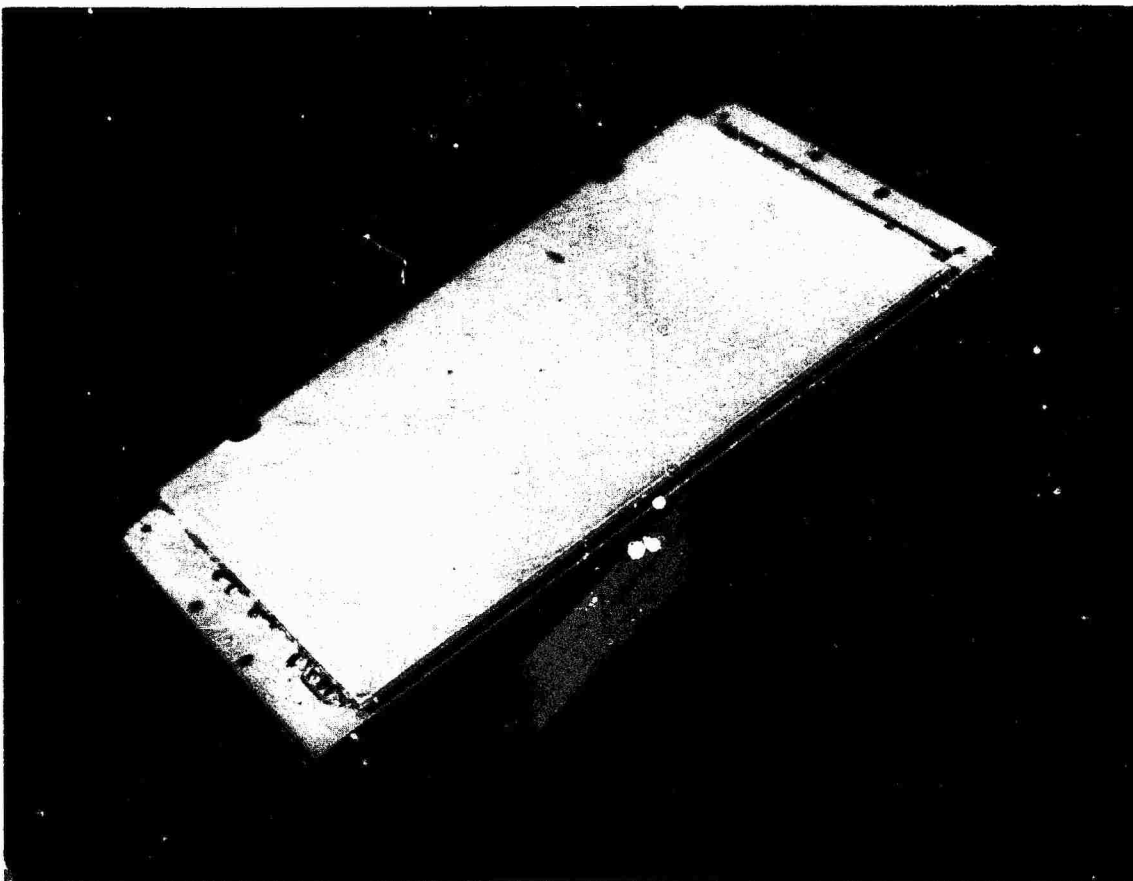


Figure 16. Circuit board damper installation³⁵

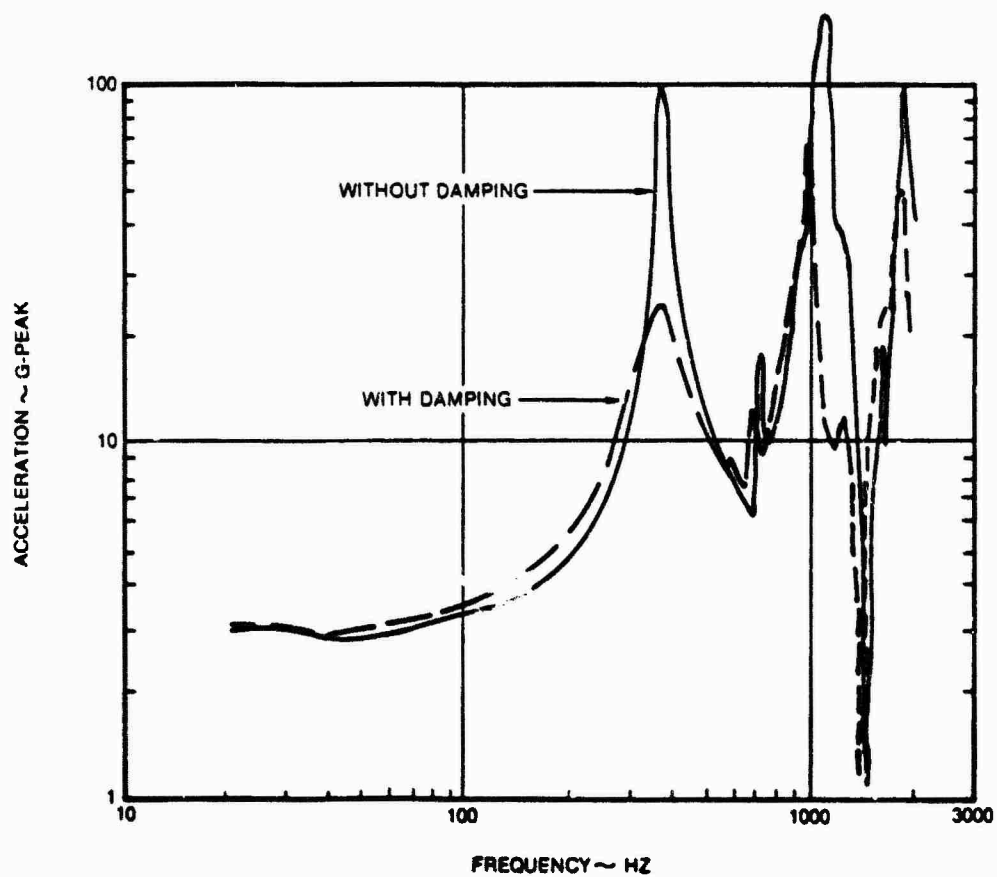


Figure 17. Effect of damping on circuit board response³⁵

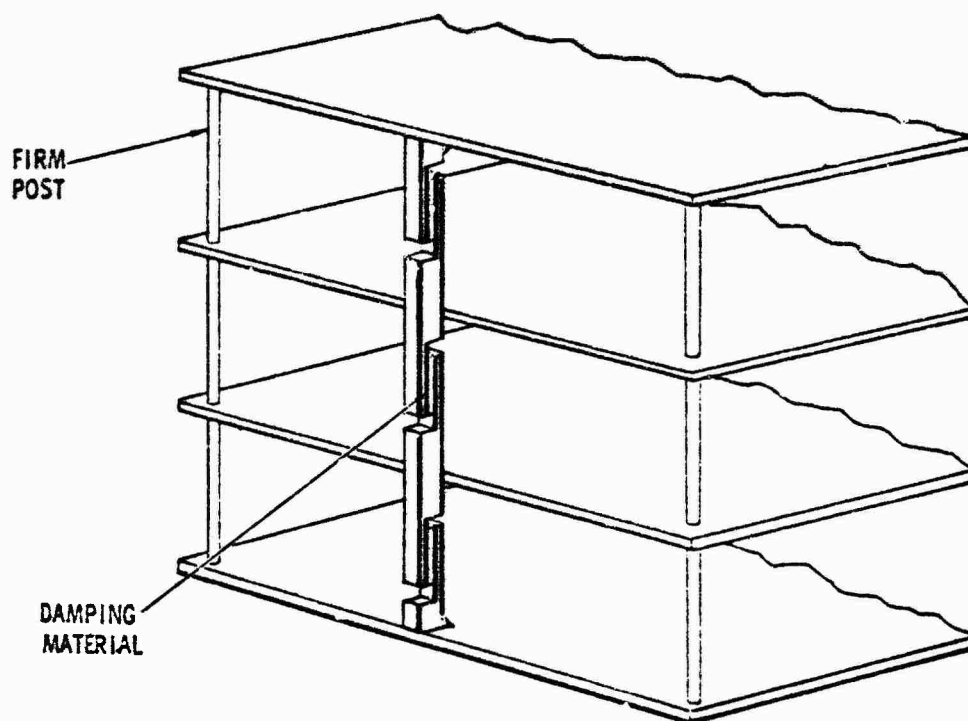
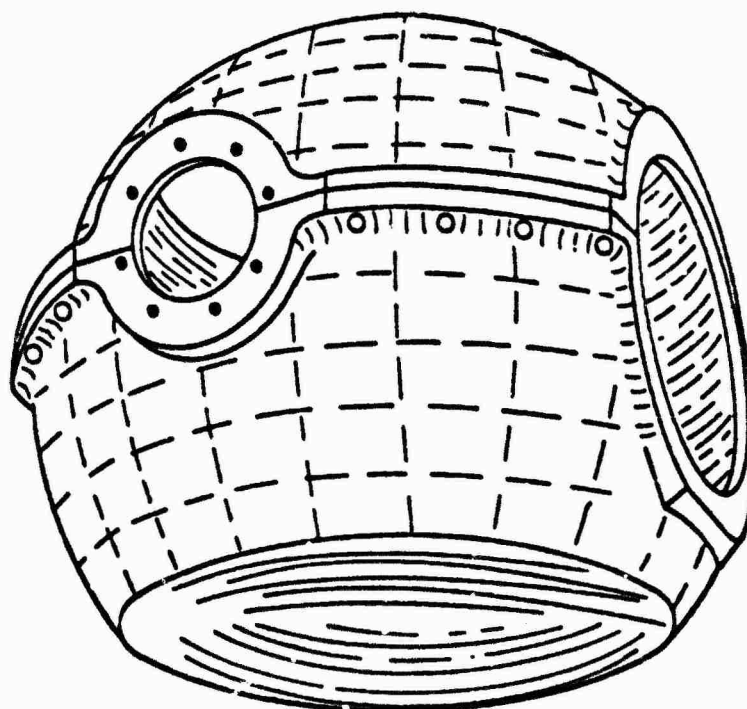


Figure 18. Damped links in stack of circuit boards



SPHERICALIZED GIMBAL HAS
EXCESS MATERIAL, STIFFNESS
REMOVED

Figure 19. Gimbal damping approach

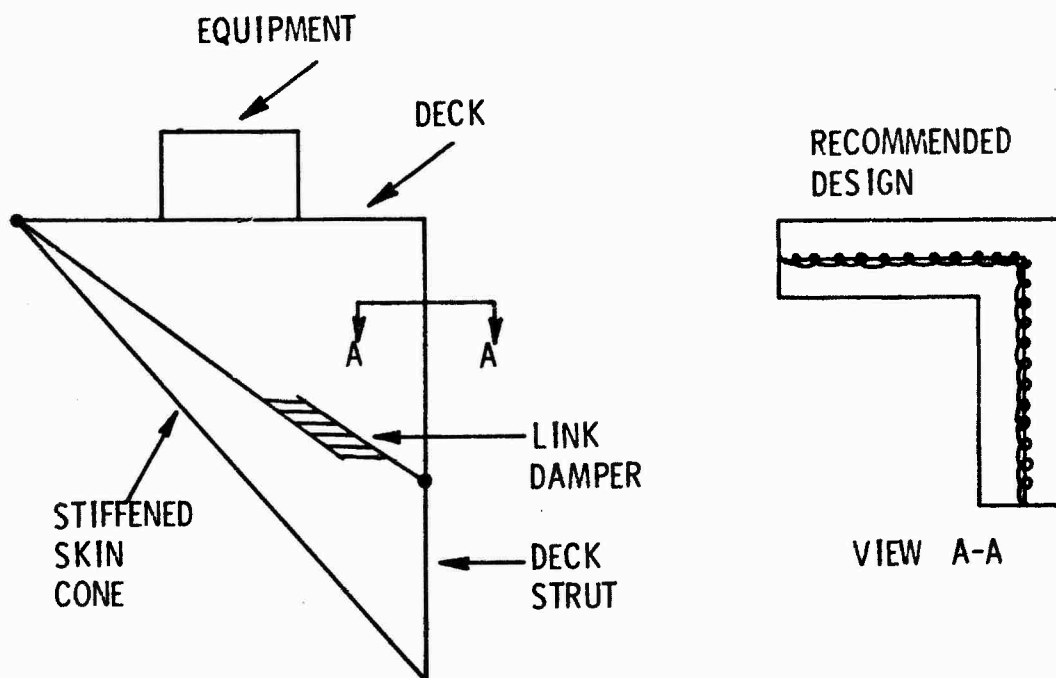


Figure 20. IUS equipment shelf with damping link⁴³

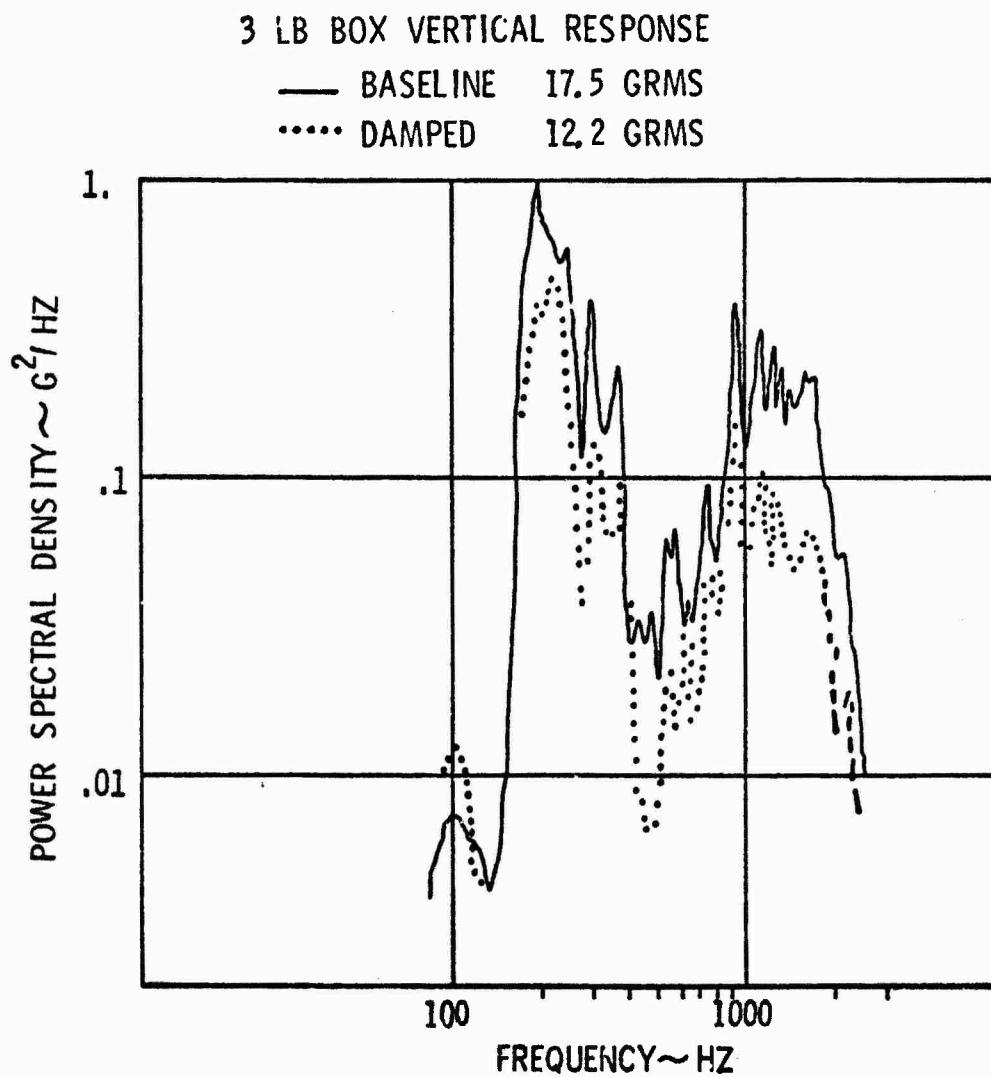


Figure 21. Effect of damping on response of IUS equipment shelf⁴³

BRAZED HONEYCOMB AND THIN
LAYER OF SOFT VEM FOR
THERMAL CONDUCTIVITY

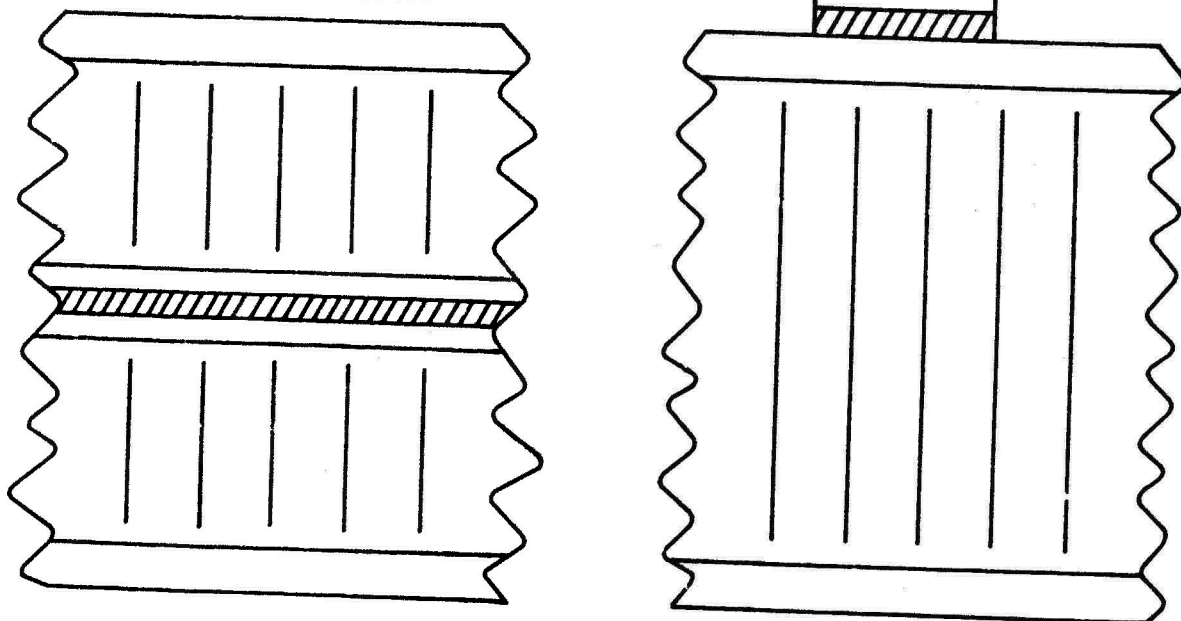


Figure 22. Damped equipment support structure

Par
B. DUPERRAY et L. GAUDRIOT
SOCIETE METRAVIB
24 bis, Chemin des Mouilles
19130 ECULLY
FRANCE

I - INTRODUCTION

Le bilan présenté ici est celui d'une société de service engagée depuis plus de dix ans dans les problèmes de vibrations et de bruit intéressant un large secteur d'applications industrielles, mécaniques et électriques, constructions navales et spatiales notamment.

Parmi les diverses techniques usuelles mises en oeuvre pour contrôler ces problèmes vibratoires et acoustiques (dimensionnement judicieux, techniques de filtrage, monitoring), il est apparu très tôt que l'accroissement d'amortissement des structures par apport de matériaux viscoélastiques notamment, pouvait présenter un très grand intérêt.

Après des études de validation fondées sur des approches théoriques et expérimentales, nombre de cas concrets ressortissant à des domaines d'application très divers ont été abordés, certains avec succès. On a pu remarquer que dans tous les cas où un résultat favorable a été obtenu, cela a correspondu à une bonne connaissance du comportement dynamique des structures, un choix adéquat des matériaux, ainsi qu'une bonne connaissance de leurs caractéristiques dynamiques.

Ainsi, outre l'aspect modélisation dynamique des structures, qui est une des activités de base de la société, il a été également nécessaire de susciter la promotion de produits amortissants bien adaptés et une collaboration étroite avec la SOCIETE NATIONALE DES POUDRES ET EXPLOSIFS a été mise en place dans ce but.

Enfin, il a également été nécessaire de développer un appareillage spécifiquement adapté à la caractérisation des paramètres dynamiques des matériaux (viscoélasticimètre - planche I), qui a trouvé par ailleurs un marché international.

Aujourd'hui, la Société METRAVIB continue de s'employer au transfert des techniques d'amortissement à un secteur industriel large, ce qui a incité notamment à se préoccuper du développement de produits nouveaux tels que :

- composites réalisés à partir de résines amorties renforcées par des fibres de verre,
- matériaux pour haute température, notamment verres et céramiques, initiés par une collaboration avec le Docteur D.I.G. JONES de WRIGHT PATTERSON AIR FORCE BASE.

Toutefois, la question du meilleur parti à tirer de ces techniques, tant du point de vue performances que de celui du coût, se pose désormais de manière particulièrement aigue et c'est là une interrogation qui reste sous-jacente au fil de l'exposé.

II - EXPOSE GENERAL DES CAS D'APPLICATION

Nous allons exposer quelques cas d'application des techniques d'amortissement par produits viscoélastiques, de complexité croissante, dont les résultats se sont avérés positifs. Nous présenterons ensuite la philosophie générale qui s'en dégage à notre point de vue. Nous la compléterons par les réflexions que nous inspire notre expérience de promoteur de ces techniques dans le secteur industriel.

- L'application la plus immédiate des produits viscoélastiques à fort amortissement se trouve dans les composants mécaniques d'une catégorie qui relève de ce qu'on peut appeler la "mécanique du caoutchouc". L'exemple le plus typique est celui d'un plot élastique amorti. Nous présentons, ci-après, les caractéristiques d'une telle réalisation dont l'intérêt évident se manifeste par la faible surtension de la courbe de transmissibilité et par la pente de filtrage (12 dB/octave) dans une gamme large de température -
Planche 2 -

- Un exemple également manifeste est fourni par le cas des tôles minces, vibrant en régime relativement libre sous des sollicitations de contour, qui se révèlent être des sources de bruit importantes.

Nous citerons l'exemple constitué par des jupes d'alternateur auxquelles un traitement par revêtement simple a permis une atténuation de l'ordre de 3 dB, ramenée à l'ensemble sur la fréquence de rotation et de 4 dB pour un tiers de la surface traitée sur l'harmonique deux - Planche 3 -

- Un cas plus particulier est constitué par l'amortissement d'un réservoir de combustible liquide de fusée. Un gain d'amortissement par revêtement simple partiel des parois de quelques pourcents s'est ainsi révélé déterminant vis à vis de l'accrochage du phénomène POGO du lanceur DIAMANT B - Planche 4 -

- La mise en oeuvre de l'amortissement dans les embases des auxiliaires qui équipent les bâtiments de la MARINE a été explorée de façon plus systématique dans le but de diminuer les niveaux vibratoires transmis à la coque. Il en est ressorti un gain appréciable sur le bruit rayonné dans l'eau, gain essentiellement fonction de l'amortissement et de la surcharge apportée aux structures support qui propagent l'énergie vibratoire. On donne ci-après l'exemple d'un groupe électrique sur coque de sous-marin - Planche 5 -

- Un cas d'emploi plus indirect de l'amortissement est constitué par l'application à des transformateurs électriques de distribution de faible puissance (~ 100 KVA), destinés à être placés en étage dans les immeubles. Ce cas résulte d'une étude menée en collaboration avec les Services des Etudes et Recherches de l'ELECTRICITE DE FRANCE.

L'amortissement direct des parois de la cuve s'avère inopérant du point de vue acoustique du fait du caractère forcé imposé par les vibrations magnétostrictives du noyau à la composante rayonnante du champ vibratoire des parois. Un remède à cette situation consiste à réaliser un très fort raidissement de la cuve. Il en résulte un gain sur l'harmonique 2 en régime forcé, mais ce gain se trouve contrebalancé par des pertes sur les harmoniques de rang plus élevé, où les parois présentent un régime à caractère résonnant, maintenant rayonnant. L'amortissement par revêtement contraint est alors pratiqué pour atténuer ces effets, et assurer ainsi le gain global en bruit recherché. - Planche 6 -

III - COMMENTAIRES SUR LES EXEMPLES PRECEDENTS

La dernière application dont l'intérêt industriel reste à prouver, illustre l'avantage que peut apporter l'amortissement dans la correction d'effets secondaires, qui apparaissent dans une restructuration visant à agir au niveau de caractéristiques primaires : redistribution des raideurs et masses. Ces effets secondaires peuvent être par exemple : le décalage des résonances par rapport au spectre des excitations, la distribution des parts résonnantes et non-résonnantes, la modification des implications, telles qu'acoustiques.

Si un tel point de vue devait se généraliser à l'épreuve des faits, il imposerait la prise en compte des possibilités de l'amortissement, à la conception même du projet dynamique de structure, en tant que facteurs fondamentaux de son architecture. Il va sans dire que cela supposerait la mise à disposition d'une gamme très large de matériaux amortis avec une technologie d'emploi adaptée à la variété des environnements, ainsi que d'une maîtrise profonde du rôle à leur faire jouer dans les comportements dynamiques d'ensemble.

Il s'agit là d'un point de vue qui apparaît aujourd'hui encore futuriste. Si l'on songe en effet que la technique du soudage a mis vingt ans pour s'imposer vis à vis de celle du rivetage, et que celle de l'assemblage par collage apparaît tout juste dans le domaine industriel après plus de dix ans d'application dans le domaine aéronautique, on peut penser qu'une diffusion des techniques d'amortissement, de portée élargie sur le plan des comportements dynamiques, demandera des délais encore plus étalés !

Compte tenu en effet des produits disponibles à l'heure actuelle, de leur coût, des difficultés technologiques, de leur mise en oeuvre, ainsi d'ailleurs que du niveau très aval de la conception d'équipements dont les aspects vibratoires sont envisagés, il n'apparaît pas possible d'avancer à présent l'amortissement comme un remède suffisamment éprouvé auquel on puisse toujours penser s'adresser en dernier ressort.

Ainsi, faute d'être très conscient de cet état de fait, on se trouve confronté à la situation de vouloir demander trop à l'amortissement et l'on se heurte immédiatement aux réticences des utilisateurs : les contraintes de mise en oeuvre et d'environnement sont jugées souvent inacceptables, les performances apportées par les matériaux dont on dispose sont considérées comme trop pointues, les coûts apparaissent en général prohibitifs. Or, il est évident qu'on ne pourra apporter de meilleures réponses techniques aux questions posées que lorsque le marché industriel de ces produits pourra s'ouvrir ; on est donc placé à ce point de vue dans un système bouclé, dont l'évolution ne pourra être que lente et dont la motricité peut être imaginée comme reposant sur le développement particulier donné à ces techniques dans les secteurs technologiques traditionnellement porteurs : spatial, aéronautique, automobile, etc ...

Or, dans ces secteurs mêmes, la question de l'intérêt de la mise en oeuvre de techniques amortissantes est actuellement posée. Nous allons faire état à ce sujet de l'expérience limitée acquise en coopération avec le domaine spatial français.

Nous présenterons d'abord schématiquement le cadre général des problèmes dynamiques au sein desquels s'inscrivent les études menées, ces études visant à explorer les possibilités offertes par l'amortissement dans le but de réduire les niveaux vibratoires auxquels sont soumis les divers équipements des lanceurs, et ce essentiellement pour des problèmes de tenue à la fatigue - Planche 7 -

Dans ce cadre, il a été entrepris une étude générale à caractère méthodologique relative aux surtensions à attendre d'équipements liés à des structures support amorties par revêtement viscoélastique. D'autre part, il a été considéré deux problèmes particuliers intéressants respectivement un support d'équipement du SPACELAB avec la firme ERNO (Bremen) et l'isolation acoustique de la coiffe du lanceur ARIANE avec le C.N.E.S.

Aucune de ces solutions n'a pourtant donné lieu à ce jour à application opérationnelle. Nous les présentons néanmoins à titre d'exemple et dégageons ensuite le rôle dévolu à l'amortissement dans le déroulement des projets spatiaux actuels.

Le premier exemple consiste dans l'étude du couplage d'un équipement sur plateau "nid d'abeille" à un cône support inter-étage. Il s'agit d'explorer l'intérêt de l'amortissement du cône vis à vis de la réponse dynamique de l'équipement. Le recours à une méthode de synthèse modale par modes complexes a permis de rendre compte de l'amortissement résultant sur les modes couplés. On donne à titre d'exemple, les courbes d'impédances ponctuelles calculées et mesurées dans le montage présenté sur la photo - planche 8 -

L'amortissement de 4 % à 6 % conféré aux premiers modes (embase bloquée) correspond à un gain de 15 dB à attendre dans la sollicitation vibratoire verticale d'entraînement du cône, et ce pour une augmentation d'un tiers de la masse du cône.

Le deuxième exemple intéresse une plaque support d'équipements thermostatée (cold plate support structure) du Laboratoire Spatial Européen (E.S.A.). Le problème a été posé comme un problème d'amortissement pur : il s'agissait de conférer au plateau support "nid d'abeille" en appui sur son contour, un coefficient d'amortissement moyen de 10 % sur les premiers modes propres de flexion (100 Hz à 600 Hz). Compte tenu des conditions d'environnement et de mise en place sur la structure existante, le choix technologique s'est porté sur un revêtement contraint avec contre-plaque d'alliage léger, et un matériau polyuréthane satisfaisant aux conditions de température (0°C à 45°C) et aux normes d'inflammabilité, de dégazage et de toxicité - Planche 9 -

Le troisième exemple a rapport au projet d'isolement acoustique de la coiffe du lanceur ARIANE.

D'une part, la structure de la coiffe est pré-définie : tôle d'alliage d'aluminium avec raidisseurs circonférentiels et longitudinaux. D'autre part, la masse à consacrer au traitement acoustique est fixée. La question est donc posée de faire le meilleur usage acoustique de ce crédit de masse. Une analyse statistique de fréquence d'anneau où le transfert s'effectue principalement par les modes résonnants de très forte densité. Dans cette zone, un traitement amortissant des panneaux par revêtement simple doit permettre la meilleure efficacité. Une solution mixte, par traitement comprenant un matériau amortissant plus un matériau absorbant acoustique intérieur, a été préconisée pour assurer les caractéristiques théoriques suivantes (voir planche 10) - Cette solution n'a pas été retenue -

Si ces quelques exemples présentent un intérêt de principe, le fait qu'ils n'aient pas donné lieu à implémentation sur des lanceurs diminue en fait beaucoup leur portée. Leur intérêt n'est pas néanmoins négatif dans la mesure où ils ont permis de dégager un premier point de vue vis à vis de la mise en œuvre d'amortissement chez les architectes spatiaux. Nous nous faisons ici leur porte-paroles pour le présenter dans ses grandes lignes.

L'idée qui prévaut actuellement est en fait de considérer l'amortissement comme un remède de dernière heure, que l'on garde en réserve, pour pallier les défauts révélés, soit par le calcul prévisionnel, soit au cours des essais. Ce remède consiste alors en des traitements particuliers appliqués localement que l'on envisage concurremment à d'autres remèdes plus immédiats : raidissement des structures ou surqualification des équipements.

Après examen de cas d'étude abordés précédemment, il apparaît clairement que l'on se trouve dans une situation encore très éloignée du point de vue futuriste énoncé. Si l'on cherche des causes à cet état de fait, on est conduit à invoquer, soit les contraintes liées à la mise en œuvre de l'amortissement qui sont difficilement acceptées par les architectes spatiaux, soit le manque d'imagination des promoteurs de ces solutions qui sont en position de valoriser cette technique.

En conclusion, revenant au rôle moteur attendu du secteur spatial vis à vis des techniques d'amortissement, compte tenu des possibilités d'application qui sont apparues en cours d'étude, la question est posée de savoir si ce domaine est effectivement désigné pour jouer le rôle de promoteur initialement pressenti pour ces techniques.

V - CONCLUSION GENERALE

Les quelques exemples présentés d'application de l'amortissement attestent du caractère pratique positif de l'emploi de ces techniques.

Il s'agit toutefois de cas particuliers à partir desquels il apparaît très difficile de faire un véritable bilan sur l'utilisation générale de l'amortissement. Les raisons sont à rechercher à notre avis dans le défaut d'unicité latent des idées directrices qui ont présidé aux mises en oeuvre de ces techniques.

Il s'agit en effet d'emplois, soit trop à priori, soit trop à posteriori, mais non vraiment intégrés à la conception même des structures, dans la perspective précise des objectifs dynamiques souhaités. Il faut reconnaître en effet que la mise en oeuvre de matériaux spécifiquement adaptés à la dissipation de l'énergie vibratoire ne peut être clairement envisagée que dans le cadre de ce que l'on pourrait entrevoir comme un art de la conception statique qui a culminé dans la création architecturale. Cet art qui pourrait reposer sur la conception propagative de l'énergie par ondes impliquerait en particulier une connaissance très approfondie de la variété des sollicitations dynamiques, jointe à un sens très précis du meilleur usage à faire de la grande variété de matériaux disponibles.

On est évidemment loin de ce schéma si l'on considère que les aspects dynamiques ne sont actuellement abordés qu'à posteriori, par calculs et essais, les structures étant conçues sur des bases quasi statiques essentiellement.

L'avenir particulier des techniques d'apport d'amortissement procèderait donc dans cet esprit du développement parallèle de :

- méthodologie de conception dynamique,
- matériaux spécifiquement adaptés aux finalités vibratoires.

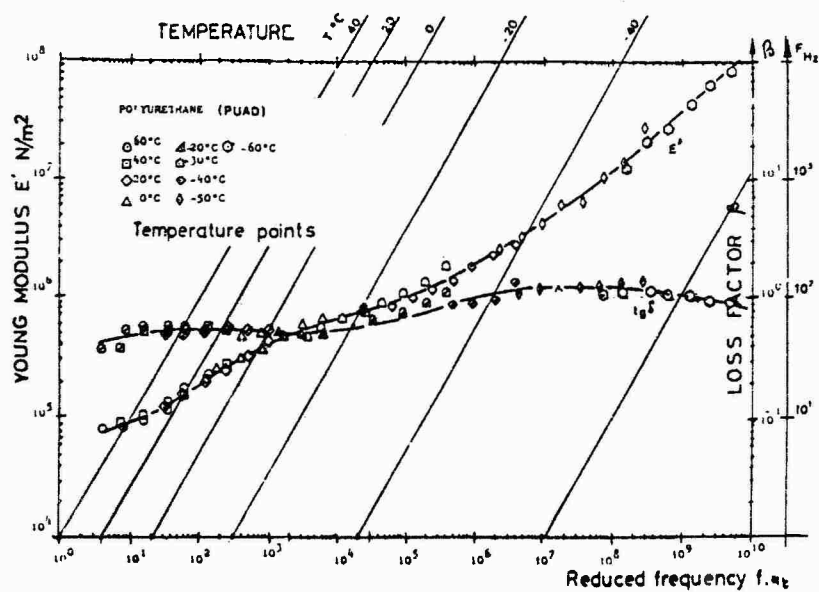
On ressent là une évolution générale dont on ne distingue pas encore clairement la progression.

On pressent néanmoins à travers les quelques résultats positifs acquis la nécessité de soutenir l'effort mesuré, consacré actuellement du développement des matériaux et de leurs techniques d'application. faute d'orientations précises, cet effort reste pourant diffus et les implications pratiques ponctuelles ; cette situation ne reflète à notre avis que le fait que les matériaux amortissants sont apparus dans la palette des architectes industriels d'une façon que l'on doit reconnaître comme prématurée.

+++++



VISCOELASTICIMETER MAK 03 - Planche I -



REDUCED VARIABLES FOR POLYURETHANE . PUAD . [SNPE]

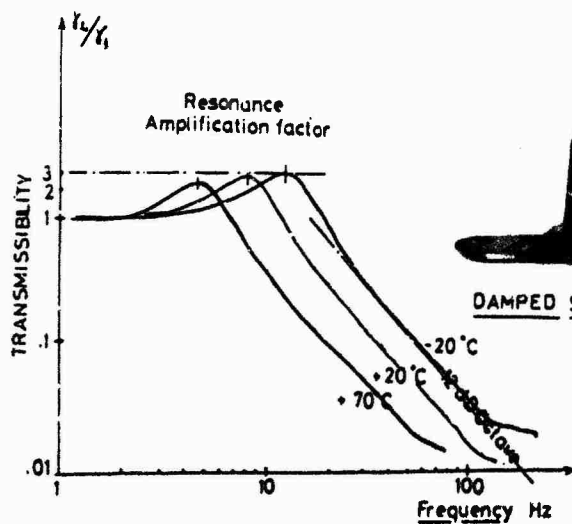
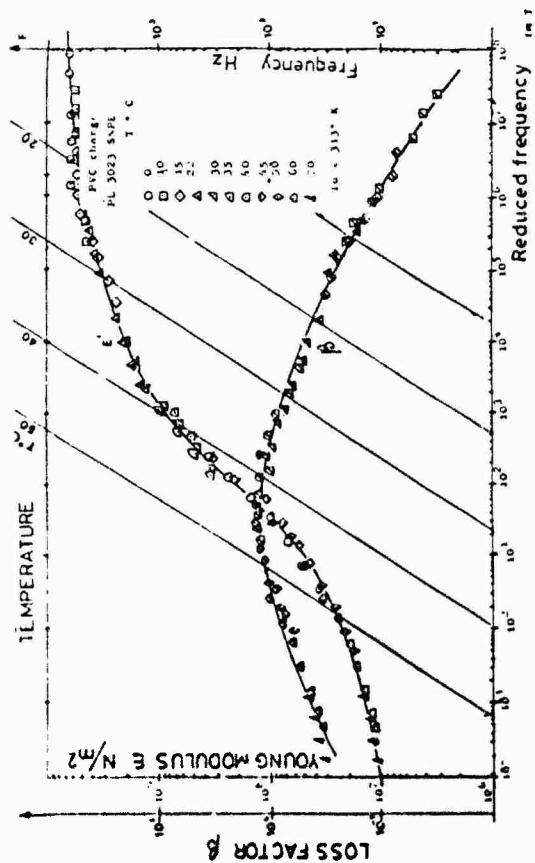


PLANCHE: 2



REDUCED VARIABLES FOR NEPURANE PL3023 [SNPE]

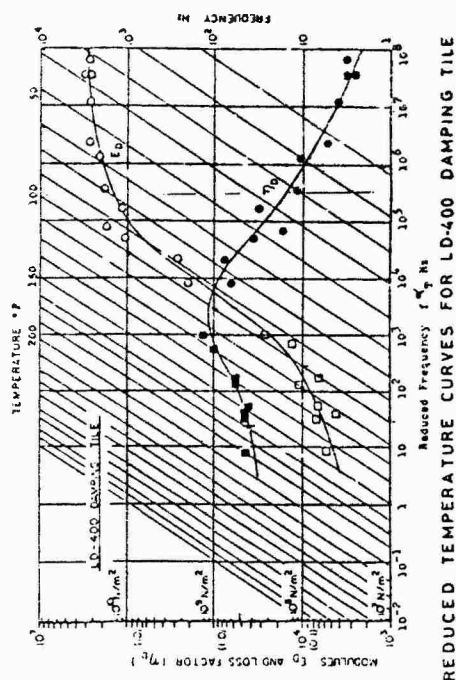


DAMPED PART BY A VISCOELASTIC LAYER

	50 Hz		100 Hz	
	before	after	before	after
β	3 mW/m^2	1 mW/m^2	5 mW/m^2	12 mW/m^2
Global gain	-3 dB		-4 dB	

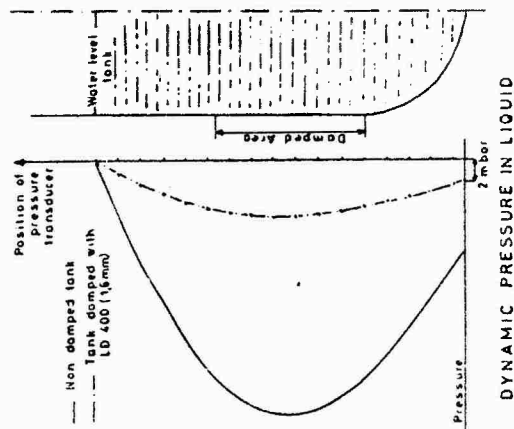
NOISE ABATEMENT APPLICATION

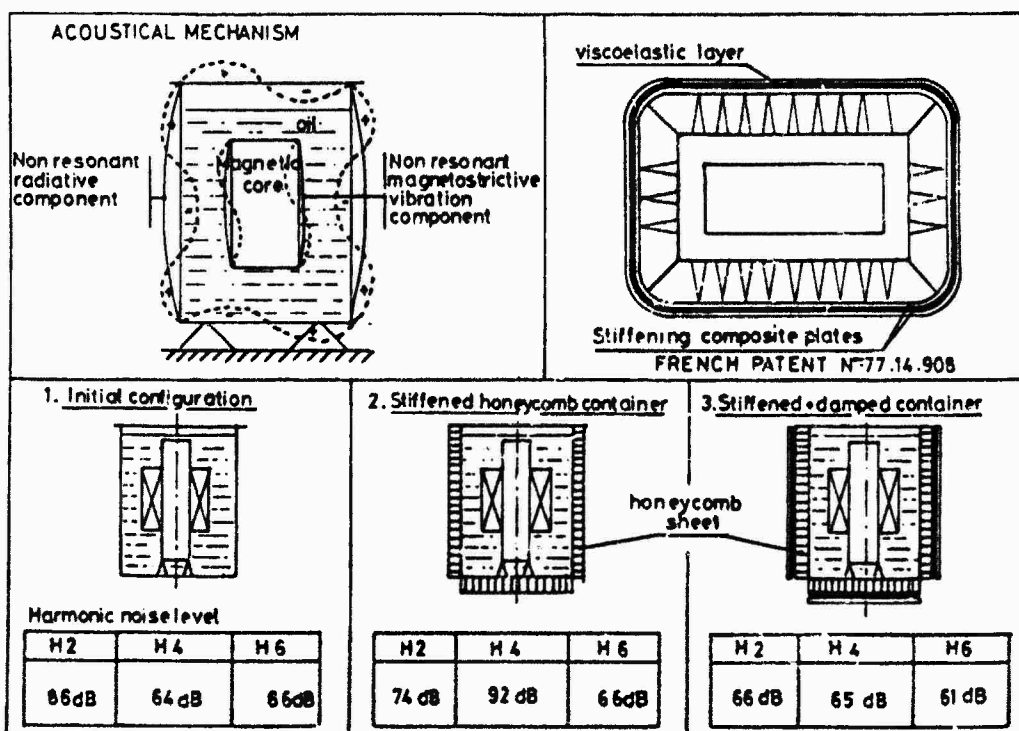
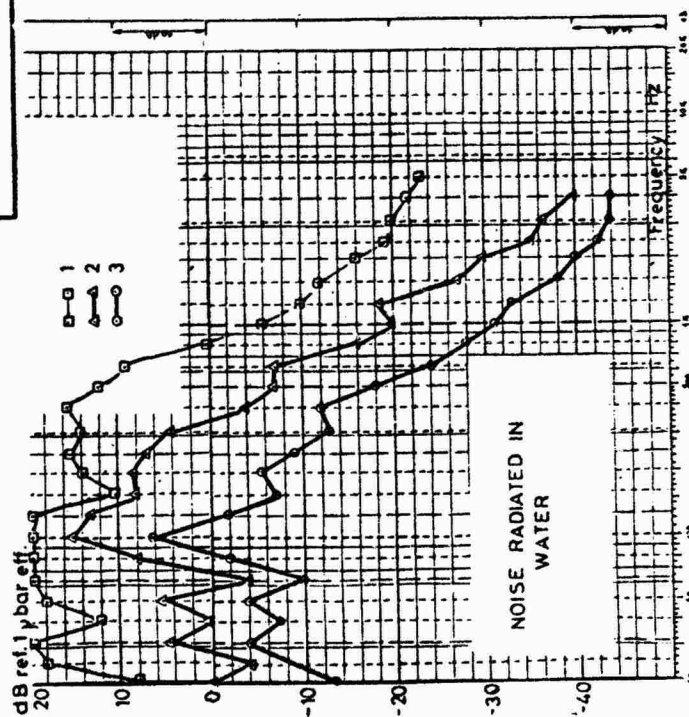
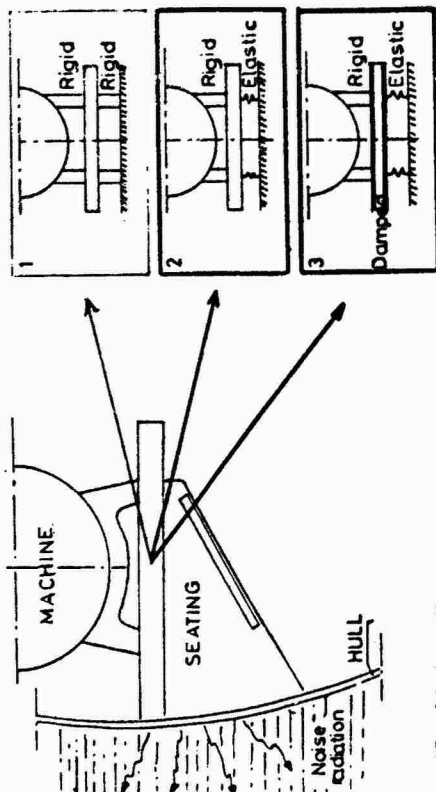
PLANCHE 3



TANK DAMPING POGO EFFECT

PLANCHE 4





ELECTRIC TRANSFORMER STIFFENING + DAMPING

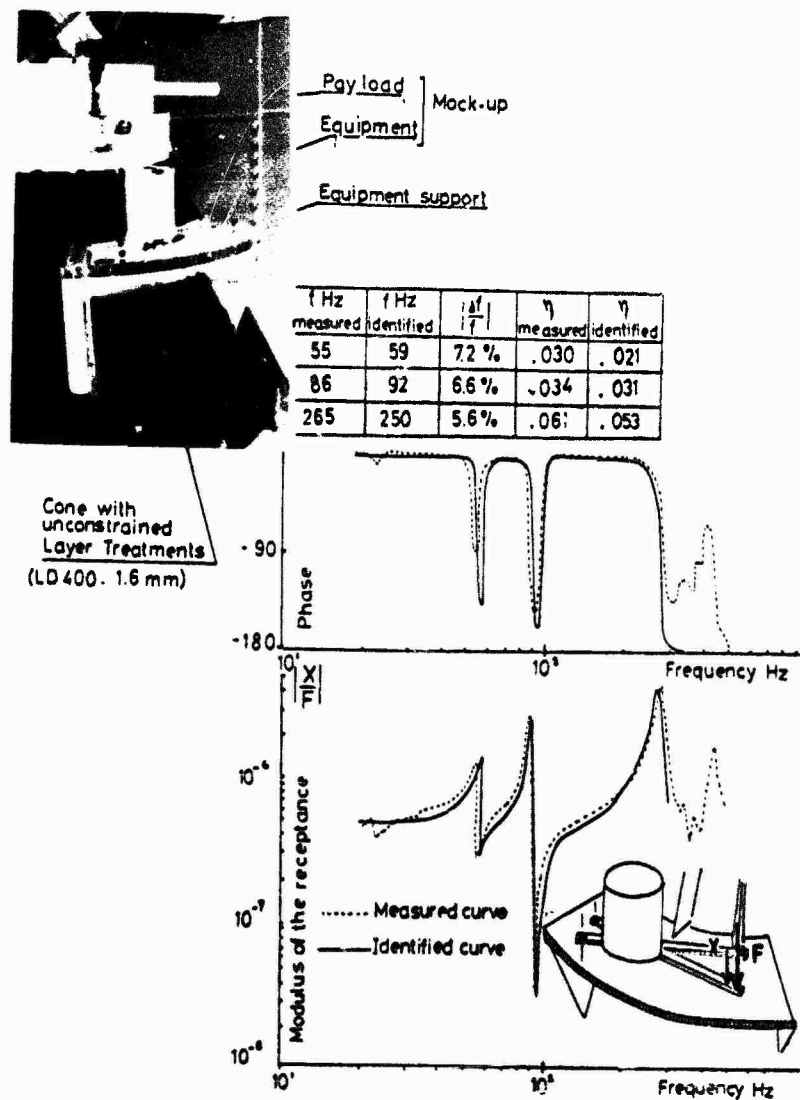
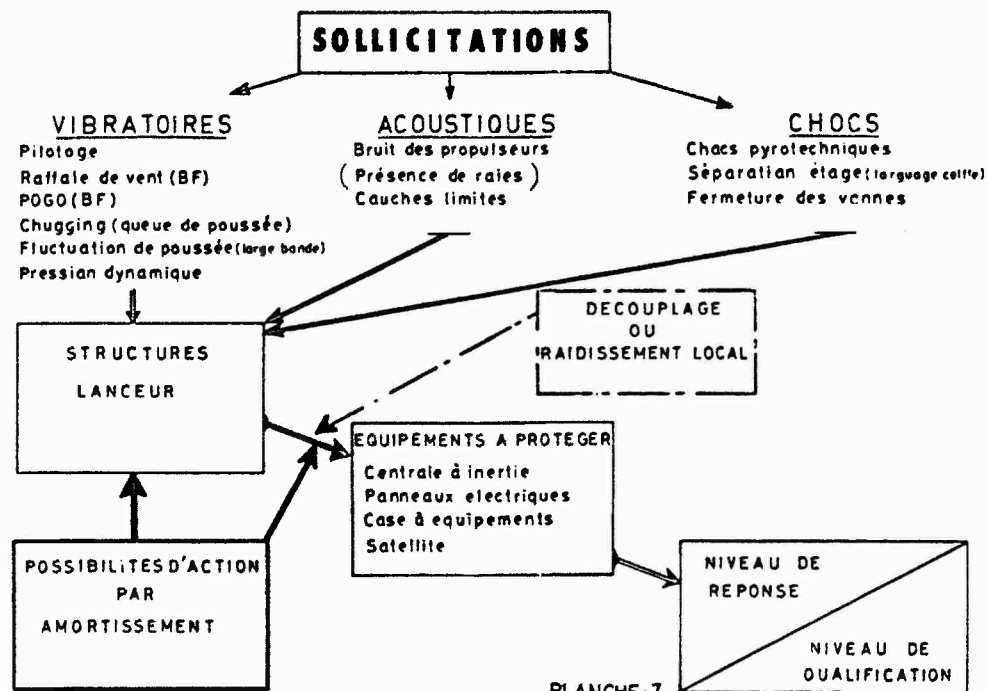
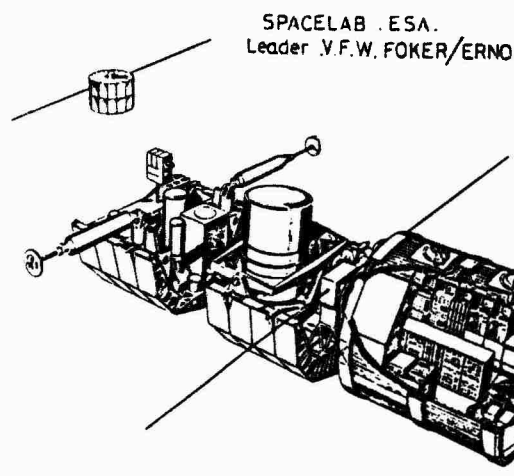
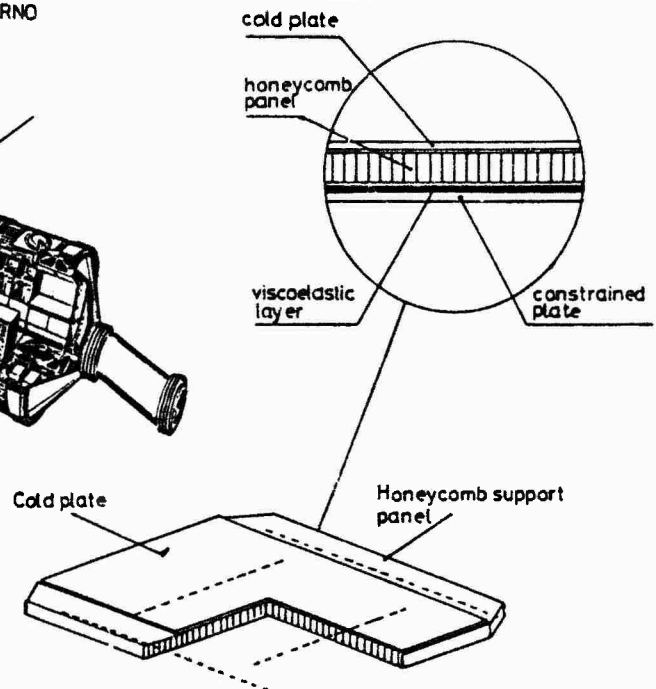


PLANCHE 8



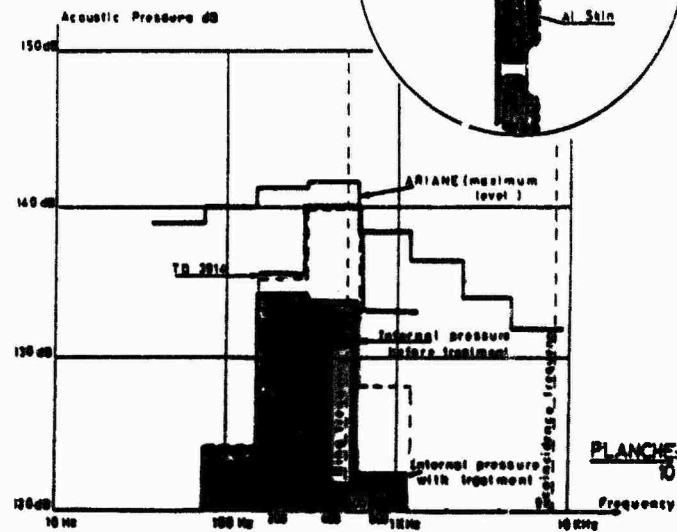
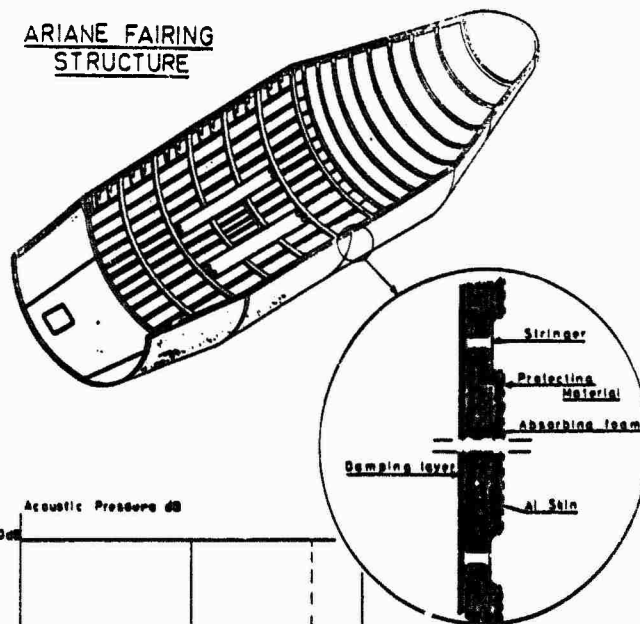
POSSIBLE SOLUTION



DAMPING OF A COLD PLATE SUPPORT STRUCTURE .C.P.S.S.

PLANCHE: 9

ARIANE FAIRING STRUCTURE



ACOUSTICAL ISOLATION of the FAIRING STRUCTURE

DAMPING EFFECTS IN JOINTS AND EXPERIMENTAL TESTS ON RIVETED SPECIMENS

by

Luigi Balis Crema
Antonio Castellani
Istituto di Tecnologia Aerospaziale
Via Eudossiana 16 - 00184 Roma - Italy

and

Alfonso Nappi
SIAI Marchetti
21018 Sesto Calende - Italy

SUMMARY

In this paper the importance of dynamic damping is highlighted and particular attention is given to the effect of riveted joints on energy dissipation. The state of the art in the field of joint damping is illustrated with reference to past experience and to several theories on damping mechanisms.

Then a series of tests carried out on specimens with riveted joints is discussed. Experimental results are pointed out with the intent of giving a further contribution to the knowledge of joint damping.

INTRODUCTION

The importance of damping prediction in complex structures and the high interest in the contribution given by different types of joints is shown by recent research activities carried out in this field [1, 2, 3, 4]. Obviously the study of energy loss is not a new subject, but in the last few years damping effects have become decisive for the success of aerospace projects, the main problems being connected with acoustic fatigue, aeroelastic supercritical vibrations, spinned satellite instability and POGO effect [3, 5, 6].

In the first part of the present work the principal problems on joint damping discussed in most recent publications are briefly introduced.

A general demand on the development of experimental research has soon come out, since the theoretical approach does not appear sufficient to acquire a good knowledge of the problem and to make satisfactory previsions on the dynamic behavior of complex structures. Damping prediction at joints is essential to make use of numeric simulation programs and to account for energy dissipation mechanisms by means of proper coefficients [7].

In the second part of this paper a series of tests carried out at the Institute of Aerospace Technology (Rome University) is discussed; riveted specimens with different types of joints have been considered and the experimental work represents a preliminary investigation with the aim of developing tests to determine the different behavior between jointed and non-jointed specimens by using the testing facilities presently available. The satisfactory outcome of these tests encourages to continue this kind of investigations by using more and more complex specimens in presence of those environment conditions which are of interest in the aerospace field (temperature and pressure).

1.1 GENERAL REMARKS

Joints are always present in any complex structure and great attention is given to their design both for static strength requirements and for fatigue resistance; in many instances, however, also their damping capacity is considered very carefully. In actual fact material damping is not always sufficient to limit resonant vibration amplitudes and stresses; in such cases structural damping may represent the solution of the problem and joints play a paramount role in energy dissipation processes: this is proved, for instance, by the simple consideration that built-up structures tend to show higher damping properties than similar one-piece structures [1].

Even material damping is quite a difficult phenomenon to understand; nowadays, however, numerical data are easily available at least for the most usual materials; the values of the "damping ratio" generally lie within a well known range.

As to built-up structures, their dynamic behavior cannot always be found out experimentally because of their complexity and dimensions; furthermore, when tests are carried out with sufficient accuracy, their cost is very high; therefore the possibility of making reliable predictions would be extremely desirable.

Structural damping has been studied quite deeply, with particular emphasis given to energy dissipation mechanisms at joints, since they show excellent damping capacity and are universally recognized to be the main source of energy loss.

In the following sections brief information will be presented on some results and theories, so as to give a general picture about the state of the art in the field of structural joints.

1.2 INTERFACE LAYER DAMPING

Comprehensive studies and remarkable research activities have been carried out to determine the effect of viscoelastic inserts on the increase of structural damping [8]; their use, however, is limited by the reduced stiffness they cause [1]. Viscoelastic inserts in bolted joints may have interesting practical applications.

In Ref. 9 the damping capacity of viscous inserts is widely discussed: tangential and normal displacements are considered. Furthermore, also the case of rotation about an axis perpendicular to the mating surfaces is investigated. Good agreement between theory and experimental tests is found; it is also demonstrated that energy loss is dependent only on two material properties, the incompressibility of the medium and its viscosity in simple shear. Other damping mechanisms do not show any particular effect in all cases (tangential, normal and angular motion) [9].

Finally, it is well known that viscoelastic layers have been used rather extensively to increase the damping capacity of built-up structures with low weight penalty: to achieve satisfactory energy dissipation it can be sufficient to add viscoelastic material, for instance by introducing a viscous insert between the panel and the stringers in a stiffened plate. A detailed discussion of the several items of this problem is presented in [4].

1.3 BUILT-UP STRUCTURES

Realistic joints are normally dependent on several complex parameters and unknowns, so that analytical studies are a difficult task; in Part 2 an attempt will be made to give some information about tests on riveted fastenings, but before discussing this subject a brief presentation will be made of previous studies on simple joints and built-up structures.

Generally, it is possible to observe that Coulomb friction is the main damping mechanism in joints characterized by relative tangential motion between the mating surfaces; of course, there is an optimization problem involving pressure and other parameters if the highest possible energy loss is to be obtained. Furthermore it is demonstrated that in many structures a small deviation from the optimized values can lead to a reduction of damping. Obviously serious problems due to fretting and corrosion may represent a difficulty so that different solutions are often preferred (for instance lubricated surfaces or adhesive inserts).

A detailed discussion of the damping effect due to uniform clamping pressure in lap joints is given in Ref. 10, where the following relationship is developed for the energy dissipation per cycle:

$$D_r = \frac{\Delta F^3}{12 w \mu p} k_l^{-1} [(1-k)^{-1} - 3k]$$

where w is the joint width, p the clamping pressure, μ the friction coefficient, k_l the extensional stiffness of the lower plate and ΔF the amplitude of the shearing force; finally if k_u is the extensional stiffness of the upper plate, it is:

$$k = k_l / (k_l + k_u)$$

It should be observed that the equation is valid only for load displacement curves which form a closed loop [10].

A similar formula is derived in Ref. 2 for the energy dissipation per cycle in rotary joints, consisting of two cylindrical members in contact over a circular surface:

$$D_c = \frac{2 \pi \mu^2 p^2 r^4}{3 S} (1 - 2h + 2h^3 - h^4)$$

where:

$$1/S = 1/l_1 G_1 + 1/l_2 G_2$$

$$h = \text{const} = (4 \pi \mu p r^3 / 3 - \Delta M)^{1/3} / (4 \pi \mu p r^3 / 3)^{1/3}$$

Apart from μ and p , already defined, the symbols used have the following meanings:

- r = outside radius of contact surface
- ΔM = amplitude of alternating torque
- $l_1 ; l_2$ = axial length of first and second member
- $G_1 ; G_2$ = shear modulus of first and second member

The relationship was obtained by assuming that the applied torque is transferred through shear friction stresses; such stresses, given by the product between friction coefficient and clamping pressure, are assumed to be constant and to exist only where relative motion has taken place; otherwise they are set equal to zero. The assumptions just described represent a remarkable simplification of real joints, but the results of the analysis are convalidated by experimental tests [2].

It has already been pointed out that if shear motion is prohibited the damping capacity of joints is rather low, on the other hand "loose" joints reduce structural stiffness and involve serious fretting problems; there is, however, an intermediate solution: joints can be fastened tightly enough to prevent translation and allow relative rotations; in this case the stiffness loss is very little and the damping effect is good.

A detailed discussion of the problem can be found in Ref. 11, where an analysis is carried out by means of a computer program fit to represent the friction joint.

Ref. 12 is an extensive study on the damping capacity of built-up beams with riveted joints: a theoretical analysis is carried out for beams with no sliding motion at joints; the theory appears to be in good agreement with experimental results, that show an energy dissipation roughly proportional to the third power of the stress amplitude when vibration amplitudes are small; otherwise the energy loss is proportional to a lower power [12].

Generally speaking, there is an optimum condition characterized by the highest damping capacity. If this condition takes place fastenings are neither loose nor perfectly tight but somewhere in between. It should be noticed, however, that such situation can not normally be realized in practice, since it would cause structures to be rather loose and inefficient.

The response of built-up plates at high frequency was studied in Ref. 13, where an attempt is made to identify the dominant damping mechanisms; experiments at different pressures and at frequencies much higher than the panel fundamental resonance frequency have shown that the damping capacity is mainly due to an air pumping effect which appears when the mating surfaces move apart; according to the test results, the pressure (which depends on the applied torque) is of no importance. The joints considered were tight enough to prohibit any relative motion and the amplitudes were rather small, so as to avoid damping measurements dependent on the vibration amplitudes [13].

It has also been demonstrated that damping of stiffened plates depends on the frequency, on the presence of lubricants and on the width of the contact area between stringer and panel.

A tremendous work has been faced during the design of the Space Shuttle, where the problem of structural joint modeling was given great attention; the approach techniques developed during the design phase are widely discussed in Ref. 7: in this context it will be enough to summarize just a few basic concepts which can be extended to other structural damping problems.

First of all it should be remembered once again that the dependance of joint damping on other parameters is not linear: nevertheless a linear model can be used by introducing an equivalent viscous damping.

This assumption is justified by considering that the sinusoidal response to a sinusoidal excitation is practically not influenced by damping non linearities. Furthermore, when riveted joints in plate elements are considered, it should be noted that the energy dissipation is characterized by three different stages: material damping, local plastic deformation and dynamic friction losses: they are due, respectively to small displacements (elastic region), larger motions (plastic region) and relative slipping of the mating surfaces [7].

1.4 CONCLUDING REMARKS

Through the analysis of the references examined a clear demand on experimental tests can be noticed, since theoretical formulations do not lead to reliable damping predictions because of the uncertainties they involve; this concept is well grounded particularly when joints are present and authors agree in the necessity of tests on complex structures owing to the increase

ing importance of damping in structural design.

In actual fact, the need of experimental work should not be underestimated, since significant data on the subject are very rare, especially when riveted joints are considered.

These considerations have encouraged the beginning of a systematic experimental analysis on the damping effects in riveted joints and the preliminary results are shown in the following section (Part 2).

PART 2

EXPERIMENTAL TESTS

2.1 DESCRIPTION OF SPECIMENS

A series of specimens realized at SIAI Marchetti has been tested at the Institute of Aerospace Technology (Rome University) to study the effect of rivets on energy dissipation.

All the specimens were made of aluminum alloy (2024-T3-QQ-A-250/4); the main properties of the material are reported in Table I [14].

TABLE I

Density	$2.77 \cdot 10^3 \text{ kg m}^{-3}$
Modulus of elasticity in tension	$7.26 \cdot 10^{10} \text{ N m}^{-2}$
Shear modulus	$2.90 \cdot 10^{10} \text{ N m}^{-2}$
Ultimate tensile stress	$4.32 \cdot 10^8 \text{ N m}^{-2}$
Proportional limit in tension	$2.75 \cdot 10^8 \text{ N m}^{-2}$
Elongation at rupture	$10 \div 15\%$

Two sets of specimens have been used and the principal difference can be found in the change of their width:

- S 1) width : 15 mm
length : 280 mm
- S 2) width : 65 mm
length : 250 mm

The joints have been realized by means of different rivets and their specifications are reported in Figures 1, 2, 3. For both sets of specimens three types of joints have been tested, namely lap joint, butt joint (with single strap), butt joint (with double strap), as shown in Figures 1 and 2.

In Fig. 3 the different specimens with riveted-fastened laminates are illustrated; at last, a comparison has been made with specimens made out of an aluminum alloy plate (thickness : 2 mm) without joints.

TABLE 2

SPECIMEN		JOINT *	RIVET	THICKNESS (mm)	LENGHT (mm)	WIDTH (mm)
S 1	a	lap	MS20426 AD3-3	1	280	15
	b	b.s.s.				
	c	b.d.s.				
	a'	lap	MS 20470 AD5-5	1		
	b'	b.s.s.				
	c'	b.d.s.				
	g	r.f.l.	MS 20426 AD4-4	2		
	g'	r.f.l.	MS 20470 AD5-5			
	i	---		2		
S 2	d	lap	MS 20426 AD3-3	1	250	65
	e	b.s.s.				
	f	b.d.s.				
	h	r.f.l.	MS 20426 AD3-3	2		
	l	---	---	2		

- * b.s.s. = butt - single strap
b.d.s. = butt - double strap
r.f.l. = riveted - fastened laminates

2.2 MEASUREMENT METHOD AND TEST PROCEDURE

The testing equipment used to evaluate damping is composed by the system shown in Fig. 4 and consists of the following instruments: oscillator, vibration exciter, capacitive detector, amplifier and recorder [15].

The specimen is clamped on a mounting, while the electromagnetic exciter and the vibration detector can move along a slide which is fixed on the same mounting. A frequency range between 2 and 2,000 Hz can be examined, a digital frequency-meter and an oscilloscope allow to determine resonant frequencies correctly. It is well known that several difficulties are involved, since measurement is influenced by vibration amplitudes, transducers position, clamping pressure, specimen characteristics, and so on.

Experiments have been carried out making any possible effort to maintain identical conditions, with the purpose of obtaining repetitive and comparable results; particular attention has been given to reproduce the same constraint conditions and to keep comparable vibration amplitudes.

Non-dimensional damping coefficients vs. specimen vibration amplitude (peak-peak) are reported in Fig. 5, which refers to normal test conditions; it can be noticed that the vibration amplitude has no effects in the working conditions selected. The non-dimensional damping coefficient is measured by means of two classical methods, namely frequency sweep (amplitude sweep with constant force) and decay transient [16].

The measurement of the damping coefficient through the frequency sweep method has been carried out by using different values of the ratio between the amplitudes: the band width has been evaluated, respectively, at -3 dB (ratio between amplitudes: $\lambda = 1/\sqrt{2}$) and at -14 dB ($\lambda = 0.20$).

As shown in Fig. 6, the various methods lead to values that differ only in a small percentage. The results reported in the following sections represent mean values.

2.3 EXPERIMENTAL RESULTS

A series of tests has been made in the frequency range between 15 and 100 Hz; the resonant frequency variation has been obtained, for each specimen, by changing the length of its free side. All the results are referred to the excitation of the first bending mode. The experimental results are presented through a set of diagrams (from Fig. 7 to Fig. 11) where damping coefficients vs. frequency are reported. Each diagram shows the damping effect due to different types of joint, for a given rivet: a comparison is made with the specimen without joints.

In Fig. 7 damping coefficients for specimens a, b, c, of series S1, are shown: these specimens are characterized by the three joints described before and have been made by using the same rivet MS20426 AD3-3. In Fig. 8 the results obtained for specimens a', b', c' (with rivet MS20470 AD5-5) are reported, while Fig. 9 refers to the damping coefficients typical of specimens g and g' (series S1) with riveted - fastened laminates.

As pointed out before, all the results of Figures 7-9 are compared with data obtained by testing specimen *i* (without joints).

In Fig. 10 the damping coefficients for specimens *d, e, f*, of series *S 2* (with rivet *MS 20426 AD3-3* and the three joints considered, are compared) with the values concerning specimen *i* (without joints); in Fig. 11, finally, a comparison is made between specimen *i* and specimen *h* of series *S 2* (with riveted - fastened laminates).

2.4 TESTS IN VACUUM CHAMBER

The effect of atmosphere on global damping can be evaluated by carrying out tests in vacuum; therefore some specimens of both series have been tested in a vacuum chamber available at the Institute of Aerospace Technology [17]: its diameter is 457 mm (18") and its height 762 mm (30").

The general lay-out of the equipment is shown in Fig. 12, while in Fig. 13 damping coefficients at normal pressure are compared with the values obtained at a pressure lower than 10^{-5} Torr.

2.5 ANALYSIS OF RESULTS

As pointed out before, the purpose of the research was to evaluate the contribution of riveted joints to global damping properties: the effect due to riveting has been exhibited through the comparison with specimens without joints.

Figures 7, 8, 10 show a sensible increase of damping coefficients in jointed specimens and their behavior as a function of frequency is similar to the behavior of the specimen without rivets. Damping coefficients of series *S 2* (Fig. 10) are higher than in series *S 1* (Fig. 7,8); this effect is probably due to the different constraint conditions used for the two sets of specimens.

As a matter of fact damping coefficients represent global values for the system that is being examined; therefore the behavior of distinct systems must be necessarily different.

This effect, however, has not represented any problem for the comparison between riveted and non-riveted specimens within the same series.

On the contrary no remarkable differences have been noticed by changing either the joints or the rivets, this result seems to be in agreement with References [1] and [13].

The mean percentage increase determined in jointed specimens (in comparison with the non-jointed one) is reported vs. frequency in Fig. 14.

Finally, specimens consisting of riveted - fastened laminates (Fig. 9 and 11) appear to have the same damping properties of the specimen without rivets, this effect is probably due to tensile stresses caused by the rivets [8] and this in agreement with the results obtained by [18].

As far as atmosphere is concerned, Fig. 13 shows that energy dissipation is about 25% higher; this in agreement with References [17, 18, 19].

2.6 CONCLUSIONS AND FUTURE DEVELOPMENTS

The analysis of the results obtained for elementary structural components shows that significant data concerning energy loss in riveted joints can be obtained by means of normal testing facilities. Therefore, the next step may be a systematic research on similar specimens, to evaluate the effect of temperature and vacuum (which are of high interest for space applications) and to study the dependence of damping on vibration modes. Further developments shall lead to extensive tests on more complex structural components, such as stiffened panels.

The tests just presented and the future program represent an attempt of collecting experimental data with the aim, as far as possible, of defining a methodology (founded on empirical bases) which shall serve as a guide towards dynamic response prediction for complex aerospace structures [20].

REFERENCES

- [1] E.E. Ungar: "The Status of Engineering Knowledge Concerning the Damping of Built-up Structures"
Journal of Sound and Vibration, Vol. 26-1, 1973, pp. 141-154.
- [2] R.S. H. Richardson - H. Nolle: "Energy Dissipation in Rotary Structural Joints"
Journal of Sound and Vibration, Vol. 54-4, 1977, pp. 577-588.
- [3] P. Santini - A. Castellani - A. Nappi: "An Introduction to the Problem of Dynamic Structural Damping"
AGARD - R - 663, 1978.
- [4] L. Rogers: "Conference on Aerospace Polymeric Viscoelastic Damping Technology for the 1980's"
AFFDL - TM - 78 - 78 - FBA, July 1978.
- [5] P. Santini: "Influenza delle non linearità strutturali sulle vibrazioni aeroelastiche dei pannelli"
L'Aerotecnica Missili & Spazio, N. 1, 1971, pp. 85-90.
- [6] H. Försching: "Grundlagen der Aeroelastik", Cap. 2, pp. 134 - 145.
Springer - Verlag, 1974, Berlin, Heidelberg.
- [7] R.M. Gates: "Effects of Damping on Mode Shapes"
NASA - CR - 150357, 1977.
- [8] B.J. Lazan - L.E. Goodman: "Material and Interface Damping", cap. 36
Shock and Vibration Handbook, edited by C.M. Harris and C.E. Crede, Mc Graw-Hill Book Company Inc., New York, 1961.
- [9] T.J. Mentel: "Joint Interface Layer Damping"
Journal of Engineering for Industry, 89, November 1967, pp. 797-805.
- [10] A.F. Metherell - S.V. Diller: "Instantaneous Energy Dissipation Rate in a Lap Joint - Uniform Clamping Pressure"
Journal of Applied Mechanics, 35, March 1968, pp. 123-128.
- [11] C.F. Beards - J.L. Williams: "The Damping of Structural Vibration by Rotational Slip in Joints"
Journal of Sound and Vibration, 53 (3), 1977, pp. 333-340.
- [12] T.H.H. Pien: "Structural Damping of a Simple Built-up Beam with Riveted Joints in Bending"
Journal of Applied Mechanics 24, March 1957, pp. 35-38.
- [13] E.E. Ungar - J.R. Carbonell: "On Panel Vibration Damping Due to Structural Joints"
AIAA Journal, Vol. 4, N. 8, August 1966, pp. 1385-1390.
- [14] UNAVIA, Commissione Tecnica di Unificazione nell'Aeronautica, 811-02, foglio 1/3, September 1966.
- [15] R. Barboni - L. Balis Crema: "Determinazione Sperimentale delle Caratteristiche Viscoelastiche"
L'Aerotecnica Missili & Spazio, N. 2, 1972, pp. 117-127.
- [16] H. Gauzy: "Measurement of Inertial and Structural Damping"
AGARD, Manual of Aeroelasticity, Vol. 4, Cap. 3, pp. 1 - 23.
- [17] L. Balis Crema - M. Marchetti - I. Peroni: "Misure Sperimentali di Caratteristiche Dinamiche di Compositi"
in corso di pubblicazione.
- [18] R.R. Mc Withey - R.J. Hayduk: "Damping Characteristics of Built-up Cantilever Beams in a Vacuum Environment"
NASA TN D-3065, November 1965.
- [19] W.E. Howell: "An Experimental Investigation of the Damping Contribution of an Elastomeric ablator on Aluminum Beams"
NASA TM X-2852, April 1974.
- [20] C.S. Chang: "Nonlinear Dynamic Analysis of Structures"
Final Report, Volume II: "Structural Joint Damping", Contract NAS8-21435, June 1970.

ACKNOWLEDGMENTS

The Authors wish to thank Prof. Paolo Santini (Director of the Institute of Aerospace Technology) and Dr. Alessandro Brena (Technical Director of SIAI Marchetti) for the support given to the present work. Prof. P. Santini is also acknowledged for his assistance and his comments. Besides the Authors have appreciated the cooperation of Mr. Antonio Pozza and Mr. Giuseppe Siclari during the experimental tests and the aid of Mr. Alberico Blasi for the art work.

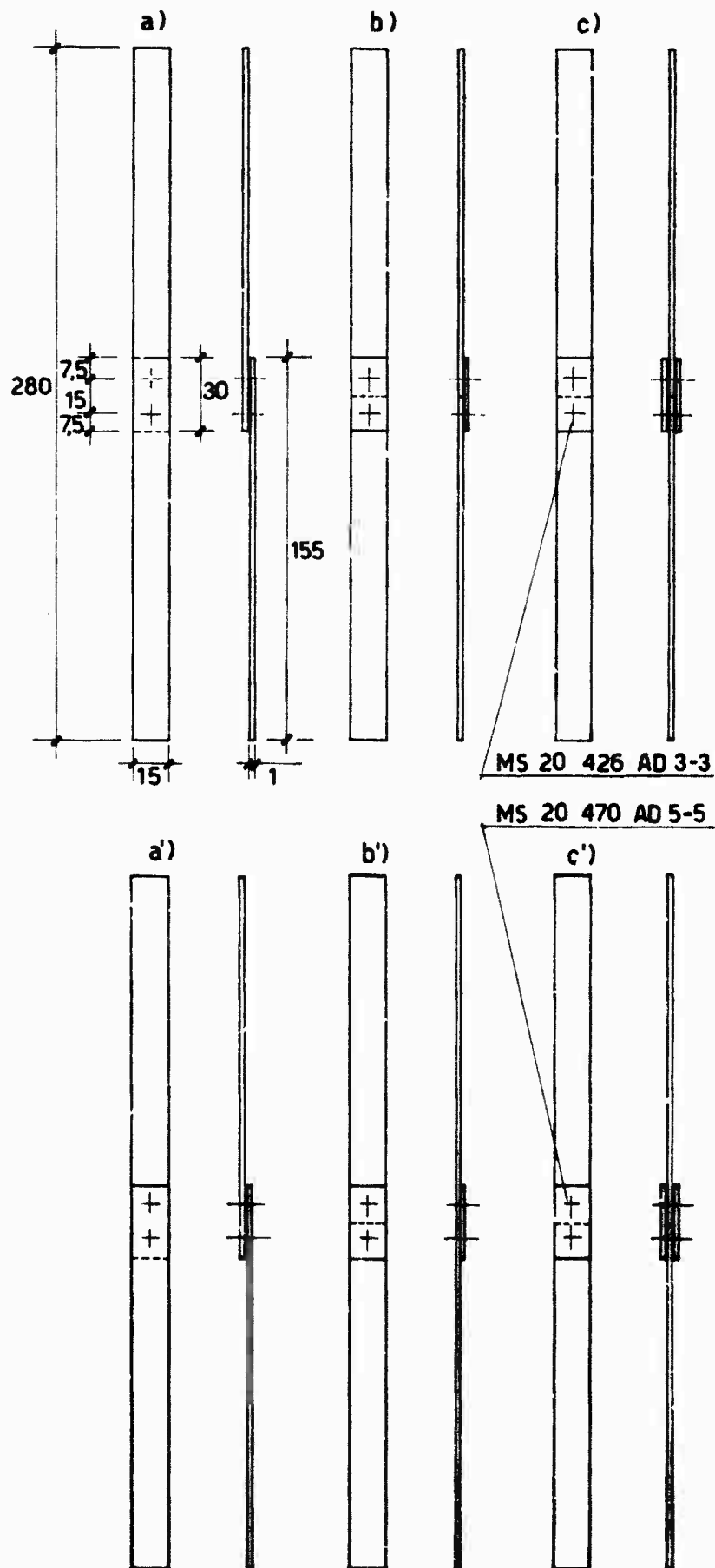


Fig. 1 - Details of test specimens.

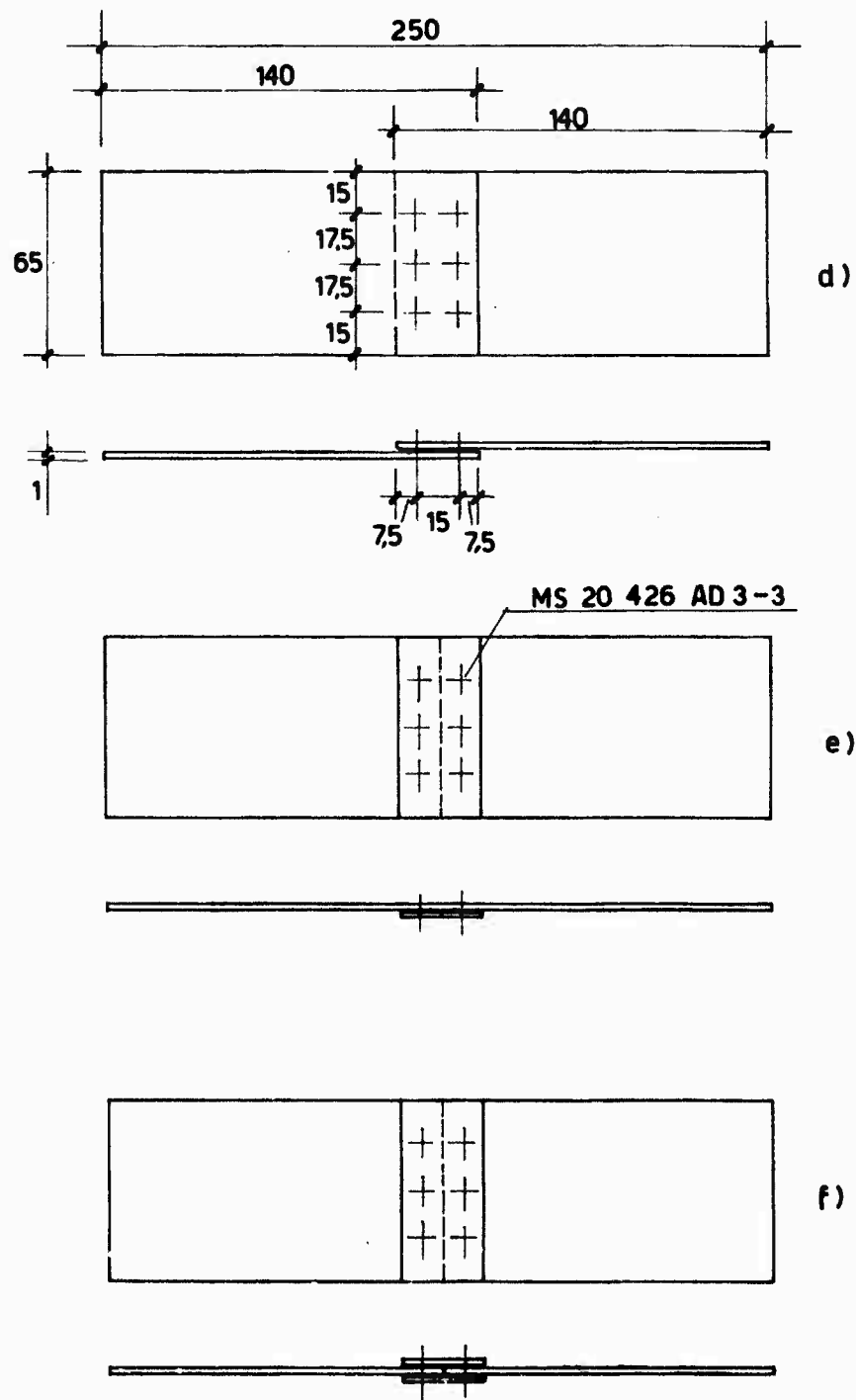


Fig. 2 - Details of test specimens.

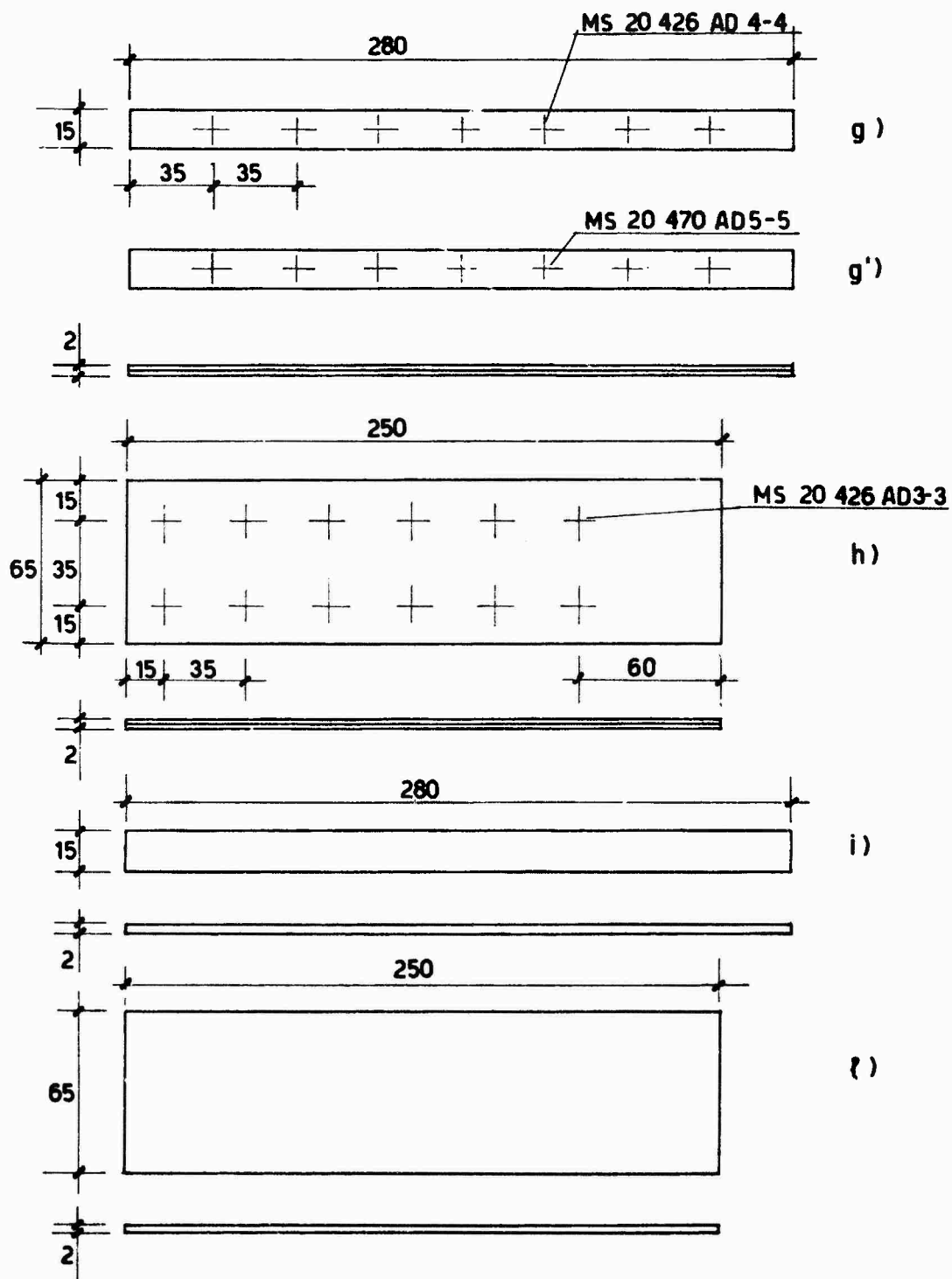


Fig. 3 - Details of test specimens.

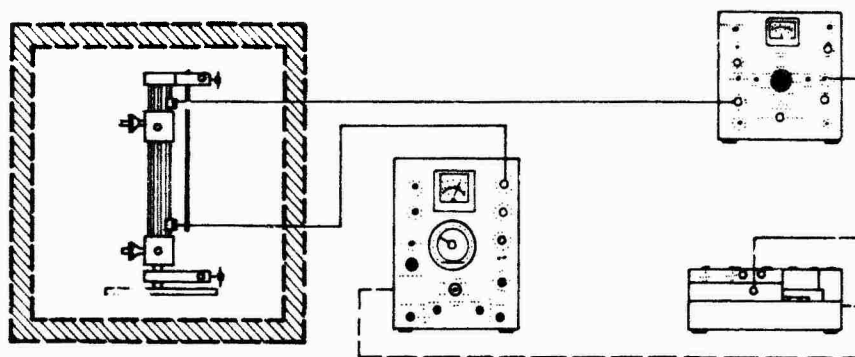


Fig. 4 - Schematic diagram of experimental set-up.

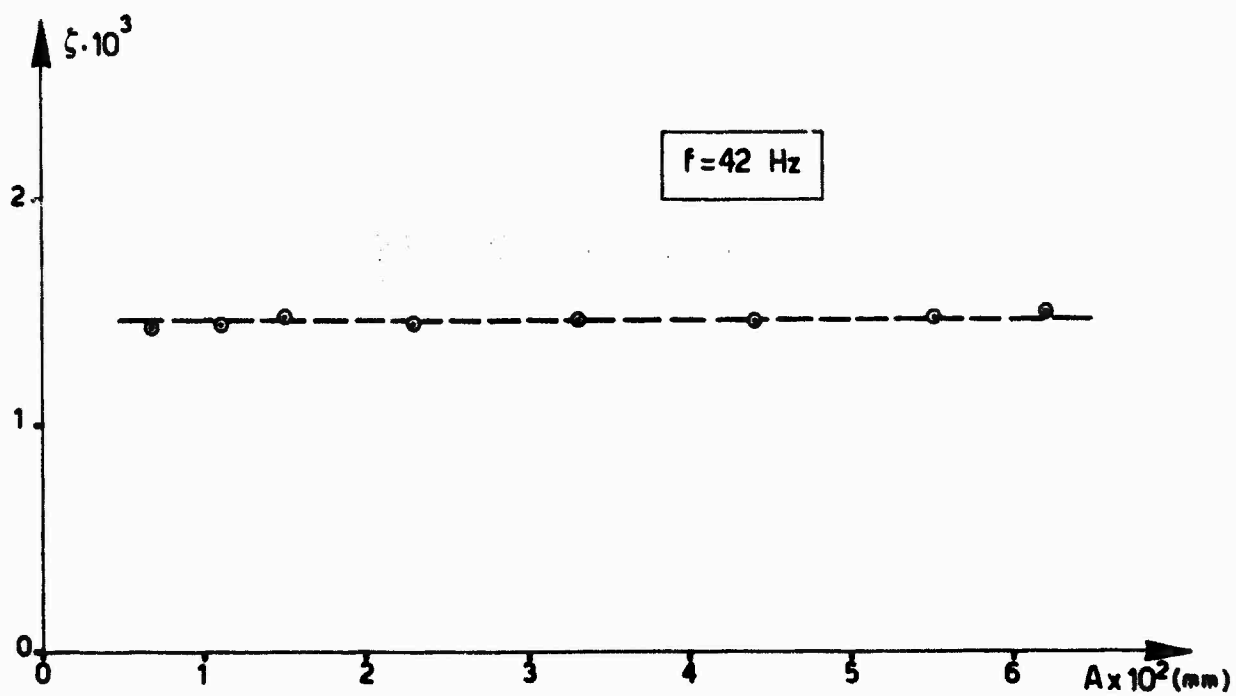


Fig. 5 - Damping coefficient ζ versus tip amplitude A

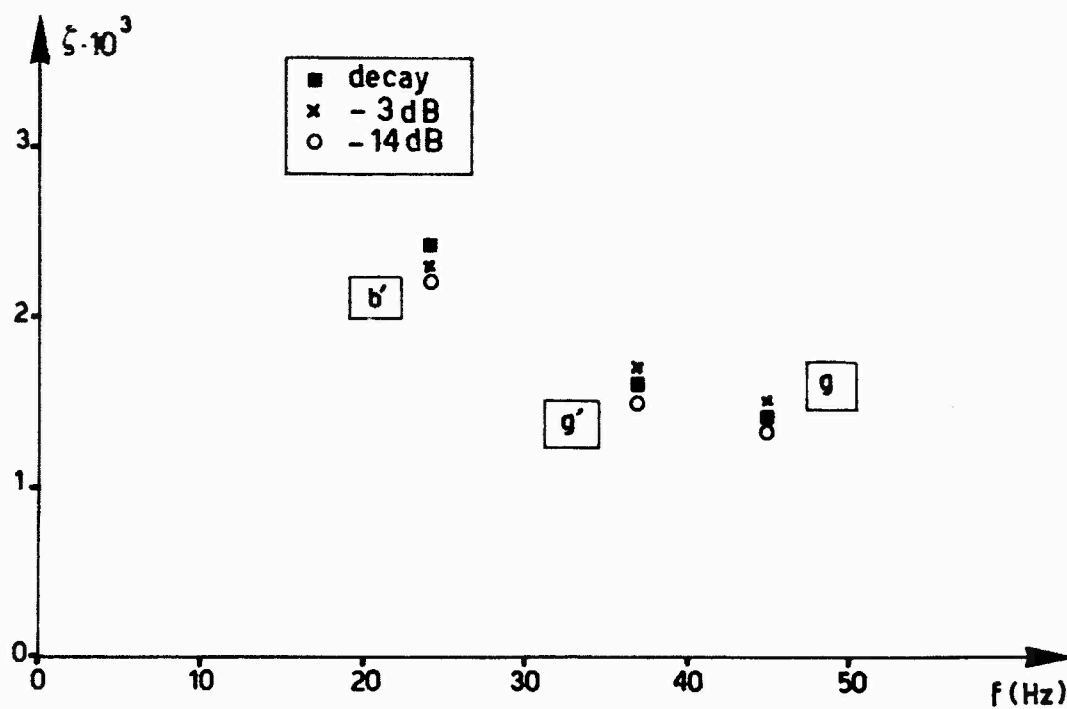


Fig. 6 -- Comparison between the employed measurement techniques.

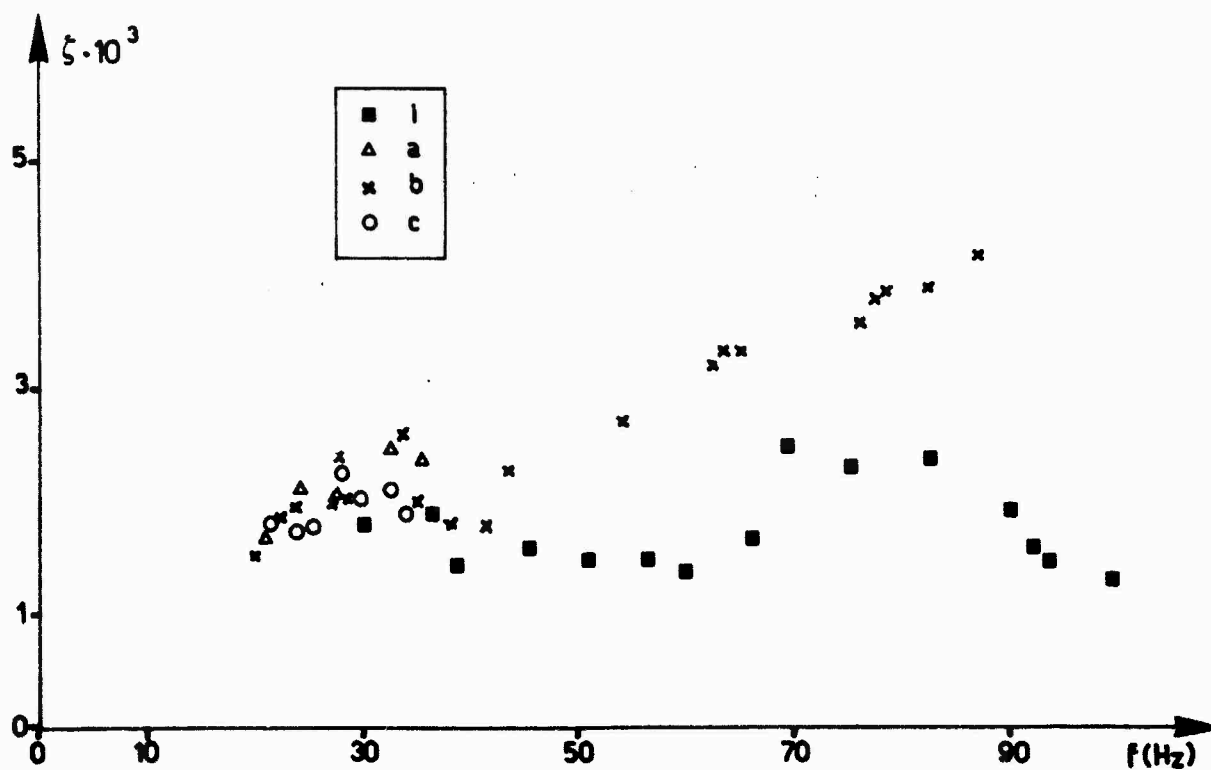


Fig. 7 -- Damping coefficient ζ versus frequency f .

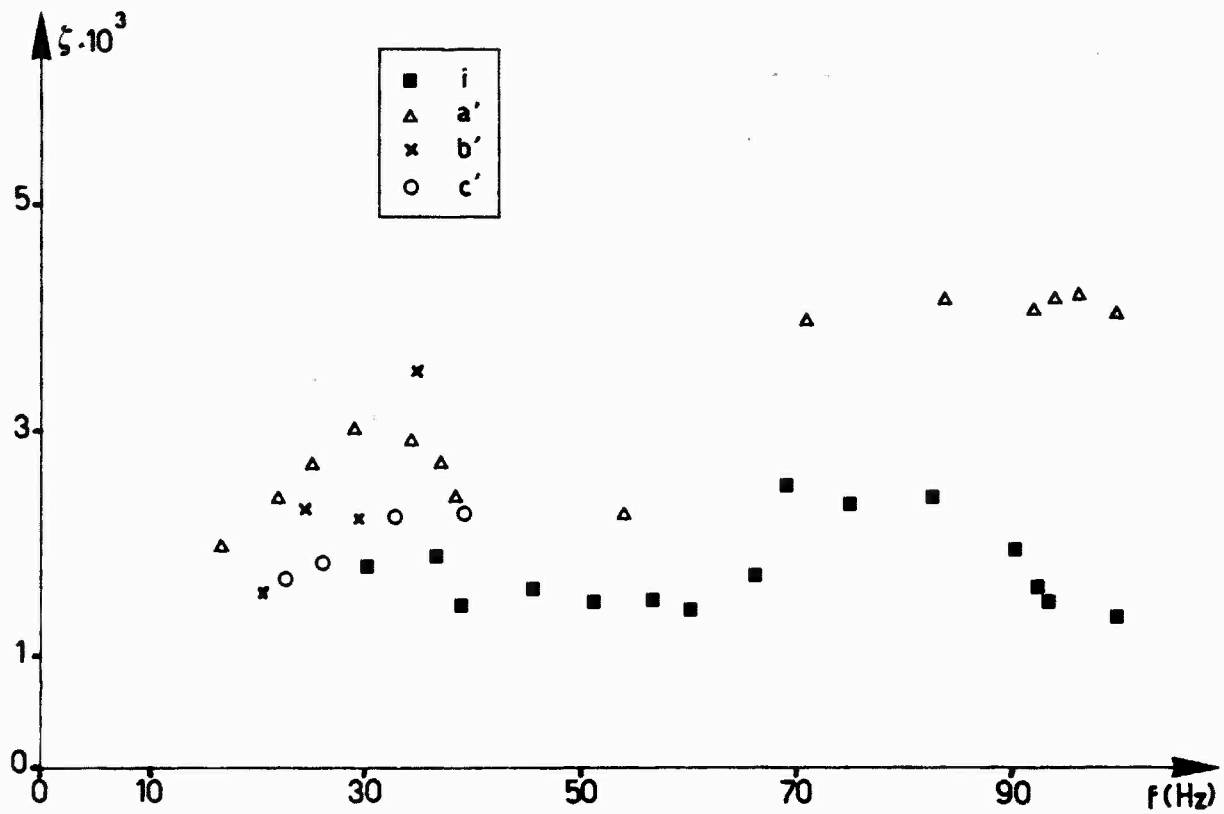


Fig. 8 — Damping coefficient ζ versus frequency f .

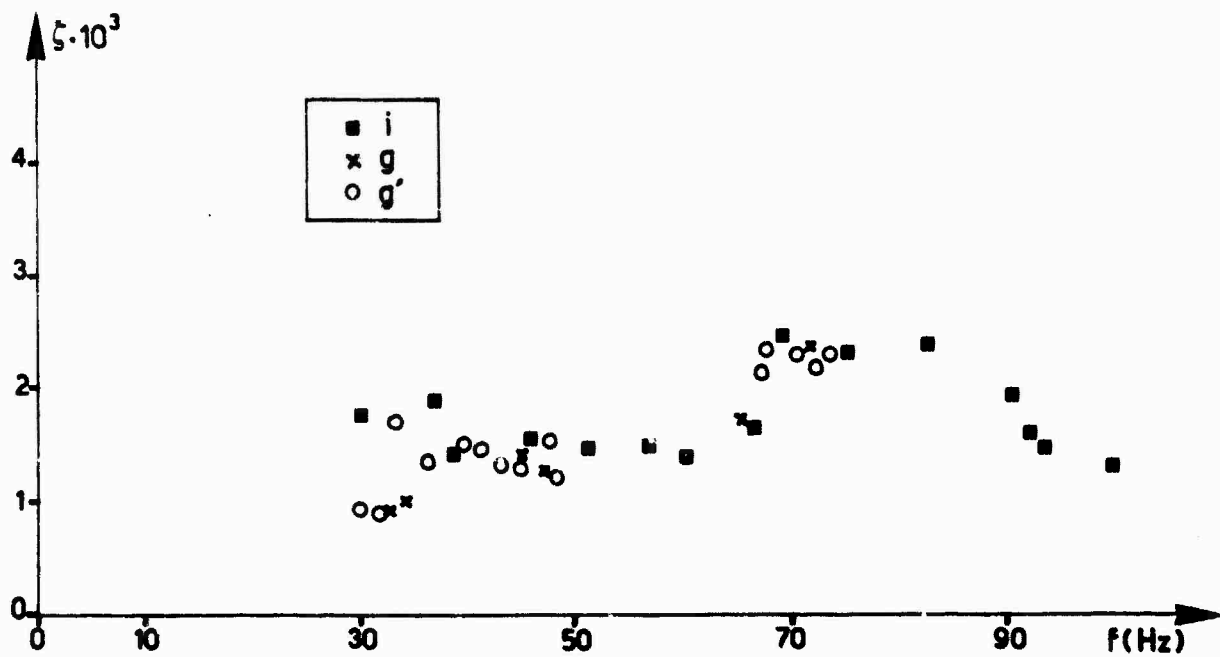


Fig. 9 — Damping coefficient ζ versus frequency f .

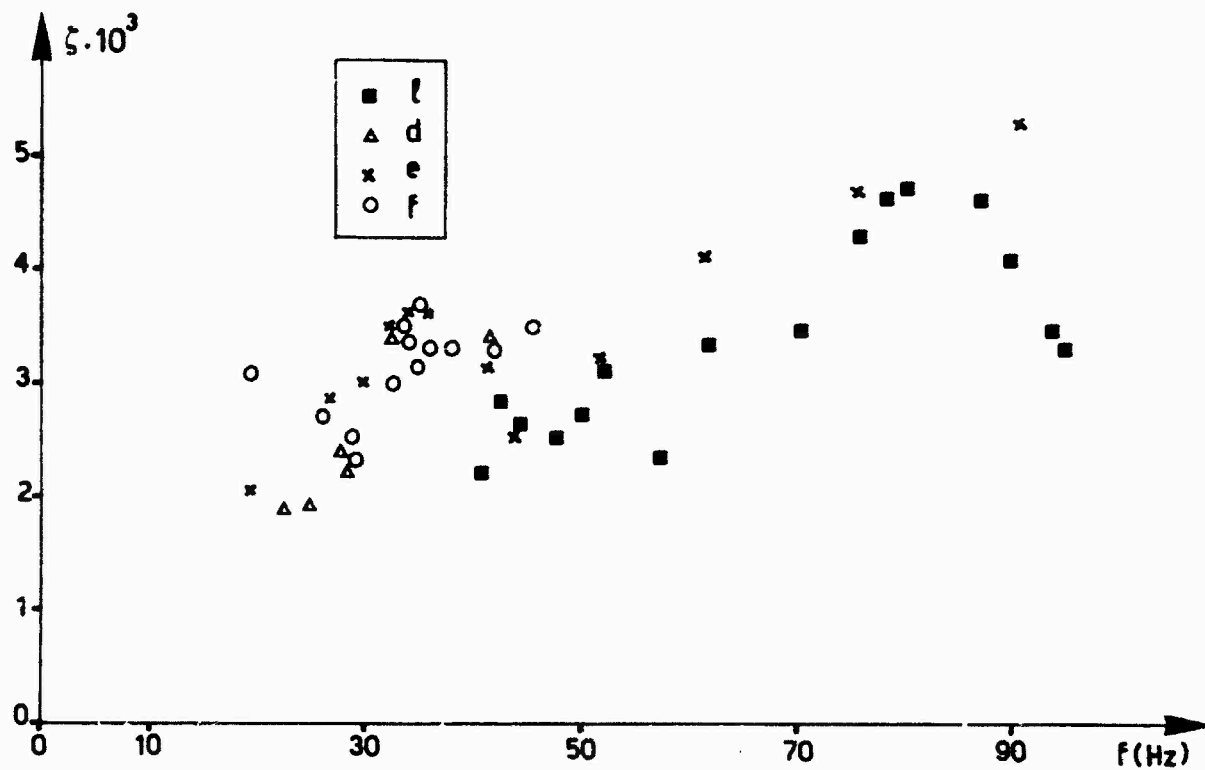


Fig. 10 - Damping coefficient ζ versus frequency f .

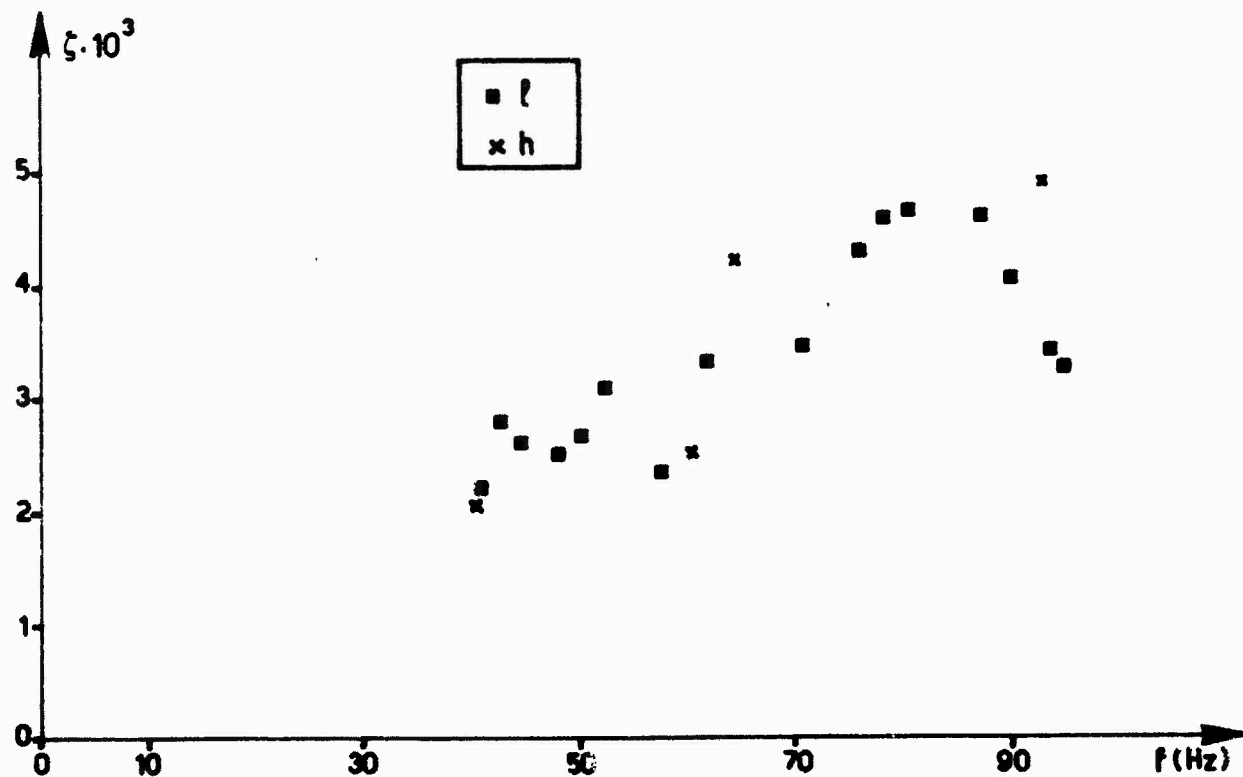


Fig. 11 - Damping coefficient ζ versus frequency f .

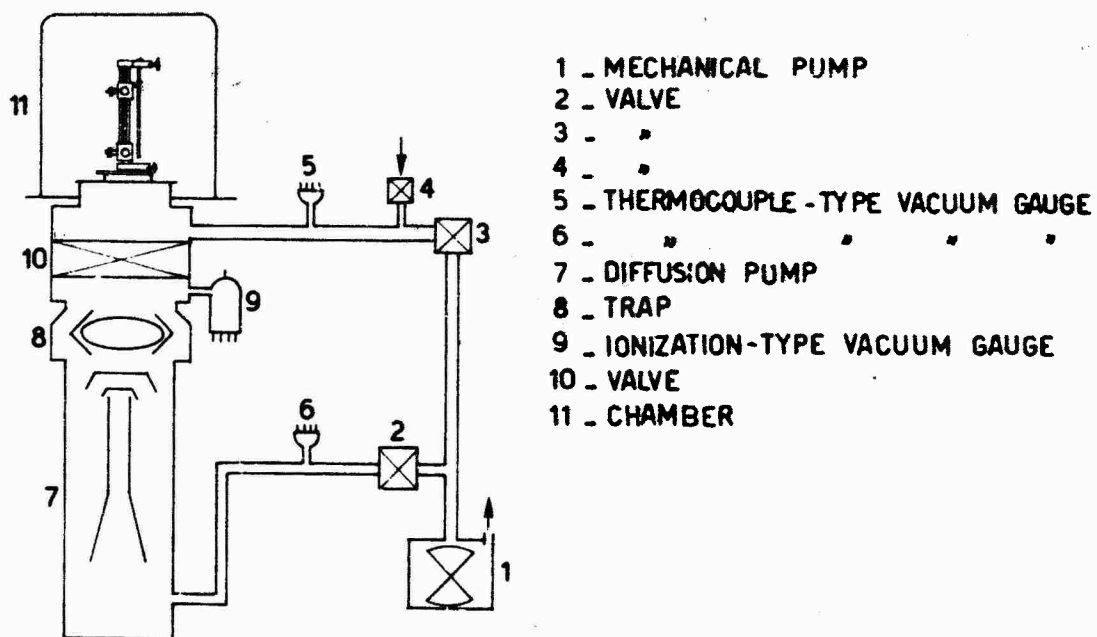


Fig. 12 - Schematic diagram of vacuum system.

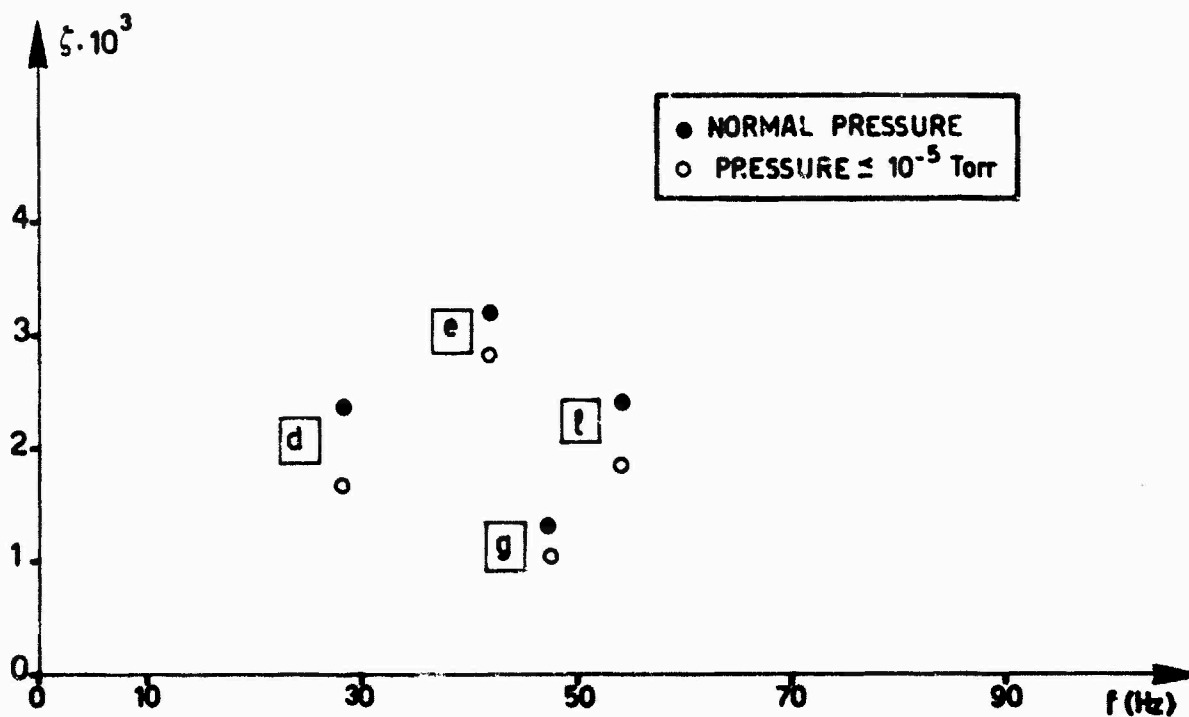


Fig. 13 - Vacuum effect on the damping coefficient ζ .

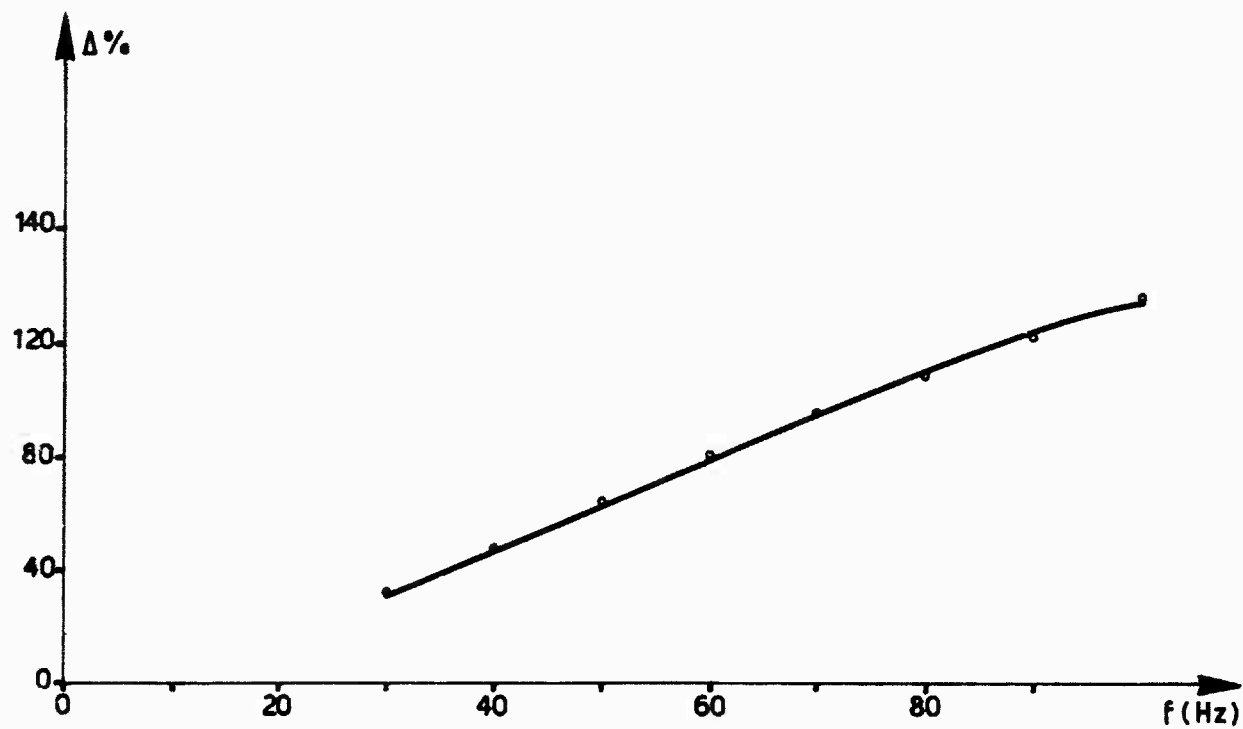


Fig. 14 - Per cent increment for the riveted specimens of the damping coefficient Δ versus frequency f .

REPORT DOCUMENTATION PAGE

1. Recipient's Reference	2. Originator's Reference AGARD-CP-277	3. Further Reference ISBN 92-835-0244-2	4. Security Classification of Document UNCLASSIFIED
5. Originator	Advisory Group for Aerospace Research and Development North Atlantic Treaty Organization 7 rue Ancelle, 92200 Neuilly sur Seine, France		
6. Title	DAMPING EFFECTS IN AEROSPACE STRUCTURES		
7. Presented at	the 48th Meeting of the AGARD Structures and Materials Panel held in Williamsburg, VA, USA on 2-3 April 1979.		
8. Author(s)/Editor(s) Various	9. Date October 1979		
10. Author's/Editor's Address Various	11. Pages 200		
12. Distribution Statement	This document is distributed in accordance with AGARD policies and regulations, which are outlined on the Outside Back Covers of all AGARD publications.		
13. Keywords/Descriptors			
Dynamic response Vibration damping Structural analysis		Composite materials Elastic analysis Aeroelasticity	
14. Abstract			
<p>The objective of the Specialists' Meeting was to make available pertinent information and reliable rules to account for the effects of structural damping on problems of elastic stability. The most general aspects of structural damping were covered; physical roots, mathematical formulation, damping characteristics of aerospace structural components, effects on dynamic response, investigation of damping in composites and effects in joints.</p>			

<p>AGARD Conference Proceedings No.277 Advisory Group for Aerospace Research and Development, NATO DAMPING EFFECTS IN AEROSPACE STRUCTURES Published October 1979 200 pages</p> <p>The objective of the Specialists' Meeting was to make available pertinent information and reliable rules to account for the effects of structural damping on problems of elastic stability. The most general aspects of structural damping were covered; physical roots, mathematical formulation, damping characteristics of aerospace structural components, effects on dynamic response, investigation of damping in composites and effects in joints.</p> <p>P.T.O.</p>	<p>AGARD-CP-277</p> <p>Dynamic response Vibration damping Structural analysis Composite materials Elastic analysis Aeroelasticity</p>	<p>AGARD Conference Proceedings No.277 Advisory Group for Aerospace Research and Development, NATO DAMPING EFFECTS IN AEROSPACE STRUCTURES Published October 1979 200 pages</p> <p>The objective of the Specialists' Meeting was to make available pertinent information and reliable rules to account for the effects of structural damping on problems of elastic stability. The most general aspects of structural damping were covered; physical roots, mathematical formulation, damping characteristics of aerospace structural components, effects on dynamic response, investigation of damping in composites and effects in joints.</p> <p>P.T.O.</p>	<p>AGARD-CP-277</p> <p>Dynamic response Vibration damping Structural analysis Composite materials Elastic analysis Aeroelasticity</p>
<p>AGARD Conference Proceedings No.277 Advisory Group for Aerospace Research and Development, NATO DAMPING EFFECTS IN AEROSPACE STRUCTURES Published October 1979 200 pages</p> <p>The objective of the Specialists' Meeting was to make available pertinent information and reliable rules to account for the effects of structural damping on problems of elastic stability. The most general aspects of structural damping were covered; physical roots, mathematical formulation, damping characteristics of aerospace structural components, effects on dynamic response, investigation of damping in composites and effects in joints.</p> <p>P.T.O.</p>	<p>AGARD-CP-277</p> <p>Dynamic response Vibration damping Structural analysis Composite materials Elastic analysis Aeroelasticity</p>	<p>AGARD Conference Proceedings No.277 Advisory Group for Aerospace Research and Development, NATO DAMPING EFFECTS IN AEROSPACE STRUCTURES Published October 1979 200 pages</p> <p>The objective of the Specialists' Meeting was to make available pertinent information and reliable rules to account for the effects of structural damping on problems of elastic stability. The most general aspects of structural damping were covered; physical roots, mathematical formulation, damping characteristics of aerospace structural components, effects on dynamic response, investigation of damping in composites and effects in joints.</p> <p>P.T.O.</p>	<p>AGARD-CP-277</p> <p>Dynamic response Vibration damping Structural analysis Composite materials Elastic analysis Aeroelasticity</p>

<p>Papers presented at the 48th Meeting of the AGARD Structures and Materials Panel held in Williamsburg, VA, USA on 2-3 April 1979.</p> <p>ISBN 92-835-0244-2</p>	<p>Papers presented at the 48th Meeting of the AGARD Structures and Materials Panel held in Williamsburg, VA, USA on 2-3 April 1979</p> <p>ISBN 92-835-0244-2</p>
<p>Papers presented at the 48th Meeting of the AGARD Structures and Materials Panel held in Williamsburg, VA, USA on 2-3 April 1979.</p> <p>ISBN 92-835-0244-2</p>	<p>Papers presented at the 48th Meeting of the AGARD Structures and Materials Panel held in Williamsburg, VA, USA on 2-3 April 1979.</p> <p>ISBN 92-835-0244-2</p>

Bl 20
4
AGARD

NATO  OTAN

7 RUE ANCELLE · 92200 NEUILLY-SUR-SEINE
FRANCE

Telephone 745.08.1G · Telex 610176

**DISTRIBUTION OF UNCLASSIFIED
AGARD PUBLICATIONS**

AGARD does NOT hold stocks of AGARD publications at the above address for general distribution. Initial distribution of AGARD publications is made to AGARD Member Nations through the following National Distribution Centres. Further copies are sometimes available from these Centres, but if not may be purchased in Microfiche or Photocopy form from the Purchase Agencies listed below.

NATIONAL DISTRIBUTION CENTRES

BELGIUM

Coordonnateur AGARD - VSL
Etat-Major de la Force Aérienne
Quartier Reine Elisabeth
Rue d'Evere, 1140 Bruxelles

CANADA

Defence Scientific Information Service
Department of National Defence
Ottawa, Ontario K1A 0Z2

DENMARK

Danish Defence Research Board
Østerbrogades Kaserne
Copenhagen Ø

FRANCE

O.N.E.R.A. (Direction)
29 Avenue de la Division Leclerc
92 Châtillon sous Bagneux

GERMANY

Zentralstelle für Luft- und Raumfahrt-
dokumentation und -information
c/o Fachinformationszentrum Energie,
Physik, Mathematik GmbH
Kernforschungszentrum
7514 Eggenstein-Leopoldshafen 2

GREECE

Hellenic Air Force General Staff
Research and Development Directorate
Holargos, Athens, Greece

ICELAND

Director of Aviation
c/o Flugrad
Reykjavik

ITALY

Aeronautica Militare
Ufficio del Delegato Nazionale all'AGARD
3, Piazzale Adenauer
Roma/EUR

LUXEMBOURG

See Belgium

NETHERLANDS

Netherlands Delegation to AGARD
National Aerospace Laboratory, NLR
P.O. Box 126
Delft

NORWAY

Norwegian Defence Research Establishment
Main Library
P.O. Box 25
N-2007 Kjeller

PORTUGAL

Direcção do Serviço de Material
da Força Aérea
Rua da Escola Politécnica 42
Lisboa
Attn: AGARD National Delegate

TURKEY

Department of Research and Development (ARGE)
Ministry of National Defence, Ankara

UNITED KINGDOM

Defence Research Information Centre
Station Square House
St. Mary Cray
Orpington, Kent BR5 3RE

UNITED STATES

National Aeronautics and Space Administration (NASA)
Langley Field, Virginia 23365
Attn: Report Distribution and Storage Unit

THE UNITED STATES NATIONAL DISTRIBUTION CENTRE (NASA) DOES NOT HOLD
STOCKS OF AGARD PUBLICATIONS, AND APPLICATIONS FOR COPIES SHOULD BE MADE
DIRECT TO THE NATIONAL TECHNICAL INFORMATION SERVICE (NTIS) AT THE ADDRESS BELOW.

PURCHASE AGENCIES

Microfiche or Photocopy

National Technical
Information Service (NTIS)
5285 Port Royal Road
Springfield
Virginia 22161, USA

Microfiche

Space Documentation Service
European Space Agency
10, rue Mario Nikis
75015 Paris, France

Microfiche

Technology Reports
Centre (DTI)
Station Square House
St. Mary Cray
Orpington, Kent BR5 3RF
England

Requests for microfiche or photocopies of AGARD documents should include the AGARD serial number, title, author or editor, and publication date. Requests to NTIS should include the NASA accession report number. Full bibliographical references and abstracts of AGARD publications are given in the following journals:

Scientific and Technical Aerospace Reports (STAR)
published by NASA Scientific and Technical
Information Facility
Post Office Box 8757
Baltimore/Washington International Airport
Maryland 21240, USA

Government Reports Announcements (GRA)
published by the National Technical
Information Services, Springfield
Virginia 22161, USA



Printed by Technical Editing and Reproduction Ltd
Harford House, 7-9 Charlotte St, London W1P 1HD

ISBN 92-835-0244-2